THE UNIVERSITY *of* EDINBURGH

E. coli motility and growth: a biophysical study

Alys Jepson

A thesis submitted in fulfilment of the requirements
for the degree of Doctor of Philosophy
to the
University of Edinburgh
October 2014

Abstract

This thesis comprises two parts, both concerned with the study of *Escherichia coli* bacterial suspensions. The first part investigates *E. coli* motility whilst the second part explores *E. coli* growth in the presence of the antimicrobial peptide pexiganan.

In Part 1 I measure the three-dimensional diffusion of non-motile cells in an active suspension of *E. coli*, using Differential Dynamic Microscopy (DDM). It is found that tracer diffusivity is enhanced linearly as a function of the bath activity, defined as the product of the number density of active bacteria and their average speed. The absolute enhancement is measured to be 1.8 ± 0.1 times smaller that that published previously in the vicinity of a surface, in agreement with theoretical predictions of enhanced diffusion by far-field advection. The diffusivities of non-motile mutants with and without paralysed flagella are enhanced to the same extent, despite a difference in hydrodynamic radii. In addition, the protocol for growing, preparing and measuring motile *E. coli* is optimised using DDM.

In Part 2 I investigate how *E. coli* density in liquid media supplemented with pexiganan influences the measurement of its Minimum Inhibitory Concentration (MIC). Growth curves, peptide bioassays and single cell microscopy are used. It is found that population density drops rapidly when pexiganan is introduced, but regrowth occurs within 24 hours at sub-MIC concentrations. The shape of the density curve is explained by peptide depletion linked to cell death and immediate recovery of cells exposed to the peptide. As expected from these findings, the system displays a substantial inoculum effect, quantified with a fitted power law. Substantial variation is seen between replicate MIC assays; an inherent property of the system which derives from the drop to small numbers of viable cells before regrowth. Finally, I show that DDM measurements of *E. coli* motility in antimicrobial peptides can provide an alternative, high-throughput density curve.

Lay summary

The thesis is presented in two parts.

Part 1 of the thesis studies the topic of bacterial swimming. When actively swimming bacteria are added to a liquid it shows interesting properties, one of which is increased mixing. Measuring such properties is important to understanding physics on the scale of a bacterium and why bacteria have evolved to swim. To measure increased mixing, this study adds inactive particles to a liquid containing swimming *E. coli*. The movement of the particles is monitored while the concentration and speed of the *E. coli* is varied.

The experiments were analysed using Differential Dynamic Microscopy (DDM), a technique not used before by research in this field. I found that in 3D, the diffusive movement of particles was enhanced, but to a lesser extent than has been seen previously next to a wall. DDM was also used to investigate the growth, preparation and measurement of swimming *E. coli*.

Part 2 of the thesis studies the topic of bacterial growth in the presence of an antimicrobial peptide. Antimicrobial peptides are an unused class of antibiotics with the potential to treat bacterial infections. Resistance to traditional antibiotics is viewed as a critical worldwide problem. Therefore, research into both new antibiotics and better tests of their action on bacteria, is topical.

This study focuses on the Minimum Inhibitory Concentration (MIC); a test that measures the minimum concentration of antibiotic required to prevent bacterial growth. Clinically, the MIC is used to compare antibiotics and determine dosage. I found that the MIC of the antimicrobial peptide pexiganan was dependent on the density of *E. coli* present at the beginning of the test. This is because, as individual bacteria die, pexiganan is depleted, allowing survivors to regrow. Therefore, the MIC of pexiganan is above the concentration required to kill a bacterium, a conclusion that could influence its clinical use. Lastly, the swimming measurements developed in Part 1 of the thesis were able to show the death and regrowth of *E. coli* in pexiganan.

Declaration

I declare that this thesis was composed by myself, that the work contained herein is my own except where explicitly stated otherwise in the text, and that this work has not been submitted for any other degree or professional qualification except as specified.

Parts of this work have been published in [1].

(*Alys Jepson, October 2014*)

Acknowledgements

Firstly I thank my supervisor Professor Wilson Poon for his guidance throughout my PhD, and my second supervisor Dr Rosalind Allen for her invaluable input towards the end. Thanks also to Jane Patterson for listening and patiently answering all of my questions.

I would like to particularly thank Dr Vincent Martinez for his practical help, his patience and his unswerving enthusiasm for any project involving DDM. A massive thanks to Dr Jana Schwarz-Linek who taught me about *E. coli* and provided me with friendly assistance in the lab. I would also like to thank Dr Angela Dawson and Dr Gary Dorken for biology advice and specifically assistance with transformations, Diarmuid Lloyd and Dr Teuta Pilizota for getting me started with single cell microscopy, Dr Mathias Reufer and Dr Rut Besseling who had helpful suggestions in the beginning and all other Tuesday morning group meeting participants for discussions on my projects over cake.

I am indebted to the other inhabitants of office 1511 over the last four years, Steve, Fred, Giulia, Matt and the printer for stimulating conversations on a range of random topics, for their understanding nods when I returned explaining how another experiment had not worked, for providing snickers bars at the right time and for never asking me to be quiet when I needed to talk. Likewise, thanks to Dario, Alex, Jay and others for sharing lab experiences.

Thank you to all my friends, in Edinburgh and further afield for their feigned or genuine interest in my science, especially to those who gave me lifts to the mountains when I needed to get away. I am thankful to my parents and sister for their continuing love and support and for rapidly proofreading sections of text at critical times.

Finally, thanks to Timmy for his encouragement throughout my PhD and for sharing Scottish adventures with me.

This work was supported by a SUPA scholarship.

Contents

List of Figures

List of Tables

Chapter 1

Introduction

Bacterial biophysics researches life in one of its simplest living forms, namely single prokaryotic cells. Bacteria have a collective terrestrial biomass greater than that of all plants and animals, and their activity influences our well-being as well as the dynamics of our planet. By researching the wide range of phenomena caused by bacteria, as well as their survival in diverse environments, we can acquire an understanding of physical processes on their length scale. This, in turn, gives an insight into bacterial behaviour. This thesis presents two biophysical studies of living bacteria, conducting measurements on bacterial activity.

Microscopy of wild-type *E. coli* allows direct identification of these cells as active entities. The cells may be moving, propelling themselves through their environment. Motility was one of the first properties to differentiate bacteria as living organisms rather than inactive colloids. On further inspection, over a longer time-scale, the cells grow and divide, increasing their numbers. Both of these activities have interested biologists for centuries, but more recently have become popular topics of research for physicists.

The thesis first focuses on bacterial motility. Physicists have studied all aspects of bacterial motility, from the propulsion mechanism itself to the swirling patterns of collective motion. Motility has also been used as a tool to create active suspensions which show different physical properties to their passive counterparts. **Part 1** of this thesis is an investigation into how the swimming activity of an *E. coli* population affects its environment; specifically the diffusion of non-motile particles.

Chapter 2 introduces previous work on the phenomenon of enhanced diffusion, which

is the increase in the diffusivity of passive tracers in an active suspension.

Chapter 3 gives an overview of Differential Dynamic Microsocopy (DDM), the method employed in this thesis to characterise enhanced diffusion and swimming *E. coli*. The set-up for experiments on enhanced diffusion and its verification are detailed.

Chapter 4 presents results on the enhanced diffusion of passive bacteria in a suspension of swimmers, discusses the study conducted and draws conclusions.

Chapter 5 bridges the two parts of the thesis. Results gained with DDM on experimental protocols for obtaining and working with motile *E. coli* in conditions relevant for the study of enhanced diffusion and antimicrobial peptides are presented.

The thesis then moves on to discussing *E. coli* growth. The dynamics of bacterial growth is one of the central themes of microbiology and is an interdisciplinary area of research spanning length and time scales from the molecular to the population level. From a medical perspective, understanding and controlling bacterial growth and death is critically important to the treatment of infections and the maintenance of a balanced microbiome. **Part 2** of the thesis is an investigation into how the environment can affect the activity of *E. coli* populations; specifically their growth and death in suspensions containing the antimicrobial peptide pexiganan. The dynamics of the system influence the Minimum Inhibitory Concentration (MIC) measured, a common estimation of the efficacy of an antibiotic.

Chapter 6 introduces antibiotic susceptibility measurements, antimicrobial peptides and previous research on pexiganan.

Chapter 7 details the methods used to monitor *E. coli* growth.

Chapter 8 presents the results of pexiganan MIC assays, time-kill curves and single cell microscopy, discusses the experimental results by simulating a simple model and finishes with a comparison to MIC results from two other agents.

Chapter 9 discusses how the results collected contribute to current research and concludes the study.

Chapter 10 links the second part of the thesis back to the first part. The motility of *E. coli* in a medium containing an antimicrobial peptide is measured with DDM.

Chapter 11 concludes and underlines the main findings of this thesis.

A publication relating to the work in Part 1, Chapter 4 is included as an appendix.

Part I

Enhanced diffusion and motility

Chapter 2

Introduction: Enhanced diffusion

2.1 Background

One of the most important and famous contributions in the history of the study of Brownian motion, or diffusion, was made by Einstein in 1905 [2], when he realised that the jiggling motion of a particle in a solution was due to thermal buffeting from the molecules making up the solution, hence proving the atomic nature of matter. Atomistic theory gave physics an additional perspective, a microscopic perspective. But the physical descriptions of the macroscopic and the microscopic worlds had very different characters. An explanation was needed of how the macroscopic description of a system was a consequence of the microscopic evolution of that system. Statistical mechanics bridged the two levels.

Today, equilibrium statistical mechanics is far advanced, some would say almost complete [3]. The focus of theoretical research has shifted to non-equilibrium systems where the role of dynamics is central. In general, processes outside equilibrium require theoretical analysis which is far from trivial and there remain many unexplained properties of non-equilibrium systems. Experimental investigations in soft matter were crucial for confirming and driving the theory behind equilibrium [3]. Now there is a need for soft matter non-equilibrium experiments to compliment the large amount of theoretical research into non-equilibrium physics [4].

This need is one reason for the interest shown in active suspensions by the soft matter community. Active suspensions are systems driven far from equilibrium, even in a steady state, by an activity inherent within them [5]. Usually the activity is the

transfer of chemical energy to mechanical energy. Many interesting properties are seen in these suspensions, such as collective motion causing large scale coherence [6]. Common natural examples of active matter displaying this property include flocks of birds, schools of fish and bacterial populations. Active suspensions are seen throughout nature, as biological systems are kept out of equilibrium by their metabolic activity [7]. Not that this area is limited to biological systems, there have been chemically engineered active colloids, driven by chemical reactions, displaying the same phenomena [4].

This study investigates a property of an active suspension, composed of non-active and active constituents, to see how it varies with 'activeness.' The property studied is the diffusion of non-active components, of the same scale as the active constituent. It is well established that their motion, due to Brownian motion and the activity in the fluid, is diffusive and can be characterized with a diffusion constant [8].

Research into this question to date has found the diffusion constant D of a passive tracer is increased linearly with density of active bacteria due to indirect or direct interactions [8–13]. The seminal paper in this field was by Wu and Libchaber (2000) [8] who were the first to study the motion of non-motile beads in a solution of *Escherichia coli*. They stated that,

> 'Beads in a bacterial bath represent a new dynamic system with much of its statistical and hydrodynamic properties yet to be explored.'

Despite a number of studies following this publication, the simplest experimental situation of bulk diffusion in a dilute swimmer suspension has yet to be explored. This study differs from previous research as it uses non-motile bacteria as the passive tracer and it measures their diffusion in the bulk of a sample, far from any wall. The study expands upon work published in the Department by Wilson *et al.* [13] using Differential Dynamic Microscopy.

2.2 Swimming *E. coli*

Escherichia coli is a gram-negative, rod shaped bacterium, $2 - 3\mu$m in length and $\sim 0.8\mu$m in width, found in nature in the human gut. It is the most widely studied bacterium and is straightforward to grow and handle. As a consequence *E. coli* is often chosen as a model microorganism in microbiological and biophysical studies. Thousands of documented *E. coli* mutants are available as well as strains which have been specifically engineered for purposes such as protein production or gene cloning.

For motility work K-12 derivative strains are frequently used [14], and their motility is well understood [15].

Motility is one of the most visually striking phenotypes of prokaryotes. It distinguished them as living entities in the first observation of microorganisms by van Leeuwenhoek in the early 1800s [16]. Bacterial swimming speeds range from 1μm/s (*e.g. Halobacterium halobium* [17]) to 1000μm/s (*e.g. Candidatus Ovobacter propellens* [18]) which are physical limits imposed by the diffusion of nutrients and the rotational speed of the motor [19], but commonly used experimental *E. coli* swim at the order of $10-20\mu$m/s. This section briefly introduces the constraints imposed by the hydrodynamics of swimming at the length scale of a bacterium, before discussing how the motility apparatus evolved by *E. coli* meets these constraints. A popular early publication on how an *E. coli* generates thrust to propel the cell body is 'Life at Low Reynolds number' by Purcell (1977) [20].

The Navier-Stokes equation describes the application of Newton's second law to a Newtonian fluid element subject to forces from the pressure (p) gradient, the viscous stress and external agents (f),

$$\rho(\partial v/\partial t + v.\nabla v) = \nabla p + \eta\nabla^2 v + f \tag{2.1}$$

where v is the flow velocity, η is the fluid viscosity and ρ is the fluid density. For a system of length scale L and speed U, the ratio of the inertial term $\rho v.\nabla v$ (scales as $\rho U^2/L$) to the viscous term $\eta\nabla^2 v$ (scales as $\eta U/L^2$) gives the dimensionless Reynolds number [14, 21],

$$Re = \rho UL/\eta. \tag{2.2}$$

In the case of a swimming *E. coli* in water, traveling at a speed of $U \sim 10\mu$m/s, the Re is calculated to be $\sim 10^{-5} << 1$. Inertia plays little to no role and the inertial terms in the Navier-Stokes equation can be neglected, leaving the linear Stokes equation,

$$0 = \nabla p + \eta\nabla^2 v + f. \tag{2.3}$$

A Stokes flow is instantaneous, laminar and time-reversible. Whereas a human swimming in water coasts for meters when they stop (Re $\sim 10^4$, turbulent regime, dominated by inertia), an *E. coli* dominated by viscosity coasts for less than 1Å when it stops swimming.

The absence of inertia for a swimming bacterium has consequences for their chosen mechanisms of motility. The time-reversible nature of a stokes flow results in a situation where reversible movements do not generate propulsion. Purcell [20] used the example of a scallop to illustrate this idea, often now known as the 'scallop theorem'. A symmetric scallop opening and shutting at Re $<<$ 1 simply moves back and forth, gaining no net displacement.

Numerous non-reciprocal, cyclic motions have been evolved to achieve swimming at low Reynolds number [22]. These include the cilia of the algae *Chlamydomonas* which are moved back and forth in a breast stroke motion [23] and the wave propagating flagellum of a *Spermatozoa* [24]. *E. coli* possess multiple $(5-20)$ flagella, 20nm in diameter and up to 10μm in length, distributed randomly around the cell body. Although well studied now, before the 1970s it was unknown how these filaments generated propulsion, with some researchers arguing that they were waved and others arguing that a traveling wave was propagated along their length [21]. Then Berg and Anderson (1973) [25] proposed that the flagella filaments were rotated at their base by a molecular motor, confirmed experimentally by Silverman and Simon (1974) [26] by tethering the hook of a de-flagellated mutant to a glass slip. They saw the cell body rotate at up to 20 revolutions per second, providing evidence of the first rotary motor to have been seen in a living creature.

The schematic in Figure 2.1(a) shows a peritrichous *E. coli* bacterium with its flagella bundled into a rotating helix at the rear, propelling the cell body forwards [27]. For simplicity, the flagella bundle is usually modeled as a single propelling helix. Figures 2.1(b+c) illustrate the thrust generating mechanism employed. Figure 2.1(b) displays a small cylindrical section of the filament moving at velocity v in the direction shown by the arrow. The force f needed to drag the rod through fluid at this velocity is represented alongside. Due to the asymmetry of a cylinder, causing there to be more drag perpendicular to the cylindrical axis than along it, f is not along the direction of v. Propulsion relies on this fact, as when multiple cylindrical sections are added together to form a rigid helix (Figure 2.1(c)), rotated at an angular velocity ω, a net force acting in the negative z direction must be applied to keep the rotating helix in place. A rotating asymmetric propeller, in the absence of an applied force, must translate.

At the base of each flagellum there is a flexible hook connecting it to the bacterial flagella motor, an assembly which rotates the flagellum. The bacterial flagella motor is a rotary nano-machine, powered by a flux of H^+ or Na^+ ions across the cytoplasmic membrane due to an electrochemical gradient called the proton/sodium-motive force

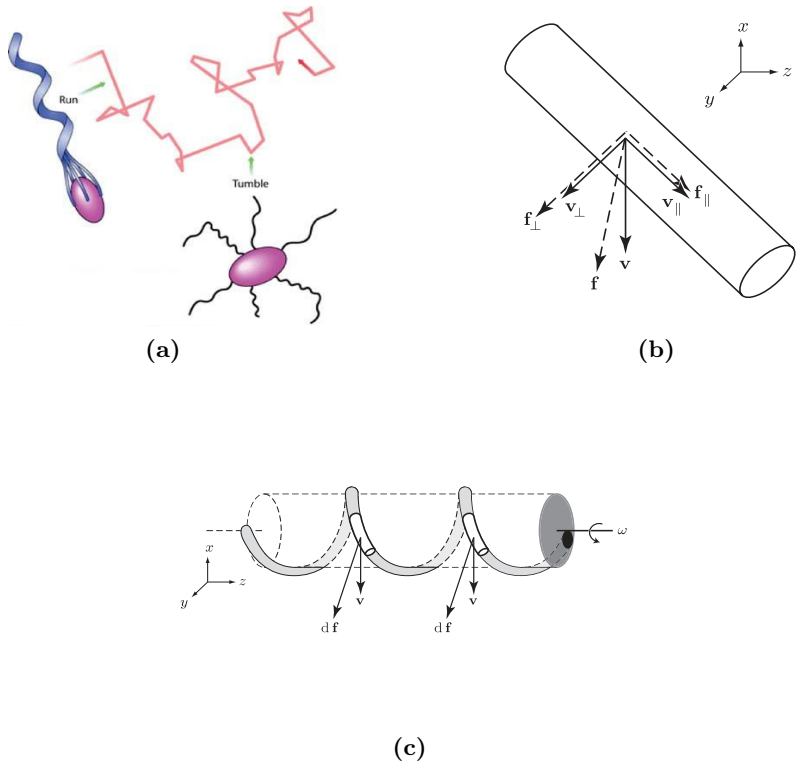

Figure 2.1 Schematics of propulsion from (a) [27] and (b+c) [21]. (a) Swimming behavior of *E. coli* in unstimulated chemical conditions. During a run the flagella are bundled whereas while tumbling they are distributed randomly around the body. (b) Cylindrical rod at low Re moving with velocity v due to a force f. In the diagram the velocity component along the axis of the rod is equal to that perpendicular to it, but the resolved forces must be different to account for the difference in drag coefficient. (c) A rotating rigid helix demonstrating the propulsion mechanism of a flagella bundle. Two small sections have been singled out for consideration. Discussed in text.

(PMF/SMF). The outside of the cell is more positively charged and at a lower pH than the inside, leading to a physiological PMF of $150-200$mV [28]. The motor is composed of a 45nm diameter rotor, and up to 10 stators anchored in the cytoplasmic membrane. Each stator acts independently and additively with respect to the others and passes 37 ± 2 ions per revolution [29]. Rotation speeds of up to 120Hz have been measured for the H^+ driven motor, but Na^+ driven motors are faster; the chimeric motor in *E. coli* has been measured to rotate at 900Hz. Figure 2.2 shows both a schematic and an electron micro-graph of the H^+ driven *E. coli* flagella motor. For more details see [28].

Self-propelled microorganisms are force and torque free, as any force/torque exerted on fluid is balanced exactly by fluid drag. Thus the cell body is required to rotate in the opposite direction to the flagella at an angular velocity Ω where,

$$\Omega = \omega - \omega_m = |\omega| + |\omega_m| \tag{2.4}$$

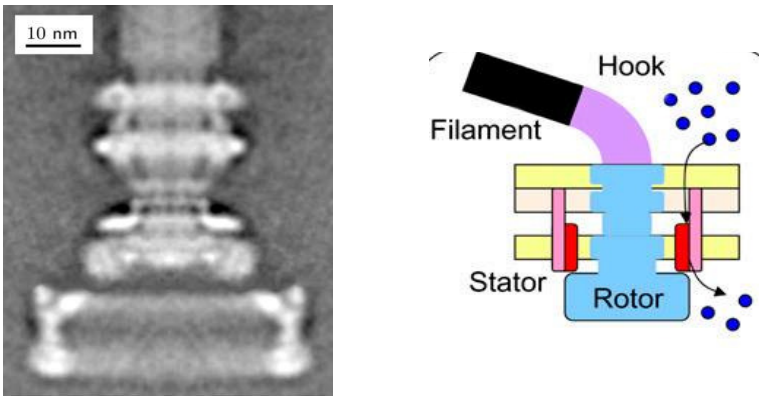

(a) **(b)**

Figure 2.2 (a) An average of 100 electron micrograph images of the flagella motor assembly published by Thomas *et al.* (1998) [30] and reproduced from [21]. (b) Schematic of the flagella motor from [29]. The rotor is sitting on the inside of the cell in the cytoplasm and the yellow bands represent the cytoplasmic membrane and the outer membrane. Ions represented by blue dots move from the outside to the inside of the cell.

in the stationary frame of the body (ω_m is the motor speed). As required by the linearity of the Stokes equation, the translational and angular speeds of the body and flagella are directly proportional to the forces and torques they are subject to. The constants of proportionality, defining the propulsion matrix of a bacterium [20] have been measured for *E. coli* by Chaddhopadhyay *et al.* [31]. Algebraic manipulation of the equations relating v, Ω and ω to the drag forces and torques on the cell body and flagellum leads to the result that the propulsion speed is directly proportional to the motor speed ω_m, with a constant of proportionality determined by cellular geometry. Measurements have shown that, within a wide range, ω_m is also proportional to the PMF [32]. Therefore, changes in speed are an indication of changes in the PMF of the cell. This is assuming that the cell is not actively regulating its speed in response to changing conditions by generating cyclic di-GMP [33, 34].

By counterclockwise rotation of the motors (viewed from the end of the flagellum towards the cell body), the individual flagella filaments bundle together at the rear of the cell body, and propel the cell forward. The dynamics of bundling has been studied for some time [35] and is the subject of continuing research. Wild-type *E. coli* change their direction of propulsion randomly each ~ 1 second, facilitated by the ability of their motors to change from counterclockwise rotation to clockwise rotation. When one or more of the motors reverse direction, usually, but not always, the handedness of the filament is switched [36] from left-handed to a right-handed helix with half the previous pitch [37]. This causes the associated flagellum to un-bundle, leading to cell

reorientation [38]. A typical tumble lasts 0.1 seconds. The overall motion described in the long-time limit is a random walk with a step time on the order of a second. *E. coli* perform chemotaxis, the movement up a chemical gradient, by sensing a chemical species and lengthening the steps or runs in a given direction by reducing the probability of a tumble. Their random walk becomes biased in the direction of a chemo-attractant [35], widely believed to be one of the primary selective advantages of motility [14, 39].

Initially it was thought that an additional reason for flagella or cilia motility was to stir the local environment of the cell, increasing nutrient uptake compared to waiting for delivery by passive diffusion. Simple calculations [21] show that cilia would have to sweep at above 1000μm/s for this argument to be plausible, which is not witnessed. That said, recent work on enhanced diffusion [40] implies that the run length of an *E. coli* is optimised to encourage the movement of passive particles, potentially sources of nutrients or oxygen. Although unlikely that this was the primary evolutionary drive in the development of motility, it may have provided an additional benefit.

2.3 Brownian motion and diffusion

Traditionally, Brownian motion is considered to have been discovered by Robert Brown in 1827 [41] but there are other earlier examples of literature which mention observations of the effect, for example in a Roman poem (60 BC) which describes the motion of dust particles [42]. Brown was a botanist studying pollen grains suspended in water under a microscope when he saw small particles displaying a jiggling motion. The mathematical description of what Brown observed was attempted a couple of times before the end of the 19^{th} century but a physical description of Brownian motion was first published almost 80 years after Brown's paper. Sutherland and Einstein both completed their mathematical explanation in the same year (1905), Sutherland having presented his at a conference the year before [2, 43]. As already discussed, Einstein used Brownian motion as an indirect proof of the existence of atomic matter. Perrin (1920) [44] went on to use photographic imaging and microscopy to experimentally study Brownian motion, setting the scene for the type of experiments done on the study of enhanced diffusion, presented in this thesis.

The displacement probability distribution of a spherical particle undergoing Brownian

motion is a Gaussian [45]:

$$P(\Delta R(\tau)) = \left\{ \frac{3}{2\pi\langle \Delta R^2(\tau)\rangle} \right\}^{3/2} \exp^{-\frac{3\Delta R^2(\tau)}{2\langle \Delta R^2(\tau)\rangle}}, \tag{2.5}$$

where ΔR is the particle's three dimensional displacement in time τ. The particles mean squared displacement in time τ is,

$$\langle \Delta R^2(\tau)\rangle = 6D_0\tau. \tag{2.6}$$

The diffusion constant due to Brownian motion D_0 is given by the Stokes-Einstein equation,

$$D_0 = \frac{k_B T}{6\pi\eta r}, \tag{2.7}$$

where k_B is Boltzmann's constant, η is the viscosity of the liquid, T is the temperature (K) and r is the radius of the particle.

Given that the mathematical description of Brownian motion is complete, research today focuses on how nature has evolved to use Brownian motion and also how the movement of microscopic particles in non-equilibrium situations differs from Brownian motion. For example, transport within the cell, movement across membranes and bacterial metabolism all depend heavily on diffusion [21].

Diffusion refers to the process of particles moving from regions of higher to lower chemical potential (commonly thought of in terms of concentration) due to the thermal kicks provided by the solvent molecules (Brownian motion). Any stochastic displacement process which causes the mean squared displacement ($\langle \Delta R^2(\tau)\rangle$) to go linearly with time ($\langle \Delta R^2(\tau)\rangle \propto \tau$) can be characterized with an effective diffusion constant D_{eff}, which will be referred to as D. For example, the 'run and tumble' motion of *E. coli*, a random walk with a step length of ~ 10 μm, can be assigned a D. By convention, in this field of study, 'passive diffusion' refers to Brownian motion, and 'enhanced diffusion' refers to the motion of particles whose $\langle \Delta R^2(\tau)\rangle$ is linear with time, but whose D is larger than that predicted by the Stokes-Einstein equation.

Microscopic particles such as *E. coli* undergo rotational and translational diffusion. Tavaddod *et al.* [46] published work on the passive translational and rotational diffusion coefficients of flagellated and de-flagellated non-motile *E. coli*, which were 3.2μm in

length and 0.9μm in width and had external flagella filaments $\sim$10μm long. They report that the translational and rotational coefficients were reduced by a factor of $\sim 1.4 - 1.5$ and ~ 3.5 respectively, by the presence of flagella. The inactive flagella increase the effective hydrodynamic radius approximately 1.5 times for their mutants of *E. coli* K12. Changing the strain could change the magnitude of this factor as it would be sensitive to the length and number of the flagella, their geometry and their positions on the body. The flexibility of the flagella and the details of the hooks which attach them to the body could also affect the result.

The study presented in this thesis also investigates the translational diffusion of flagellated and de-flagellated *E. coli*, but instead of measuring Brownian diffusion constants only, the cells are placed in active suspensions.

2.4 Active suspensions and the self-propulsion of *E. coli*

As already mentioned, active suspensions contain active matter which is able to use energy from its surroundings to produce systematic motion [5]. The resulting time evolution of the system breaks time inversion symmetry which would be forbidden in equilibrated environments [47]. Physicists are interested in all aspects of active suspensions such as the mechanisms driving propulsion of active matter [48] and exclusion processes [49], but in particular in the properties arising as a consequence of active processes [5]. For example, the regime of collective behavior or 'flocking' can be regarded as an ordered phase of matter requiring statistical mechanics and condensed matter physics to explain it.

There is much theoretical work on the properties of active matter in all environments, but especially on active fluids [50], activated by microscopic particles rather than macroscopic fish, perhaps because this relates to experiments in soft matter physics on these systems. Microscopic suspensions are appealing model systems as energy transfer to the fluid is homogeneous and parameters such as density and swimming speed can be experimentally controlled. The active particles are also large enough that it is still possible to directly observe them.

Consequently, the experimental side of active fluids is widely studied using both motile microorganisms and synthetic particles. Chemically engineered active particles have been used [51] less frequently than living cells for the purpose of studying the non-equilibrium properties of these suspensions. There is still considerable work going into their design [52] and their method of mobility by chemical reactions releases air-

bubbles, affecting the properties of a suspension. This can be a problem depending on the question being asked. Furthermore, besides being a playground for non-equilibrium physics, applying physics to suspensions of living matter rather than synthetic matter, addresses biological questions *e.g.* biofilm formation [47]. Commonly, *E. coli* are used as their motility is well understood [25], although other bacteria and algae have also been used. Suspensions containing bacteria or algae are more applicable to this work than synthetic motile colloids so further discussion of active suspensions assumes living, active components.

Suspensions of microorganisms exhibit the same regime of collective motion as macroscopic active matter. Spatial and temporal patterns much larger than the size of an individual bacterium have been seen in bacterial cultures and have been called swirls and jets [53]. A theoretical description of their formation as a non-equilibrium phase transition is the focus of substantial theoretical research [54]. Other properties of the suspension studied theoretically and experimentally have been enhanced mixing and transport, changes in the viscosity [55] and rheological properties [50].

The property studied here, the enhanced diffusion of passive particles in the suspension, relates to mixing and transport within the fluid. From a physical point of view, this property is a way of watching the mechanism of momentum transfer to the fluid by providing a tracer. Momentum transfer by bacteria has been used to drive man-made micro-motors [47] and experiments have been done with *Bacillus subtilis* to power gears with asymmetric teeth [56]. From a biological point of view, understanding enhanced diffusion in an active suspension may be key to understanding the methods evolved by microorganisms to reach nutrients [8]. There is evidence that marine bacteria motility may be linked to the recycling of organic debris and mixing in the oceans [9, 57]. From a technical point of view, mixing and transport in microfluidic devices, used regularly in microorganism experiments, are heavily dependent on diffusion [10].

There are two classes of active fluid, extensile and contractile. A suspension of *E. coli* bacteria is extensile whilst a suspension of *Chlamydomonas* algae is contractile, due to fundamental differences in the way they swim [50]. This distinction is related to the fluid flow around the swimming microorganism and outside of theoretical work on active fluids the two types of swimmers are called 'pushers' and 'pullers'. A pusher pushes fluid away from it which moves towards its midriff (*e.g. E. coli*) while a puller (*e.g. Chlamydomonas*) does the opposite. It has been predicted that extensile and contractile fluids display very different rheological properties [50] and large scale fluid transport [9] to one another. Pullers are not expected to show the large scale coherence seen in suspensions of pushers at high densities [9], as they do not align spontaneously

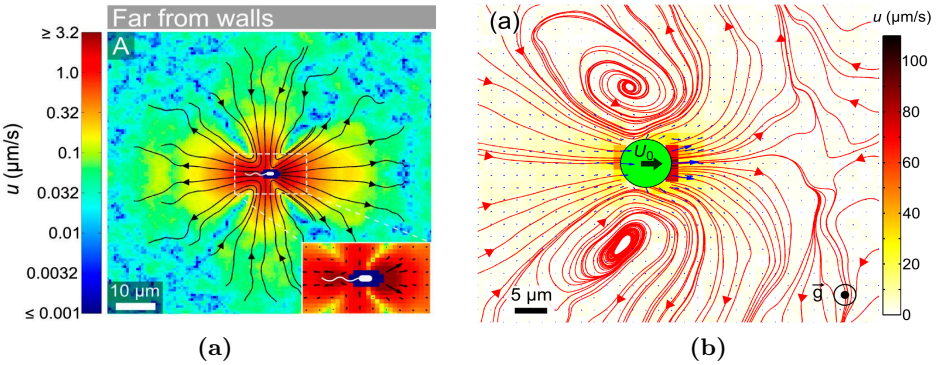

Figure 2.3 Average flow fields of single cells published in (a) [58] and (b) [59]. (a) The average flow field created by a single swimming *E. coli* 50 μm from a surface. Flow speeds are represented by a logarithmic colour scheme and direction of flow is indicated by arrows. The inset highlights the flow asymmetry close to the cell body. (b) The average flow-field created by a single swimming *C. reinhardtii*. Streamlines are shown in red and velocity vectors in blue. Flow speeds are indicated by a colour scheme.

with their neighbors at high densities.

In the regime of Stokes flow, the 'stokeslet' is the flow resulting from a passive point particle being pulled through a fluid by a single force while a 'stresslet' is the flow field from two equal and opposite forces (a force dipole). If r is the distance from the moving particle, the effect of a stokeslet on the surrounding fluid reaches further, as it decays as $1/r$, whereas the stresslet decays as $1/r^2$. For large microorganisms, $\sim$200μm in radius, the stokeslet flow due to gravity must be considered, as well as the forces applied to the fluid due to motility. However, smaller extensile or contractile swimmers are commonly modeled by a single force dipole, of positive or negative sign respectively, with thrust and drag forces displaced a distance apart, roughly the size of the swimmer [59].

Experimental measurements to investigate the validity of these models have shown that there is a regime close to the swimmer which the stresslet does not model well. The flow field around swimming *Chlamydomonas* [59] and *E. coli* [58] were measured experimentally by Drescher *et al.* by simultaneously imaging the swimming cells and fluorescent microspheres in the fluid around them (Figure 2.3). They found that for the extensile *Chlamydomonas* the stresslet model fits the flow field for $r > 7R$ ($R = 5\mu$m in this case), but closer to the cell the flow field was better represented by a triplet of force singularities, with two placed either side of the body where the flagella pull back and one representing the drag. Although the force dipole describes the flow field of a motile *E. coli* much better than that of a *Chlamydomonas*, it overestimates the flow at distances up to 6μm from the bacterium. When the model is fitted to the experimentally measured flow field the distance l between the point forces of magnitude F= 0.42pN

was $l = 1.9\mu$m. Interestingly, the point of drag acts significantly behind the cell body.

2.5 Enhanced diffusion

As already said, in the context of this work, enhanced diffusion is when passive micron-sized particles or bacteria display motion characterized by diffusion coefficients larger than those predicted for their size and temperature by the Stokes-Einstein equation. Experiments investigating enhanced diffusion place micron-sized beads in an active suspensions. When a passive particle encounters the flow field or comes into direct contact with a self-propelled microorganism, its motion is increased.

Accordingly, in dilute enough systems where the resolution of individual encounters is possible there are two separate effects contributing to the passive particle motion, Brownian motion and interactions/encounters. It is popular to consider the suspension of swimming bacteria or algae as an effective thermal bath, randomly kicking the passive particles exactly like the molecules in Brownian motion, but on a different scale [8].

2.5.1 Experimental work

The framework for studying and characterizing enhanced diffusion was presented in a pioneering paper by Wu and Libchaber (2000) [8]. They imaged and tracked the movements of 10μm and 4.5μm polystyrene beads in a bath of fluorescent *E. coli*, confined to a freely suspended soap film. The depth of the film was measured to be roughly the diameter of the particles, creating a quasi-2D environment. A previous publication by the authors had studied the passive motion of the beads in an identical film and discovered it to be diffusive with a Brownian diffusion coefficient (D_0) of the same order of magnitude as the bulk value [60].

When motile *E. coli* were incorporated into the film, the mean squared displacement of the tracer beads showed two additional features to the passive case (Figure 2.4). Firstly, at times shorter than a characteristic time $t_c \sim$1 seconds the beads underwent super-diffusion; their mean squared displacement was proportional to t^α, with $\alpha = 1.5 - 2$. Secondly, at longer times the behavior of the beads returned to diffusive behavior ($\alpha = 1$), with an effective diffusion coefficient that was significantly above that predicted by the Stokes-Einstein equation. The concentration of bacteria in the film was varied up to 5.4×10^{10} cells/ml, to probe the effect of bacterial density on these two features for the 10μm beads only. The researchers stated that by eye, the bacteria swam smoothly

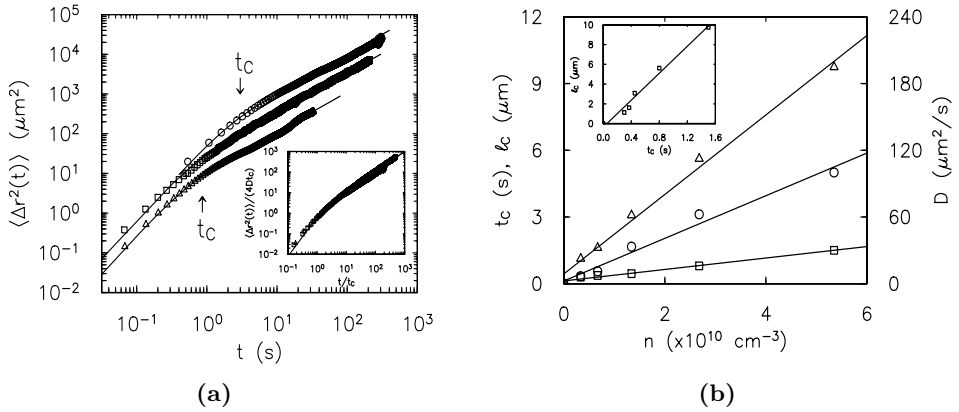

(a) **(b)**

Figure 2.4 The enhanced diffusion of 10μm beads, from [8]. (a) The mean squared displacement of beads in a concentration of (triangles) 0.67, (squares) 1.34 and (circles) 5.35 $\times$ 10^{10} cell/ml. The crossover between superdiffusion and diffusion t_c increases as concentration increases. The inset shows scaling. (b) The circles show the effect of bacterial concentration on D.

at the lower densities studied, while at higher densities, collisions and hydrodynamics randomized their directions. Swirls and jets, observed when their concentrations were high, indicated that large-scale collective motion was taking place.

Super-diffusive regime

Wu and Libchaber [8] showed that t_c increased linearly with bacterial concentration. Their explanation for this regime was that there were ballistic-like segments of particle motion due to bacterial bombardment. They constructed a theoretical Langevin-type equation to model the dynamic fluctuations of the beads. However, their theoretical explanation of the short-time behavior has since been challenged by Gregoire *et al.* [61], who reproduced the super-diffusive rather than ballistic nature of the trajectories measured by modeling the collective dynamics of swimming bacteria with a Vicsek model.

The super-diffusive regime was also the subject of a later study by Valeriani *et al.* [6]. These researchers compared their two-dimensional vectorial Vicsek model with experiments on 4μm polystyrene beads trapped between two treated glass coverslips 5-7μm apart in a suspension of *Bacillus subtilis*. At both of the densities studied, 0.03 and 0.09 surface density (corresponding to 1.25×10^9 and 3.75×10^9 cells/ml), collective behavior was observed. They argue that their experimental set-up was preferable to that of Wu and Libchaber as they use a thinner sample geometry and larger bacteria, preventing tumbling events and ensuring less movement in the third dimension. Additionally, unlike in the soap film, there was no evaporation and no

chemical repellant, which could have affected swimming. Their findings mirrored the earlier measurements; super-diffusion at early times (although lower values for α were obtained) and an increase of t_c with concentration, both qualitatively predicted by their model. An important conclusion of their theoretical work was that steric collisions play an important role in the collective behavior of the swimmers, as well as hydrodynamic interactions.

Diffusive regime

In addition to studying the super-diffusive regime, both of the experiments mentioned above [6, 8] measured the long-time diffusion coefficient D to be significantly enhanced with respect to the passive case. D was enhanced $\sim 1000\times$ by 5.4×10^{10} *E. coli*/ml and $\sim 100\times$ by 3.75×10^{9} *Bacillus*/ml. Wu and Libchaber found a linear increase in D with bacterial concentration ($0.1 - 10$ volume %) and presented the appealing picture of a higher concentration representing a higher effective temperature. No attempt was made to measure the proportion of motile bacteria in the suspension, or to quantify the different swimming behaviors observed at different concentrations.

In summary, further work on enhanced diffusion in microbial suspensions has adapted the experimental situation and has broadened the applicability of the findings. One primary focus has been to study lower concentrations of swimmers ($0.001 - 0.1\%$) [13, 62, 63]. As is the case in the study presented here, researchers were interested in simplifying the experimental situation by removing interactions between independent swimmers and eradicating collective motion. Experiments which have maintained a 2D nature to facilitate particle tracking have investigated the implications of confinement [62, 63]. Novel methods and different micro-organisms have been used to extend the study to 3D [11–13]. Improved image analysis has enabled the quantification of the bath activity, highlighting the importance of the bacterial swimming speed as well as density [62]. The remainder of this section provides the details of these contributions to the field.

The most relevant recent experimental work, both to the original study and to that presented in this thesis, was published by Miño *et al.* in 2010 and 2012 [62, 63]. They monitored latex tracer beads in suspensions of wild-type *E. coli*. The objective of the researchers was to measure the effective long time diffusion constant (D) of the beads in varying fluid activity, controlled by the density and speed of motile *E. coli*. Although densities of *E. coli* as high as 10^{10} cell/ml were used, no collective motion was observed. For the corresponding bacterial concentration, the probability of direct collision between swimmers is much lower in a 3D sample chamber than in a 2D film

or chamber.

Although their suspensions were not confined to 2D, and the majority of measurements were made inside a chamber of height h=110μm, the researchers only considered the bacterial and tracer motion in the vicinity of the glass surface (within 5μm). Wild-type *E. coli* are known to dwell at surfaces due to hydrodynamic attraction, although the effect is less pronounced than for smooth swimmers. There is evidence that they smooth out their run and tumble motion to preferentially swim in large clockwise circles as a consequence of the torque-free condition [64, 65]. The distance of the tracer beads from the glass surface was not measured, but was inferred to be distributed according to the Boltzmann factor from comparison of their Brownian diffusion coefficient with that expected in the bulk. Given the small number of beads monitored in each field of view ($\sim$ 10), the lack of measured information on distance from and possible interactions with the surface, is a disadvantage to these experiments.

In their first set of experiments [62], as well as adding either 1μm or 2μm tracer particles, the researchers added Percoll to the active suspension to prevent the sedimentation of bacteria. Cover slips were treated with Poly-Vinyl-Pyrrolidone (PVP) (molecular weight unstated), which was also mixed at low concentrations (0.005%) into the media, to prevent bacteria sticking to the glass. Uncleaned PVP contains unidentified small molecules, able to increase the motility of *E. coli* if added at concentrations $\geq$ 0.05% [66]. Although the concentrations used were far below this in the bulk, PVP concentrations in the vicinity of the glass were not quantified.

Miño *et al.* noticed that not all of the bacteria displayed ballistic motion, a significant proportion were diffusive. For a given preparation protocol they were unable to control the ratio of inactive to active cells in the sample [67]. They postulate that the motility behavior is dependent on the micro-environment (although presumably this should not vary between cells in their sample) and the position of the cell in the cell cycle. To measure the fraction of ballistic trajectories, a protocol was developed to separate their trajectories (further discussed in Chapter 3). In this way they were able to precisely measure the activity in the fluid, as well as the tracer motion, rather than simply having knowledge of the bacterial concentration in the chamber, as was the case for previous experiments.

Rather than only varying the concentration of bacteria, their average speed and motile fraction were also altered. Cells were grown to late exponential phase in LB and then washed twice by centrifugation into a motility buffer, and left for an hour. In some cases the smallest, 'baby cells' (assumed to be at an early stage of the cell cycle) were

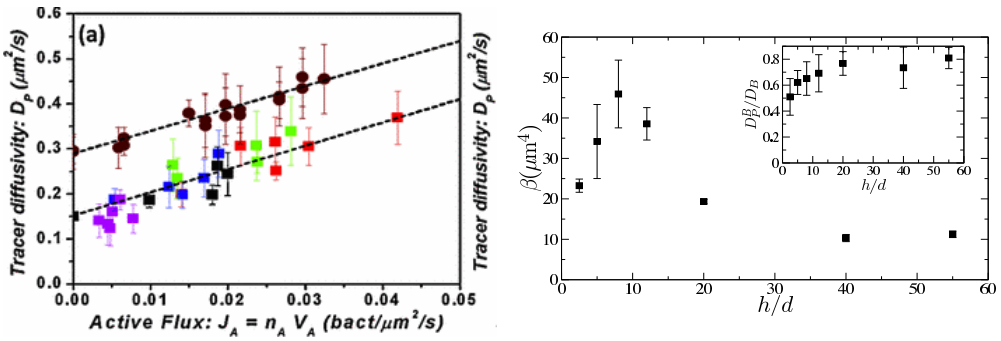

(a) (b)

Figure 2.5 Figures published by Miño and co-workers in [62] and [63] respectively. (a) Enhanced diffusion scaling with J_A for tracers size 1μm (circles) and 2μm (squares) in unbouyant conditions (density matched). Each colour describes a different experimental protocol, not described here, leading to different swimmer speeds. (b) Effect of confinement (h) on β, where d is the radius of the tracer. Inset shows effect of confinement on the Brownian diffusion coefficient.

then sorted by centrifugation from this population, as they exhibited higher speeds than the remainder of the population. These cells were used alone, or mixed with mature populations (cells assumed to be at a late stage of their cell cycle), to explore a range of activities. The weakness of this approach was that the average length of bacteria varied from 1.12 to 2.5μm in different samples. An intermediate fluid activity contained a wide distribution of both cell lengths and swimming speeds, and hence variety in the swimmer flow fields.

To characterise the bacterial motion, 20 second movies at 20 frames per second (fps) were used. To characterise the motion of the beads, 300 second movies at 1 fps were used. No verification that the speed of the bacteria and the bacterial density next to the wall does not change in over 5 minutes of data acquisition is presented.

The researchers found that for both sizes of tracer particle used, the diffusivity scaled linearly with a quantity named the activity flux $J_A = n_A v$, defined as the number density of active bacteria n_A multiplied with their mean velocity v (Figure 2.5(a)). This is a generalisation of the concentration scaling that was found previously; as this was the first instance of v being varied. The equation of the linear curve seen, where D_0 is the Brownian diffusion constant of the latex beads, was;

$$D = D_0 + \beta J_A. \tag{2.8}$$

Mino *et al.* proposed that the prefactor β which is a length to the fourth power, is

physically significant, and found $\beta = 5\mu\text{m}^4$ for unconfined buoyant conditions (Percoll added) [63]. The prefactor β was insensitive to probe diameter, but was sensitive to the nature of the active component. When self-propelled Au-Pt rods were used instead of *E. coli*, β rose to $13\mu\text{m}^4$.

In the second publication by Mino *et al.* in 2012 [63], the researchers improved on the speed variation protocol by using cells of a similar maturity and size in each sample, whilst changing the pH. By varying the pH from 5 to 9 they obtained average speeds from 4μm/s to 20μm/s, a factor of 5 different, rather than the factor of 2 obtained with their previous protocol. However, they present a figure indicating that at a pH of 6.9 average speeds ranging from $8.5 - 16\mu$m/s are obtained, with large standard deviations associated, suggesting that their protocol for growing motile cells may not be as reproducible as ideal. They were unable to density match with Percoll whilst changing the pH as viscosity was also affected. As a consequence, after sample preparation they had to wait 'some minutes' for the beads to sediment and the distribution of bacteria to stabilise, before beginning acquisition.

A tracer particle of diameter 2μm was added to all suspensions. By varying pH and density, β was measured to be $13\mu\text{m}^4$, significantly higher than when density matched. The reason for this difference is not fully explained, but as the average height of the tracers is less, surface effects would be expected to play a greater role. However, the parallel drag correction factor for the Brownian diffusion coefficient was measured to be the same in buoyant and non-buoyant conditions.

The researchers went on to vary the sample confinement at a single pH by lowering the upper cover-slip to reduce the height of the chamber (Figure 2.5(b)). At each height h, the density of bacteria was varied to obtain a measurement of β. No effect was seen until h was reduced to $\sim 20\mu$m, below which β increased to a peak value at $h = 8\mu$m, $8\times$ that of β measured in an unconfined ($h = 110\mu$m) chamber. Further confinement reduced β once more. The researchers do not comment on whether the narrowest confinements affect the swimming behavior of cells. For example, it is possible that tumbles were not possible at $h < 5\mu$m. Although these experiments indicate that diffusion would be enhanced less in 3D, where there is no confinement, it does not predict by how much, as the physics of the enhancement could be different next to a wall than in bulk fluid.

Although there have been 3D measurements of enhanced diffusion in suspensions of swimmers, studies have either been limited [12], or have been undertaken in sufficiently different situations [10, 11] to prevent direct comparison with the work of Wu and Libchaber or Miño *et al.* For example, a rheological study of a 3D bacterial suspension

noted enhanced diffusion but did not fully investigate it [12]. The exception is the preliminary 3D data shown in a publication by Wilson *et al.* [13], which is the work this project has continued.

Leptos *et al.* [11] tracked a 3D suspension of the algae *Chlamydomonas reinhardtii*, 10μm in diameter, swimming with an extensile breaststroke motion at $\sim 100\mu$m/s. The cell concentrations used ($10^6 - 10^7$ cell/ml) were dilute and no collective motion was observed. Speeds measured were in the imaging plane, so although the cells were moving in 3D, any motion in the direction perpendicular to the imaging plane was disregarded. The researchers mention that the three dimensional speed distribution would differ from the speed distribution presented.

Tracer particles (2μm diameter) showed displacement probability distribution functions composed of a Gaussian core and exponential tails. As swimmer concentration increased, the core broadened, indicating a linearly enhanced diffusion coefficient which reached $\sim 6\times$ its Brownian value at 2.2 volume %. Individual particle trajectories showed unclosed loops as an algae passed, clearly indicating the importance of hydrodynamic interactions over collisions in this system. Given the fundamental differences in the way *E. coli* and algae swim, their different sizes and the fact that algae have time-dependent strokes, these results are not directly comparable with bacterial studies. Yet recent theoretical work on the hydrodynamic descriptions of enhanced diffusion, presented in the next section, offer the hope of quantitative comparisons in the future.

Finally, instead of using tracer particles whose size is on the order of the active micro-organisms, Kim and Breuer [10] measured the diffusion coefficient of the high molecular weight molecule Dextran ($M_w = 7.7 \times 10^4$, $R_g = 7.7$nm). Unlike in all of the other experiments mentioned, D was measured by imaging a PDMS Y-shaped microchannel which forms two streams that mix due to diffusion. By measuring the intensity profile across the 40μm channel at various distances from the mixing point, the diffusion coefficient of fluorescent Dextran in one of the streams could be measured. Motile wild-type and constantly tumbling *E. coli* were introduced into the fluorescent stream and the changes in D recorded. Both caused concentration dependent enhanced diffusion, although the wild-type caused roughly twice that of the tumblers. As a control they additionally added non-motile bacteria, which were also seen to enhance the diffusion of Dextran, but to a lesser extent than the motile cells. They postulate that this is caused by the Brownian motion of the inactive cells and their flagella. Evidently this is a different experimental situation, with different mechanisms of enhancement than when the tracers are larger, as adding a dilute non-active component would not enhance

the diffusion of μm scale tracer beads.

2.5.2 Calculations

Following the experimental findings by Miño *et al.* [62, 63] (and in one case the experimental findings reported in this thesis [1]), there have been three main theoretical calculations of β, considering swimmer-tracer hydrodynamic interactions. Far-reaching hydrodynamics are more relevant to dilute, active suspensions than direct collisions (as were studied in [6] for a dense suspension in 2D), justified in [40].

There are a number of assumptions and results which are common to all of the theoretical work covered in this section. Swimmers are assumed to be independent *i.e.* all work is modelling a dilute system in the absence of collective motion. They are also assumed to be identical and isotropic in their orientation and motion, and to interact with tracers in statistically independent events. Tracers are assumed to move at the velocity of the fluid at their centers, identically to point-like particles, as experiments have shown that enhanced diffusion does not rely on their diameter [62]. All calculations have reproduced the super-diffusive regime discovered by Wu and Libchaber and the dependence of the long-time diffusion coefficient on activity flux rather than concentration, discovered by Miño *et al.* [62, 63].

Calculations of β for *E. coli* suspensions were preceded by other publications on the theory of tracer movement. Dunkel *et al.* [68] demonstrated that swimmers induce loop-like tracer trajectories, which survive the effect of Brownian motion for typical experimental conditions. Of more direct relevance here is a publication of kinetic theory analysis of swimmer-tracer hydrodynamic interactions developed by Lin *et al.* [69] for contractile squirmers (spheres in Stokes flow which move their surface at a steady tangential velocity, considered first by Lighthill (1952) [70]). The framework Lin *et al.* presented is briefly introduced before the similarities and differences between each of the three pusher (extensile) calculations are described.

A diagram defining the parameters influencing an interaction event is reproduced in Figure 2.6 (see [69] for details). Two impact parameters are needed; a the initial perpendicular distance to the particle, and b the distance from the start of the trajectory to the point of closest approach. The motion of the particle is determined by a series of additive kicks from passing squirmers, each of which moves the particle by $\Delta(a,b)$. Squirmers change direction randomly after a path length λ, occasionally trapping a tracer in their wake and transporting it a path-length before it is released.

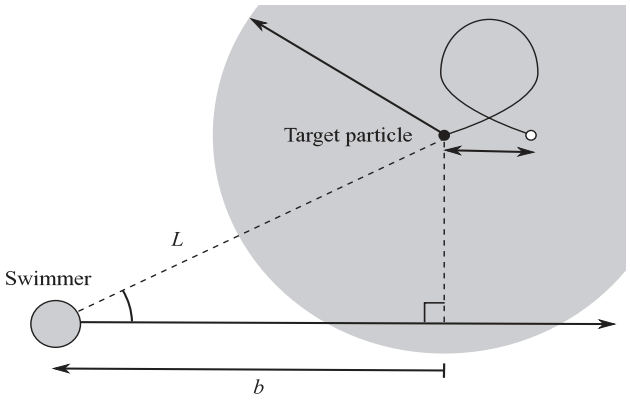

Figure 2.6 Schematic from [69] showing the situation described in theoretical work. The net displacement of the tracer Δ depends upon the impact parameters a and b. λ is the path length of the swimmer. The initial position of the tracer is represented by a black dot, and the final position by a white dot. The 'interaction disk' of radius R is shaded in grey.

Simulations were performed to compare theoretical predictions with the experimental displacement PDFs (Probability Distribution Functions) measured by Leptos *et al.* [11]. Although they predicted exponential tails to their PDFs similar to those seen in the experiments, it was not clear whether the origin was the same. Their theory predicted that if swimmers changed direction, then the loop-like trajectories of passive tracers in their flow field, would not close, leading to net displacement and enhanced diffusion. These un-closed loops are precisely what was observed in the tracked trajectories of beads in the vicinity of *Chlamydomonas*. Additionally, the magnitude of the enhanced diffusion was in good agreement with the experiments provided the velocity field strength was chosen appropriately. Squirmers are a good model for spherical extensile swimmers such as *Volvox* or *Chlamydomonas*, but do not describe the velocity field of a motile *E. coli*.

Miño *et al.* (2012) [63] (the first β calculation of the three) constructed a similar theory, but which considered the far field advection of swimming *E. coli* with infinite path lengths rather than squirmers with finite paths. A swimmer was found to be better represented by two point monopoles than a dipole, as this allowed a smaller cut-off value for the minimum distance between swimmer and tracer to be used. This cut-off is necessary as their theory did not predict well the displacements resulting from close encounters. Additionally, their theory neglected the circular motion of bacteria next to a surface.

The pre-factor β, measured in their experiments, was understood from the theory to be a product of the swimmer-tracer cross-section of interaction and the mean squared

displacement of a single scattering event. They showed that β depends heavily on distance of the tracer from the surface, a variable that they could not control in their experiments. The average β predicted ($2\mu\text{m}^4$) from assuming that tracer distance from the wall is distributed according to the Boltzmann distribution was ~ 7 times below their experimental results, but matched the dependence on confinement qualitatively. Their 3D prediction of $\beta = 0.48\mu\text{m}^4$ was ~ 4 times below their 2D value, explained by comparing the swimming efficiency in bulk to the reduced efficiency at the wall (at the wall the swim speed is slower for the same magnitude of force). The discrepancy between the theoretical and experimental results of these researchers, and the absence of a measurement in 3D, presented an opportunity for further work in this area.

The second (directly applicable) theory of enhanced diffusion in an *E. coli* bath was developed in collaboration with the experimental results presented in Chapter 4 of this thesis (by other researchers in the department). An overview of the work is given in this section, rather than after the experimental results, to facilitate a direct comparison with the other theoretical work in this field. The theoretical results were published alongside the experimental data shown in this thesis [1] and expanded upon in [40].

The model used was a modified version of the theory by Lin *et al.* [69]. Swimmers were approximated as point dipoles and values of numerical parameters for swimming were taken from Drescher *et al.*'s measurements of the dipolar field [58]. Near field interactions, where the field is inadequately described as dipolar and additional interactions due to charge, adhesion *etc.* are likely, were argued to be largely irrelevant. This is due to the rarity of direct collisions and the likelihood that hydrodynamic interactions would push particles away before collision. However, the researchers point out [40] that while this applies to tracers on the order of a bead or bacterium, for much smaller tracers, (*e.g.* the Dextran in [10]), that can come closer to the core of a swimmer, their enhancement would be significantly larger and dominated by near-field interactions.

Numerical simulations demonstrated that the enhancement β was higher ($\sim 7.19\mu\text{m}^4$) than in the previous calculation by Miño *et al.*, due to the inclusion of random direction changes representing tumbles. As for squirmers, direction changes lead to greater enhanced diffusion by causing tracers to describe part-loops. A detailed discussion of how swimmer characteristics affect the numerical pre-factor determining β is presented in [40]. They predict that the enhancement of tracers should depend strongly on the path length of the swimmers λ. As λ approaches infinity, tracer loops almost close, reducing the enhancement. Interestingly, maximum enhanced diffusion is obtained for biologically relevant run-lengths and reduces again for very short run-lengths (below

$\sim 10\mu$m), a result which was observed experimentally for tumblers by Kim and Breur [10]. Despite discrepancies between the extension of this model to a 2D situation and the experimental wall measurements by Miño *et al.*, the β predicted provides a good estimate.

Finally, recent analytical work by Pushkin *et al.* [71, 72] is the third example of β being calculated for an *E. coli* suspension. An explicit value for β was published after the experimental data presented in this thesis [72], but was based on preceding work presented in [71]. In brief, Pushkin *et al.* [71] claim that far-field advection only accounts for 85% of the enhancement in 3D, and an additional physical mechanism of fluid entrainment the remaining 15%. Entrainment is the near field effect of tracers getting caught in the wake of a swimmer, accounted for partially in the theory for squirmers but not in either of the pusher models for *E. coli*. This addition increases the 3D prediction of β to $\sim 9\mu\text{m}^4$. For quasi-2D suspensions of dipole swimmers or for suspensions of quadrupole swimmers, entrainment is argued to dominate.

2.6 Aim

The experimental and theoretical situations are summarized in Tables 2.1 and 2.2. For experimental studies that did not explicitly measure β, the assumption that all of the bacteria were swimming at 15μm/s was necessary to calculate approximate values. All of the theoretical work in calculating β has been for dilute suspensions representing *E. coli*, ([69] did not explicitly calculate β for squirmers), but the experimental results in [63] are the only study that can be compared with the theoretical predictions. Other experimental work in dense suspensions, using molecular tracers or extensile swimmers have indicated β values an order of magnitude larger.

It is apparent that there is an area missing from the experimental work published so far on enhanced diffusion in bacterial active suspensions, namely measurements of tracer beads in dilute 3D suspensions of *E. coli*. To make progress on the study of tracers in active suspensions these are needed, both as a measurement in the simplest conditions without wall interactions, and as a comparison with well developed theories. This gap has been partially filled by work here in the Edinburgh group [13], but there is room for a more thorough study. Here I use non-motile bacteria as tracers, as in [13], due of their similarity to the active component and for practicality. However, the aim was to further develop measurements of the system by separating the tracer contribution to the diffusion coefficient measured from that of non-motile bacteria from the motile

Table 2.1 Experiments on tracer diffusion.

	Dimensionality	Active component	Tracer	β (μm^4)
[8]	Soap film	*E. coli* (collective motion)	Beads 4.5 and 10μm	~ 90
[11]	3D	*Chlamydomonas*	Beads 2μm	~ 915
[10]	3D	*E. coli*	Dextran molecules	~ 650
[63]	Next to a wall	*E. coli*	Beads 2μm	13 ± 0.7

Table 2.2 Theory on tracer diffusion in a bath of *E. coli* approximated by point dipoles.

	Dimensionality	Effect(s) included	β (μm^4)
[63]	Next to wall	Advection	2.0
[63]	3D	Advection	0.48
[40]	3D	Advection	7.19
[72]	3D	Advection + Entrainment	9.0

strain.

More specifically, one of the aims of this project was to scrutinise whether the variable J_A is appropriate for the study of enhanced diffusion in general, or whether its applicability is limited to the systems of Miño and co-workers. If applicable, the primary aim was to calculate β for the system.

By making the experimental situation truly 3D, it is simplified. Normally, in the study of a system, research begins with the simplest experimental situation. In the case of this system, experiments in 2D or close to walls facilitated measurements, but complicated interpretation. If interactions with surfaces are present, many additional questions are raised and additional verifications are required. A 'cleaner' experiment is possible in the bulk, there is no need to add compounds such as PVP to the motility medium, or to wait minutes once sealing the chamber for the tracer beads to sediment.

Chapter 3

Methods: Enhanced diffusion

In this chapter the methods used to study the enhanced diffusion of non-motile, tracer cells in a suspension of swimming *E. coli* are described.

3.1 Introduction to methods

Two complementary techniques are used widely to study the dynamics of colloidal and biological systems; Dynamic Light Scattering (DLS) and microscopy. Light scattering works in reciprocal space and provides average information on the entire sample, whilst microscopy works in real space and allows a detailed inspection of sample constituents. Attempts have been made to use DLS and microscopy simultaneously by building laser scattering apparatus into a microscope [73]. This allows more information to be gathered than from one technique alone. Additionally, microscope based DLS has been used for studying properties of red blood cells [74]. These optical apparatus are limited to labs with considerable expertise to build the setup. Differential Dynamic Microscopy (DDM), the method used in this thesis, allows a use of microscopy itself to study the reciprocal space and gather the same information as is possible to obtain from Dynamic Light Scattering (DLS).

There are two categories of measurements needed in experiments on enhanced diffusion. The diffusion constant of the passive tracer must be measured. Additionally, the bacterial parameters (the average speed of the bacteria and proportion of bacteria swimming) must be measured to quantify the activity of the fluid. To date the primary technique employed for both measurements has been to record image sequences in real space, using microscopy, which are then analysed with tracking. Tracking measures

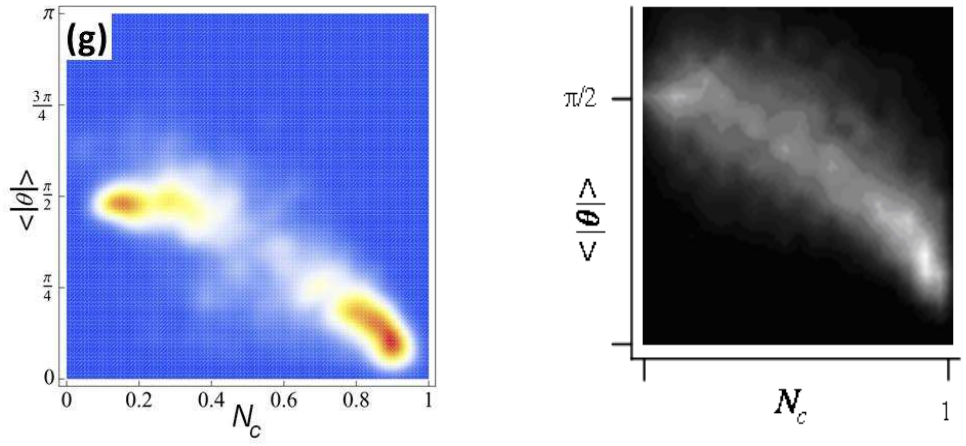

(a) **(b)**

Figure 3.1 Trajectories plotted in $N_c, \langle\theta\rangle$ space. (a) Taken from [62] for *E. coli* next to a wall. The probability density fades from blue to red for low probability to high probability. Clusters are centered close to where they would be centered for purely diffusive and ballistic motion. (b) For wild-type *E. coli* in the bulk. The probability density fades from white (high) to black (low). Clusters are not well defined making it difficult to distinguish between the two populations.

the movement of particles by recording them in a movie, following their positions in consecutive frames and then linking them to form trajectories. The technique has been used extensively in colloidal science [75], and was the method used for first quantifying bacteria motility [38]. Historically, small numbers of particles were tracked manually, but today, it is possible to access code based on the theory presented in [75], which can simultaneously identify and track large numbers of particles.

A study by Miño *et al.* [62], introduced already, recognized that a proportion of the bacteria in their suspension did not swim and devised a protocol for separating the tracks of diffusive bacteria from those swimming ballistically. They greatly enhanced their statistics by plotting their trajectories in the parameter space displayed in Figure 3.1(a). The parameters are defined to be the average angle between successive steps $\langle\theta\rangle$ and $N_c = Tdr/Ldt$, where dr is the mean step size a particle makes with a step time dt, T is the trajectory duration and L is the diameter of a circle which encompasses the entire trajectory. Purely diffusive trajectories are expected at $[0, \pi/2]$ and purely ballistic trajectories are expected at $[1, 0]$ in the $N_c, \langle\theta\rangle$ plot. In reality there are clusters of trajectories near these points for *E. coli* and tracers next to a wall.

The tracking technique in itself does not limit the experiment to 2D, as it is possible to track in 3D [75] and also to find a 3D diffusion constant by tracking a 2D projection of a 3D system. However, the extra dimension complicates the analysis for a number of

reasons. With regards to tracking the tracers, they can become obscured by bacteria at the high concentrations usually used. With regards to tracking the bacteria, a $\times 20$ or $\times 40$ magnification is needed to accurately track micron sized objects, but the larger the magnification, the greater the reduction of the field of view, causing the fastest bacteria moving in the focal plane to leave while data is being recorded. Consequently, tracking a 3D system biases towards bacteria which appear to move slowly, because their motion has a component along the direction perpendicular to the focal plane. Additionally, although the diffusive and ballistic tracks can be separated using the protocol described above, it is not straightforward to distinguish between the two clusters in 3D, causing problems for the measurement of the proportion of motile bacteria (Figure 3.1(b)).

Measuring bacterial dynamics with light scattering, in principle suitable for experiments of this nature (demonstrated in the next section), would allow 3D measurements. However, light scattering has been used little to measure bacterial motility, due to the impracticality of detecting scattered light at small enough angles to access the time and distance scales of a swimming bacterium. To illustrate, a typical *E. coli* swims at a speeds of around 10μm/s, so a detector must be able to access scattering vectors of $q < \frac{2\pi}{10}$, which corresponds to angles below 3°. Conventional DLS measures at angles above 20°, going below this requires custom made apparatus, while above 3° any precession or wiggling of the bacteria contributes to the measurement. An early study explored the capability of DLS for measuring bacteria motility [76], but the limitations of apparatus were never overcome to the extent that it took over from tracking as a tool to measure the velocity of bacteria regularly.

3.1.1 The Intermediate Scattering Function

The Intermediate Scattering Function (ISF) is usually the quantity of interest in DLS experiments [77]. The ISF is defined as the normalised correlation function of the Fourier component of density (ρ) fluctuations;

$$f(\vec{q},\tau) = \frac{\langle \Delta\rho(\vec{q},t)\Delta\rho(\vec{q},t+\tau)\rangle}{\langle |\Delta\rho(\vec{q},t)|^2\rangle}. \tag{3.1}$$

where $\vec{q}$ is the wave vector and

$$\Delta\rho(\vec{q},t) = \int \Delta\rho(\vec{r},t)e^{i\vec{q}.\vec{r}}dr, \tag{3.2}$$

with $\Delta\rho(\vec{r},t) = \rho(\vec{r},t) - <\rho>$ representing the fluctuations in density at position $\vec{r}$,

around an average density $< \rho >$.

The ISF is also the dynamic structure factor $S(\vec{q},\tau)$ normalised by the static structure factor $S(\vec{q}) = S(\vec{q},\tau = 0)$,

$$f(\vec{q},\tau) = S(\vec{q},\tau)/S(\vec{q}) \tag{3.3}$$

where $S(\vec{q},\tau) = \langle \Delta\rho(\vec{q},t)\Delta\rho(\vec{q},t+\tau)\rangle$ and $S(\vec{q}) = \langle |\Delta\rho(\vec{q},t)|^2\rangle$.

The dynamic structure factor $S(\vec{q},\tau)$ of a material measures correlations in space between particles and their time evolution. For N identical at positions r_j (j=1...N),

$$S(\vec{q},\tau) = 1/N\langle \sum_{j,k} e^{-i\vec{q}.(\vec{r}_j(t+\tau)-\vec{r}_k(t))}\rangle, \tag{3.4}$$

where $< .. >$ denotes ensemble averaging. For non-interacting particles [77],

$$f(\vec{q},\tau) = \langle e^{i\vec{q}.\Delta\vec{r}_j(\tau)}\rangle_j, \tag{3.5}$$

where $\Delta\vec{r}$ is the displacement of the particle in time τ.

Assuming the system is ergodic, $f(\vec{q},\tau)$ decays from $f = 1$ at $\tau = 0$ to $f = 0$ as τ increases, over a characteristic timescale. The functional dependence of $f(\vec{q},\tau)$ between these two extremes depends on the composition and behaviour of the sample. If the particles are undergoing Brownian motion, the calculation of the average (Equation 3.5) using the Gaussian displacement distribution (Equation 2.5) gives the analytic result [77],

$$f(q,\tau) = e^{\frac{-q^2}{6}\langle \Delta r^2(\tau)\rangle} = e^{-q^2 D\tau}, \tag{3.6}$$

where $\langle \Delta r^2(\tau)\rangle$ is the mean squared displacement (MSD).

For motile microorganisms which are swimming isotropically (such as *E. coli* in the absence of a chemical gradient) where $\Delta r = vt$, assuming straight trajectories, the ISF reduces to [77],

$$f(q,\tau) = \int_0^\infty P(v)\mathrm{sinc}(qv\tau)dv, \tag{3.7}$$

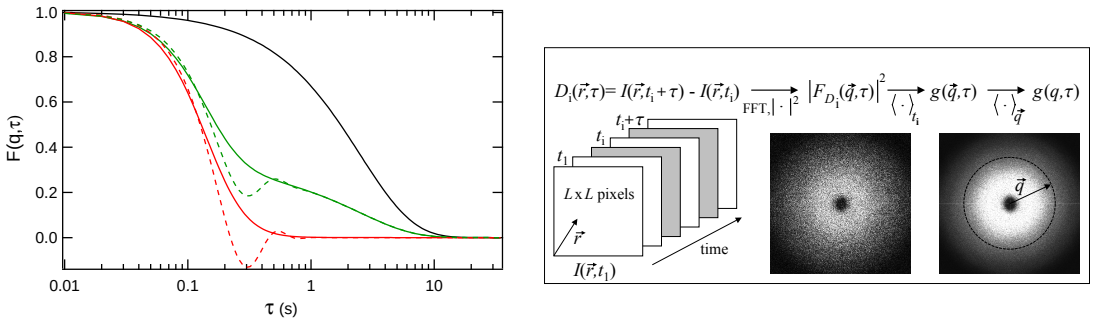

(a) **(b)**

Figure 3.2 (a) Theoretical $f(q,\tau)$ against τ at $q = 1\mu\text{m}^{-1}$ for (black) diffusing particles, (red) isotropic swimmers with $P(v)$ described by a Schultz distribution and (green) a 30:70 mixture of the two. $D = 0.4\mu\text{m}^2/\text{s}$ and $v = 15\mu\text{m/s}$ with a wide swimming speed distribution, $\sigma = 8.6\mu\text{m/s}$ (line), or a narrow distribution, $\sigma = 3.3\mu\text{m/s}$ (dashed line). See below for definition of Schultz distribution and σ. (b) Schematic of image processing in the DDM procedure, published in [79].

where $P(v)$ is the velocity distribution of the motile microorganisms. For a population of bacteria in which a proportion α are swimming and also undergoing Brownian motion and $(1-\alpha)$ are undergoing Brownian motion only the whole ISF reads [78]:

$$f(q,\tau) = e^{-q^2 D\tau}[(1-\alpha) + \alpha \int_0^\infty P(v)\text{sinc}(qv\tau)dv]. \tag{3.8}$$

By fitting a function of the form of Equation 3.8 to the measured ISF, the proportion of motile swimmers, the speed of the motile swimmers and the diffusion constant of the non-swimmers can be extracted. Figure 3.2(a) shows the calculated $f(q,\tau)$ for diffusing spheres, isotropic swimmers (using typical *E. coli* input parameters) and a mixture of the two. The ISF for a mixed population shows a two stage decay; a fast process dominated by swimming and a slower decay dominated by diffusion.

Theoretically, DLS could provide the measurements needed for this study of enhanced diffusion, by measuring the ISF of a mixed population. However, as already mentioned, practical limitations of the technique mean that appropriate length-scales for the study of *E. coli* motility are not accessible.

3.1.2 Differential Dynamic Microscopy

Put simply, DDM is a method of measuring the ISF of a system, by recording images in real-space, using microscopy. The advantage of DDM over DLS for this project on enhanced diffusion is its ability to work at large length-scales, the equivalent of low

scattering angles in DLS. The advantage of using DDM over tracking is that it facilitates measurements in 3D. Images can be recorded at a lower magnification, increasing the field of view and causing the effect of perpendicular motion to be negligible [13, 79].

Binary mixtures were the first samples to be studied using DDA (Differential Dynamic Algorithm) by Croccolo *et al.* (2006) [80], but it was Cerbino and coworkers (2009) [81, 82] who showed experimental evidence that bright-field microscopy could be used to study the dynamics of colloidal particles in the reciprocal space (DDM). They believed that DDM could complement tracking methods for certain systems and be useful in many situations where tracking proves difficult, for instance in concentrated systems and for particles too small to be resolved individually. Since the initial studies, DDM has been used to study the aggregation of colloidal nano particles [83] and the anisotropic diffusion of magnetic colloids [84]. In particular, DDM has been successfully applied to measure the ISFs of motile microorganisms, such as the algae *Chlamydydomonas reinhardtii* [79], and of relevance to this thesis, *E. coli* [13, 79]. In general, as well as allowing a choice of spatial region, advantages of DDM over DLS include its ability to be applied to optically absorbant samples and to fluorescence microscopy, exploited in the project presented here.

DDM involves recording a movie *i.e.* taking time-lapse images of a sample. Each image taken of the sample is described by an intensity profile $I(\vec{r},t)$ which changes in successive images as the particles change location. The Differential Image Correlation Function (DICF) $g(q,\tau)$ is measured by taking the difference between $I(\vec{r},t)$ and the same quantity τ time later to obtain $D(\vec{r},\tau)$. This then undergoes a Fourier transformation to become $(F_D(\vec{q},\tau))$ and is averaged over different initial times t to obtain $g(\vec{q},\tau)$. If sample dynamics are isotropic, $g(\vec{q},\tau)$ can be averaged azimuthally for each q, at different values of τ, to obtain $g(q,\tau)$. This process is shown schematically in Figure 3.2(b).

Assuming that the intensity fluctuations in the image are proportional to the number density fluctuations of particles, it can be shown that [13],

$$g(q,\tau) = A(q)\left(1 - \frac{\langle \Delta\rho(q,t)\Delta\rho(q,t+\tau)\rangle}{\langle |\Delta\rho(q,t)|^2\rangle}\right), \tag{3.9}$$

where $A(q)$ depends on the imaging system and contains potential information on the

size of particles in the sample. This expression includes the ISF, therefore,

$$g(q,\tau) = A(q)[1 - f(q,\tau)] + B(q) \tag{3.10}$$

where $B(q)$ is included to account for camera noise. For an alternative, more general, derivation of this relation, see [84].

The DICF $g(q,\tau)$ measured experimentally from the time-lapse images is fitted, at each q in the range measured, with Equation 3.10. The ISF, $f(q,\tau)$, is given by Equation 3.6 or 3.8 depending on the composition of the sample. This requires a choice of $P(v)$ in the case of motile microorganisms. For *E. coli*, the microorganism of interest to this study, $P(v)$ is peaked [76, 78, 79]. A Schultz distribution has been used previously [13, 79], allowing Equation 3.8 to be solved analytically. The Schultz distribution is given by,

$$P(v) = \frac{v^Z}{Z!}\left(\frac{Z+1}{\bar{v}}\right)^{Z+1} \exp\left(-\frac{v}{\bar{v}}(Z+1)\right) \tag{3.11}$$

where the variance σ^2 is related to Z via $\sigma = \bar{v}(Z+1)^{-1/2}$.

The time scales accessible to DDM are limited only by the frame rate and the duration of the experiment [79, 81]. The length scales accessible are determined by the size of a pixel (dependent on the magnification used and the camera employed) and the frame size used [79]. For *E. coli*, an optimum q range is within $0.5 \leq q \leq 6\mu\text{m}^{-1}$, as above $q = 6\mu\text{m}^{-1}$ wobbling of the cell body contributes to the signal, and below $q = 0.5\mu\text{m}^{-1}$ straight line swimming can't be assumed. A $10\times$ magnification has typically been used [13, 79], imaging $\sim 10^4$ bacteria in a field of view. Once final values for parameters (v, σ, α, D) have been obtained, by averaging over fitted results in the chosen q range, contributions from thousands of bacteria have been averaged over, making DDM a high-throughput method.

Martinez *et al.* [79] validated the results obtained from applying DDM to an *E. coli* suspension. For smooth swimming *E. coli* (run only), v, σ and D showed good agreement when compared directly to results from particle tracking of the same sample (it was not possible to reliably measure α in 3D with tracking). For measuring the average properties of the suspension, DDM was deemed less laborious, faster and returned better statistics than tracking, which typically averages over only $\sim 10^2$ bacteria. It was also checked that DDM could be performed on bright-field,

phase-contrast or fluorescence microscopy. All three imaging techniques returned the same results, but phase contrast is preferable as it displays a better signal to noise ($A(q)/B(q)$) ratio.

In deriving Equation 3.9 it is assumed that motion of the bacteria in the z axis does not influence its image contrast. As the depth of field is finite, Martinez *et al.* [79] checked the validity of this assumption by performing DDM on simulated particles whose contrast was smeared according to their z axis position. It was found that for the experimental set-up and procedure used (the same as those described in this thesis, section 3.3) results were not influenced by motion in the z axis *i.e.* results were independent of the depth of field. Finally, the modelled ISF in Equation 3.7 assumes straight swimming *E. coli* that do not tumble. When wild-type (WT) *E. coli* were measured and fitted with the same ISF, the average speed v showed some q dependence [13, 79] (see section 3.3.2). It was verified [79] that this is as expected from simulations of particles undergoing direction changes, and is due to the increased probability of a direction change at low q lowering v at these length-scales.

Since the development of DDM for *E. coli* suspensions, the technique has been used within the Edinburgh group for research on *E. coli* motility in complex environments. These have included polymer [66] and small molecule solutions [85], droplets [86] and porcine mucus. In this thesis DDM is applied to WT *E. coli* in the study of enhanced diffusion (Chapter 4), in the study of bacterial preparative protocols (Chapter 5) and in the study of antimicrobial peptide action (Chapter 10).

Other microorganisms require suitable theoretical models of their ISF to allow research into their motility with DDM. *Chlamydomonas reinhardtii* displays a more complex motion on different time and length scales to *E. coli*, requiring an understanding of additional contributions to the decay of the ISF [79]. But, given the usefulness of DDM once experimental procedures have been optimised, it is unlikely it will be long before it is used with many other simple swimmers such as *Pseudomonas*. It may also prove useful for characterising the motility of *E. coli* at surfaces, which would require an alternative ISF. However, note that, whilst under development for a given microorganism, DDM is dependent on tracking to inspect motility details (allowing a model of the ISF to be proposed) and to verify initial results.

The remainder of this chapter first describes the microbiological methods used to prepare WT *E. coli* for DDM measurements, before detailing the collection and analysis of DDM data for this thesis.

3.2 Microbiological methods

3.2.1 Bacteria and culture media

Bacteria: The non-pathogenic K-12 derived strain of *Escherichia coli* wild-type (WT) AB1157 was used as the active, motile particles throughout. AB1157 was chosen as it is a highly motile strain, often used in experiments on motility.

Two non-motile mutants of AB1157, transformed by A. Dawson and J. Schwarz Linek were used as passive tracers. The motA mutant has paralysed flagella which do not rotate due to a disruption in the stator complex of the motor [87]. The fliF mutant does not have any flagella, as the first step of flagella synthesis is disrupted [88]. Both transformants were kanamycin resistant.

With assistance from G. Dorken, using A. Dawson's protocol, both non-motile mutants were transformed to introduce the fluorescent GFP-encoding plasmid pHC60 [89] and tetracycline resistance.

In one instance fliC, a non-motile mutant of AB1157, de-flagellated but retaining its hooks was used.

Culture Media: Three media/buffer were used in this study.

Luria Broth (LB) [90] - LB is composed of 10g/L Tryptone, 5g/L, Yeast Extract and 5g/L NaCl. LB and LB agar (containing 15g/L of agar) were purchased from the department of Biology. The maximum doubling rate of *E. coli* in aerated LB liquid culture is $20 - 30$ min at 37°C.

Tryptone Broth (TB) - TB is commonly used as the growth medium when a highly motile population is required [91, 92]. TB was prepared by dissolving 10g of Bacto Tryptone and 5g of NaCl in 1 liter of distilled water. The media was autoclaved immediately after preparation. The maximum doubling rate of AB1157 in aerated TB liquid culture at 30°C was measured to be ~ 50 min.

Berg Motility Buffer (BMB) - Adler and Templeton (1967) [92] studied *E. coli* swimming in different environmental conditions and showed that a phosphate buffer with a chelating agent at pH=7 was sufficient for swimming, whilst preventing growth. Since this finding, other closely related minimal buffers have been developed for biophysical experiments on bacterial motility. BMB was prepared by mixing 20ml of 3.3M NaCl, 1ml of 1M EDTA, 3.8ml of 1M KH_2PO_4 and 6.2ml of 1M K_2HPO_4, and

adding distilled water up to a volume of 1L. The media was autoclaved immediately after preparation.

Storage: For long-term storage of *E.coli*, 2ml of a culture grown overnight in LB was centrifuged at 4500rpm for 5min, the supernatant discarded, and the pellet resuspended in 1ml of LB. Eight hundred μl of the bacterial suspension was vortexed with 800μl of 20% glycerol in a sterile cryotube and then stored at -80°C. When used, bacteria were recovered from the vial by streaking onto an LB agar plate. Plates were incubated for 24 hours in a stationary 30°C incubator before being removed, wrapped in parafilm and stored in a 4°C fridge. Plates were discarded after 1 week.

3.2.2 Preparation of a motile suspension

See Chapter 5 for an investigation and justification of the growth and preparation protocols.

Density: The number density of cells was judged by their optical density (OD) in solution, a measure of turbidity. OD was measured at 600nm in a Cary spectrophotometer, with the sample in 1ml cuvettes. Dense solutions, above OD=1, were diluted for measurement to reduce multiple-scattering effects.

Growth of a motile culture: Single colonies were picked from the agar plates for growth in a liquid culture for experimentation. A colony was placed in 10ml of LB and incubated overnight (16 ± 2 hours) at 30°C and 200rpm. Three hundred and fifty μl of the culture was then diluted with 35ml of TB and the flask returned to the incubator for 4 hours. Simultaneously the OD of the overnight culture was checked for normal growth and 1ml was removed to check for aggregation (below). When removed after 4 hours incubation the culture had grown to OD=0.5$\pm$ 0.1. The mutants were grown and washed identically to WT AB1157 except that kanamycin and tetracycline were added to both growth steps to protect against loss of the mutations.

When both WT and mutant cells were required simultaneously, the mutant culture was re-inoculated and removed from the incubator 40 min before the WT culture to stagger the washing procedure.

Aggregation protocol (created by Dr. J. Schwarz-Linek): On occasion the cells formed aggregates in the overnight culture and the exponential culture, and were unusable for the experiments. It is postulated that aggregation is caused by a change in bacterial phenotype, causing the excretion of the surface protein Ag43, which plays

a role in biofilm formation [93].

To verify that aggregation had not occurred before continuing with the wash, 1 ml of the overnight culture was centrifuged, the pellet re-suspended in motility buffer and deposited into a cuvette. The cuvette was checked visually at the same time as the exponential culture was removed from the incubator. If the cells had aggregated, they sedimented over the four hours. The cuvette no longer showed a uniform turbidity, but had clear media at the top and a dense suspension at the bottom. Normally, if no aggregation occurred, the turbidity did not change enough to be judged visually in 4 hours, as the sedimentation rate of a single, non-motile *E. coli* can be calculated to be 0.27mm an hour [94]. Aggregates $\sim$10$\times$ the size of a single bacterium would achieve sedimentation rates of cm per hour.

Filtering: A filtration washing procedure transferred the bacteria from the TB growth media to BMB for the experiments. A sterile Nalgene filtration unit consisting of two compartments separated by a Milipore 45μm filter was used. The filter was soaked in BMB for $\sim$ 1 min before being carefully placed centrally on the unit with sterile tweezers. The upper half of the unit was then screwed tightly onto the lower before the 35ml culture was slowly poured down the side of the unit and onto the filter. The liquid drips slowly through the filter, leaving the bacteria on the filter or suspended in any liquid remaining ontop of the filter. Gravity alone does not result in practical dripping rates, so a suction tube was connected from the lower half of the unit to a running water tap to apply a small amount of additional suction through the filter. Between the unit and the tap the tube passed through a 70% Ethanol bath to ensure that no viable bacteria were sucked into the running water.

When the level of TB had fallen to approximately 3mm above the filter, leaving $\sim$3ml of liquid, 35ml of BMB was pipetted into the unit. It was allowed to run down the opposite side of the unit to the culture previously, and onto the filter. It was important to prevent the filter from running dry during the procedure, as this resulted in a greater proportion of non-motile bacteria after the wash. This washing step was repeated 3 times. The water flow was adjusted to maintain a constant rate of dripping through the filter and a consistent wash speed between experiments, with the whole process requiring 45$\pm$ 10min. When $\sim$ 1-3ml of liquid remained on the filter after the third wash, a sterile cut pipette tip (the end of the tip was removed with scissors to widen the constriction and reduce flagella shearing) was used to transfer the liquid to a plastic 50ml polystyrene test tube (Greiner). Smaller tubes do not have a wide enough diameter for the filter to be inserted. The filter was removed from the unit using sterile tweezers and deposited on the side of the tube. The liquid was run back and forth along the tube and over the

filter by gently tipping the tube, until the bacteria on the filter were re-suspended. The final suspension had an OD of between 5 and 15 depending on the volume of liquid left on-top of the filter after the final washing step.

Dilution: OD was calibrated to colony forming units (CFU) to give OD=1, corresponding to $1.55 \pm 0.05 \times 10^9$ cell/ml, for *E. coli* in BMB after the preparation detailed above. Optical densities between OD = 0.01 and OD = 0.5, corresponding to bacteria concentrations $0.155 - 7.75 \times 10^8$ cell/ml were obtained by dilution with BMB. All pipetting of motile cells was performed slowly, with cut tips.

Formaldehyde: To measure the diffusion coefficients of dead WT AB1157, fliF and motA they were washed as normal, diluted to OD=0.5 and 0.5ml of 1.2% formaldehyde was added to 2ml of bacterial suspension. The addition of formaldehyde and the preparation of the samples for the microscope took place under a fume hood. Plate counts showed that after $\sim$ 30 min only 0.002% of cells remained viable.

Glucose: To increase the average speed of the swimming *E. coli*, samples were prepared at OD=1 and then diluted 2$\times$ with BMB containing glucose at 0.006 wt%.

3.2.3 Calculating volume fraction

To calculate a volume fraction of bacteria ϕ from the number density of cells, a measurement of the length and width of the bacteria was made. AB1157 were washed as for motility experiments, and 1μl of OD=0.5 was deposited onto a BMB agar (2g agar in 10ml of BMB) pad, confined in an adhesive gene frame (further details of this process can be found in section 7.7.1). When the liquid was judged by eye to have evaporated or been absorbed into the agar, a glass coverslip was stuck ontop of the pad, confining the cells between the agar and the coverslip.

The cells were imaged with a $\times$100 oil-immersion phase contrast PH3 objective through the cover slip. The automated image capturing software Microtron was used to capture a z-stack of a single x-y field of view with images in the stack 0.1μm apart. This allowed a judgement of the center of a bacterium to be made, and an image chosen for further analysis (Figure 3.3). The procedure also confirmed that the bacteria were orientated perpendicular to the cover slip.

Crude measurements of length (from tip to tip) and width (measured roughly half way down the length) for 60 cells were done using ImageJ. Optical point-spread function uncertainty was judged to be within the uncertainty of manually deciding where the

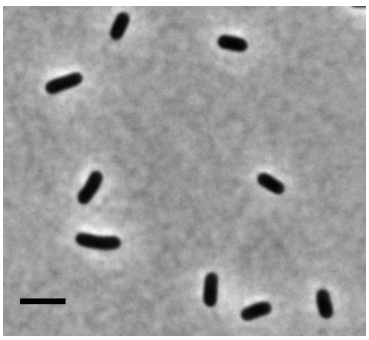

Figure 3.3 Phase contrast image (319 × 290 pixel) at ×100 magnification of stationary *E. coli* on BMB agar. Image is section of the frame, size 1600 × 1200 pixel, in which 60 bacteria were used to judge the average volume of an AB1157 bacterium grown in TB and washed into BMB as for motility experiments. Scale bar=3μm.

cell edge was. The average volume of a bacterium was calculated assuming it to be a cylinder. The protocol was judged to be sufficiently accurate for the need, which was to quote the volume fractions, based on body volume, of active bacteria in our suspensions.

Cell length was polydisperse, ranging between 1.7μm and 3.8μm. The average length of a bacterium with its standard deviation was $2.4 \pm 0.6\mu$m, and its width $0.86 \pm 0.07\mu$m. Assuming a cylindrical cell shape, the average volume of a bacterium was calculated to be $V = 1.4 \pm 0.1\ \mu\text{m}^3$ (quoted with uncertainty rather than standard deviation). The majority of the experiments were carried out at OD=0.5, corresponding to a volume fraction $\phi \sim 0.1\%$.

3.3 Experimental protocol and setup

This section describes how to apply DDM to a bath of swimming wild-type *E. coli* (following the analysis presented in [13, 79] closely), or to diffusers alone, before moving on to describe the experimental procedure for combining the two to investigate enhanced diffusion.

3.3.1 Collecting DDM data

Directly before taking the measurements, a suspension of bacteria in motility buffer was gently mixed by tilting the containing tube. A glass capillary of depth 400μm (50×8 × 0.4mm VitroTubes, Vitrocom) was held horizontally and $\sim 170\mu$l of the suspension was slowly pushed in with a pipette. A 1ml pipette tip has a orifice of similar diameter to

the capillary. When full, the ends of the capillary were sealed with Vaseline by hand, making sure visually that no air could pass the seals. If capillaries were not sealed, the fluid underwent drift, complicating analysis. Often small pockets of air were present at each end after sealing, which were tolerated as the measurements were consistently made in the middle of the capillary. If the capillary proved difficult to fill, appeared dirty on the inside, or contained bubbles in the bulk after filling, it was discarded and the sample was re-loaded into a new capillary.

The cells were always imaged 100μm from the bottom of the capillary in the bulk of the suspension. After placing the capillary on the microscope stage the microscope was focused on the lower glass wall and then the focus was moved 100μm upwards. It was more important to efficiently find the field of view for recording each time than to avoid areas which contained darker patches due to dirt on the outside of the capillaries. DDM analysis is not influenced by static contributions to the images.

For a sample containing WT *E. coli*, only one method was used to measure the swimming parameters; DDM from phase contrast images. For a sample of mutant fluorescent diffusers, D could be measured with DDM from a phase contrast movie or a fluorescence movie. In fluorescent movies, a greater magnification and a slower frame rate (in comparison with phase contrast movies) were used to generate a sufficient signal to measure diffusion.

Phase contrast microscopy on a Nikon Eclipse Ti inverted microscope with a high speed camera (Mikrotron MC 1362) was used to record the sample at 100 fps. Magnifications of $\times 10$ were used with a frame size of 500 pixels. The field of observation at $\times 10$ magnification was $702 \times 702\mu\text{m}^2$ and $\sim 40\mu$m in depth, imaging $\sim 10^4$ bacteria (at OD=0.5) of length ~ 1 pixel. Movie sequences were recorded for 38 seconds. The light source was adjusted to illuminate the sample at a level shown in Figure 3.4(a).

Fluorescence microscopy on the same microscope using the same high speed camera was used to record the sample at 20 fps. The sample was irradiated with $450 - 490$nm light from a Chroma EGFP filter cube at maximum intensity. A Nikon Plan Fluor $\times 20$ objective with numerical aperture $= 0.5$ at a frame size of 1024 pixels were used. The field of observation at $20\times$ was $719 \times 719\mu\text{m}^2$ and $\sim 20\mu$m in depth. Movie sequences were ~ 800 frames long (~ 40 seconds). An example of a single frame is shown in Figure 3.4(b).

While $\times 20$ magnification probes shorter length-scales than are needed for the measurement of swimming speed, it provides an well-suited q range (up to $\sim 4\mu\text{m}^{-1}$) for the measurement of micron sized particle diffusion.

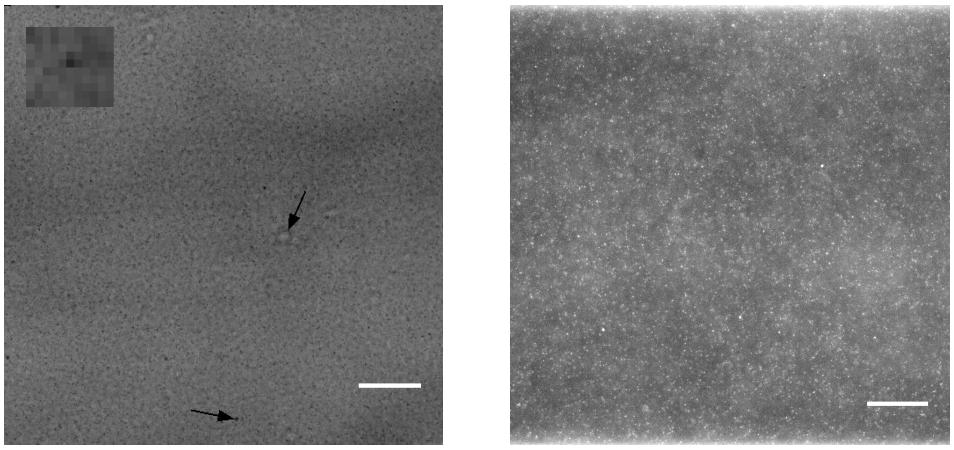

(a) **(b)**

Figure 3.4 Microscopy of an *E. coli* suspension. (a) Single frame of size 500×500 pixel taken in phase contrast at 10× magnification. Arrows point to static contributions due to dirt. Inset: magnification of 11×10 pixels in which one bacterium is imaged. (b) Single frame of size 1024×1024 pixel taken in fluorescence at 20× magnification. Brightness and contrast are adjusted in (b) to show features. Approximately 10^4 cells are imaged in each frame. Scale bars=100μm.

3.3.2 Analyzing DDM data

In order to analyze the raw images to obtain the DICFs using DDM they were processed using Labview code on an 8-core processor. For each delay time τ, every third frame was taken as an initial time for 100 frames *i.e.* frame 1,4,7 ...313. Equation 3.10 was then fitted to the measured DICF using least squares fitting in IGOR Pro. $f(q,\tau)$ was modelled by Equation 3.6 or 3.7 depending on sample composition. This returned the parameters v, D, α, A, B and Z defined previously, for each q. Further details of this procedure can be found in reference [79]. The fraction of non-motile bacteria (b) is defined as $b = 1 - \alpha$. In the following, b is frequently quoted rather than α, depending on the experimental situation.

Examples of DDM data: Wild-type population

A sample containing WT AB1157 at a concentration of 7.8×10^8 cell/ml was analysed as described in [13, 79]. Figure 3.5(a) shows the $g(q,\tau)$ and Figure 3.5(b) the reconstructed $f(q,\tau)$ (ISF) for 5 different q values. It can be seen from the reconstructed ISFs that the sample is composed of both motile and diffusive bacteria, the former causing the decay at short times and the latter at longer times. The implication of this for the experiments on enhanced diffusion are discussed later, but here the notation 'M' for

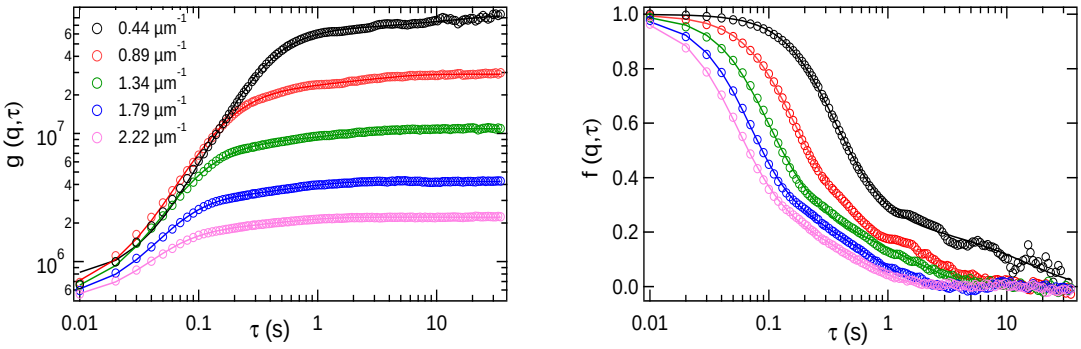

(a) **(b)**

Figure 3.5 DDM of WT *E. coli*. (a) DICFs $g(q,\tau)$ measured (symbols) and fitted (lines). (b) Measured ISFs $f(q,\tau)$ (symbols), reconstructed using Equations 3.8 and 3.10 and fitted (lines).

motile WT and 'N1' for non-motile WT populations, is introduced. Given that the two timescales are clearly separated, the ratio of the amplitude's of these two decays quantifies the proportion of motile (α) to non-motile (b) bacteria in the sample M:N1 [13, 79].

Figure 3.6 shows the values of the fitted parameters for every q measured. To obtain a value for v, σ, b and D for this sample, with an appropriate uncertainty, each is averaged over a given q range. All parameters are extremely noisy at low q, as the ISF has not fully decayed in the range of τ probed, invalidating the fit [13, 79]. Therefore the average is taken between $q = 1\mu\text{m}^{-1}$ to $q = 2\mu\text{m}^{-1}$ for the swimming parameters v, b and σ where they are largely q independent. The average for D is usually extended to the largest q measured at $\times 10$ magnification, as diffusion operates over shorter length-scales than swimming.

The average swimming speed v has some q dependence which is believed to be due to the tumbling motion of these wild-type bacteria, as smooth swimming mutants do not show the same dependence [79]. As q decreases, the length-scale probed increases, and the probability of the bacteria tumbling in a given time period goes up, resulting in a lower measured speed (discussed in [79]). The q dependence results in a larger quoted uncertainty in v than for a smooth swimming mutant.

The sample demonstrated in Figure 3.6 has $v = 14 \pm 1\mu\text{ms}^{-1}$, $b = 0.28 \pm 0.04$, $\sigma = 1.2 \pm 0.3\mu\text{ms}^{-1}$ and $D = 0.44 \pm 0.07\mu\text{m}^2\text{s}^{-1}$, with uncertainties representative of q dependence. The measurement of D is noisy as the proportion of non-swimming bacteria is small, making the fit to the diffusive decay more difficult. The diffusion of the swimming bacteria impacts little on the measured D (checked with simulations in

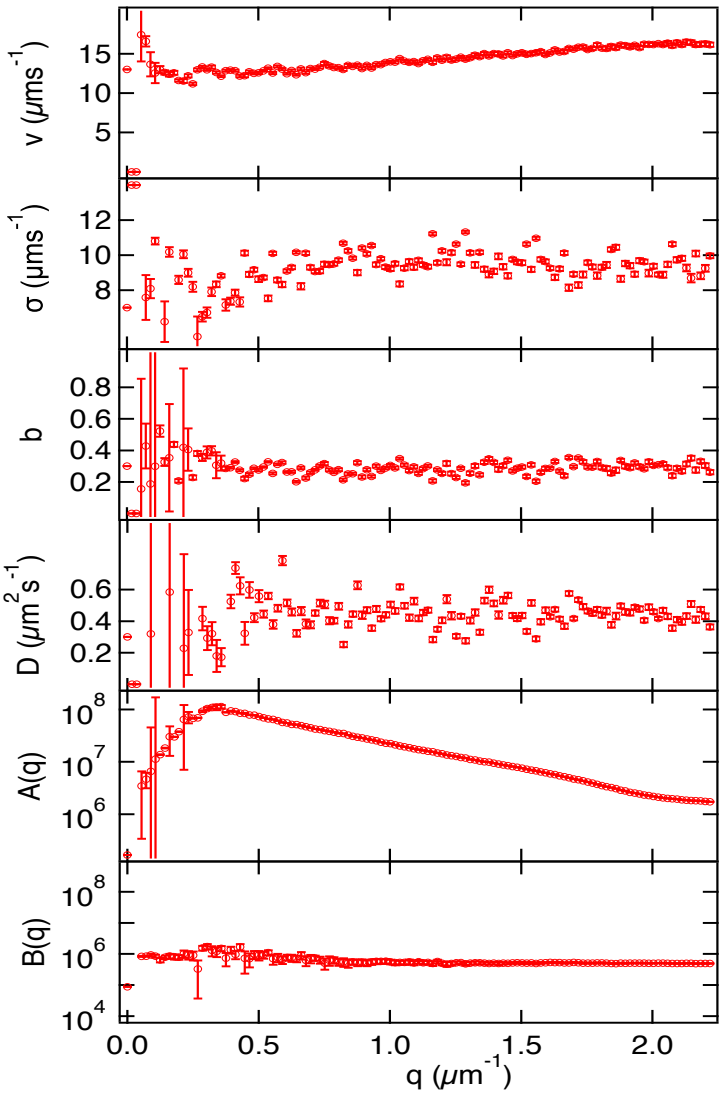

Figure 3.6 Fitted parameters against q for WT *E. coli*. Parameters $b(= 1 - \alpha)$, D, $A(q)$ and $B(q)$ are defined by Equations 3.8 and 3.10, while v and σ are parameters of the Schultz distribution, Equation 3.11.

[13]), therefore D is assumed to be the effective diffusion coefficient of the non-motile WT in the sample (N1).

Examples of DDM data: Diffusive population

Before mixing the mutant diffusers with the WT bacteria to probe enhanced diffusion it was necessary to verify that the Brownian diffusion coefficient D_0 of diffusers alone could be measured using both phase contrast microscopy and fluorescence microscopy. Note that the addition of the pHC60 plasmid did not affect the Brownian diffusion coefficient of either mutant.

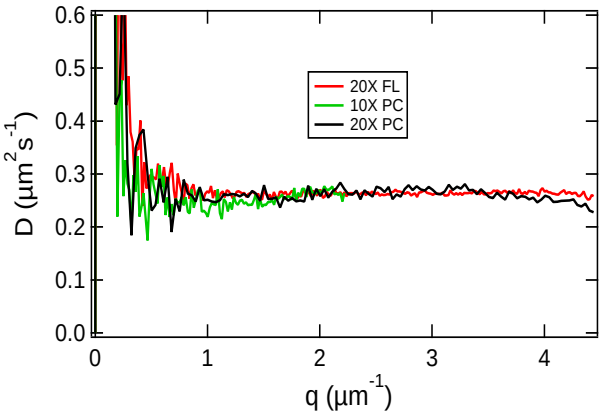

Figure 3.7 D_0 against q for motA at OD=0.5. Measured in phase contrast (PC) at $\times 10$ magnification (green) and $\times 20$ magnification (red) and by fluorescent signal (FL) at $\times 20$ magnification.

A sample containing motA at OD=0.5 (7.8×10^8 cells/ml) was recorded using phase contrast microscopy at $\times 10$ and $\times 20$ magnification and using fluorescence microscopy at $\times 20$. The DICF measured was fitted with Equations 3.10 and 3.6. The reconstructed ISF's had one diffusive contribution to their decay (not shown).

Figure 3.7 shows the fitted D_0 with q for each measurement made. All measurements agree within error over the q range $1 < q < 3.5\mu\text{m}^{-1}$, but above this D drops slightly. This has been observed in both phase contrast and fluorecence movies (although not seen prominently in the fluorescence measurement shown here), and corresponds to the length scale which begins to be on the order of the size of the bacterium. This could cause additional contributions to the decay of the ISF, invalidating the purely diffusive fit. Additionally, once q is $4.4\mu\text{m}^{-1}$ the ISF decays to 0 within ~ 0.7 seconds, meaning the model of diffusive decay is only fitted to the first $\sim$ 13 data points, inevitably leading to more noise.

3.4 Protocol followed for experiments on enhanced diffusion

As the proportion of non-motile cells in a washed WT AB1157 culture does not vary significantly from day to day between cultures, it was necessary to add more non-motile cells to investigate enhanced diffusion, either motA or fliF. These mutants act as passive tracers in the active suspension of WT bacteria. This results in three sub-populations in each sample; motile WT AB1157 (M), non-motile WT AB1157 (N1) and the added

Table 3.1 Example of a range of samples which varied α while keeping ϕ and v constant. Samples labeled 0 to 10, with corresponding fraction of wild-type suspension and fraction of mutant suspension (both at OD=0.5) incorporated into a total volume of 1ml.

Number	Fraction WT	Fraction mutant
10	1	0
9	0.9	0.1
8	0.8	0.2
7	0.7	0.3
6	0.6	0.4
5	0.5	0.5
4	0.4	0.6
3	0.3	0.7
2	0.2	0.8
0	0	1

non-motile population, named 'N2'. For each set of samples, in which the suspension activity was varied, only one of the mutants was required, which was distinguishable from the N1 population with fluorescent microscopy.

The activity $J_A = n_A v = \alpha v \phi / V$ (where n_A is a number density of swimmers, ϕ is the volume density of bacteria, V is the volume of a single bacterium and α is the proportion of swimming bacteria) in a range of samples was varied by independently varying α, v or ϕ. Most data was collected varying α while keeping ϕ and v constant, by mixing washed suspensions of WT and mutant (N2, either fliF or motA) diluted to OD=0.5 ($\phi \approx 0.1\%$) at different ratios. Table 3.1 shows a typical range of samples which varied α (total volume of 1ml) prepared in 2ml tubes (Star Lab).

The average speed v was increased by preparing 0.5ml samples at OD=1 and then adding 0.5ml of glucose solution at 0.006 wt% in BMB, immediately before imaging. This resulted in an overall concentration of OD=0.5 and an average motile population speed of $\sim 25 \mu \mathrm{ms}^{-1}$. Motile bacteria are able to utilize glucose to swim faster [85, 92]. DDM returned a flatter $v(q)$ for bacteria in a glucose solution, possible due to one of, or a combination of, three factors. It is possible that the tumbling rate of the bacteria is reduced by glucose, but even if not, at a higher v bacteria would travel further without tumbling. Therefore, tumbling would only influence the v measured at low q (estimated by $q = 2\pi/25 = 0.25 \mu \mathrm{m}^{-1}$), reducing the observed effect of tumbling in the range of averaging. The third possibility is that the increased v biases measurements towards slower bacteria at high q.

A few data points were taken where the overall concentration ϕ was not kept constant. Concentration was varied between OD=0.2 (3.1×10^8 cell/ml) and OD=0.5 (7.8×10^8

cell/ml) at constant α, by mixing 9 parts WT to 1 part motA and adjusting the optical density of both suspensions before mixing. Both ϕ and α were changed by keeping the ratio of WT to fliF constant but changing the ϕ of only the WT suspension before mixing to between OD=0.05 and 0.5 (7.8×10^7 and 7.8×10^8 cell/ml).

A range of samples were prepared before measurements began. The samples were not loaded into the capillaries until immediately before the measurements took place under the microscope. A series of measurements began with a sample containing the WT only (number 10 from Table 3.1) and ended with another measurement of the same sample (from the same tube). All measurements were taken as efficiently as possible, always within ~ 1.5 hours of each other. The motility of *E. coli* in BMB decreases with time (see section 5.2).

Capillaries were prepared, and phase contrast $\times 10$ movies were recorded, in exactly the same way as for a suspension of WT only described above. The phase contrast movies returned v, α (or b) and D_{N1+N2} (the average diffusion coefficient of both non-motile populations combined). Immediately afterwards a $\times 20$ fluorescence movie was recorded in which only the mutant motA or fliF bacteria were visible, returning D_{N2} (the average diffusion coefficient of the N2 population alone). The microscope and software were returned to the settings required for the phase contrast movies before the next sample was loaded into a capillary. Not only was a shutter closed to block any blue light but the filter wheel was turned so that the phase contrast movie was not recorded with filtered light.

The remainder of this chapter discusses possible problems associated with the procedure, and justifications for its use.

3.4.1 Checking the non-motile fraction

A proportion $(20\% - 40\%)$ of the AB1157 cells did not move after the wash procedure. This meant that by adding non-motile mutants using the procedure described above, b (proportion non-motile) was changed in the range $0.2 - 1$ and α (proportion motile) in the range $0 - 0.8$. Using the first measurement of the samples containing AB1157 only (M+N1) for each culture, the proportion of N1 on that particular day could be measured and the expected α or b for each sample calculated.

An example is shown in Figure 3.8 for a range of samples in which ϕ is constant, and the fraction of WT suspension to motA suspension was varied. The b predicted from the first WT only measurement is plotted in red. The b measured for each sample by

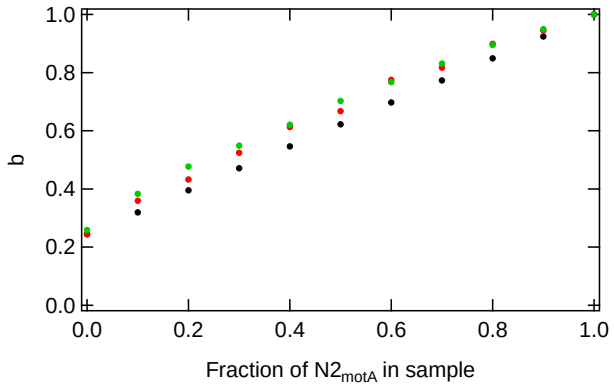

Figure 3.8 Checking the non-motile fraction in samples. b measured by DDM (red), calculated by knowing M:N1 and the composition of the sample (black) and calculated taking time dependence of M:N1 into account (green). Error bars omitted to ease interpretation.

DDM does not follow this line. The disagreement is due to the time dependent nature of N1 in the WT culture. With time, in BMB, the proportion of N1 increases, which is measured with the final WT sample of the series. Taking this time dependence into account by assuming a linear increase, b can be re-calculated and is shown on the graph, reassuringly matching closely with the value measured by DDM.

3.4.2 Fixing procedure

Some fitting difficulties were encountered in the analysis of the phase contrast movies. The difficulty at high proportions of motile bacteria is that the contribution of purely diffusive bacteria to $f(q,\tau)$ is small, resulting in a noisy $D(q)$, shown previously in Figure 3.6. As D of the tracers is measured separately using fluorescence, this is not a concern.

The problem at low proportions of motile bacteria is that they contribute little to the decay of $f(q,\tau)$ which results in very noisy (with q) and lower than expected average values for b and v (Figure 3.9). In order to measure b it is possible to fix the average speed and/or the standard deviation of the speed distribution to values measured for samples from the same bacteria culture but at higher motile proportions. The differences obtained by fixing v and σ to the values obtained from the WT only sample in Figure 3.6 (data taken as part of the same experiment) can be seen in Figure 3.9. Fixing v and σ aids the fit substantially, returning much less noisy measurements of b and D with q, allowing meaningful averages to be taken. These averages depended little on the exact values of the fixed v and σ, within a reasonable range. Averaging over all possible initial times in the DDM analysis of the movie (rather than every

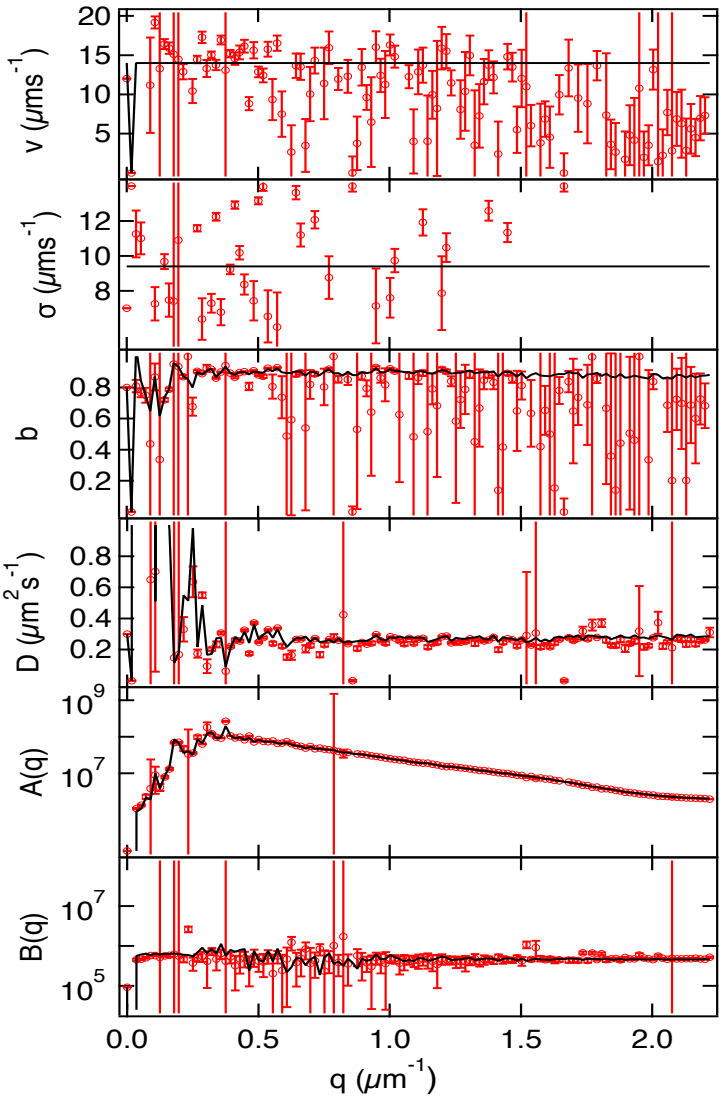

Figure 3.9 Fixing procedure for samples containing a low motile fraction. Free fitted parameters (red symbols) against q for a sample containing 8 parts motA to 2 parts WT *E. coli*. Fitted parameters with v and σ fixed to values from Figure 3.6 (black lines).

third) only improved the appearance of the data marginally, and did not change the average values of b and D measured.

The WT only sample, the analysis of which is presented in Figure 3.9 was composed of 80% motA (N2) and 20% AB1157 (M+N1), therefore b (N1+N2) was expected to be ~0.86. By fixing v and σ, b was measured to be 0.88±0.02, matching that expected within uncertainty. This is an extreme example, samples were not prepared with lower motile fractions than this. For samples with higher proportions of motile bacteria, although the measurement of v and b is made easily, fits were done fixing the same parameters, in order to verify that they did not alter the outcomes.

This fixing procedure relies on the assumption that v of the motile bacteria across all samples is very similar. Given that all the motile bacteria come from the same culture and were washed together this is a fair assumption. As already said, each experiment began and ended with a sample containing WT AB1157 only. Over the time period of the experiment ($\sim 1-2$ hours) the average speed consistently slowed by only $1-2$ μm/s, which was taken into account when fixing speed values for samples measured towards the end of the experiment.

As v is one of the parameters used to quantify the activity of the suspension, it is important to obtain an accurate measurement of it in each sample. As this was not possible, one additional verification that v did not in reality reduce in low α samples was required. Dark Field microscopy was used to measure a series of samples in which α was varied. The technique, described in the following paragraphs, probes the body rotation frequencies of the motile bacteria.

As a consequence of the torque free condition on a swimming bacterium, the rotation of the flagella, driven by the flagella motor, causes the bacterium body to rotate in the opposite direction [20]. The body rotational frequency Ω is expected to be proportional to the swimming speed for a Newtonian fluid, as in the present case [31].

Dark field illumination and imaging of a suspension of swimming *E. coli* results in time dependent fluctuations in image intensity. These result from any wiggling motion of the bacterium's body that causes it to move in and out of the focal plane. Simple models describing the wiggling of a swimming *E. coli* have been analyzed and discussed [95]. Researchers noticed experimentally that the flagella bundle often has an axis of rotation different to that of the body, meaning that each time the body rotates it circles the axis of motion once, causing a wiggle of frequency Ω.

A recently developed dark field microscopy method was used to measure Ω [66, 96]. The method is higher throughput and faster than previous measurements of Ω, which have been a laborious processes undertaken on single cells [31, 95, 97, 98].

An image sequence was recorded using dark field illumination with $\times 10$ magnification (Figure 3.10(a)), by turning the condenser to PH3, increasing the frame rate to 500 frames per second and turning the light source high. Roughly 3500 frames at frame size 500 pixels were recorded, resulting in a ~ 3 second movie. The dark field image sequences were processed by dividing each frame into square tiles of length 5 pixels. The pixel values in each tile were summed to give a single value, and this was repeated for each image, to give a tile intensity which changed over time. The power spectrum of each tile was calculated separately and then all the tiles were averaged to give a final

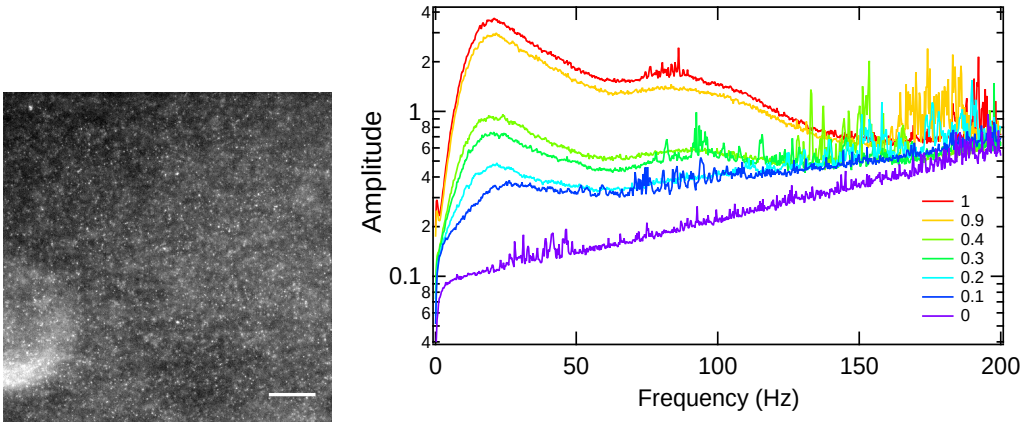

(a) (b)

Figure 3.10 Dark field microscopy. (a) Single dark field imaged frame of size 500×500 pixel, recorded at 10× magnification. Scale bar=100μm. (b) Dark Field power spectra of 7 samples composed of a fraction WT suspension (OD=0.5) shown in the legend. The remainder of each sample was composed of motA suspension (OD=0.5).

curve, averaging contributions from $\sim 10^4$ bacteria.

The power spectra of samples whose composition are described in the legend, are shown in Figure 3.10(b). There are two peaks in the power spectrum. It was originally thought that a higher frequency peak observed experimentally was the flagella frequency, but more recently, theoretical work taking the peritrichious nature of the flagella into account, suggests that the high frequency peak observed is more likely to be a higher harmonic of the body rotational frequency [96]. There is no sign that the position of the first peak, due to the body rotation [66, 96], shifts to lower frequencies at lower fractions of motile bacteria. This finding confirms that the swimming speed is similar within the range of swimmer concentrations in these samples, if they contain WT bacteria from the same culture. Finally, for samples where a direct measurement of v is not possible, the uncertainty in the average speed used to calculate J_A reflects this.

3.4.3 Swimming in fluorescent light

Had irradiation by light of wavelength $450 - 490$ nm (GFP excitation) influenced the behaviour of any of the sample components, then the protocol described for experiments on enhanced diffusion could not have been used. To verify that this was not the case, phase contrast movies were recorded following the standard procedure for analysis with DDM, but with the sample also being irradiated by GFP filtered light.

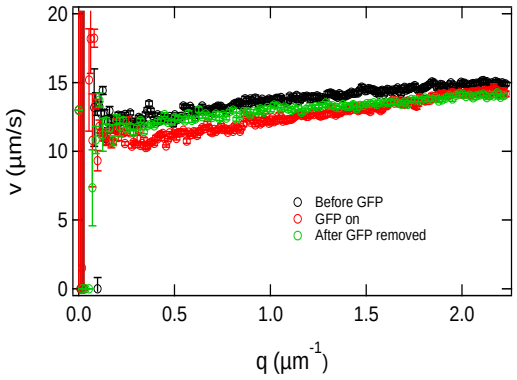

Figure 3.11 Swimming in fluorescent light. Average swimming speed v against q from DDM analysis of a sample before, during and after being exposed to 40 seconds of $450 - 490$ nm wavelength light.

Both the proportion of non-motile cells and their diffusion were unaffected by the light. Figure 3.11 shows $v(q)$ data for a sample of WT only before being irradiated with GFP excitation wavelengths, during, and afterwards. The sample was loaded into the capillary, a movie was recorded following the usual procedure, saved and then the GFP light was turned on (at maximum intensity) for the duration of another movie (40 seconds). The light was then turned off while this movie was saved and a final movie was recorded. While being irradiated, the gradient of $v(q)$ is influenced slightly, reducing the average speed by $1 - 2\mu$m/s. Thirty seconds after the light is removed $v(q)$ has returned to within uncertainty of pre-irradiation.

Each day that fluorescence microscopy was used, the speed during exposure was again verified and a decrease of $1 - 2\mu$m/s was the largest effect seen. In general, the effect of the light was deemed insignificant. It was verified that if all results shown in the following chapter were adjusted according to the maximum effect on v witnessed, the conclusions of the study are not influenced.

Interestingly, although not of direct relevance to this study, CFP (Cyan Fluorescent Protein) excitation wavelengths ($425 - 445$ nm) cause a steep $v(q)$ at early times, believed to indicate an increased tumble rate. After $\sim$ 4 min irradiation v slows considerably and loses the dependence on q.

These findings were not unexpected, light between 390nm and 530nm was shown to affect the motility of both *Salmonella* and *E. coli* in 1975 [99]. On prolonged exposure to bright unfiltered light cells became constantly tumbling, then smooth swimming, then were paralysed. It was found that if the light was filtered to exclude the wavelengths 390-530nm the bacteria swam normally. This range incorporates both GFP and CFP

wavelengths. The results presented here suggest that wavelengths below 450nm affect the motility of *E. coli* more than those between 450 and 530nm, but further work would be needed to quantify this statement.

3.4.4 Fluorescence measurements

Due to the protocol used, the overall density of the tracer population N2 varied between samples. For samples with high proportions of motile cells, and hence a high activity, the number of fluorescent non-motile bacteria was as low as 7.5×10^7 cell/ml. As fewer cells meant a lower signal, measuring D was more difficult. Consequently, a check that the measurement of $D_{0,N2}$ (the Brownian diffusion coefficient of the N2 population) was density independent was required.

Fluorescent measurements of $D(q)$ for motA in BMB are shown in Figure 3.12(a) for OD=0.5, 0.25 and 0.05. In the range $1 < q < 2.5\mu\text{m}^{-1}$ all three traces agree within error. At $q > 2.5\mu\text{m}^{-1}$, D drops for the lowest density sample (OD=0.05) and at $q > 3.5\mu\text{m}^{-1}$ D drops for all three samples. Again, the lowest density is an extreme example, only a couple of samples were measured at N2 densities this low, requiring averages to be taken below $q = 2.5\mu\text{m}^{-1}$. For the majority of samples D was averaged in the range $1 < q < 3\mu\text{m}^{-1}$ with a visual check that D was q independent in this range.

Observation of the reconstructed $f(q, \tau)$ at OD=0.05 hints at an additional contribution to the decay at long times for high q, invalidating the diffusive fit (Figure 3.12(c)). The density dependence of the effect suggests it may be due to number fluctuations. Significant changes in the number of diffusers (N) at the length-scale of observation (scaling as $\sqrt{N}$) make definition of the baseline difficult. At each length-scale, or q, there are ten times more diffusers at OD=0.5 than OD=0.05, therefore the onset of the effect is at a lower q (higher length scale) for the lower density.

Another potential cause of the D measurement failure at high q is demonstrated in Figure 3.12(b) where $A(q)$ and $B(q)$ are plotted for each of the samples for which $D(q)$ is plotted in Figure 3.12(a). As the density of motA increases, the point at which $A(q)$ intercepts $B(q)$ moves to higher q. This can be interpreted as a measure of the ratio of signal to camera noise. Camera noise becomes larger than the signal at a much lower q for the lowest density, increasing difficulty in fitting $f(q, \tau)$.

At the black level (BL) minimum of BL=50 it was not possible to see the tracers by eye at a frame-rate of 20 fps, so the BL was increased. To check that the exact black

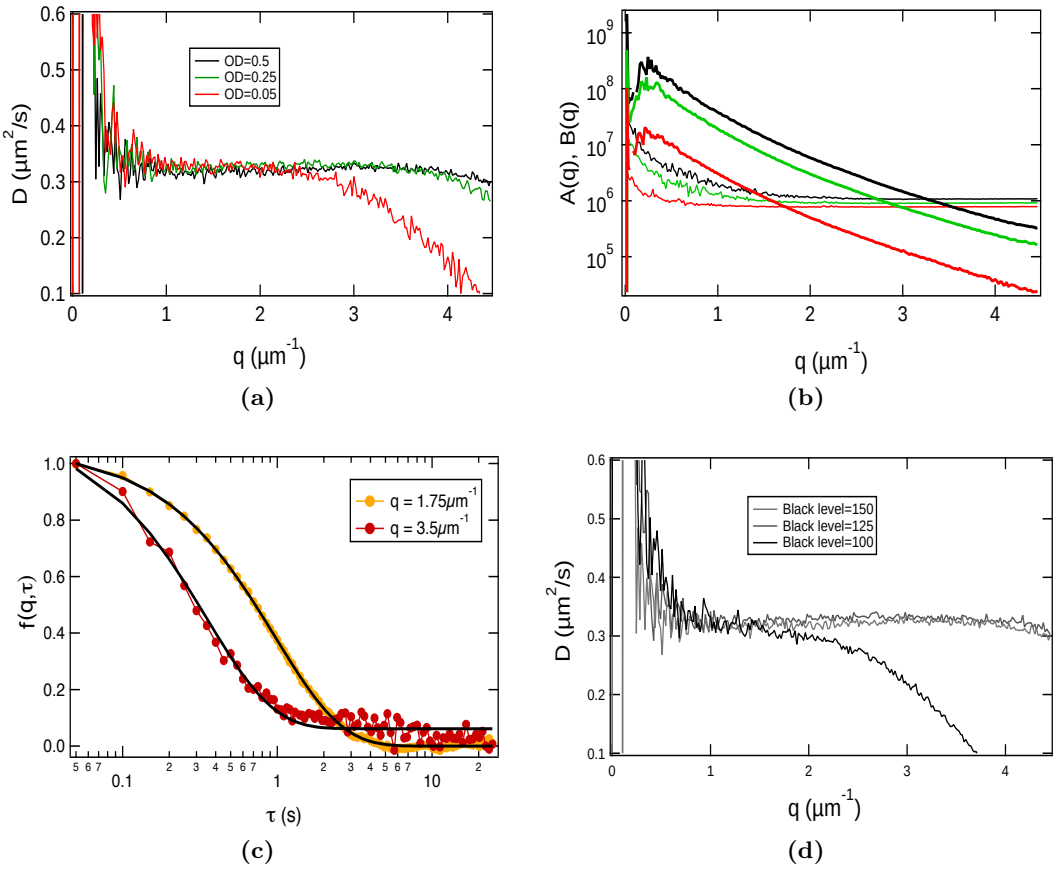

Figure 3.12 Measuring D with fluorescence. (a) $D_{0,N2}$ and (b) A (thick line), B (thin line) plotted against q for samples containing mutant motA at optical densities shown in the legend. (c) Reconstructed ISF at two values of q for OD=0.05. (d) $D_{0,N2}$ against q at three different black levels for the same sample of motA at OD = 0.5.

level chosen did not influence the measurement of D, three movies of the OD=0.5 samples were taken at different BLs. At BL=100 the signal was not strong enough to measure D, possibly due to number fluctuations in the low number of bright cells imaged. However, at both BLs tested above BL=100 the $D(q)$ traces agreed (Figure 3.12(d)). This was also checked for lower densities, which confirmed that BLs in the range of $125 - 150$ were sufficient for a measurement of D.

Chapter 4

Results, Discussion and Conclusion: Enhanced diffusion

This chapter is split into two sections. The first section presents the results obtained on the enhanced diffusion of non-motile bacteria in an active suspension. The second section discusses the results and draws conclusions from the findings.

4.1 Results: The enhanced diffusion of non-motile bacteria

The protocol followed for experiments on the enhanced diffusion of fluorescent, non-motile, mutant tracers was presented in Chapter 3. In this section, an example of raw data collected following this protocol is presented. This is followed by results of the analysis for all data sets. In the course of this study it was noticed that these measurements could provide information on the nature and enhanced diffusion of the native non-motile AB1157 (N1). Results from experiments designed to yield this information are shown after those on the enhanced diffusion of the non-motile mutants.

4.1.1 The Intermediate Scattering Functions measured with DDM

Figure 4.1(a+b) shows the measured ISFs, for $q = 0.53 - 2.22\mu\text{m}^{-1}$, obtained from a phase-contrast movie of a sample composed of 7 parts WT AB1157 (M+N1) to 3 parts motA (N2). There are two clear contributions to the decay, the ballistic component,

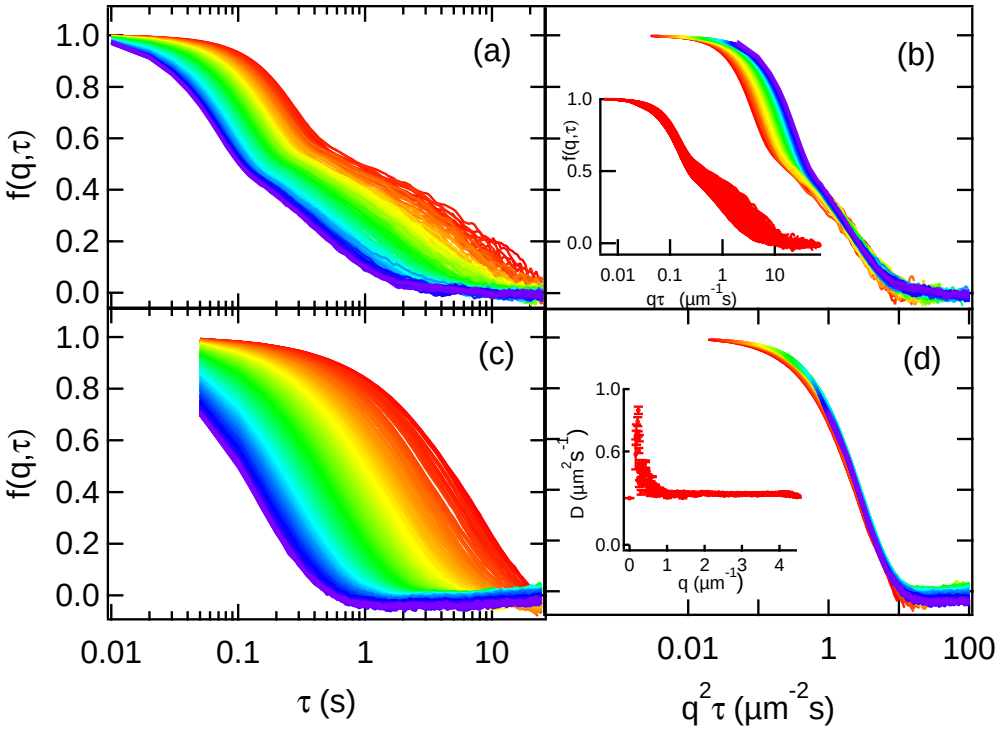

Figure 4.1 Measured ISFs, (a+b) from phase contrast movie of a sample containing $\alpha \sim 0.5$ and $v \sim 15\mu\text{m}/s$ at $\phi = 0.1\%$. Plotted against (a)τ (b) $q^2\tau$ showing diffusive decay collapsing (inset) $q\tau$ showing ballistic decay collapsing. q increases in a rainbow scale from red $q = 0.53$ to purple $q = 2.22\mu\text{m}^{-1}$. (c+d) Measured ISF from the fluorescence movie of the same sample plotted against and (c)τ (d) $q^2\tau$, showing decay due to diffusion collapsing. q increases in a rainbow scale from red $q = 0.62$ to purple $q = 4.46\mu\text{m}^{-1}$.

collapsing against $q\tau$ (shown in the inset of Figure 4.1(b)), and the diffusive component collapsing against $q^2\tau$ (Figure 4.1(b)). Despite there being two non-motile populations in the sample (N1 and N2), only one apparent diffusive process is measured, indicated that the diffusion constants, D_{N1} and D_{N2}, are too close to be differentiated. Fitting of the $g(q,\tau)$ functions returns $\alpha = 0.48 \pm 0.02$, $v = 14.8 \pm 0.3\mu m/s$ and $D_{N1+N2} = 0.37 \pm 0.02\mu\text{m}^2/\text{s}$.

Figure 4.1(c+d) shows the ISFs for $q = 0.62 - 4.46\mu\text{m}^{-1}$, from a fluorescent movie of the same sample, in which only N2 is visible. The τ range begins at 0.05 seconds rather than 0.01 seconds as the frame-rate was reduced to 20fps for the fluorescent movie. The q range is twice as wide as for the phase contrast movie, as the magnification was doubled. The collapse against $q^2\tau$ over such a large q-range confirms that although the tracer movement may be super-diffusive on short timescales, this method of analysis allows a measurement of the long-time dynamics and therefore the effective diffusion coefficient.

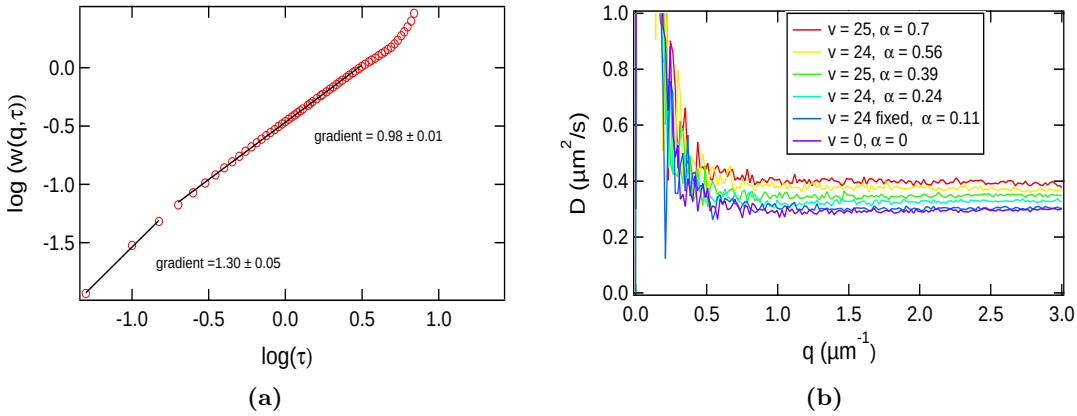

Figure 4.2 The width function plotted for a single q value and $D(q)$ plotted for 8 samples. (a) Log$(w(q,t))$ plotted against log(τ) at q=1.31μm^{-1}. Best fit lines fitted by Igor Pro, with corresponding gradient stated alongside. (b) Fitted $D(q)$ from 8 fluorescence movies of samples with varying α. Values for v (in μm/s) and α ($\alpha = 1 - b$), obtained from the phase contrast movie of each sample, are shown in the legend. For clarity, these are samples which contain glucose, in order that the effect on D_{N2}^{motA} can be seen easily.

As a check, log$(w(q,\tau))$ was plotted against log(τ) (Figure 4.2(a)), where the width function $w(q,\tau)$ = -ln$(f(q,\tau))/q^2$ [100, 101]. By analogy with the mean squared displacement, any deviation from a slope of one signifies deviation from diffusive behavior. This plot is shown for a single value of q in Figure 4.2. A hint of super-diffusion is seen at short times, but after $\tau \sim 0.2$ seconds (log$(\tau) \sim -0.7$) the slope is measured to be ~ 1. Plots at other q values, within the range of averaging, demonstrate similar, overlapping curves.

Fitting of the corresponding $g(q,\tau)$ functions to the ISFs shown in Figure 4.1(c) returns $D_{N2}(q)$, as shown in inset of Figure 4.1(d). Averaging over $1 < q < 3$ μm^{-1} gives $D_{N2}^{motA} = 0.326 \pm 0.003$ μm^2/s. The diffusion coefficient of N2 alone does not agree with that of N1+N2. This discrepancy is the subject of the section 4.1.3; in this section it is the measurements of D_{N2} which are of interest.

The analysis detailed above was applied to all samples prepared as described in the methods section. Figure 4.2(b) shows $D(q)$ for 8 samples at $\phi = 0.1\%$ (OD=0.5), where $v \approx 25\mu$m/s (glucose added) and α varied between 0 and 0.7. As the activity of the fluid is increased by increasing α, D_{N2} rises but remains q independent in the averaged range. The values of D_{N2} quoted in the next section are averages over the q range, with their corresponding standard deviation.

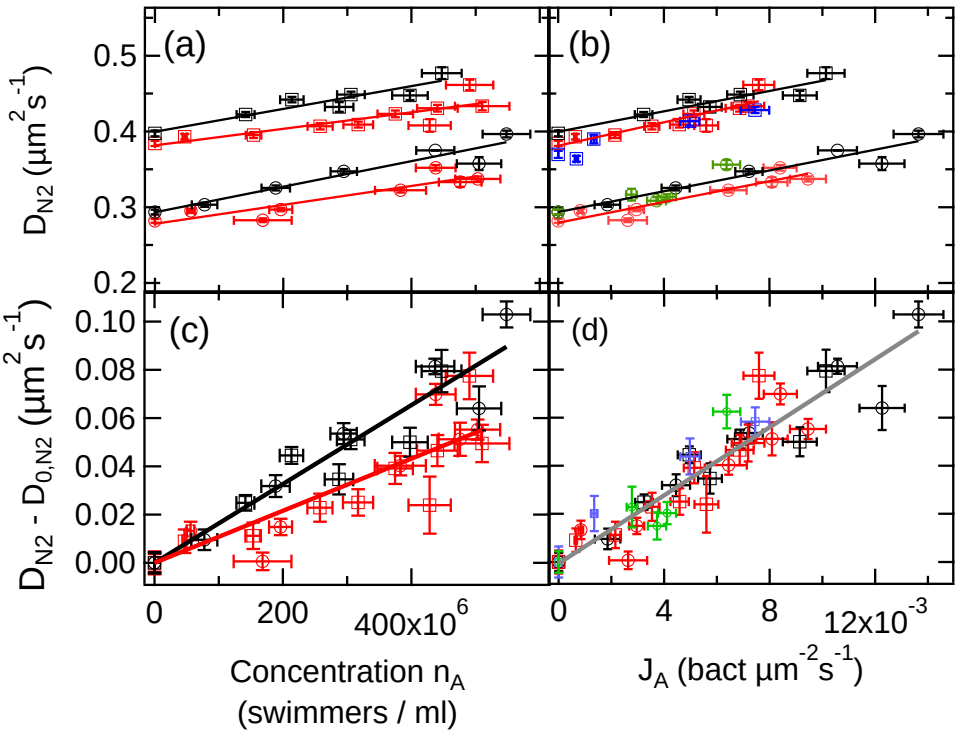

Figure 4.3 Enhanced diffusion of passive tracer bacteria measured as a function of n_A and J_A. (a) and (b) plot D_{N2} of motA (circles) and fliF (squares) in suspensions of AB1157 containing no glucose (red) or glucose (black), while α is varied. Best fit lines fit each bacteria at each speed separately. Green and blue points correspond to data taken varying ϕ or both ϕ and α. (c) and (d) plot the enhancement of D above D_0 for both motA and fliF data with and without glucose in the sample. Best fit lines fit all red data (motA+fliF) and all black data (motA+fliF). The error bars are one standard deviation.

4.1.2 Diffusion of fluorescent, non-motile bacteria

Figure 4.3 shows the enhanced diffusion of non-motile mutants motA (circles) and fliF (squares) in a bath of motile WT swimmers, without glucose (red) or with glucose (black). The same four data sets are plotted four different ways, D_{N2} against both n_A and J_A and $D_{N2} - D_{0,N2}$ against both n_A and J_A (recall that $D_{0,N2}$ is the Brownian diffusion coefficient of the N2 population). All of the information is contained in (a) and (d) alone, but providing (b) and (c) in addition eases interpretation.

Firstly, the non-motile mutants do not have matching Brownian diffusion coefficients. It was found that $D_{0,N2}^{fliF} = 0.39 \pm 0.02 \mu\text{m}^2/\text{s} \approx 1.4 \times D_{0,N2}^{motA}$ in absence of swimmers indicating that the effective hydrodynamic radius of fliF is ~ 1.4 times smaller, as Tavaddod *et al.* [46] found for de-flagellated mutants. Although the D_0 of both non-motile strains varied between days due to different cultures and sensitivity to temperature, there was always a significant difference between the two strains. Note

that in the calculation of $D_{N2}-D_{0,N2}$, $D_{0,N2}$ is taken as the measurement of the mutant suspension alone during the same experiment *i.e.* from the same culture, within ∼60 minutes of all other measurements. From Figures 4.3 (a+b) it appears that adding glucose to non-motile cells increases $D_{0,N2}$. This was not the case, $D_{0,N2}$ happened to be higher from the culture grown on those days, whether glucose was added or not.

As the number of swimming bacteria per sample $n_A = \phi\alpha$ (with ϕ in units of cell/ml) increases with increasing α (constant ϕ and v), the average D_{N2} of the tracer population, either motA or fliF rises *i.e.* their diffusion was enhanced. When plotted against n_A ((a+c)), there is a linear increase of D_{N2} at each of the swimmer speeds, with a clear separation between the two. This is most evident in Figure 4.3(c) where the difference between D and D_0 has been plotted. For a given α, and therefore a given n_A, the faster the average speed of the swimming bacteria, the larger the enhancement.

When D_{N2} is plotted against J_A in Figure 4.3(b), all four data sets have very similar gradients β. Interestingly, despite the difference in their nature, motA and fliF are enhanced to the same extent. This has been shown previously for 1 and 2μm tracers next to wall [62], but nevertheless is intuitively surprising as motA has passive flagella distributed around the cell body.

Panel (b+d) include additional data taken for motA, varying ϕ while at constant α and v (green), and for fliF varying both ϕ and α (blue), in order to verify the dependence on J_A rather than any of the individual variables. This data agrees well, confirming also that the concentration of tracer bacteria does not affect their diffusion; they are independent diffusers as expected from section 3.4.4.

When the enhancement $D-D_0$ is plotted against J_A in Figure 4.3(d), all data collapses onto the same line, as expected from previous experimental work [62] and theoretical work [69]. An unweighted free fit through all of the data, shown on the figure as a grey line, gives a gradient $\beta = 7.1 \pm 0.4\mu\text{m}^4$ and an intercept of $-0.0006 \pm 0.002\mu\text{m}^2 s^{-1}$. Fixing the line to pass through (0,0) changes the gradient to $7.0 \pm 0.2\mu m^4$, while weighting with the errors in enhancement changes the free fit gradient to $7.3 \pm 0.2\mu m^4$ and the fixed intercept gradient to $7.1 \pm 0.1\mu\text{m}^4$. Although the uncertainties in D are not Gaussian but come from averaging separate measurements at different length-scales, noise in the measurement is close to being Gaussian (verified for some $D(q)$ traces). If all four data sets are fitted separately (without the blue and green data points) then an average of their gradients gives $\beta = 7.0 \pm 0.5\mu\text{m}^4$. As all of these alternative fits give values of β within the uncertainty of the free fit, the gradient of the free fit is quoted as our measurement of β.

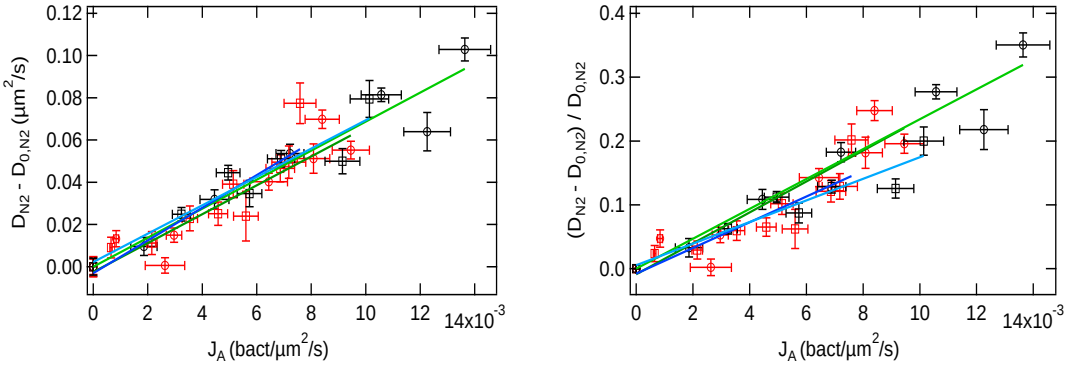

(a) **(b)**

Figure 4.4 Collapse of the data normalised *vs* un-normalised. Enhanced diffusion of motA (circles) and fliF (squares) in suspensions of AB1157 containing no glucose (red) or glucose (black), plotted against J_A (a) un-normalised to D_0,(b) normalised to D_0. Best fit lines to fliF data (green) and motA (blue) without glucose (dark) and with glucose (light).

To justify the collapse of $D - D_0$, as Miño and co-workers used previously, rather than $(D - D_0)/D_0$, both are plotted for all four data sets in Figure 4.4. If non-glucose (black) and glucose (red) data is fitted together, it appears by eye as if the collapse is as good as in Figure 4.3(d) (not shown). However, best fit lines fitted to each data set separately demonstrate a separation between motA and fliF data if $(D - D_0)/D_0$ is plotted (Figure 4.4(b)), whereas there is no separation if $D - D_0$ is plotted (Figure 4.4(a)).

To summarize, the data supports the use of the equation $D = D_0 + \beta J_A$ to describe the enhanced diffusion of passive tracers in a 3D bath of swimming *E. coli*, with β measured to be $7.1 \pm 0.4 \mu m^4$.

4.1.3 Diffusion of all non-motile bacteria

The average diffusion coefficient measured by the phase contrast movies, rather than the fluorescent movies, is presented in Figures 4.5 for selected data sets. Despite both N1 and N2 contributing to the decay of the ISF it is only possible to measure one diffusive process (shown in Figure 4.1). Theoretical ISFs were built for a motile population and two non-motile populations with differing diffusion coefficients. Fitting the built ISFs confirmed that for two differing Ds within the range anticipated as plausible for non-motile cells, the two populations could not be fit separately. The D obtained from fitting the theoretical ISF with a single diffusive process was between those of the two populations.

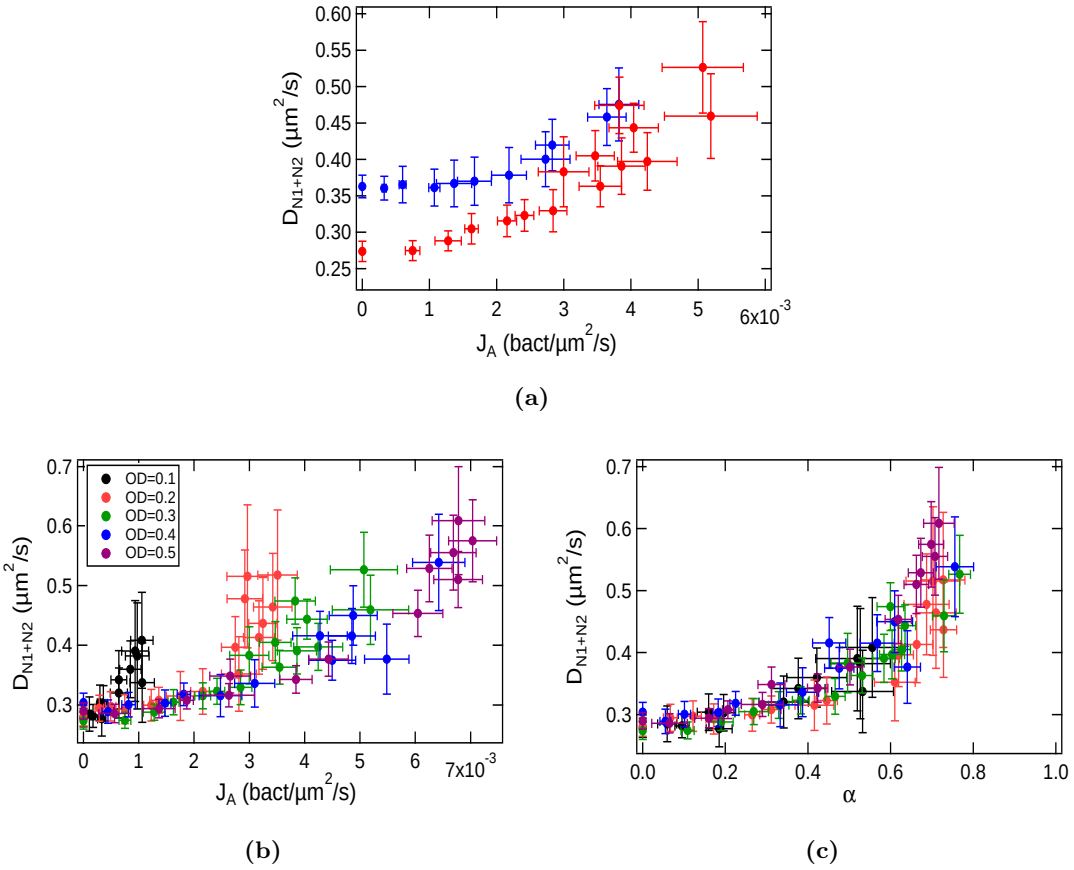

Figure 4.5 Diffusion coefficients measured from phase contrast movies. (a) D_{N1+N2} for N2= motA (red) and N2= fliF (blue). (b) D_{N1+N2} for N2=motA at 5 different concentrations plotted against J_A and (c) α.

D_{N1+N2} shows a different pattern of enhancement plotted against J_A than the D_{N2} data discussed already. D_{N1+N2} for the same samples (or identical preparations) as the black data in Figure 4.3 where J_A was varied by varying α in the samples (constant ϕ and v (no glucose)), do not show linear enhancement with J_A. Furthermore, flif and motA no longer show the same shape of enhancement, with D^{fliF}_{N1+N2} showing no enhancement until higher values of J_A than D^{motA}_{N1+N2} (subtle but reproducible).

Further measurements of D_{N1+N2} were made for motA by varying α in samples at 5 different values of ϕ between OD=0.1 (1.55×10^8cell/ml) and 0.5 (7.75×10^8cell/ml), the results of which are shown in Figure 4.5(b). The data no longer collapses against J_A but shows a strong dependence on α which can be seen in Figure 4.5(c).

In order to explain why these results are different from those in the previous section, information about the population N1 was needed. The N1 population are non-swimming AB1157 bacteria which are present in a suspension where the majority of cells were motile. From measurements of exponentially growing, unwashed AB1157

in TB, it is known that prior to being transferred into motility medium $\alpha \approx 0.9$. After the washing procedure α decreases to $0.6 - 0.8$ (see Chapter 5 for discussion of this decrease). Therefore, N1 is a combination of cells which were non-motile during growth and cells which lost motility during the wash. To investigate the N1 cells alone, separating them from motile cells was considered, but in the timescale necessary was deemed impractical.

Two approaches were used to explore D_{N1}. Firstly, it was necessary to verify that the diffusion coefficient of a WT AB1157 was not measurably different to its motA mutant. This was done using formaldehyde to kill cells. Secondly, it is observed from Figure 4.5(b) that D_{N1+N2} recorded at the highest J_A for each ϕ show a dependence on concentration. These points correspond to samples containing no mutant population, therefore D_{N1+N2}=D_{N1}. Thus, a series of samples containing WT bacteria only were measured at differing ϕ to confirm the dependence.

Diffusion of bacteria killed with formaldehyde

Given that motA is a mutant of AB1157, a non-motile, undamaged AB1157 bacterium is expected to have the same hydrodynamic radius as motA. To verify that this was the case, formaldehyde was used to kill the cells. Formaldehyde did not influence D_0^{motA} within error. AB1157 lost motility (and viability) in formaldehyde and their D_0 was measured to be within uncertainty of D_0^{motA}. As up to 80% would have displayed motility when viable, these cells dominate the measurement of D, giving us no further information about the N1 population. Nevertheless, it proves that there is no measurable difference in hydrodynamic radius between the two strains.

FliF and fliC (a mutant possessing a hook, but no flagella) had similar D_0, both dead and alive. For the three non-motile mutants, although the dead D_0 was within the error bars of D_0 for the alive cells, it was marginally lower in each case. Whilst not relevant to this project, the cause of the slight change of D_0 with viability could be an interesting avenue to pursue as it has been suggested previously by Tavaddod *et al* (unpublished). These researchers believe that the active channels covering the outer membrane of an alive bacterium could form local jets of fluid, resulting in a small ballistic contribution to their mean squared displacement, and a higher measurement of D.

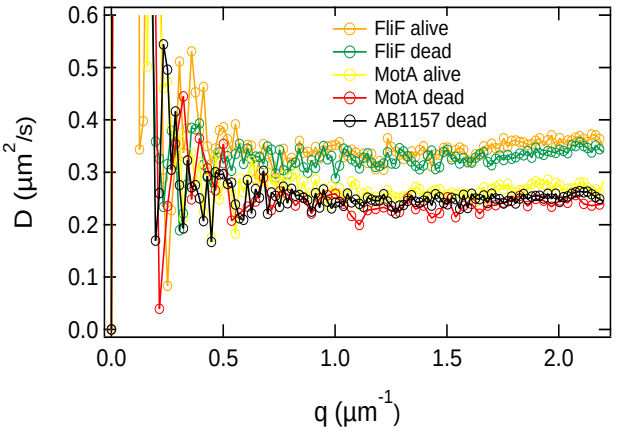

Figure 4.6 $D(q)$ measured by DDM for viable and un-viable bacteria of the same strain (specified in legend).

The inferred diffusion constant of the native non-motile population

To obtain $D_{0,N1}$ alone, without any enhancement due to the motile cells, a series of dilutions of the same WT AB1157 washed culture were made, preparing suspensions between OD=0.01 and 0.5 (ϕ=0.002-0.1%). This varied J_A in a series of measurements by varying ϕ, without changing α or v (small changes in these parameters with density is the subject of further research currently).

D_{N1} is shown in orange on Figure 4.7(a). Points at low values of J_A are noisy, in part due to the difficulty of fitting the diffusive part of the measured ISF at densities this low (OD=0.01 M+N1). It is clear that $D_{0,N1}$ is significantly higher than $D_{0,N2}^{motA}$ and is closer to $D_{0,N2}^{fliF}$. A best fit line to this data has an intercept of 0.37 $\pm$ 0.02 μm^2/s, within error of $D_{0,N2}^{fliF}$, suggesting that N1 are non-motile due to a lack of flagella. Their flagella may never have grown or have been sheared off during the washing procedure.

D_{N2} (green and black) from fluorescence measurements and D_{N1+N2} from phase contrast measurements at OD=0.5 (blue and red) are plotted alongside D_{N1} for comparison. While D_{N1} is enhanced linearly with J_A, the enhancement gradient β is larger than that of either motA or fliF. This feature provides an explanation for the shape of the D_{N1+N2} with J_A curve. Given the experimental protocol, the ratio of N1 to N2 increases as J_A is increased by increasing α in a series of samples. As N1 and N2 have a differing D behavior with J_A, the protocol leads to the dependence on α observed. In addition it accounts for why at low α D_{N2}^{fliF} does not increase as rapidly as D_{N2}^{motA}. The addition of a small proportion of WT bacteria to motA not only enhances their diffusion with activity, but increases the diffusion measured in phase contrast due

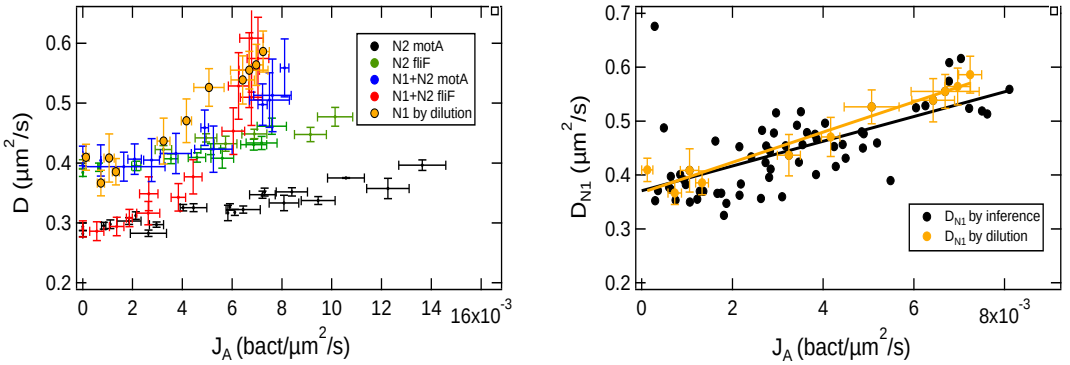

(a) **(b)**

Figure 4.7 Diffusion coefficient of the native non-motile population. (a) D_{N1} obtained by dilution (orange), plotted alongside D_{N1+N2} (blue and red) and D_{N2} (green and black) (b) D_{N1} obtained by inference from D_{N1+N2} and D_{N2} results (black) and D_{N1} obtained by dilution (orange).

to N1 having a higher Brownian diffusion coefficient.

By assuming that D_{N1+N2} measured is a straightforward average of the two populations, according to the ratio of their amount in the sample, and by knowing the dependence of D_{N2} on J_A, D_{N1} can be inferred from the results of a phase contrast movie. To illustrate, for a sample composed of motA and WT in a ratio of 3:7, with $\alpha = 0.7$ in the WT solution, the ratio of all 3 populations M:N1:N2 is 49:21:30. Knowing α, ϕ and v, J_A can be calculated and hence D_{N2} from $D = D_0 + 7.1 J_A$. D_{N1+N2} is composed of N1 and N2 at a ratio of 21 to 30, so D_{N1} can be calculated.

D_{N1} was calculated for all of the data shown in Figures 4.5(a+b) and plotted alongside the measurements made by dilution in Figure 4.7(b). All D_{N1+N2} points below $D_{0,N2}$ for the data series (due to noise in the measurement of no enhancement) were neglected, as they would lead to a prediction of D_{N1} far below what is reasonable. Despite being scattered, the data points roughly follow the orange data points obtained by dilution. Best fit lines fitted to each set of data agree on the intercept $D_{0,N1}$ within error, and give $\beta = 28 \pm 2 \mu m^4$ (dilution) and $\beta = 23 \pm 3 \mu m^4$ (inference).

To improve the estimate of β for N1 more experimental data would be needed, but the data presented is sufficient to establish that β is significantly above that of the non-motile mutants. This is a surprising result, which suggests the nature of the interactions between swimmer and N1 diffuser are different than those between swimmer and non-motile mutants.

4.2 Discussion and Conclusion

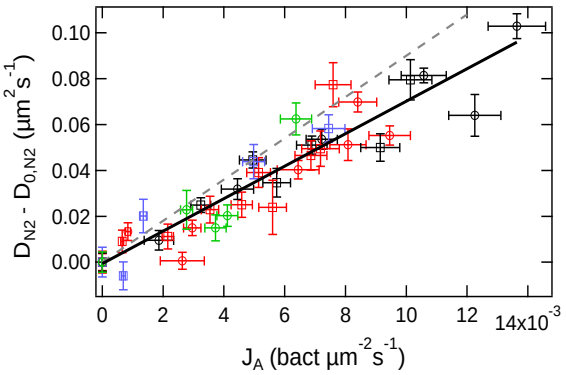

Figure 4.8 Comparing enhanced diffusion results with a prediction from the literature. Figure 4.3 (d) replotted with a best fit line through all data (black) and a line of gradient $\beta = 9\mu\text{m}^4$ (grey dashed), representing the prediction in [72].

The enhanced diffusion of passive bacteria in dilute suspensions of *E. coli* in 3D was found by this study to scale with activity flux, as it does next to a wall [62, 63]. The prefactor β was measured to be $7.1\pm\ 0.4\mu\text{m}^4$. These results are in agreement with the numerical simulations performed in collaboration with this work, published in [1], with further details presented by Morozov and Marenduzzo in [40]. The theory considered the far-field advection of tracers in a dilute suspension of run and tumble *E. coli*, predicting a β of $7.19\mu\text{m}^4$.

The theoretical work of Miño *et al.* [63] predicted a β of $0.48\mu\text{m}^4$ in 3D for non-tumbling *E. coli*, far below that measured here. This disagreement highlights the importance of swimmer tumbles in the enhanced diffusion of tracer particles in this system. For the theory of run and tumble swimmers in [1] and [40] the typical run-length of wild-type *E. coli* was used in the calculation of β, for a comparison with the experimental results presented here. Incidentally, simulations showed that this run-length was close to maximising the enhanced diffusion of passive tracers in a dilute suspension. It may be that the run-length of wild-type *E. coli* evolved from a need to increase the diffusion of passive particles in their vicinity, as well as being driven by chemotaxis [40].

Pushkin *et al.* [72] incorporated near field trapping of particles in a swimmer wake to their analytical theory and predicted a β of $\sim 9\mu\text{m}^4$. The incompatibility of this prediction (highlighted by Figure 4.8) with the results presented, suggests that near field interactions do not raise β by 15% in this environment, contrary to the belief of these researchers. Note that a weakness of all theoretical β predictions is that the active particles swim with a single speed rather than a distribution of speeds, as is observed

experimentally.

Despite motA possessing inactive flagella $\sim 10\mu$m in length, its β measured was the same as that measured for de-flagellated fliF. This implies [1] that both tracers are in the 'PIV regime' (Particle Imaging Velocimetry), a regime where small particles follow the streamlines of a flow field. Particles leave the PIV regime when corrections, scaling as $(R/l)^2$ [102] (due to size (R) and average swimmer-tracer distance (l)), approach 1. For motA ($R \sim 10\mu$m) at the cell concentration used $(R/l)^2 \sim 0.5$. Therefore, it is anticipated that by increasing the total bacterial concentrations as little as $3\times$ above that used in this study, motA will leave the PIV regime and the physics of enhanced motion will change. This is the subject of a further investigation in the group.

There were some limitations and weaknesses to the methods used in this study. Although bacteria containing a fluorescent plasmid provided sufficient signal for measurement with DDM, other fluorescent strains with a weaker fluorescent signal did not. Additionally, no experimental verification that glucose did not influence the tumble rate was possible. Glucose is a chemo-attractant and *E. coli* are able to change their swimming behavior within seconds of an external stimulus being applied [103]. A high-throughput, rapid method to quantify the tumble rate, as part of, or alongside DDM measurements, could yield valuable information.

It was found that non-motile AB1157 have a Brownian diffusion coefficient closer to that of de-flagellated *E. coli* than flagellated cells. Their diffusion was enhanced to a greater extent by suspension activity than that of either fliF or motA. In a preliminary data set, Miño *et al.* [67] also found that the non-motile bacteria in his samples displayed enhanced diffusion with a higher β ($81 \pm 5\mu\text{m}^4$), than measured for the passive tracers. Note that in Wilson *et al.* [13] D_{N1+N2} was plotted, and it was assumed that N1 and N2 populations were identical, which is not the case.

The findings presented suggest that the N1 cells interact differently with the swimmers than the N2 tracer population. It is possible that although the motion of N1 cells can be assigned a diffusion coefficient, they are not passive. If flagella shearing has resulted in the loss of whole or part flagella, then constant tumbling or twitching motions may result.

Further study to determine the cause, both of the N1 population and the mechanism of their enhanced diffusion, is important avenue of future exploration. All studies utilising motile *E. coli*, for the study of bacterial motility or active suspensions, would benefit from further understanding, as this population is always present in samples. Fluorescent microscopy of the flagella could provide information on the nature of the

non-motile cells.

Measurements in 3D were facilitated by DDM. Despite advantages of using this technique over tracking in the study of enhanced diffusion, there remain outstanding questions raised by the analysis. For example, when measuring low concentrations of swimmers or diffusers it would be informative to quantify the effect of number fluctuations on the ISF. In addition to further DDM measurements, future study of the same system with tracking could indicate whether the trajectories observed experimentally are loop-like, as expected from theoretical work [40].

The natural progression to this study would be the investigation of more concentrated suspensions. As already mentioned, the physics of enhanced diffusion will change as near-field interactions between tracer and swimmer become more important. Higher concentrations of swimmers result in collective motion, rather than independent swimming. In this regime, the enhanced motion of tracers is unlikely to be characterised by a diffusion coefficient. Furthermore, it would be interesting to work at a high enough concentration of non-motile particles that they begin to interact with each other.

There have been two further publications on the topic of enhanced diffusion since the completion of this study. Pushkin *et al.* [104] have investigated confined enhanced diffusion theoretically and found that enhancement decreases as the system size decreases. When the system size is 0.8 times that of the bacterial run-length, enhancement is reduced by a factor of two compared to that in an un-confined system. An experimental study of confined geometries would require careful characterisation of the distribution of activity within them. There has been work in the group on motile *E. coli* in emulsion droplets [86]. The bacterial distribution within the droplet depends both on the size of the droplet and the density of bacteria. Now characterised, this system may prove a useful environment in which to add tracers and study confined enhanced diffusion. It is possible to apply DDM to a field of view containing several droplets, but as yet controlling the size of the droplets and the density of bacteria within them has not been possible.

Molina and Yamamoto [105] have numerically simulated a suspension of squirmers (both pushers and pullers) and have recovered a scaling with activity for the effective hydrodynamic diffusion coefficient of the swimmers, as well as the tracers. Their simulations indicate that D of the swimmers has a gradient close to one with activity, while D of the tracers agreed with that of the swimmers at higher activities but was lower at low activities (ϕ <0.05). Extracting the translational diffusion coefficient of the swimmers is not currently possible using DDM, as non-motile cells, always present

dominate the diffusive contribution to the ISF.

In conclusion, this study represents the first measurement of enhanced diffusion in a 3D *E. coli* suspension with DDM. It confirmed that the diffusion of passive non-motile bacteria is enhanced with the activity of the suspension and measured β to be 7.1$\pm$ 0.4μm^4. The findings were in agreement with published theory [1, 40].

Chapter 5

Motility: Preparing and using motile bacteria

5.1 Background

In the study of enhanced diffusion, control and knowledge of the suspension activity was crucial to the collection of meaningful data. During the project, it was realised that characterisation of *E. coli* motility under our preparation procedures was a valuable exploration in its own right. Previous research into enhanced diffusion has not always followed preparation procedures believed to be optimum (see section 2.5). This chapter justifies the use of protocols detailed already, but is presented afterwards, as the research was not conducted as preparation for the experiments on enhanced diffusion, but as a consequence of increased awareness and curiosity developed during the study.

Active suspensions are used for the purpose of antibiotic susceptibility testing in Chapter 10; where the focus is the motile bacteria themselves rather than a property of their suspension. Again, meaningful data collection required further understanding of *E. coli* motility in the environmental conditions required, and in turn adjustment of the environmental conditions to allow measurements to be made. The final results section of this chapter relates specifically to the study on pexiganan which follows.

In general, this chapter gives pragmatic advice to researchers using bacterial motility as a tool in their investigations. It also further demonstrates the ability of DDM to quantify *E. coli* motility.

5.2 Introduction

E. coli has become a model system for the study of bacterial motility and active suspensions. Commonly, these studies transfer the motile bacteria from a growth medium into a motility medium, for use in the experiments. The reasoning behind this protocol and the composition of the motility medium were presented in a now classic paper by Adler and Templeton (1967) [92]. They discovered that a phosphate buffer (pH=7) with the chelating agent EDTA maintained motility, without the need for an energy source. The use of cells in this motility buffer omits the complications of chemotaxis and density changes due to growth. Adaptations to the precise transfer or washing procedure and minimal buffer composition have been developed since this seminal study, however further research contributing to the understanding behind motility protocols has been sparse.

As well as designing a chemically defined motility medium, the study by Adler and Templeton investigated factors influencing motility in the medium such as the stimulation of motility by an energy source (while growth remains inhibited), oxygen depletion in sealed sample chambers, pH, temperature, and the number of dilution steps in the washing protocol. They also investigated motility in their growth medium prior to washing and the factors influencing it including the pH and temperature during growth, the phase of growth and the addition of glucose to the growth medium.

Despite the impressive scope of qualitative findings in this publication, quantification of their findings can now be much improved upon with modern methods. Adler and Templeton judged motility by inoculation of a capillary tube at one end at time = 0, and then by removal and incubation of fluid from different distances from the origin. This judged 'the frontier of migration' rather than the average speed, a semi-quantitative result heavily skewed by any highly motile bacteria in the population. Both tracking procedures and DDM have allowed measurements of motility to be less laborious and more informative. In particular, DDM has the ability to measure the average speed v and non-motile fraction b of a population of *E. coli* in 3D [13, 79].

The ability to quantify motility has lead to an exploration of the *E. coli* motility protocol used by researchers in this group, involving the repetition of aspects of Adler and Templeton's classic study. The areas investigated in this chapter can be broadly split into 3 groups; growth of a motile culture, the washing procedure into a motility medium and the measurement protocol in both motility and growth medium. Below, the findings of Adler and Templeton and other previous researchers are presented,

alongside a statement of what was investigated for this chapter.

1. Growth: Firstly, a culture of *E. coli* must be grown. Motility depends on the medium, the temperature and the growth phase of the bacteria. Adler and Templeton grew *E. coli* in a defined, phosphate buffered, growth medium containing 20 amino acids required to synthesize proteins. They mention that the organic part of the media could be replaced by casein hydrolysate, hence the majority of motility research since has used undefined Tryptone broth (TB), which results in reproducibly motile cultures [64]. Even so, some researchers grow motile *E. coli* in Luria Broth (LB) instead of TB, such as Miño *et al.* [62] who used *E. coli* in their research on enhanced diffusion. Luria broth also contains Tryptone, but is supplemented with 5g/L yeast extract. Once washed from LB into motility buffer, Miño *et al.* then left cells to recover speed for 1 hour before use in the experiments. Speeds in the range $4-12$ μm/s were typical, with b being difficult to control from day to day [67]. They found that if the smallest cells were chosen by centrifugation then higher speeds were measured.

Adler and Templeton [92] demonstrated that the optimum temperature for maximum motility was below 37°C, as above this organisms grew fewer flagella. Moreover, cells in the exponential phase of growth were more motile than those in lag or stationary phases. A study by Amsler *et al.* [106] used cell tracking to find that the motility of *E. coli* grown in TB peaked in the post-exponential phase, reaching 15μm/s. This correlated with a two-fold increase in both flagella length and flagella number density per cell volume. They postulate that in a nutrient rich environment, favourable for growth, there is no advantage to synthesising flagella and moving. As the nutrient concentrations decrease in the culture, the environment becomes more stressful, promoting motility. The subsequent decrease of motility in the stationary phase was not due to reduction in flagellum synthesis but a three-fold decrease in torque produced by the flagellar motors, likely to reflect a decrease of energy available to the bacteria [106]. This chapter presents a study on the motility of exponential and stationary cultures, in LB and TB at 30°C and 37°C.

2. Preparation: Secondly, the grown cells are washed from the growth medium into a motility buffer. Adler and Dahl [91] used centrifugation followed by gentle resuspension in motility medium to wash the bacteria. Adler and Templeton [92], using the same procedure, found that by washing the cells free from growth medium four times rather than two, the total distance moved by the frontier was reduced by 33%, but when they performed yet another wash the distance was not further reduced. Filtration has since been used as an alternative to centrifugation [64], to reduce the duration of the wash and to increase the bacterial yield. This chapter reports data on the effect of filtering a

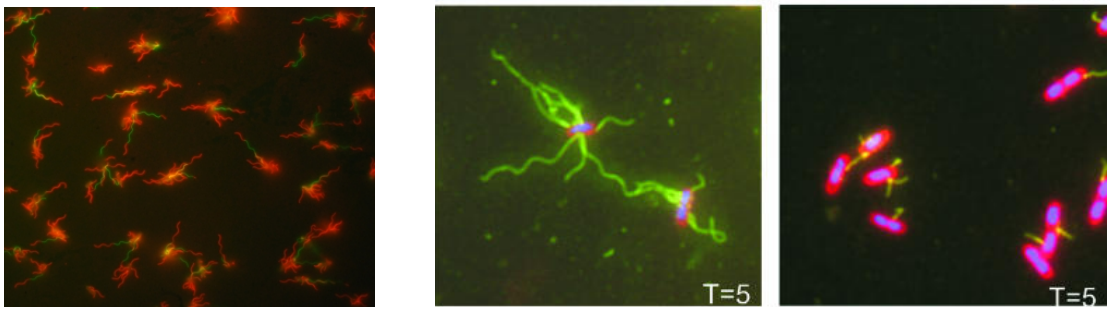

(a) **(b)**

Figure 5.1 Images of flagellar filaments taken from [107] and [108] respectively. (a) The flagellar filaments of *E. coli* imaged with fluorescent microscopy. Cells firstly labelled with Alexa Fluor dye 488 (green), incubated for 3 hours, and then labelled with Alexa Fluor dye 546 (red). (b) Exponentially growing *Salmonella* cell bodies and flagella imaged with fluorescent microscopy 5 min after blending (right) or no blending (left). DNA was stained with DAPI, cell membrane with FM4-64 and filaments were immunostained using fluorescein isothiocyanate.

motile culture from a growth medium to a motility medium, and compares it to rapid and slow centrifugation protocols.

Motility preparation protocols state that motile cells require gentle treatment to avoid shearing of the flagella [64, 91]. However, quantitative proof that normal pipetting speeds and frequencies can influence either v or b of an *E. coli* population has not been published. Depending on the wash procedure, between growth and measurement, a culture may undergo 5 to 20 pipetting actions. This chapter investigates the influence of pipette tip diameter and pipetting speed on the motility of the sample.

Literature on flagella shearing has subjected bacteria to more violent techniques than pipetting. Forceful ejection through a 22-gauge needle tips can be used to cause breakage of *E. coli* flagella due to shearing [107]. Turner *et al.* report that before shearing *E. coli* grown in TB and washed into motility buffer had normally distributed flagellum lengths of mean $\sim$6.6μm. After shearing, flagellum lengths were exponentially distributed, with the shortest lengths the most probable and a mean of 1.6μm. Despite the removal of the flagella cap, sheared filaments regrew on addition of fresh TB, at the same growth rate as was observed in un-sheared filaments. The growth rate, inferred from the staining of old and new filament segments with different fluorescent colours (see Figure 5.1(a)), varied between cells and did not slow with increasing length. The researchers postulate that the length of an un-sheared flagellum is limited naturally by breakage.

Rosu and Hughes (2006) [108] used a blender to expose *Salmonella* cells in LB to shear forces, as a non-lethal method of removing flagella. This method resulted in complete

loss of bacterial motility for both stationary phase and exponentially growing cells, but exponential cells displayed an average of $1-2$ short flagella per cell after blending (Figure 5.1(b)), whilst stationary cells retained less. Breakage was observed to occur throughout the filament or at its base. Within 30 min of shearing, exponential cells had regained motility to almost the extent of the un-sheared control. Regrowth of flagella in stationary phase cells was greatly inhibited.

3. Measurement: Finally, after growing and preparing a motile culture for measurement, the measurement procedure itself can influence its motility. Appropriate conditions for measurement depend on the research question. Frequently, unconfined oxygenated suspensions are of interest. Yet samples must be loaded into capillaries, or other confined chambers for imaging under a microscope. These impose biological and physical limitations on the culture. If, as in all the motility work presented in this thesis, the capillaries are completely sealed to prevent drift, the bacteria are measured in an oxygen restricted environment. The fastest swimmers have a higher likelihood of reaching a glass surface, and depending on their tumble rate, of remaining in its vicinity [109], potentially lowering v measured by DDM in the bulk. Hence, the time spent in the capillary before measurement, and the density of cells in the suspension are variables which could influence the result.

The limitation of interest to this study is the biological effect of oxygen depletion. Adler and Templeton [92] observed that motility in minimal buffer supplemented with glutamine ceased within $10-20$ min in a sealed capillary, but persisted for days in an oxygen unrestricted droplet. If an anaerobic energy source, such as glucose, was available, motility without oxygen was observed.

A paper under preparation here in the Edinburgh group [85], quantifies these findings. After initially sealing a capillary containing bacteria in motility buffer, v drops $\sim 2\mu$m/s in the first 10 min (Figure 5.2(a)). The reduction in speed then slows to $\sim 1\mu$m/s an hour, marginally above the slowing in the oxygenated tube. When oxygen is depleted, v drops to 0μm/s over a few min (Figure 5.2(b)). Fluorescent lifetime imaging microscopy (FLIM) measured the oxygen concentration in the capillary, and confirmed that oxygen is reduced linearly with time until the sudden drop in v, at which point it bottoms out (calibrated to be little to no oxygenation) (Figure 5.2(c)). The time of the v drop is dependent on the density of cells, allowing an oxygen utilisation rate of $1-3\times10^{-12}$ μmol/min/cell to be calculated [85].

When glucose is added to the motility medium (Figure 5.2(d)), v increases $\sim 1.7\times$ and the oxygen utilisation rate increases $\sim 10\times$ due to aerobic glycolysis. After oxygen

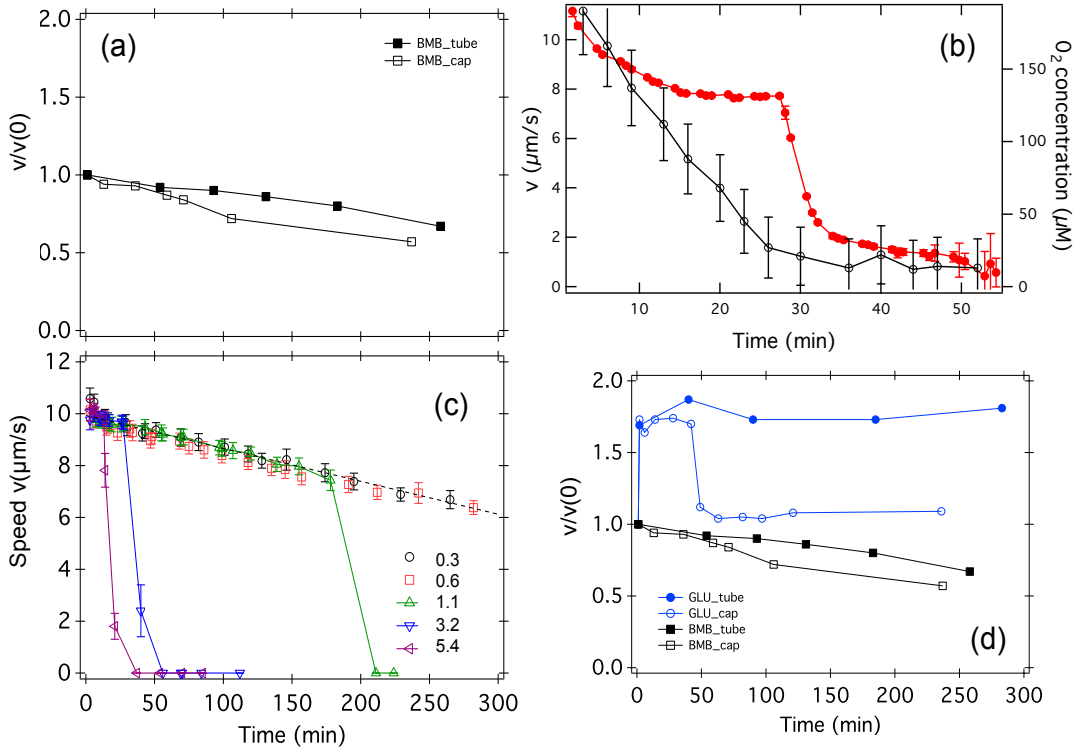

Figure 5.2 Motility of *E. coli* in different conditions of measurement, from [85], in preparation. (a) v normalised to the initial time point for *E. coli* at OD=0.3 in BMB. The suspension is in a test tube (open symbols) or a sealed capillary (closed symbols). (b) v as a function of time in a capillary for 5 ODs as indicated. (c) v as a function of time in a capillary for OD=3. The concentration of oxygen is measured using FLIM. (d) Normalised v with time in BMB containing glucose (18mM) added at $t = 0$ min, from the tube and in the capillary, compared to in BMB alone.

depletion, cells are able to maintain motility through anaerobic glycolysis, at a v similar to that in the absence of glucose.

In some investigations there is a need to study the motility of *E. coli* whilst growing *i.e.* in a growth medium rather than a motility medium. A preliminary study into the effect of antibiotics on the motility of *E. coli* (some of the results are presented in Chapter 10), required the bacteria to be in TB rather than BMB as the majority of antibiotics influence actively growing cells to a further extent than non-growing cells [110]. To interpret the results, an examination of the influence of oxygen deprivation in a sealed capillary on motile cells in TB and in TB containing antibiotics was conducted as part of this chapter. These results are compared to $v(t)$ from the tube in TB.

5.3 Experimental methods

Bacteria and media: *E. coli* AB1157 were used. Luria Broth (LB), Tryptone Broth (TB) and Berg Motility Buffer (BMB) were prepared as described in section 3.2.1.

Density: Throughout this chapter *E. coli* densities are expressed as optical densities (OD). For cells grown to OD=0.5 in TB at 30°C, this OD corresponds to $0.75 \pm 0.1 \times 10^9$ cell/ml, and changes in OD are directly related to changes in cell density. For cells grown under other conditions this calibration may change, but these calibrations were not measured as part of the study.

Standard growth protocol: Presented in section 3.2.2. Referred to as the 'standard protocol' as it was used in the previous chapters and is the growth protocol used for the preparation of all motile cells in the remainder of this thesis. A single colony was suspended in LB and incubated at 30°C and 200rpm overnight for 16 hours. The culture was then diluted 100× into TB and incubated for 4 hours at 30°C and 200rpm.

Growth experiments: Stationary cultures: Single colonies of *E. coli* AB1157 were suspended in 10ml of LB or TB and incubated at 30°C or 37°C overnight for 16 hours. Cultures were in stationary phase and had optical densities in the range $3-4$. OD of the overnight culture was measured and the culture diluted to OD=0.3 in fresh LB or TB medium. Measurements were made $5-15$ min after dilution.

Late-exponential cultures: An overnight culture in LB was diluted 100× into 35ml of TB or LB and incubated at 30°C or 37°C for the time required to grow to OD=0.5. The culture was diluted to OD=0.3 in the appropriate medium. Measurements were made $5-15$ min after dilution. The standard protocol was one of the growth conditions studied.

Microscopy to measure cell length: Phase contrast (PH3) microscopy at 100× magnification was conducted using an oil-immersion objective on a Nikon Eclipse Ti inverted microscope. Culture drops of volume 20μl, grown under one of the eight growth conditions investigated, were pipetted onto cover slips. After 2 min, >30 cells had either sedimented onto, or were swimming in the vicinity of, the cover slip. The microscope was focused on sedimented cells perpendicular to the slip, and a movie was recorded. Image J was used to measure the lengths of 30 bacteria in the field of view, oriented perpendicular to the slip. Uncertainty derived from the point-spread function was deemed to be within the uncertainty from manually deciding the location of the cell ends. Average lengths are quoted with their corresponding standard deviation.

Filtration: The filtration procedure followed the protocol outlined in section 3.2.2. In order to remove cells after each filtration step, the remaining $1-3$ml of liquid ontop of the filter was gently swirled to resuspend cells, and 0.5ml of the suspension removed with a pipette. The OD was measured and the suspension diluted to OD=0.3 in BMB for measurements. To investigate whether the suction pressure used for filtration affected the motility, two filtration units were run simultaneously, each with half of a split culture. One unit was run with the water tap flowing at a high rate, the other at a low rate.

To explore whether mechanical damage occurred during filtration, a culture grown in TB was washed into TB following exactly the same protocol as was used for BMB.

Cells washed 3 times using filtration were diluted in BMB to OD=3. This suspension was then diluted $10\times$ immediately before measurement in BMB, TB and mixtures of the two media.

Centrifugation: Two centrifugation protocols were used. In the first 'rapid centrifugation' protocol, 1ml of a culture (OD=0.5 in TB) was placed in an micro centrifuge tube and centrifuged at 8000rpm for 2min. The supernatant was discarded, leaving a volume of $\sim 30-80\mu$l in the tube and 1ml of BMB was added. Resuspension was achieved by slowly pipetting $\sim 2-3\times$ with an 1ml tip. The procedure was repeated 3 times. In order to remove cells after each washing step, 4 replicate eppendorfs were prepared, each undergoing a different number of washing steps. The suspensions in each were diluted to OD=0.3 in BMB for measurement. The washing procedure was repeated washing the cells into TB rather than BMB to probe mechanical damage.

In the second 'slow centrifugation' protocol, 10ml of the culture was centrifuged at 1700rpm for 10 min. The supernatant was discarded and the cells resuspended in the remaining liquid ($\sim$0.5ml) by gently turning the tube. One ml of BMB was added and the suspension turned once more until full resuspension was achieved and no pellet seen. Another 9ml of BMB was then added. The whole procedure was repeated twice. After each washing step 500μl of the suspension was removed and diluted to OD=0.3 in BMB for measurement.

Pipetting: Diameter of tip orifice: Pipette tips of volume 1ml and 200 μl were cut using scissors to widen the diameter of the tip orifice. They were autoclaved before use. Two hundred μl of an bacterial suspension in either TB or BMB at OD=0.3 was placed in 5 eppendorf tubes. Both cultures had been grown using the standard protocol and then one was washed with filtration into BMB. Each tube was pipetted (set volume 190μl) up and down $20\times$ with a different pipette tip. A manual pipetting

speed thought to be intermediate within a range of manual pipetting speeds possible, and close to the maximum speed of the mechanised pipette, was used throughout. Care was taken not to form bubbles. The motility of the suspension was measured immediately after pipetting. The diameter of the tip orifice used was measured with a ruler. A series of measurements began with an un-pipetted control and progressed with decreasing tip diameter. A final un-pipetted control was measured after the five pipetting measurements to check the time dependence of v and b in the suspension.

Pipetting speed: To investigate the effect of pipetting speed on motility, electronic pipettes (Eppendorf Xplorer) were used. They were operated at their maximum speed of 8, which ejects the fluid in 0.9 seconds, and at an intermediate speed of 4, which ejects the fluid in 2.8 seconds. Two hundred μl of suspension was pipetted into two eppendorf tubes. One of the samples was subjected to pipetting (set volume 190μl).

Recovery on glucose addition: Two hundred μl of AB1157 suspension in BMB diluted to OD=0.5 in an eppendorf was pipetted either 5$\times$ or 20$\times$ with the mechanized pipette at speed 8. One half of the volume was then removed (by pipetting very slowly with a cut tip) and placed in another eppendorf for glucose addition. One hundred μl of 0.1mM glucose in BMB was added and the eppendorf tipped gently to ensure mixing. A capillary was loaded immediately for measurement. The other half of the original volume was also removed into a new eppendorf and one hundred μl of BMB was added.

Recovery with time: One ml of bacterial suspension at OD=0.3, in either TB or BMB, was pipetted up and down (volume of 200μl) as fast and as frequently as possible for $\sim$1 min. The motility was measured immediately afterwards as well as at several time-points during the subsequent 70 min.

Motility measurement, tube protocol: To study motility under oxygenated conditions, for all of the situations described above, a 'tube protocol' was used. A volume of 170μl of resuspended cells was loaded into a 0.4 x 8 x 50mm capillary and both ends were sealed with Vaseline.

All movies were recorded in phase contrast at 10$\times$ magnification following the procedure in section 3.3. Two or three movies were recorded depending on the medium (explained in full later in the chapter). Movies were recorded in the middle of the capillary, 2cm from the sealed ends, and 100μm above the bottom wall. For any time-series measurements a fresh capillary was loaded from the test suspension in the tube.

Measurement, capillary protocol: To study motility under oxygen restricted conditions a 'capillary protocol' was used. Resuspended cells were loaded identically

to the tube protocol. DDM was used to measure the motility inside the capillary with time, with the $t = 0$ point beginning $30 - 60$ seconds after loading. Measurements were performed roughly in the middle of the capillary, in the same location each time.

Antibiotics: *E. coli* at OD=0.5 in TB were placed into 1ml tubes. A small volume of antibiotic stock ($10-25\mu$l) was added to the tube, to result in a magainin2 concentration of 20μM, a pexiganan concentration of 5μM or a kanamycin concentration of 0.62mM. The tubes were gently tipped to ensure mixing, and then 170μl was removed for measurement. See the second part of the thesis for an introduction to the antimicrobial peptides pexiganan and magainin2.

DDM analysis: All movies were analyzed following the procedure presented in section 3.3.2. The primary focus of this chapter was to measure the average speed of the motile cells v the proportion of non-motile cells b.

5.4 Results

5.4.1 Motility protocol: Growth

The effect of growth media (LB *vs* TB), temperature (30°C *vs* 37°C) and growth phase (OD=0.5 *vs* stationary phase), on the motility of *E. coli* AB1157 was investigated. The growth conditions are labelled LB/TB$_{30/37,0.5/stat}$. The focus was to verify the protocol for the preparation of a motile culture for further use; not to conduct a study into the motility of *E. coli* during growth. Thus, the grown bacteria were diluted to a density practical for the measurements (OD=0.3) in *fresh* growth medium, rather than in supernatant from the culture they were grown in. As measurements took place $5 - 15$ min after dilution, time to adapt to the new environment is limited. However, it is important to be aware that the behaviour measured is a phenotype of the bacteria from a given set of growth conditions, exposed to fresh media at room temperature. An interesting further study could compare the results presented to those from cultures grown in the same way and then diluted into supernatant and measured at the temperature of growth.

Figures 5.3, and 5.7 summarise the DDM measurements of all eight growth conditions. The measured DICF $g(q, \tau)$ was fitted with Equations 3.8 and 3.10 and the Intermediate Scattering Functions $f(q, \tau)$ reconstructed from the fitted values for $A(q)$ and $B(q)$. The fit parameters of interest to this study were the average swimming speed v and the non-motile fraction b, returned over the q range $0 - 2.2\mu\text{m}^{-1}$.

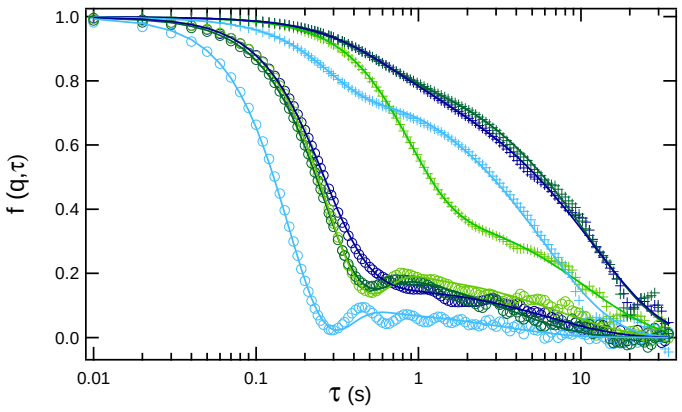

Figure 5.3 ISFs measured for WT *E. coli* grown in eight different conditions. Reconstructed $f(q,\tau)$s at q =1.15μm^{-1} grown in, $LB_{30,stat}$ (○), $TB_{30,stat}$ (○), $LB_{37,stat}$ (×), $TB_{37,stat}$ (×) and $LB_{30,0.5}$ (○), $TB_{30,0.5}$ (○), $LB_{37,0.5}$ (×), $TB_{37,0.5}$ (×). Fits plotted as solid lines.

Reconstructed $f(q,\tau)$s at q= 1.15μm^{-1}, probing a lengthscale of l= 5.5μm, are plotted for all growth conditions (Figure 5.3). At this lengthscale, all conditions show the characteristic shape expected from a fast decay due to swimming followed by a slow decay due to diffusion. The calculated $f(q,\tau)$ for a population of bacteria in which a proportion is swimming and a proportion b is diffusing fits the measured data well. From qualitative comparison of the $f(q,\tau)$s, there are motility features which can be commented upon. Strikingly, decay at early times from growth at 37°C is significantly slower than decay from growth at 30°C. $f(q,\tau)$s measured for $TB_{30,0.5}$ and $LB_{30,0.5}$ show oscillations after the fast decay process, characteristic of a narrow speed distribution $P(v)$.

In this study, bacterial swimming was of more interest than diffusion. To confirm the identity of the fast processes as ballistic, $f(q,\tau)$s are plotted against $q\tau$ in the q range $0.46-2.2\mu$m^{-1}. A collapse was seen for all conditions confirming ballistic swimming in the samples, however for $LB_{30,0.5}$ and $LB_{37,0.5}$ this procedure highlights unexpected q dependent features. As $TB_{30,0.5}$ and $LB_{30,0.5}$ produced large motile populations, plots are shown for these two conditions as examples (Figure 5.4). In TB the fast process collapses against $q\tau$. In LB, the collapse is not as convincing. All measurements collapse at early times, but the decay speed of the assumed ballistic process appears to slow with q, leading to discrepancies between measurements at later times.

Figure 5.5 displays $v(q)$ and $b(q)$ for the two growth conditions used as examples. $TB_{30,0.5}$ has a q independent b, but v shows a q dependence, dropping steadily from 25-21μm/s in the given q range. In this case, the q dependence of v is thought to be due to the high swimming speed of the bacteria combined with a low tumble rate. As

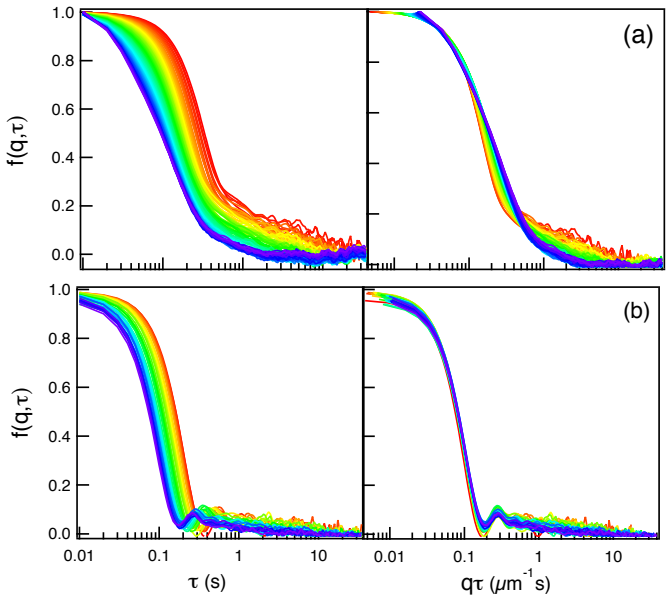

Figure 5.4 Measured $f(q,\tau)$s in the range $q = 0.46 - 2.2\mu\text{m}^{-1}$ rainbow coloured from red to blue. Plotted against τ and $q\tau$. Cells grown to OD=0.5 at 30° in (a) LB and (b) TB.

a consequence, at the highest q values, $f(q,\tau)$ does not show a well defined plateau at early times. The fit weights the contribution of slow swimmers more heavily than the fastest swimmers, resulting in a lower measured v. Moreover, it is possible that there is a depth of field effect at speeds this high, as the likelihood that the intensity of a bacterium will change within a second is higher than at lower speeds [79]. From observation of the movies, it is possible that the bacteria are tumbling less frequently than in motility medium, where a rising v with q is measured [79].

For $\text{LB}_{30,0.5}$, length-scale dependence in v is expected from the observation that $f(q,\tau)$ changes shape with q. Values of v are $\sim$10μm/s slower than in the previous example, therefore the cause of the q dependence is likely to be different. The average swimming speed decreases by 5μm/s over the q range, before plateauing above $\sim 1.5\mu\text{m}^{-1}$. Additionally, b is q dependent, dropping and become difficult to measure above $\sim 1.5\mu\text{m}^{-1}$.

The cause of the q dependence is indicated by inspection of the movies recorded. Even at 10× magnification it can be seen that cells are significantly longer than those grown in TB (Figure 5.6). Microscopy at 100× magnification yielded an average cell length with corresponding standard deviation of 4.4±1.2μm, in comparison to 2.3±0.6μm for $\text{TB}_{30,0.5}$. The maximum growth rate of *E. coli* is greater in LB, therefore a greater proportion of the cells are preparing to divide at the time of measurement than in TB. But, additionally it is known that cells coordinate their size with nutrient availability,

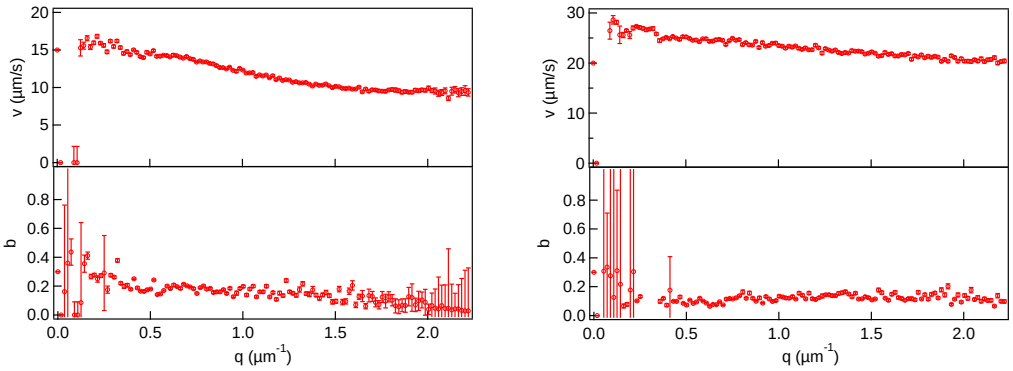

Figure 5.5 Motility in two example growth conditions. Average swimming speed v and non-motile fraction b, extracted from fitting the DICFs measured with DDM at each q. Cells grown to OD=0.5 at 30° in (a) LB and (b) TB.

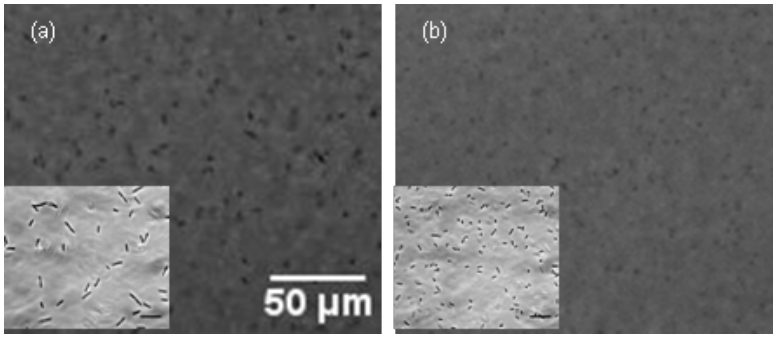

Figure 5.6 Phase contrast microscopy at 10× magnification, of cells grown to OD=0.5 at 30°C in (a) LB and (b) TB. Inset: Phase contrast microscopy at 100× magnification of the corresponding growth condition. Black scale bars = 10μm.

postulated to allow them to hold the DNA formed by multiform replication [111]. Rotational diffusion or wiggling motion of a cell body of length $l = 4.3\mu$m would contribute to the $f(q,\tau)$ at approximately $q = 2\pi/l = 1.47\mu\text{m}^{-1}$, within the range measured. As the magnitude of the diffusion constant D is as expected [1, 13] and is q independent to above $q = 1.5\mu\text{m}^{-1}$, the additional contribution to the $f(q,\tau)$ is judged to be ballistic rather than diffusive. Dynamic light scattering of bacteria has previously probed q values at which rotational diffusion is expected to contribute and recorded a ballistic scaling [76].

$\text{LB}_{37,0.5}$ showed the same pattern of q dependence as $\text{LB}_{30,0.5}$ in its DDM measurements. Microscopy at 100× magnification confirmed that the average length of cells in these cultures was $l = 4.4 \pm 1.0\mu$m. Average cell lengths with their corresponding standard deviations, a measurement of polydispersity, are summarised in Table 5.1. Cell body

Table 5.1 Average length (l) of 30 cell bodies under 8 different growth conditions with their corresponding standard deviations (δl).

	$LB_{30,stat}$	$TB_{30,stat}$	$LB_{37,stat}$	$TB_{37,stat}$
l (μm)	1.7	1.5	1.6	1.7
δl (μm)	0.4	0.3	0.3	0.5
	$LB_{30,0.5}$	$TB_{30,0.5}$	$LB_{37,0.5}$	$TB_{37,0.5}$
l (μm)	4.4	2.3	4.4	2.4
δl (μm)	1.2	0.6	1.0	0.6

length was shorter in all overnight cultures than in those grown to OD=0.5. Uncertainty in the lengths quoted is large, estimated at $\pm 0.2\mu$m, due to the crudeness of the imaging and analysis methods used. However, differences in length large enough to impact the DDM measurement are real can be observed in the images, even by eye.

Standard deviations in cell lengths (δl) are between $20-30\%$ of the average length l for all growth conditions. As l is longer for $LB_{30,0.5}$ and $LB_{37,0.5}$ a polydispersity of this proportion represents a greater range of cell body lengths in these cultures than in any others. To quantify motility for longer and more polydisperse *E. coli*, either a lower magnification could be used to access a lower q range, or an $f(q,\tau)$ model which accounts for cell body motion could be developed.

Both $LB_{37,0.5}$ and $LB_{37,stat}$ return a noisy v and b throughout the q range. There are two reasons why fitting $f(q,\tau)$ for these conditions was difficult. Firstly, a large proportion of the bacteria are non-motile (high b), so the amplitude of the ballistic decay is small (Figure 5.3 (×) and (×)). Secondly, v is low enough that there is not a clear separation of the ballistic and diffusive processes. This affects the robustness of the fit [79]. Furthermore, these cells may move differently to a simple 'run' or 'run and tumble' motion (*e.g.* constant tumbling) if flagella synthesis has been suppressed in the high nutrient environment [106].

No growth condition studied returned a v which increased with q, reinforcing the suggestion that the tumbling rate in a growth medium is lower than in motility buffer. To verify this, cells in motility buffer were resuspended into growth medium (TB and LB tested), and measured within a minute of resuspension. As well as the average v measured rising significantly (from $\sim 15\mu$m/s to $\sim 23\mu$m/s), their $v(q)$ profile changed from rising with q to showing a decrease with q. It is known that chemotactic response to stimuli is precisely related to the stimulus and occurs within seconds of the stimulus being applied [103].

The average speed v and proportion non-motile b were averaged from $q = 0.46$ to

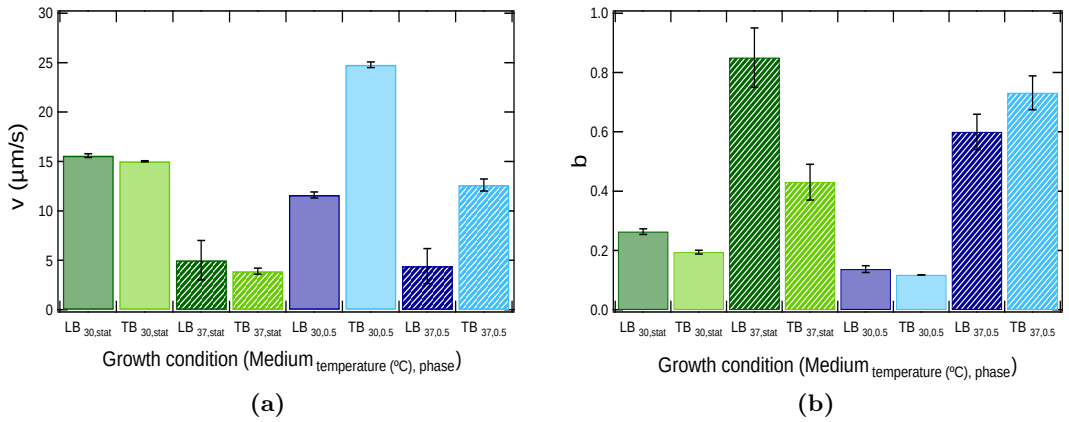

Figure 5.7 Histogram of average motility for eight growth conditions. (a) v and (b) b for WT *E. coli* grown to stationary (green) or OD=0.5 (blue) at 30°C or 37°C (cheque) in LB (dark) or TB (light).

$q = 2.0\mu\text{m}^{-1}$ (Figure 5.7). The samples for which v and b drop with q have error bars which reflect this. Results indicate that, on average, cultures grown at 37°C swim more slowly and have larger non-motile fractions than those grown at 30°C.

It is interesting that both $\text{LB}_{30,stat}$ and $\text{TB}_{30,stat}$ produce populations in which 80% of the cells are motile, with a v of $\sim 15\mu$m/s. From previous studies [106] lower motility than that seen in the stationary phase was expected. The average speed of bacteria grown in $\text{LB}_{30,0.5}$ is similar to the stationary culture (if only low q values considered) or below (if averaged over the whole q range). Conversely, for $\text{TB}_{30,0.5}$, v is 10μm/s higher than in the stationary phase and significantly faster than from growth under any of the other conditions.

In understanding the motility differences between growth media, differences in growth curves must be considered. In LB the bacteria grow faster than in TB at the same temperature, and to a higher maximum density. Therefore, at the time of measurement, stationary cultures have been in the stationary phase for longer, at a higher density. Cultures grown to OD=0.5 were grown for less time in LB than TB, and although OD=0.5 represents a similar biomass between cultures, those in LB contain larger cells at a lower cell density. Growth curves performed in a plate reader demonstrated that OD=0.5 corresponded to the same late exponential phase of growth in both media. It is possible, although unexplored, that the difference in v between $\text{LB}_{30,0.5}$ and $\text{TB}_{30,0.5}$ is due purely to geometry. In LB, l is almost double that in TB at OD=0.5. Amsler *et al* [106] highlighted the importance of cell length for the speed measured with a claim that the peak motility is in the post-exponential phase in part due to a reduction in

cell length leading to an increased density of flagella. Miño *et al.* [62] found that by centrifuging to harvest only the smallest cells, they could enhance the average motility of their suspensions grown in LB. It may be that maximum motility occurs later in the post-exponential phase for cells grown in LB, when their length begins to decrease.

The data collected confirms that amongst the growth conditions tested, growing *E. coli* in TB at 30°C to OD=0.5 produced the best motility. One of the definitions of good motility is a motile population which is well separated from the diffusive population. This is a requirement of both DDM and tracking, otherwise analysis proves difficult. For most motility experiments it is also preferable to use a culture with a high proportion of swimmers rather than diffusers. $\mathrm{TB}_{30,0.5}$ growth satisfies these needs, and the extraction of v and b is possible using the same procedure as for cells in motility buffer, with $P(v)$ given by the Schultz distribution. However, the distribution of swimming speeds is far narrower than in BMB and the fit to the oscillatory part of the $f(q,\tau)$ could be improved upon. Without weighting the fit, the proportional distribution widths σ/v measured are $\sim 2-3$ times below those of populations in BMB, but if a quantitative measurement of the width was essential, weighted fits, or fitting of the motile contribution only, could be explored. It was verified that changing the $P(v)$ distribution from Schultz to Gaussian or Log-normal did not improve the fit.

To summarise, in order to obtain a motile culture, *E. coli* should be grown at 30°C rather than 37°C, as expected from previous research [92]. A future experiment should remove samples from a culture grown at 30°C in TB throughout the growth curve to verify whether OD=0.5 the peak of motility. From the study by Amsler *et al.* [106], a sharp peak in the swimming speed would be expected at OD$\sim$0.2 (converted from their Klett units). This density was measured to be in the post-exponential phase for their strain, but remains in the exponential phase for AB1157 in TB, more likely to be a difference between density measurements than between strains.

This section has justified the continued use of the standard growth protocol for experiments utilising the motility of *E. coli*. If undertaking a study in which growth at other temperatures, or phases, or in richer media is necessary, then DDM provides a rapid and informative method of gaining quantitative observations on the motility. However, in some cases, further characterization of the motility would be needed to maximise the utility of the data collected.

5.4.2 Motility protocol: Preparation

During the preparation for measurement in a motility buffer cells are washed and diluted. This section investigates the effect on motility of transferring a motile population from the growth medium to a motility buffer by filtration, centrifugation and pipetting.

Wash

The previous section assumed that it is preferable to begin the washing procedure with a highly motile culture to achieve motile cells post-wash. This assumption, although not unreasonable, was verified by washing a culture of AB1157 grown in LB at 37°C, showing limited motility, into BMB. Neither v nor b recovered over the following 2 hours monitored, and the size of the cells did not obviously reduce. Therefore, all following work in this section focuses on washing *E. coli* grown using the standard protocol ($TB_{30,0.5}$).

Motility behaviour before and after three filtration steps into BMB (a wash), differed markedly, as can be deduced from a comparison of the DDM data presented in section 3.3.2 with that in the last section. Before being washed, motile cells have a narrow distribution of swimming speeds with v between 20 and 25μm/s, depending on the culture. The tumbling rate is believed to be low. Ten to twenty % of the sample is non-motile. After the wash, the motile population has a wider distribution of swimming speeds and a v between 12 and 17μm/s. The non-motile population has increased to $30-40\%$ of the population, and the tumbling rate is large enough to be noticed in the increase of v with q (see section 3.3.2). To investigate reasons for these changes, measurements were made during the filtration procedure and compared to two centrifugation washes.

Filtration: Figure 5.8 shows v and b measured after each dilution step of a filtration protocol. Wash number 0 represents cells in TB, and each subsequent wash involves a 1/10- 1/30× dilution of the media from TB to BMB. Each wash step reduces the average speed by $2-4\mu$m/s except for the third wash, which did not change the speed considerably from the second. The non-motile fraction rises from ~ 0.1 to 0.3 during the whole procedure. Repeats showed an unchanging b between washes 0 and 1 within uncertainty, rather than a drop.

Additional data was taken after bacteria removed at each step had sat on the bench

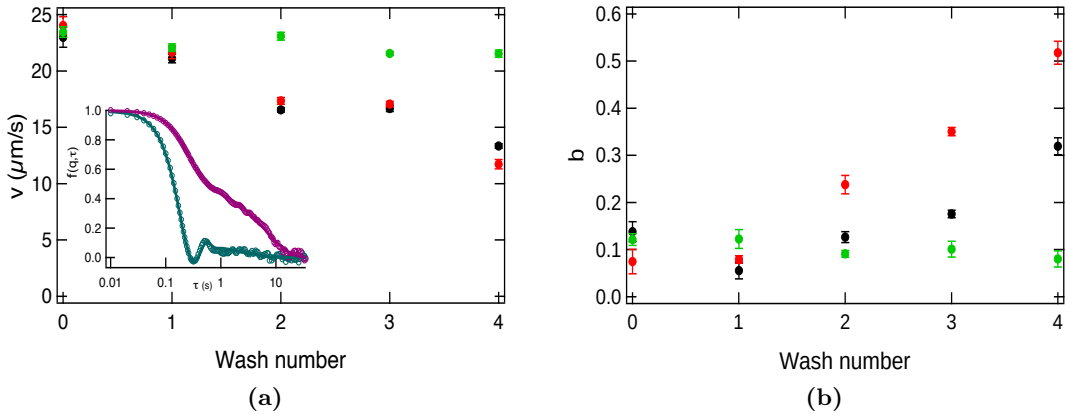

Figure 5.8 Motility during a filtration wash. (a) Average swimming speed and (b) non-motile fraction of cells undergoing a wash from TB into BMB (black) or TB (green) by filtration. Measurements of cells washed into BMB were repeated 50 min after the conclusion of the wash (red). Inset: Measured (symbols) and fitted (line) $f(q,\tau)$ of *E. coli* in TB before wash (turquoise) and in BMB after wash (purple).

for 50 min. The average speeds in TB and from each washing step remain within error bars of those measured initially. The non-motile fraction, b did not increase during this time in TB, or in a suspension washed once, but rose considerably for cells having undergone further washes.

To judge whether any mechanical damage is inflicted on the cells during filtration, two experiments were conducted. The washing procedure was repeated with TB replacing BMB. Multiple washing steps did not alter v or b within error (Figure 5.8 (green)).

Secondly, a culture underwent 3 filtration steps into BMB and was diluted to OD=3 in BMB; an experiment facilitated by the ability of filtration to harvest high densities of bacteria. Immediately before measurement this suspension was diluted 10× in TB, BMB, or a TB:BMB mixture. Resuspension into BMB, calculated to contain a $1{:}10^4$ parts TB after 3 washes and a 10 times dilution, resulted in the lowest v, identical to that of resuspension in TB:BMB $1{:}10^4$ (Figure 5.9). Resuspension into a medium containing concentrations of TB $1{:}10^3$ TB:BMB or above, increased v in comparison to resuspension in BMB. The non-motile fraction b was unaffected by the composition of the resuspension buffer.

Resuspension in TB (resulting in 9:1 TB:BMB) did not recover a v of that in the culture before washing, but remained below this level. This cannot be explained by the small amount of BMB remaining in the medium, as when bacteria from the flask (TB, unwashed) were diluted in BMB (resulting in 1:1 TB:BMB medium) their speed was not influenced. Either the washed bacteria have been mechanically damaged and

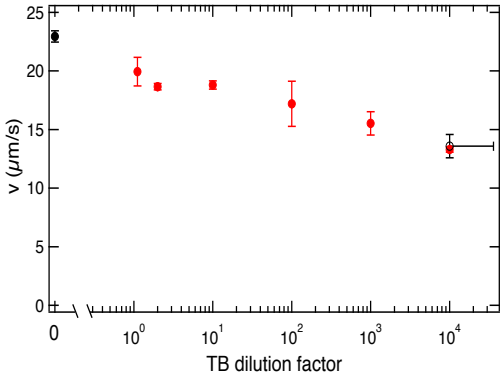

(a)

Figure 5.9 Motility on resuspension in TB from BMB. The average swimming speed of *E. coli* at OD=0.3, before washing (black filled), in BMB after 4 filtration steps (black empty) and suspended in a dilution of TB in BMB immediately before measurement (red).

are thus unable to recover their unwashed speed, or their internal energy sources have changed as a consequence of having been in BMB for $\sim$ 1 hour.

Other factors with the potential to affect the motility of a sample after filtration are the strength of suction used and the overall time spent washing. Unfortunately, it is difficult to separate these contributions as, in general, if the suction is increased, the length of the wash decreases. Note that at very high suction rates this relationship does not hold, as the filtration rate is observed to decrease again. The motility of cells washed using high suction (wash duration $\sim$25 min) was compared to that of cells washed using very low suction (wash duration $\sim$90 min). After 3 filtration steps using low suction b had risen to ~ 0.2 while at higher suction, b was increased to $b = 0.35$.

Centrifugation: Motility monitored during the fast centrifugation washing procedure showed a similar pattern as during filtration. Figure 5.10 shows v dropping during the first 2 washing steps, plateauing for the third, and then dropping marginally further with wash 4. The non-motile fraction is again unaffected by the first washing step and thereafter increases from 0.1 to 0.3. Slow centrifugation resulted in the main speed reduction occurring in the first washing step and then plateauing in the subsequent two. The non-motile fraction rose further over 3 steps, possibly due to the overall time taken for each step, meaning that cells measured after wash 3 had been in BMB for $\sim$ 40 min compared to $\sim$ 10 min under fast centrifugation.

Facilitated by the speed and relative ease of the fast centrifugation procedure compared to filtration, 10 washes were completed rather than 4 (Figure 5.11). In this particular wash, after 2 wash steps, v measured bottomed out, and did not systematically decrease further with further washes. However, b continued to increase with further wash

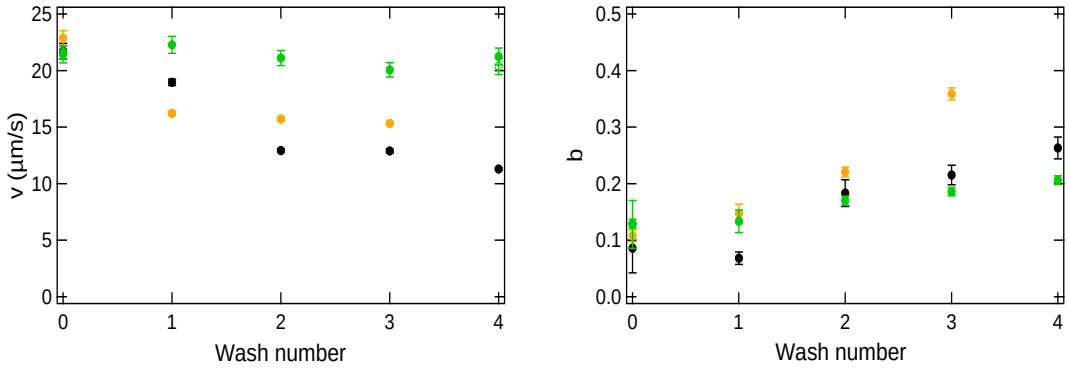

(a) (b)

Figure 5.10 Motility during a centrifugation wash. (a) Average swimming speed and (b) non-motile fraction of cells washed from TB into BMB (black), or TB (green) using the rapid centrifugation protocol. Washing from TB to BMB with the slow centrifugation protocol plotted in yellow.

steps. Data becomes noisy after many washes as the density of bacteria available for measurement begins to decrease.

The fast centrifugation procedure was repeated, washing the cells into TB rather than BMB (Figure 5.10 (green)). The average speed did not change within uncertainty over four centrifugations, however b rose marginally to 0.2.

Discussion: The results presented suggest two contributions to the drop in motility during the transfer of cells from TB to BMB; the removal of motility stimulus present in the growth medium and mechanical damage to the bacteria. Dilution of a stimulus is proposed to be the dominant cause in the reduction of v, as when the stimulus is re-introduced recovery is immediate. A more permanent effect, such as mechanical damage, is proposed to be the dominant cause in the increase in b, as reintroducing a stimulus does not affect it, and further washing steps continue the increase.

In motility medium bacteria use their endogenous energy sources to swim [85, 92], whereas in TB they are able to metabolise nutrients. It is known that providing energy sources such as glucose increases the speed, so it is perhaps unsurprising that v is higher in TB than in BMB. However, after two filtration or centrifugation steps the concentration of TB in the buffer has been lowered > 100 times, depending on the volume of fluid discarded after each step. It was unexpected that concentrations of TB this low could influence *E. coli* motility, but it has been shown that bacteria cannot be considered washed free from growth medium until TB has been diluted $1000 - 10000\times$.

After two filtration steps the concentration of TB in buffer has been lowered $100 - 900\times$,

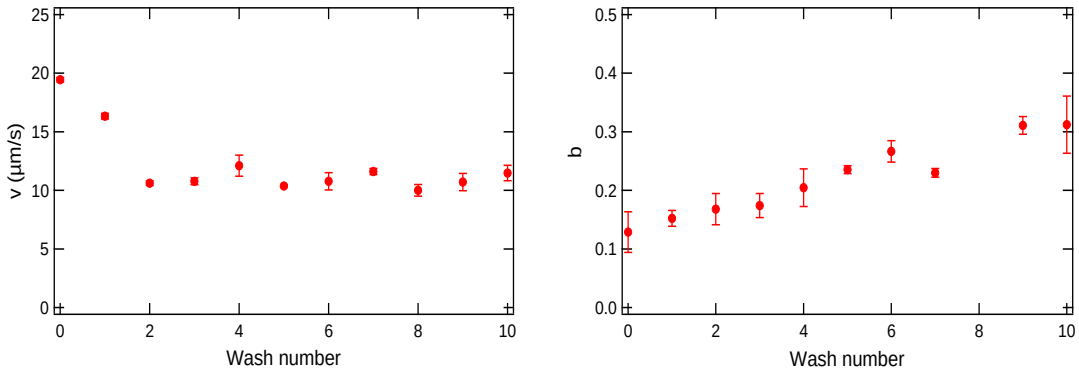

(a) (b)

Figure 5.11 Motility during ten centrifugation steps. (a) Average swimming speed and (b) non-motile fraction of cells washed from TB into BMB with 10 fast centrifugation steps.

depending on the volume remaining on-top of the filter after each step (1-3ml). The medium is typically diluted a further $\sim 10\times$ with BMB for measurement resulting in a $1000 - 9000\times$ dilution of TB. After two fast centrifugation steps the TB has been diluted $150 - 2500\times$ ($20 - 80\mu$l remaining in the micro- centrifuge tube at each step), and the medium is diluted a further $\sim 2\times$ with BMB for measurement. Therefore, if careful to discard a volume of supernatant at the upper end of the ranges quoted here, two washes is sufficient to dilute the TB to levels which do not influence v. Any further washing risks mechanical damage, resulting in more non-motile bacteria. If volumes discarded are lower it may require up to 4 washes to remove the influence of TB from the medium.

Depending on the research need, awareness of the effect of nutrients could influence the choice and duration of washing procedure. Without knowledge of the results presented there is a large amount of variation in the volume of supernatant discarded after each washing step using either filtration of centrifugation. It would be possible to design a protocol, for example a measurement of the volume remaining, to ensure that the dilution was precisely the same each time.

It was illustrated in this section that when a high density of bacteria was required, a filtration washing procedure was preferable, whilst when the duration of the wash was important, the fast centrifugation was preferable. For these experiments there was no reason to use the slow centrifugation protocol, as it proved difficult to complete more than 3 washing steps without losing a large proportion of the bacteria. Centrifuging at fewer revolutions per minute to be more gentle did not reduced b.

Adler and Templeton [92] used a centrifugation washing procedure, but did not note

the estimated nutrient dilution at each step. They reported a reduction in motility between 2 washes to 4 washes, but not between 4 and 5 washes. The researchers do not explicitly attribute this to the further dilution of metabolites in the medium, although it is indirectly suggested. The similarity in the patterns of results between the two studies is reassuring. From a comparison of the 33% reduction in distance of frontier movement between wash 2 and 4 to the 0-13% reduction in average speed measured here (depending on the wash), it can be inferred that the procedure in [91] resulted in a lower dilution of growth medium at each step. Having said this, the two motility measurements used are different quantities. Measuring the average swimming speed is a preferable quantification of bacteria motility, especially since the width of the swimming speed distribution increases during the wash.

Incidentally, both filtration and centrifugation showed the majority of the increase in the swimming speed distribution width (σ/v) occurs during wash step 1. It appears that dilution of the nutrients during this step increases heterogeneity in the population, a feature often seen in the transition of cells from exponential to stationary phase [112].

Mechanical damage to the cells is proposed as an explanation for the increase in b during the wash, as a possible reason v cannot recover to its original level on resuspension of washed bacteria in TB, and for why decreasing the filter suction decreases the effect on motility. The flagella of *E. coli* can be removed or shortened by sufficient shear forces [107]. However, some of the experiments designed to confirm that damage was taking place, indicated the opposite. Filtration of cells into TB showed little or no effect on the motility, while centrifugation of cells into TB only resulted in a small increase in b. Therefore, unless mechanical damage is dependent on media/buffer composition, these results are inconclusive. The following section hints at whether there is such a dependence.

Pipetting

During the preparation of motile *E. coli* for measurement, suspensions undergo pipetting. It is realistic to suppose that during the preparation of bacteria by filtration and dilution that suspensions undergo pipetting up to 5 times. The fast centrifugation protocol may result in up to 20 pipetting actions, as resuspension at each step is achieved by pipetting. Note that, in the washes presented above all pipetting was carried out slowly with cut tips.

Figure 5.12 shows the results of pipetting a suspension of *E. coli* in TB 20× (orange)

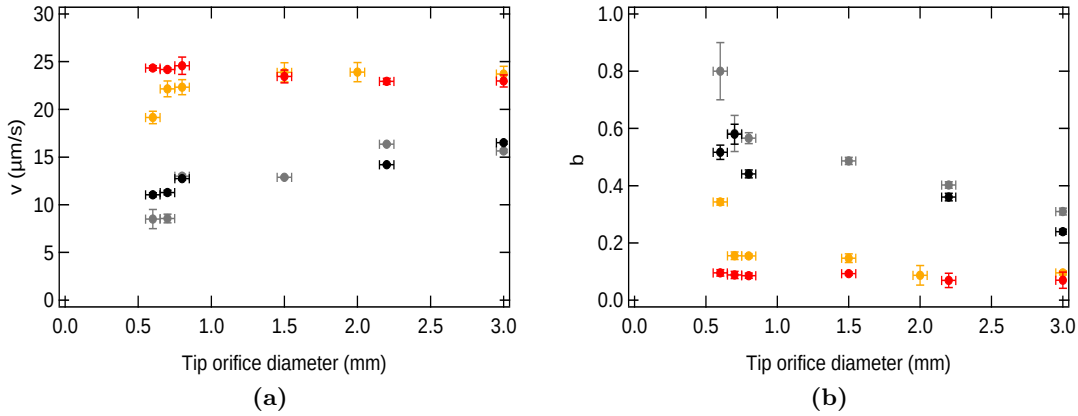

Figure 5.12 Pipette tip orifice diameter influence on motility. (a) Average swimming speed and (b) non-motile fraction of *E. coli* in TB having undergone 20 pipetting actions (orange) or 5 pipetting actions (red), and in BMB having undergone 20 pipetting actions (grey) and 5 pipetting actions (black). Plotted against the orifice diameter of the tip opening. Un-pipetted samples are plotted at a tip orifice diameter of 3mm.

or 5× (red) and in BMB 20× (grey) or 5× (black). Un-pipetted control suspensions, undergoing no more pipetting than strictly necessary for preparation and insertion into the capillary, are plotted at 3mm. Pipette tip diameters 0.8mm and 0.6mm represent normal un-cut 1ml and 200μl tips respectively. Other diameters were obtained by cutting tips. The speed of the pipette action was kept constant, rapid without creating bubbles.

The average swimming speed in either medium is unaffected by tip diameters above 1.5mm. After 20 pipetting actions with tip diameters of 0.6mm, v is $0.80 \pm 0.04\times$ that in the un-pipetted TB sample and $0.54 \pm 0.07\times$ the un-pipetted BMB sample. The non-motile fraction b is influenced by 20× pipetting at larger diameter tips than those influencing v. In TB, b is increased marginally by 1.5mm diameter tips, while in BMB, even at the largest diameter tested (2.2mm), b increases from 0.3 ± 0.01 to 0.4 ± 0.01. The smallest tip diameter used (0.6mm) increases the non-motile fraction $3.7 \pm 0.4\times$ in TB and $2.6 \pm 0.3\times$ in BMB. When a suspension in BMB was pipetted 5 times before measurement, v was reduced less, $0.66 \pm 0.01\times$ at 0.6mm. Likewise b was increased slightly less, $2.2 \pm 0.1\times$. Suspensions in TB were unaffected by 5× pipetting within error.

Electronic pipettes were used to investigate whether the speed of 5× pipetting with un-cut 200μl tips influenced motility (Table 5.2). For suspensions in BMB, 5 pipetting actions at the maximum speed of 8 reduces v to $0.85 \pm 0.02\times$ that of the control. When the speed of the pipetting was reduced by half to 4 the reduction in v drops. The

Table 5.2 Pipetting speed influence on motility. Changes in the average swimming speed (v) and non-motile fraction (b) of *E. coli* in TB and BMB after being electronically pipetted 5× at speeds 8 and 4. Values normalised to that of an un-pipetted control measured at the same time (v_0, b_0). Quoted with corresponding uncertainty.

Medium	TB	TB	BMB	BMB
Speed	8	4	8	4
v/v_0	1.02 ± 0.04	1.01 ± 0.04	0.85 ± 0.02	0.89 ± 0.04
b/b_0	1.0 ± 0.2	1.1 ± 0.2	1.56 ± 0.07	1.07 ± 0.09

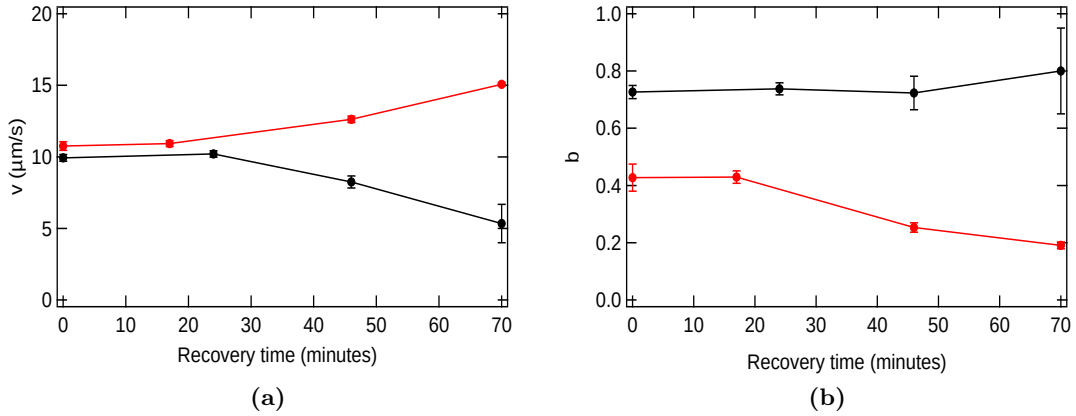

(a) **(b)**

Figure 5.13 Recovery of motility from pipetting. (a) Average swimming speed and (b) non-motile fraction of *E. coli* with time in TB (red) and BMB (black), having undergone 1 minute of continuous rapid pipetting with a 200μl tip. Capillaries were loaded for measurement immediately after the pipetting.

increase in b is eliminated by reducing the pipetting speed. Suspensions in TB were unaffected, within error, by 5 slow or fast pipetting actions.

Figure 5.13 shows the time course of recovery for suspensions pipetted violently for ∼1 min. Note that the ferocity of pipetting was uncontrolled and v measured at $t = 0$ min, immediately after the pipetting, was the same for the samples in TB and BMB coincidently. In fact, it is likely that this indicates that the sample in TB was pipetted more violently before the measurement. Despite this, it is clear that cells in BMB do not recover from this treatment, v reduces and b increases with time since the pipetting. The motility of cells in TB recovers partially over the 70 min monitored. The non-motile fraction reduces from 0.43 ± 0.05 to 0.19 ± 0.01 and v increases from $10 \pm 0.3\mu$m/s to $15 \pm 0.1\mu$m/s. Assuming all bacteria remain viable and divide to form a population with 10% non-motile (b of the corresponding control), b would be expected to reduce to 0.27 in ∼350 min (the doubling time of *E. coli* at OD=0.3 in TB at 20°C). As motility is recovered more rapidly than this, these results indicate that flagella lost during pipetting are re-grown through continued growth, as well as new flagella being

Table 5.3 Adding glucose to pipetted cells. The average swimming speed, and its proportional increase for un-pipetted, 5× or 20× pipetted *E. coli* suspensions in BMB, on the addition of 0.05mM glucose.

	Un-pipetted	5×	20×
v_c (μm/s) no glucose	14.9 ± 0.2	12.2 ± 0.3	9 ± 2
v (μm/s) glucose	23 ± 2	18.7 ± 0.4	14 ± 0.8
v/v_c	1.5 ± 0.1	1.53 ± 0.05	1.6 ± 0.3

initiated on daughter cells.

Glucose was added to *E. coli* in BMB immediately after they had been subjected to mechanised pipetting at the maximum speed of 8. Results are shown in Table 5.3. Adding 0.05mM of glucose to un-pipetted cells increases v to $\sim$25μm/s, as reported [85]. The speed is enhanced from 12μm/s to 19μm/s for a suspension pipetted 5× and from 9μm/s to 14μm/s for a suspension pipetted 20×. Proportional increase on the addition of glucose remains the same in each case. The proportion of non-motile bacteria was, within error, unaffected by the addition of glucose.

Discussion: Although pipetting results are inevitably noisy due to limitations in the control of the experiments, the trends reported are reproducible and have important implications for the preparation of motile *E. coli*. If highly motile suspensions are needed, they should be pipetted as slowly and as infrequently as possible. Rapid repeated pipetting actions are able to mechanically damage *E. coli* such that their motility is affected and is not immediately recoverable with a stimulus such as glucose. Damage was measured to be greater when cells are suspended in motility buffer as opposed to growth medium.

A Beckman-coulter information bulletin [113] uses computational fluid dynamics to show that by widening the orifice of a pipette-tip from 0.6mm to 1.4mm the maximum velocity of pipetted water (flow rate 90μl/s) is reduced ~ 4 times (0.41m/s to 0.105m/s). The maximum shear strain rate is reduced 13 times (3982s^{-1} to 313s^{-1}). This section has shown that changes in shear of this magnitude influence the measured motility of *E. coli* having undergone pipetting. In the absence of literature on the measurement of the shear necessary to remove or break the flagella of an *E. coli*, these measurements have provided an order of magnitude estimate.

This section has assumed that the shortening, or removal of flagella would reduce v or increase b. The swimming speed of a single *E. coli* is non-monotonically related to the length of its helical flagella bundle. *E. coli* grow their flagella to $\sim 10\mu$m in length, maximizing speed by being long enough to extend out of the cell body wake

without adding unnecessary drag [114]. Assuming AB1157 grow flagella to typical lengths (unmeasured), then shortening the flagella due to shearing would be expected to decrease v. Less is known about the influence of the number of flagella on v and b.

It was anticipated that growing cells are able to recover motility whilst those prohibited from growing cannot recover. The continued growth of flagella after shearing when bacteria are in a growth medium has been reported for *Salmonella* and *E. coli* in the literature [107, 108]. Although Turner *et al.* [107] did not measure the flagellum growth rate *per se*, their study inferred a growth rate in TB at 30°C that varied considerably between cells at 0 to 2μm/hour. Unfortunately these researchers did not measure the return of motility during the regrowth; flagella lengths were measured for cells immobilized on a glass slide. Although shearing in this chapter was likely to be less violent than in [107] (a pipette was used rather than a needle) the bacteria have recovered some, but not complete, motility after 70 min, suggesting a regrowth rate of the order of that measured in [107] (μm in hours). Although not the aim of the experiment in this case (see below), with further data collection, for a longer period of time, an average flagella growth rate for *E. coli* in TB at room temperature could be estimated from DDM measurements of motility.

It was not anticipated that pipetting results would also suggest that *E. coli* in BMB are more easily mechanically damaged than those in TB. Speculatively, although the transition to stationary phase is not identical to cells being removed from a growth medium and placed in a buffer, in both cases cells are transitioning from growing to non-growing in a nutrient deprived environment. Rosu and Hughes [108] noticed that mechanical breakage of flagella depends on growth phase. On average, Salmonella retained 1-2 short flagella after blending if in the exponential phase, compared to less in the stationary phase. The researchers attributed flagella retention to short nascent flagella, able to resist shearing. They inferred that the probability of breakage was related to filament length. It is known that sub-populations of *R.meliloti* lose flagella integrity (they are imaged with no, or short, broken flagella) with time when starved [115], and it may be that *E. coli* have similar mechanisms to down regulate motility when starved, leading to their flagella becoming more susceptible to shear. Another hypothesis is that unbundled flagella are more easily broken or detached from the cell body than those bundled. As mentioned, the tumble rate in BMB is believed to be above that in TB. Moreover, flagella are able to display different polymorphic forms, it could be that changes in form due to exposure to different media or a tumbling event [36] change the strength of the filament.

Although unexpected, the enhanced damage in BMB compared to TB could explain

why 4 washing steps into BMB increases b while they remain unaffected by washing into TB. Furthermore, throughout the washing procedure in TB the cells are able to grow and hence repair any damage to the flagella caused by the wash. Centrifugation washes more rapidly than filtration and did return a slight dependence of b on the number of wash steps in TB, whereas no dependence was seen with filtration.

In conclusion, these experiments have implied the reduction in motility during the washing and preparation procedure is due to two things. Firstly the cells swim slower in BMB than TB, and secondly, once in BMB they are more susceptible to mechanical damage to their flagella. Although these findings provide practical information for researchers wishing to prepare motile cultures, further experiments are needed to conclusively deduct the causes of the results seen.

5.4.3 Motility protocol: Measurement

All results presented in this chapter up to this point have been measurements from a tube *i.e.* a capillary was loaded with sample from a tube and movies taken to give results believed to be representative of motility within the tube. The capillary was then discarded and any further samples reloaded. Control measurements, if necessary, were done at the same time so that changes in motility within the tube over time did not influence results reported.

For cells in BMB, $v(t)$ from a tube was compared to $v(t)$ in a capillary in the introduction. *E. coli* in BMB slow over time, attributed to an active down regulation of motility at a well-defined rate [85]. Knowledge of how the swimming speed changes with time is useful in planning studies such as that presented on enhanced diffusion. For the same reason, awareness of $b(t)$ in a tube or capillary is also important (demonstrated by section 3.4.1). This section begins with the time-dependence of the non-motile fraction in BMB, as it is not included in the paper under preparation [85], and was therefore not mentioned in the introduction.

The section then progresses to presenting $v(t)$ and $b(t)$ in a tube and a capillary for unwashed bacteria in TB. The investigation of these measurements was motivated by the growth, washing and pipetting research already discussed in this chapter, where understanding of motility characteristics before the washing procedure was required. A second motivation was the study of AMPs presented later in the thesis, where cells were required to be actively growing rather than under starvation conditions. Other, more general, motivations for using cells in TB include the fact that post exponential

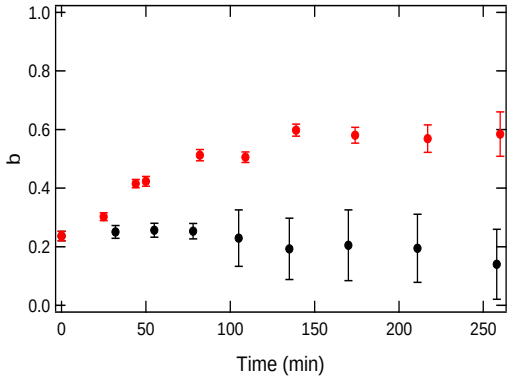

Figure 5.14 Fraction non-motile with time in motility buffer. *E. coli* at OD=0.3 in BMB. Tube measurement (red) and capillary measurement (black).

phase cells have increased homogeneity in their motility compared to a population of starving cells, a potentially convenient feature. Finally, on occasions, motile bacteria are needed rapidly and the wash represents a tedious unnecessary step which introduces damage to the flagella filaments. This section demonstrates the motility over time if the grown culture is simply removed from the incubator and diluted to the required density for experimentation; a procedure requiring 5 min.

Tube and capillary measurements: BMB

A culture grown under the standard protocol was washed into BMB using filtration and resuspended to OD=0.3. The first measurement was made $5-10$ min after the wash ended and $45-60$ min after removal from the incubator. The capillary was left stationary under the microscope and subsequent measurement were taken for the next 4 hours. For the corresponding tube measurement, fresh capillaries were filled at each time-point. Figure 5.14 shows a comparison of $b(t)$ measurements from the tube and capillary. The average speeds recorded in both slowed by $\sim 1.5\mu$m/s per hour, agreeing with the plot presented in the introduction (Figure 5.2) [85].

Strikingly, $b(t)$ does not show the same behaviour between the tube and the capillary (Figure 5.14). The non-motile fraction in a capillary, measured 100μm from its base, remains constant for the first $\sim$75 min. Subsequent measurements of b are difficult as the diffusive process in the measured $f(q,\tau)$ is ill-defined and thus $b(q)$ noisy; it is likely that there were very few diffusers in the field of view. The sedimentation rate of an *E. coli* cell body is approximately 270μm an hour [94]. All non-motile cells in the 300μm above the field of view are expected from calculations to have sedimented through it in $\sim$70 min, in agreement with the timescale measured.

In the tube, b rises for the first $\sim$140 min after the wash and then plateaus. The rise in b is not due to tube mixing before sample removal as it is witnessed when capillaries are filled from many different stationary tubes containing suspension separated at $t = 0$ min. The trends in b reported for tube and capillary have been observed separately, for several different densities, many times. Currently there is no explanation for the differences observed between them. Possibly the act of pipetting the suspension into the capillary causes a greater number of the *E. coli* to stop swimming the longer they have been in BMB, but this is an unlikely explanation and no experiments were conducted to test it.

Tube measurement: TB

E. coli were cultured using the standard protocol which results in an optical density of $0.5 - 0.55$ after 4 hours of growth in TB. Figure 5.15(a) (black) shows growth in the incubator (30°C, 200rpm). Although lower ODs at shorter times are not shown on this plot, it is known, both from this study and from the literature [107], that the minimum doubling time of the population under these conditions is $\sim$50-60 min and that the population leaves the exponential phase at OD$\sim$ 0.3. The culture is in the post-exponential phase on removal at $t = 0$ min. Later data points were taken by returning the flask to the incubator after the extraction of part of the culture for dilution.

The culture was diluted to OD=0.5 (sample 0.5), 0.3 (sample 0.3) and 0.1 (sample 0.1) at $t = 0$ min. Unlike in BMB, in which the density of bacteria is constant over a 4 hour time period, bacteria are able to continue growing in TB after preparation. Growth slows immediately on removal from the incubator compared to that of the culture returned to the incubator. When diluted to OD=0.1, growth slows to a rate comparable to that measured in a shaken 20°C incubator (grey) and only begins to deviate from this at >150 min. Deviation from incubated 20°C growth occurs earlier at the higher densities, after $\sim$50 min and $0 - 10$ min for OD=0.3 and 0.5 respectively. The absence of shaking has a greater influence on growth the higher the density.

The maximum doubling rate of *E. coli* in TB at 20°C is $\sim$ 90 min (measured with multiple replicate growth curves in the plate reader). After dilution of the growth culture to OD=0.1, initial regrowth is close to this rate; after 100 min the suspension is at OD$\sim$ 0.2. Regrowth from OD=0.3 and 0.5 are below this, reaching OD=0.49 ± 0.01 and OD=0.63 ± 0.01 after 4 hours respectively. These results are unsurprising as OD=0.3 represents a density above exponential growth in these conditions, but they

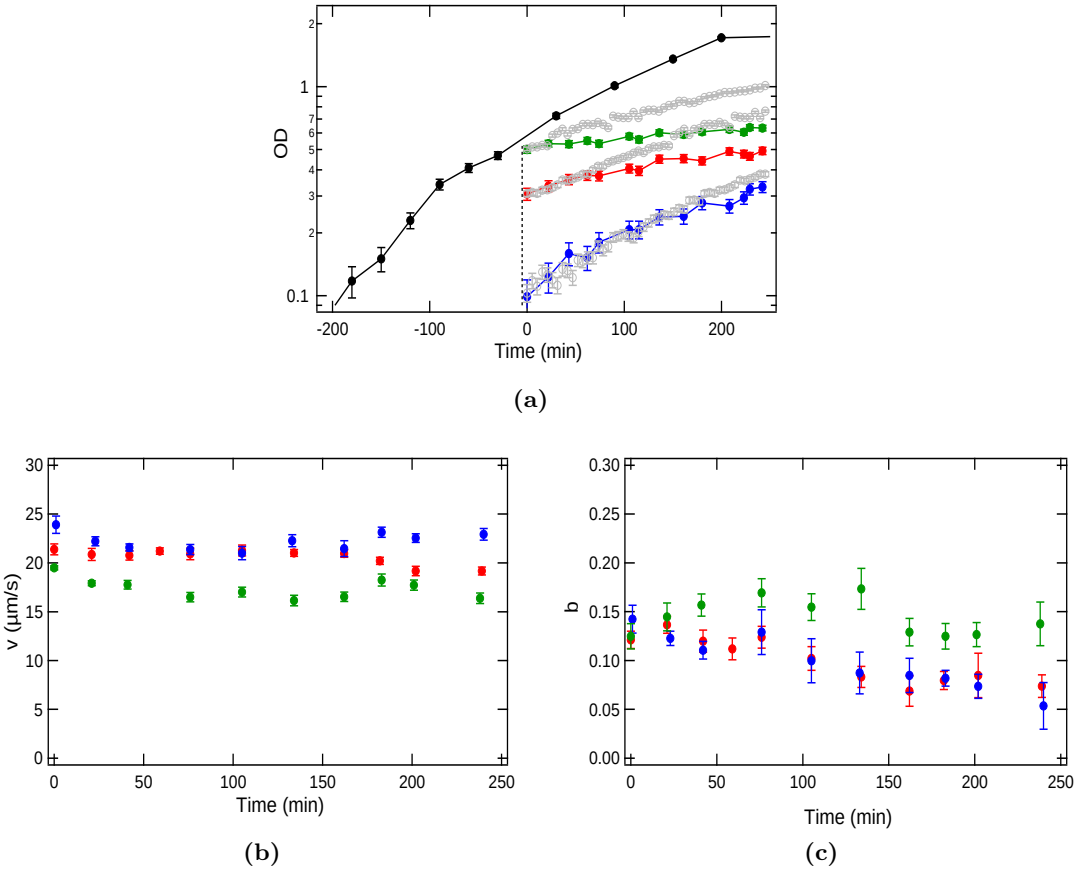

Figure 5.15 Measuring the motility of *E. coli* in TB with time after dilution to a required density. Suspensions at room temperature diluted to OD=0.5 (green), OD=0.3 (red) and OD=0.1 (blue) at $t = 0$ min. (a) Optical density measurements including additional data from a flask at 30°C and 200rpm (black) and a well at 20°C and 200rpm (grey). (b+c) DDM measurements of v and b.

remain useful measurements in the planning of experiments with *E. coli* in TB.

DDM measurements of replicate suspensions to those in Figure 5.15(a) are shown in Figure 5.15(b+c). Sample 0.5 has a lower $v(t)$ than the lower densities. The average swimming speed in sample 0.1 and sample 0.3 agree within uncertainty and remain constant for the first 150 min, after which v (sample 0.1) continues at this level and v (sample 0.3) begins to drop. From inspection of Figure 5.15(a) it can be seen that sample 0.3 is now at OD=0.45, therefore it is hypothesised that the reason for the slowed swimming of sample 0.5 is beginning to become a factor in sample 0.3. The following section demonstrates that a measurement of a lower v at densities this high is due to oxygen depletion in the capillary within the first 40 seconds of recording.

The non-motile fraction of all three samples is lower than in BMB and varies less with time. Sample 0.5 returns a noisy $b(t)$, fluctuating around ∼0.15; it is unknown whether

the drop in speed, believed to occur during the movie, influences the measurement. The non-motile fraction in samples 0.1 and 0.3 agree for the duration of the experiment and slowly decrease from 0.13 ± 0.2 at $t = 0$ (10 min outside the incubator), to 0.06 ± 0.02 after 240 min.

In summary, for the first 4 hours after being removed from the incubator, *E. coli* in TB diluted to OD= $0.1-0.3$ change less in their motility than those at the same densities in motility buffer. However, there are difficulties encountered when working with higher densities in TB, shown more clearly in the following section. Note that when the room temperature is above 20°C the growth rate of samples will increase and it may be that the v measured is higher than reported here (speeds of up to $\sim 27\mu$m/s were recorded in the summer).

Capillary measurement: TB

The average swimming speed of *E. coli* in TB is plotted as a function of time in a sealed capillary in Figure 5.16 for three densities of cells. At OD=0.5 v has already begun to drop by the time the first movie was recorded. It continues to drop to below 5 μm/s by 20 min and then maintains this level. When the cell density is lowered, the drop in v is not immediate but occurs within $5-6$ min at OD=0.3 and within 20 ± 2 min at OD=0.1. The inset of Figure 5.16 plots the time of the drop against the inverse of cell density (OD) at $t = 0$ min, indicating a roughly linear relationship for 3 data points collected. The average swimming speed after the drop is dependent on the density of cells; the lower the density, the higher v. There is no immediately apparent biological or physical explanation for this reproducible feature. Furthermore it is unknown whether the bacteria continue to grow inside the capillary and at what rate.

The abrupt drop in v is believed to occur when the cells run out of oxygen. There is evidence to support this assertion, which was confirmed for cells in BMB in Figure 5.2(c). If, after the drop in speed, the microscope is focused on the edge of the capillary, where there is often a small air bubble, the bacteria are clearly still swimming faster than in the centre. Previous research [85] has shown that in BMB containing glucose, when the oxygen is depleted, the bacteria are able to maintain motility at a lower level through anaerobic glycolysis. The energy sources in TB can also be metabolised anaerobically to maintain motility.

Assuming water contains an oxygen concentration of $\sim 0.3\mu$mol/ml, and that the

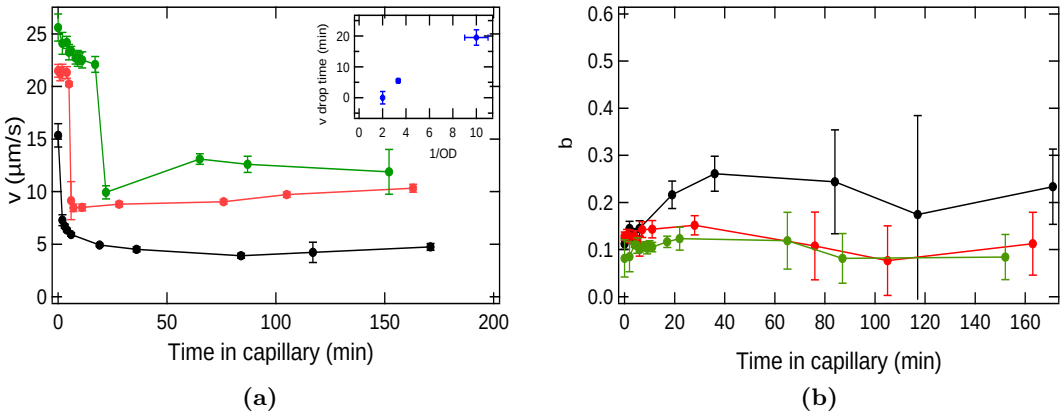

(a) (b)

Figure 5.16 Motility with time in a sealed capillary. (a) Average swimming speed and (b) non-motile fraction of *E. coli* at OD=0.5 (black), OD=0.3 (red), OD=0.1 (green) in TB. Inset: Time of speed drop as a function of the inverse of sample density (1/OD).

bacteria consume all oxygen, the oxygen utilisation rate can be calculated [85]. At OD=0.5 *E. coli* in TB consume oxygen at a rate of 300×10^{-3} μmol/ml/min, slowing to 60×10^{-3} μmol/ml/min at OD=0.3 and 15×10^{-3} μmol/ml/min at OD=0.1. Oxygen consumption rates *per cell*, calculated at each density, are in the range $1-4\times10^{-10}$ μmol/min/cell. These rates are $\sim 100\times$ above those calculated for *E. coli* grown in the same way, but transferred into motility buffer and $\sim10\times$ above those calculated for cells in motility buffer containing glucose [85].

Oxygen consumption rates quoted in the literature increase confidence in these calculations. Riedel *et al.* [116] used a respirometer to measure the oxygen consumption of *E. coli* growing in LB diluted 5 times at room temperature. In the exponential phase of growth (doubling time unstated) each cell used 2×10^{-10} μmol of oxygen per minute. The oxygen consumption rate slowed by 2 orders of magnitude on entry into the stationary phase. These results agree with the rates observed here using DDM in both the order of magnitudes recorded and the change in magnitude between growing and non-growing cells.

Future studies could repeat this experiment whilst varying the growth rate. Observing oxygen depletion in TB as a function of time after removal from the incubator, or as a function of time after resuspension from BMB back into TB, are two possibilities. Higher growth rates could be achieved in a richer medium or at higher temperatures, but as shown in a previous section these conditions reduce motility and may confuse interpretation of the data.

At OD=0.1 there is an initial drop in speed of $2-3\mu$m/s in the first 20 min before

the main drop. This initial drop is comparable to that often seen in BMB at all densities (Figure 5.2). It is not witnessed at OD=0.3 in TB, perhaps implying that the process responsible has already concluded by the time measurements of capillaries at this density begin. Further research into the density dependence of this feature in both TB and BMB is being conducted to further understanding of its cause. It is possible that its cause is biological, for example a response to the depletion of oxygen below a certain level. However, it is believed currently that it is more likely to be a physical feature of confinement. For example, it is possible the fastest swimmers accumulate at the wall over a timescale of minutes, reducing the average speed measured in the bulk. Or perhaps there is a slight imperceptible drift due to the liquid settling in the capillary, influencing the DDM measurements.

The non-motile fraction of bacteria in the capillary does not vary significantly over the first $20 - 40$ min monitored for the densities OD=0.1 and OD=0.3. At OD=0.5, b is measured to increase for the first 30 min, but v drops to $\sim 5\mu$m/s over this time-period, making the diffusive process difficult to separate from the ballistic in the analysis. As in BMB, time-points after 60 min in the capillary return noisy $b(q)$ for all 3 densities, due to sedimentation reducing the number of non-motile cells in the field of view. Fitting the measured $f(q, \tau)$ with $b = 0$ fixed does not change the v measured for these time-points.

All measurements presented earlier in this chapter were taken with full awareness of the capillary behaviour in BMB and TB, following protocols adjusted accordingly. In BMB, the first movie recorded was discarded, as it is dependent on the exact amount of time taken to load the sample. The protocol adopted for the results in this chapter was to record and analyse the first three movies taken of a capillary, and either average over the 2nd and 3rd or use the 3rd, depending on whether the speed continued to drop significantly between them. In TB, OD=0.3 was chosen as the preferred density for measurement, as it gave enough time before the drop in v to record a movie, and v was constant in time before the drop. At least two movies were recorded and analysed to verify that the speed was in the plateau region, and if so, these results were averaged.

Since the conclusion of the experimental work presented in this chapter, software has been developed by J. Arlt and V. Martinez to automate the capture and saving of sequential movies. This has allowed capillary measurements to be captured far more easily, with an increased frequency of measurement. An example of the increased resolution is shown in Figure 5.2. There is now a standard procedure of collecting $5-10$ movies of each capillary measured. More information is available than previously and for each tube measurement, the capillary measurement can be considered.

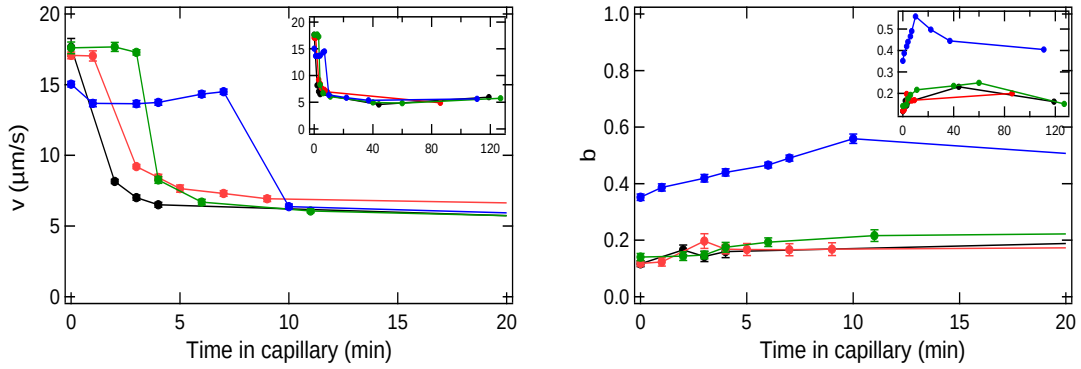

(a) (b)

Figure 5.17 Motility in a sealed capillary containing antibiotics. (a) Average swimming speed and (b) non-motile fraction of *E. coli* at OD=0.5 in TB (black), TB + 0.62mM kanamycin (red), TB + 20μM magainin2 (green) and TB + 5μM pexiganan (blue). Samples were sealed into capillaries $\sim$ 1 min before the first measurement (at $t = 0$), immediately after the addition of the antibiotics to the media. Inset: The same data plotted over the full 120min of measurement.

Capillary measurement of a suspension containing antibiotics

With no understanding of the results presented above, measurement artefacts are possible. As an example; a preliminary study of the effect of antibiotics on motility, conducted as part of this thesis, began by using *E. coli* in TB at OD=0.5. One movie was recorded after loading the capillary, assumed to be representative of the speed in the test tube. Control measurements, without antibiotic, showed large variations between replicates, now understood to be a function of the time taken to load and image the capillary. The addition of antibiotic often led to an increase in the speed measured compared to the control.

Having later monitored the speed as a function of time inside the capillary, Figure 5.17 was plotted. Instead of increasing the speed, the effect of the antibiotic agent is to prolong the period before the drop in motility due to oxygen depletion. By $t = 2$ min, v of the control has dropped significantly. It takes $3-4$ min for v of same suspension containing 20μM of magainin2 to drop, $2-3$ min for the drop in 0.62mM kanamycin to occur and $7-10$ min for a suspension of 5μM pexiganan to drop. Each sample drops to the same level within error, reinforcing the observation that post-drop v is consistent between samples at the same OD.

For the sample containing pexiganan, a potential cause of the later drop is apparent; b is increased from 0.1 to 0.35 immediately. Work in the following part of this thesis, specifically section 8.3, shows that this increase is due to partial death of the population.

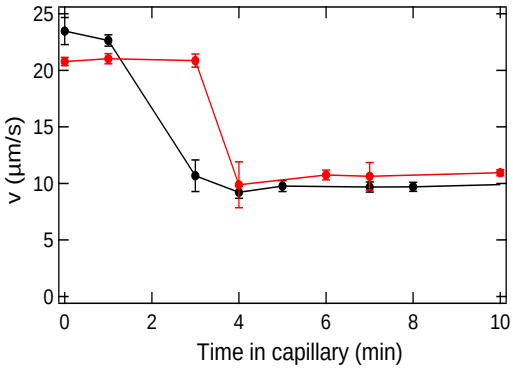

Figure 5.18 Motility in a sealed capillary containing kanamycin. Average swimming speed of *E. coli* at OD=0.3 in TB (black) and TB+ 300μg/ml kanamycin (red) for the first 10 min in a capillary.

With less bacteria viable, oxygen is consumed at a reduced rate. Neither kanamycin or magainin2 appear to have reduced v or increased b compared to the control. Having said this, *E. coli* in TB usually swim at v=20 − 25μm/s rather than the 17μm/s measured here, an indication that v of the control has already dropped at $t = 0$ min. In order to check this, the control sample was diluted to OD=0.3 in order to obtain a plateau in v before the drop. These results were compared to the same suspension with 0.62mM of kanamycin added (Figure 10.3). The addition of kanamycin slows the motile bacteria, and prolongs the plateau in v at short times. Magainin2 and pexiganan also slow the cells at short times after addition (see Chapter 10).

Knowledge of the influence exerted by the measurement procedure on motility is crucial to interpretation of results. The antibiotics tested do not increase v of *E. coli* at short times (as would be concluded from the data at $t = 2$ min alone), but reduce v at the concentrations tested. Further research is required to explain the science behind both the slowing in speed and the apparent reduction in the oxygen utilisation rate. If these antibiotics do not cause immediate death to some of the cells, then this observation suggests that their metabolism is affected. Interestingly, any affect the antibiotic has on v of the population before oxygen depletion is not manifested in the v measured after depletion; anaerobic motility is unaffected.

5.5 Discussion and Conclusion

This chapter investigated the preparation protocol of motile *E. coli*. It has justified the procedures used in other parts of the thesis, and provided pragmatic guidance on understanding motility results collected with DDM. Further experiments continuing the characterisation of *E. coli* motility for practical use have been suggested throughout the chapter. Areas of interest in the research of *E. coli* motility, requiring further work to be understood, rather than simply characterised, have been highlighted. For example; why does motility in TB increase during the late-exponential phase? why is v lower in BMB than TB? why are flagella more susceptible to shear in motility buffer? and, why does lowering v with antibiotics reduce the oxygen utilisation rate?

The reasoning behind the transfer of *E. coli* into motility buffer for use in active suspensions was mentioned in the introduction. This research has provided an additional reason, that the oxygen is depleted $\sim$100$\times$ slower than in a growth medium (TB). The average speed of a growing motile population changes abruptly on the depletion of oxygen, an unhelpful feature in many investigations. Having said this, monitoring motility in a sealed environment is indicative of oxygen utilisation rates, and could be used to probe this quantity in a variety of environments. Moreover, using *E. coli* in TB removes the need for a washing procedure and results in a more motile suspension than easily achieved in a motility medium without the introduction of supplements.

Since the pioneering studies of Adler, Dahl and Templeton [91, 92] there has been a great advance in the understanding of the mechanism of motility and chemotaxis, but little work on changing or developing motility protocols. This study has repeated aspects of Adler and Templeton's investigation, conducted almost 50 years ago, and has confirmed their findings whilst improving measurements of bacterial speed and providing additional information on the fraction of motile bacteria. Extension of the study to aspects of the protocol previously unexplored, such as the influence of pipetting, have provided more practical information for researchers utilising *E. coli* motility than was available from previous literature.

In conclusion, DDM is an effective tool for the quantification of bacterial motility in different environmental conditions. The technique was used to demonstrate that the motility of *E. coli* is a function of its growth conditions, its preparation and the measurement protocol used.

Part II

Growth in the presence of pexiganan

Chapter 6

Introduction: Pexiganan action on growth

The second part of this thesis studies pexiganan susceptibility measurements, specifically the MIC, by measuring *E. coli* growth. Pexiganan is an antimicrobial peptide which has shown potential for use as a therapeutic agent to treat bacterial infections. Antimicrobial peptides and antibiotic susceptibility measurements present topical research subjects due to our increasing reliance on traditional antibiotics while they exhibit a decreasing efficacy due to antibiotic resistance.

6.1 Background

Infectious diseases have been the leading cause of human illness throughout existence [117]. Bacterial infections cause a wide range of ailments, from mild *Pseudomonas aeroginosa* ear infections to the infamous *Yersinia pestis* bubonic plague that eradicated one third of Europe's population in the 14th century. An antimicrobial is an agent which either kills micro-organisms or inhibits their growth, called an antibiotic when the target is a bacterium (synonymous with antibacterials). Antibiotics kill selectively; this characteristic differentiates antibiotics from disinfectants or sanitisers which are non-selective killing agents.

It can be argued that the 'antibiotic era' began with the hospital use of pyocyanase, prepared from *Pseudomonas aeruginosa* by Emmerich and Low in 1899 [118]. However, the realisation that a chemical compound could be designed to target invasive microbes

only, leaving the host unharmed is attributed to Paul Ehrlich [117]. In 1904 he began a screening program which resulted in the discovery of the drug salvarsan to treat syphilis, the most prescribed drug until the 1940s [119]. There followed a race to undiscovered molecules, with large scale screening being the primary method of discovery [117]. Fleming discovered penicillin, the most widely used antibiotic to date in 1929 [120], greatly reducing the number of amputees who died of infections during the second world war.

Fleming was one of the first scientists to warn that if too little penicillin was used during treatment a potential resistance to the drug could arise. Despite the drug discovery success of the period between 1950 and 1970, no new antibiotic classes have been discovered since then. The stagnation of discovery represents a problem, as Fleming and others postulated correctly; resistance to antimicrobial agents is now widespread.

Antimicrobial resistance (AMR) is the resistance and survival of microbes after exposure to an agent at a concentration to which it was originally sensitive. The evolution of resistance can progress with speed in a bacterial ecosystem as many of the genes responsible are on plasmids that can be transferred horizontally between bacteria [121]. Some resistance inferring genes are ancient (*e.g.* penicillin resistant bacteria existed before penicillin was first used as an antibiotic) but the use of antibiotics create selective pressures that drive them into human pathogens. Therefore, although resistance is a natural and complex phenomenon, the level of AMR correlates with the level of antibiotic consumption by humans and animals [122]. Overuse, underuse or the misuse of drugs, caused by self-prescription or misdiagnosis, exposing the bacteria to sub-lethal or unnecessarily lengthy doses accelerate their evolution, exacerbating the problem.

World Health day 2011 was dedicated to raising awareness of antimicrobial resistance and it was voted to be the challenge of the Longitude Prize in 2014. A return to the pre-antibiotic era is self-evidently a problem from the point of view of death due to infections. Despite an estimated 1.5 billion being spent on the treatment of multi-dug resistant infections, 25,000 patients in the EU die each year from infections due to multi-drug resistant bacteria [123].

Novel antimicrobials to replace those which have become ineffective are needed. During the era of antimicrobial discovery, the main ecological niche explored was the soil [117]. There is the possibility of exploring other ecological niches, such as the marine environment, but there has been poor financial investment in antibiotic discovery in the last decade. Another solution is to synthetically engineer antimicrobials now that their

mechanisms are further understood, or to further develop the use of bacterial phages. Finally, there is the possibility of borrowing or mimicking the antimicrobial peptides (of which pexiganan is an example) that contribute to the natural defences of plants and animals to microbes.

Interest in AMPs has grown exponentially in the last 30 years [124]. Research has focused on peptide discovery, synthesis and biophysical characterisation of peptide mechanism of action on model membranes, resulting in the production of potent antimicrobials. However, the vast collection of findings on the molecular level have not been translated into an understanding of AMP action on bacteria [125]. Although biological measurements, almost invariable a minimum inhibitory concentration (MIC) determination and time-kill curves (introduced in section 6.2.3), are required to prove antimicrobial action, there have been few studies dedicated to the interpretation of bacterial density with time in a suspension containing an AMP. If AMPs are to reach their potential and be used clinically, without repeating antibiotic era mistakes, future treatment protocols will require a level of sophistication which is currently unobtainable.

Thus, the primary aim of this study was to gauge the meaning of the MIC threshold for the widely studied AMP pexiganan, by inspecting the growth and time-kill curves of *E. coli* in sub-inhibitory concentrations of the agent. Although, on occasions, previous research has presented sub-MIC growth curves to further the understanding of this threshold [126], they have been examined for only a few antibiotics and no antimicrobial peptides. A secondary objective to the study was to conduct population and single cell measurements to act as a reference for future research on pexiganan mechanism of action.

The introduction consists of two sections. The first section introduces the antibiotic susceptibility measurements used in this study, beginning with a description of growth in liquid culture. The section terminates with a discussion of the limitations of the MIC assay, since it is a primary focus of the study. The second section is specific to antimicrobial peptides and the research conducted on them. Pexiganan is introduced, and previous studies conducted on this peptide described. The section concludes with a discussion of perceived problems antimicrobial peptide field of research, in particular with respect to the biological measurements of efficacy.

6.2 The biological activity of antibiotics.

6.2.1 Bacterial growth

In order to judge the susceptibility of a microbe to an antibiotic, its growth in antibiotic free medium must first be understood. Bacterial growth has been one of the central focuses of bacterial physiology in the last half century, inspired at least in part by Jaques Monod's seminal studies [127]. In 1949, Monod is quoted as remarking 'The study of the growth of bacterial cultures does not constitute a specialised subject or branch of research; it is the basic method of Microbiology' [128]. Bacteria grow by increasing their mass (*E. coli* by elongation), and then sub-dividing into two cells which undergo the same process again. Bacterial growth can be studied on a single cell level, referred to as a 'cell cycle' (see reviews [129, 130]) or on the population level, described by a 'growth curve'.

The growth curve of a bacterial population is a measurement of the number or density of bacteria with time. Nowadays the measurement of a bacterial growth curve is one of the first experiments encountered by those who have chosen to study microbiology, but its use in research has diminished. In a guest commentary, Neidhardt (1999) [127] asked researchers not to forget the usefulness of growth curve observation in this era of proteomics and genomics.

When every bacterium in a culture is dividing at the maximum growth rate determined by their environment they are said to be in a state of balanced growth [131]. In this case, the rate of growth is proportional to the total number or density of growing cells N,

$$dN/dt = \mu N. \tag{6.1}$$

where μ is defined as the specific growth rate, related to the doubling time T_D by $T_D = \ln(2)/\mu$. N grows exponentially with time,

$$N(t) = N(0)e^{\mu t} \tag{6.2}$$

from an initial inoculum size of $N(0)$.

In this thesis cells are inoculated into a closed environment with a fixed amount of nutrient, *e.g.* a test tube or a well containing growth media. In a closed culture there are additional features to the subsequent growth curve, shown in Figure 6.1. Initially, unless inoculated from an identical culture, the bacteria require time to adapt to the

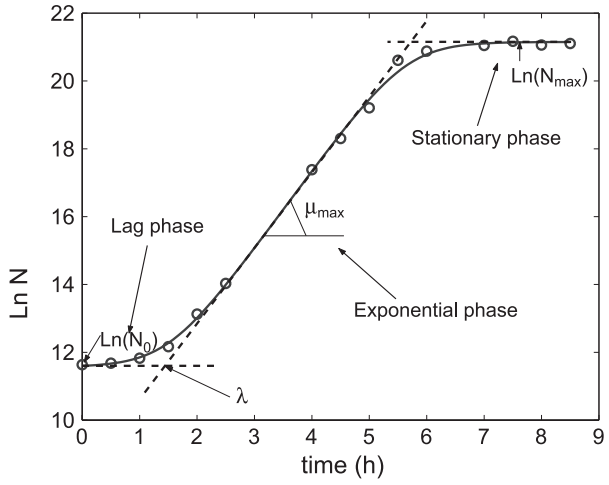

Figure 6.1 Example of a typical *E. coli* K12 growth curve from [134]. Ln of bacterial density plotted as a function of time.

new environment before they can take advantage of it. Gradually their rate of division increases [132] until they reach their maximum growth rate and exponential growth of the number/density of cells (N) commences. The early time adjustment period is called the lag phase, and the population lag time λ is defined geometrically as the time at which a straight line extrapolation of the exponential phase intercepts the initial inoculum level. Balanced exponential growth progresses until nutrient depletion leads to growth slowing and the culture enters a post-exponential, then early-stationary phase. During the stationary phase N plateaus, before beginning to drop as waste products accumulate. The stationary level N_{max} typically reflects the capacity of the media to sustain a dense culture, bacteria are able to reach higher stationary levels in rich media.

Depending on the medium, the growth curve may display two or more exponential phases (reported in section 8.1.1). Diauxic growth (two phases) occurs when the bacteria can metabolise one of the medium components more easily than another. For example, *E. coli* in LB is diauxic, with a brief lag phase at OD$\sim$ 0.3, due to the depletion of easily utilised catabolizable amino acids [133]. When the primary nutrient source has been depleted, growth slows and the population enters a short lag phase while adjusting to the second source. A second period of growth then follows, typically at a lower μ than the first.

Batch culture is only one of the experimental situations in which a growth curve can be measured, but is the most common due to its simplicity and the use of closed environments for the preparation of bacteria for experiments. Often the purpose of

measuring a growth curve is to establish μ, λ and N_{max} of a given bacterium under a specific set of conditions. These are extracted by fitting a model. Classically, empirical deterministic models were used [135]. However, in the last $\sim$ 20 years, researchers in the field of food microbiology working on mathematically modelling bacterial growth curves have argued that applying classical models to numbers of bacteria on a log scale had limited use, detracting from mechanistic interpretation [136].

In particular, Baranyi and co-workers have been concerned with the interpretation of the lag phase. By comparing the deterministic and stochastic models of cell growth they have shown that the population lag time (λ) is always shorter than individual lag times, although the connection is not straightforward [137, 138]. Likewise, the doubling time of the population is $\sim$ 30% less than the mean single cell generation time (assuming a Poisson distribution) [136]. The fastest recovering and dividing cells in a population dominate the growth curve.

Cell counting techniques are required to plot a bacterial growth curve. Two methods of cell counting, mentioned already in this thesis, play a central role in antibiotic susceptibility and this study; plate counting (colony forming units) and optical density (OD). Counting colony forming units (CFU) judges viability directly, but requires incubation overnight, whilst OD measures the turbidity of a culture, a proxy for biomass, and returns results immediately. For a growing culture, OD is related linearly to CFU within a certain range of turbidity, above which multiple scattering begins to influence the reading. OD is calibrated to a CFU for a given bacterium growing in a given set of conditions, as cell size influences light scattering.

6.2.2 Introduction to detection times

Detection times are a method of analysing growth curve turbidity data. A population growing from an initial level of $N(0)$ reaches a certain level N_{det} in a time T_{det} of,

$$\mathrm{T}_{det} = \lambda + \frac{ln(N_{det}/N(0))}{\mu}, \tag{6.3}$$

provided N_{det} is in the exponential phase (Figure 6.2(a)) [137]. Measurements of detection times T_{det} have proved useful in the study of environmental stresses or preservatives (often from the food industry), such as heat shock, NaCl and acetic acid. Typically, multiple growth curves are collected simultaneously in a multi-well plate, placed in a plate reader which monitors OD with time. In this study on bactericidal antibiotics, detection times are used for three purposes, listed below.

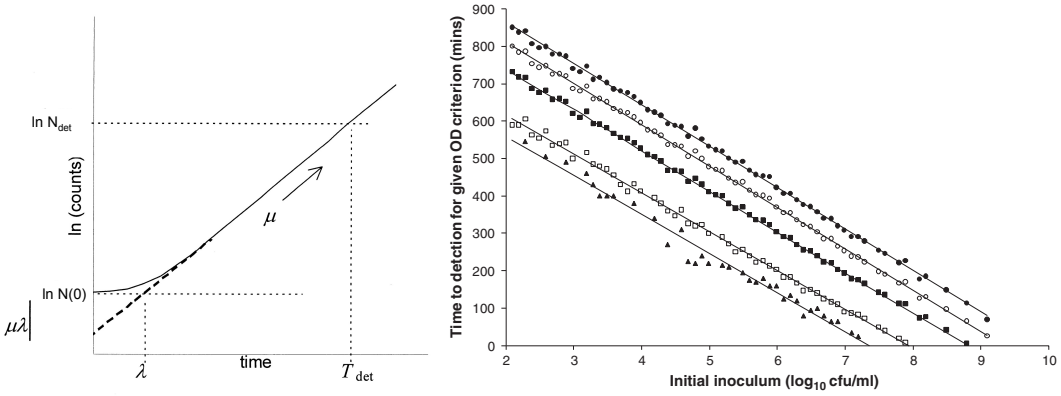

(a) **(b)**

Figure 6.2 Detection time definition and their use in measuring μ. (a) Schematic of a growth curve indicating an N_{det} chosen to be in the exponential phase and its corresponding T_{det}. Adjusted from [139]. (b) The time to detection plotted against inoculum size for *Listeria monocytogenes*. Different shaped symbols represent five different N_{det} criteria. Each choice of detection level results in the same gradient, but a different intercept. From [140].

Firstly, in order to measure μ and λ, detection times have been developed as an alternative method of analysis to fitting a model to a single growth curve [140, 141]. By varying $N(0)$ and plotting it against T_{det} of the resulting growth curve, a straight line is obtained with a gradient inversely proportional to the growth constant μ. The y intercept represents the theoretical time taken for a single bacterium/ml to reach the detection level, while the x axis intercept is the initial inoculum of the size of N_{det} [140]. The presence of a measurable lag can be inferred from the intercepts. An example from [140] for *Listeria monocytogenes* growing in a multi-well plate is shown in Figure 6.2(b) for comparison to a similar plot measured as part of this study in section 8.1.2.

Characterisation of the growth curve in this manner is valid if neither μ of λ depend on inoculum level $N(0)$, otherwise there are deviations from the straight line. For the growth rate μ, this is an accepted assumption for bacteria and has been verified for *E. coli* [142]. For inoculum levels larger than $\sim 10 - 100$ cells λ does not depend on population size either [142, 143] as it is is dominated by the fastest dividing bacteria. When the inoculum is small the heterogeneities of single cells begin to influence the population lag time, leading to more variation in detection times and an average detection time that is longer and above the straight line. The $N(0)$ below which these effects become important depends on the makeup of the population and varies between strains, thus it is verified for the strain of *E. coli* used in this study in section 8.1.3.

Secondly, detection times are also used in the visualisation of the effect of antimicrobial environments or agents on population growth. A longer lag time or a slower growth rate

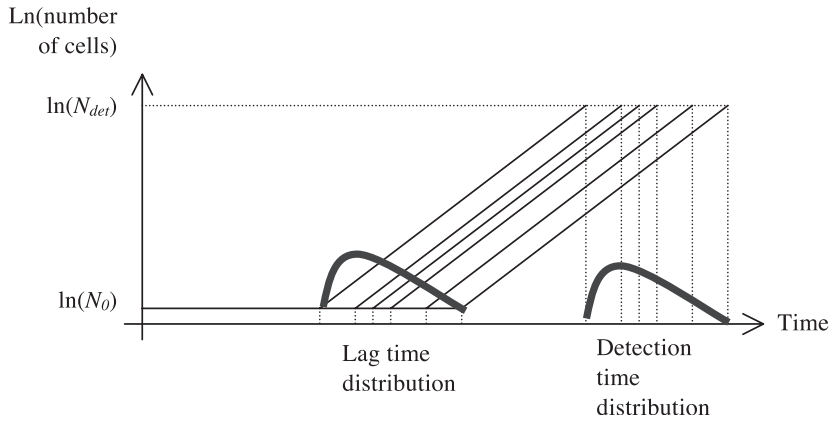

Figure 6.3 The distribution of T_{det} is the same as the distribution of single cell lag times when each population is generated from a single cell $N(0) = 1$. From [144].

lead to a longer T_{det}. An example of this use is the study of Robinson *et al.* into how the inoculum size effected the lag phase of *Listeria monocytogenes* in NaCl. In an NaCl concentration of 1.2M the mean detection time and the variation between replicates increased with decreasing $N(0)$, allowing the researchers to hypothesise reasons for the effects on growth seen.

Thirdly, detection times are commonly used as an indirect method of measuring single cell lag times, sometimes referred to as the 'dilution method' [144–149]. If every well initially contains a single cell, and each single cell generates a population with the same specific growth rate, then the distribution of detection times is a shifted distribution of the single cell lag times. This is shown diagrammatically in Figure 6.3, from [144]. In reality there are a range of $N(0)$ in wells and noise in the OD measurement, meaning that the T_{det} distribution is wider than that of single cell lag times [144]. It is possible to measure and calculate the separate contributions to distribution width in order to control for them [144], or if studying the effect of an agent on lag time (as is the case here), it is possible to compare the distribution with that of a control without the agent.

6.2.3 Measuring the biological activity of antibiotics

This part of the thesis is concerned with how antibiotics influence the growth of bacteria, *i.e.* antibiotic susceptibility measurements. Antibiotic susceptibility testing (AST) has a history as long as antibiotics themselves. A review by Wheat in 2001 [150], based on the book by Poupard *et al.* [151], points out that alongside early descriptions of antibiotic action were inevitably descriptions of methodologies to support the concept of antibiotic action. Pasteur, Koch and Erhlich describe measuring antibiotic activity

with broth methods, by noting loss of motility (the subject of Chapter 10) and with animal protection studies. In the 1920s, Fleming was the first researcher to use the ditch plate technique and an end-point broth dilution technique, a precursor to the first description of the Minimum Inhibitory Concentration (MIC) assay in the 1950s [150]. The need to standardise techniques was recognised in the 1950s, and since then the WHO has played an active role in encouraging the development of AST systems (now at least six within Europe) [150].

Common modern AST techniques, used daily in microbiology laboratories, are based on and have remained surprisingly similar to the methods described a century ago. They include disk diffusion methods, establishing a MIC with broth dilution, agar dilution or e-tests and MBC (Minimum Bactericidal Concentrations) measurements. Wheat [150] comments that 'if the limitations of these methods are understood ... the results should offer a reliable guide to susceptibility ...', implying that there is still work to be done on their understanding, one of the aims of this study.

The remainder of this section introduces the two AST techniques used in this study.

MIC measurements

This part of the thesis is mainly interested in the minimum inhibitory concentration (MIC) measurement; a method used widely for screening antibiotics against organisms. Most commonly they provide a comparison between effective concentrations of different antibiotics on the same organism, or a comparison of different microorganisms with the same antibiotic. Accurate and reproducible MIC measurements are of paramount importance to clinical practice [152]. MIC assays are used as part or all of the criteria to identify strains that have evolved resistance to an antibiotic; a resistant strain has a higher MIC than a susceptible wild-type strain.

The MIC is defined as the lowest concentration of antibiotic that inhibits visible or detectable growth in $18 - 24$ hours [153]. Dilution methods typically test a two-fold dilution series with $10 - 12$ dilutions. The work presented here uses the broth micro-dilution method, recommended as the method of choice for most routine procedures. It follows the protocol published in Nature Methods by Wiegand *et al.* in 2008 [153], following the guidelines of the Clinical and Laboratory Standards Institute (CLSI) and the European Committee on Antimicrobial Susceptibility testing. MIC assays are prepared in 96-well microtiter plates (see Figure 6.4), allowing either a visual read off of turbidity after $16 - 24$ hours, or an optical density reading by a plate reader. As

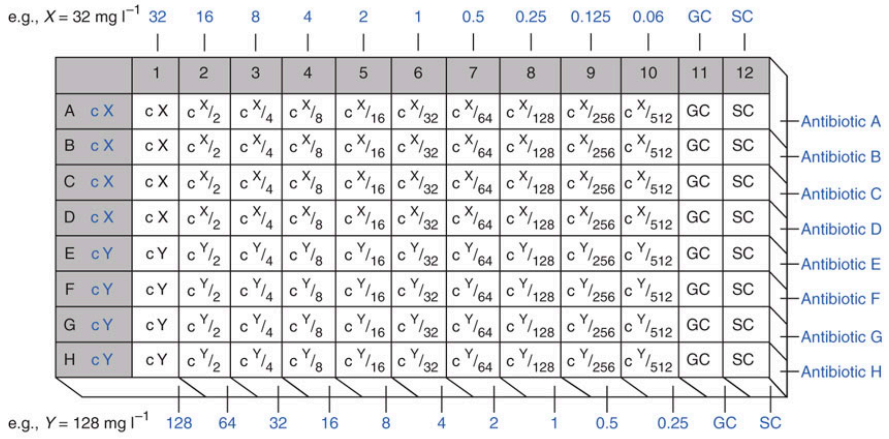

Figure 6.4 Multi-well plate set-up to determine MIC, suggested in [153]. X and Y are the highest concentrations (c) of antibiotic tested. GC: growth control, inoculum with no antibiotic. SC: sterility control, medium with no inoculum.

plate readers are automated and able to act as incubators as well as measuring optical density, it is practical to place the plate in the reader after preparation and measure optical density throughout the 24 hours of the test.

Guidelines published by national organisations such as the CLSI, outline each method in a detailed way to reduce lab to lab variability. Replicate MIC assays performed in a single laboratory show a 3-fold dilution range [154] (4 × difference between replicates), attributed to environmental factors. Inter-laboratory variation accounts for ∼50% of the variation seen in MIC quality control data [154].

MIC values play a central role in therapeutic dosing regimes, which are determined by pharmacokinetic and pharmacodynamic factors [155]. Pharmokinetics (PK) describe what the body does to the drug, the rate at which it is distributed and excreted. Pharmacodynamics (PD) describes what the drug does to the microbe, which concentrations lead to cell death or inhibit growth. The overall activity of the antibiotic is quantified in a PK/PD ratio or index, where PK and PD are represented by numbers. There are at least three different measures of PK; the peak concentration of drug at the site of infection, the time spent above the MIC, and the area under a curve of drug concentration *vs* time for 24 hours at the infection site. Despite being a single threshold value, containing a limited amount of information, the only formally used PD parameter is the MIC [156].

A closely related susceptibility test is the minimum bactericidal concentration (MBC). The MBC is defined to be the concentration at which the viability of a population is reduced to below 0.01% of the initial population in $16 - 24$ hours. The MBC can

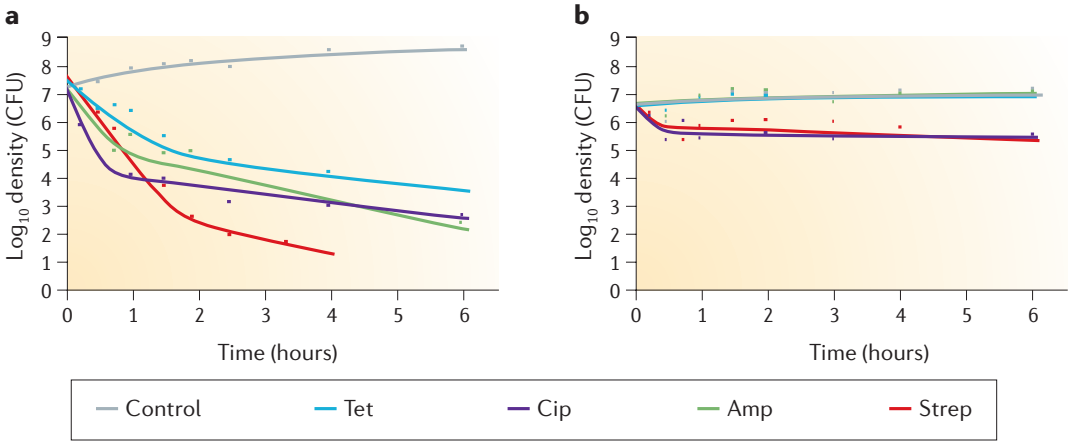

Figure 6.5 Time-kill curves of *E. coli* MG1655 exposed to above MIC levels of the antibiotics shown in the legend. Cells, (a) exponentially growing in LB (b) in stationary phase washed into saline solution. Taken from [158].

be determined from subculturing broth from MIC tests onto agar plates which do not contain the antibiotic. Antibiotics are considered bactericidal (bacteria-killing) if the MBC is no more than four times the MIC, and bacteriostatic (bacteria-inhibiting) if higher [157].

Time-kill curves

In this thesis time-kill curves are performed to complement MIC measurements. Time-kill or killing curves refer to the measurement of viable bacterial density with time, in an inhibitory concentration of an antibiotic. Usually, time-kill curves are measured by plating the test assay onto antibiotic free agar at different time-points after antibiotic addition. By providing the kinetics of antibacterial action, time-kill curves return more information than end-point methods, such as the MIC. However, as time-kill curves are time consuming to perform and as they do not return a single number, they are used less frequently as PD measurements than the MIC.

Time-kill curves have a number of common features. The early stage of bacterial death, after the introduction of an antibiotic, is exponential in many cases [159]. Afterwards the density drops slower, sometimes eventually bottoming out (Figure 6.5(a)). The slowing of the death rate and the fact that substantial fractions of bacteria survive exposure to the antibiotics is attributed to phenotypically resistant cells called persisters [158]. Although persisters are resistant bacteria, this a separate issue to antibiotic resistance, which refers to genetically resistant cells. If grown again in an antibiotic free

environment persisters produce a population with the same susceptibility to antibiotics as its ancestors. The phenotypic resistance to antibiotics displayed by persisters is believed to be due to the fact that this sub-population of cells is not actively growing, or is growing more slowly. Most antibiotics are far less effective against cells if they are not actively dividing, in fact for a given bacterium its death rate caused by an antibiotic is directly related to its growth rate [158].

Unsurprisingly, many antibiotics show a concentration dependence in their time-kill curves, although some do not. This concentration dependence manifests itself in changing exponential death rates, differing lag before the onset of exponential death or a different plateau levels of survivors [159]. Some studies are extended to investigate the effect that varying initial density of bacteria (inoculum size) has on the features of the time-kill curve. It has been consistently shown that the activity of antibiotics against a low inoculum is not necessarily a good predictor of their capability against a high inoculum [155].

The mechanisms behind concentration and density dependent features of time-kill curves are not well understood. Arguably, mathematical modelling of time-kill curves, taking into account resistant sub-populations, is ahead of experimental understanding [156, 158, 159]. Careful experiments to approach hypotheses predicted by time-kill models and to further understanding of the density timecourse are required for many antibiotic agents, attempted here for pexiganan.

6.2.4 Growth curves in antibiotics: Comparing OD to CFU

Both growth curves and time-kill curves are measurements of cell density with time. The measurements are named differently as one is performed in conditions of net growth, and the other in conditions of net death. Growth curves are measured with OD (calibrated to CFU) and time-kill curves are measured directly with CFU, as the two methods of measuring density return different information. OD is directly proportional to CFU whilst all cells in a culture are growing, but if cells lose viability (their ability to survive and to replicate in favourable conditions) and continue to scatter light, proportionality is lost.

A comparison of OD to CFU in conditions of net death contains information. Figure 6.6 shows published growth curves measured in OD for *E. coli* in three concentrations of ampicillin. By comparing the measurements shown to CFU measurements they found that the pre-lytic increase in OD was due to an increase in volume without division

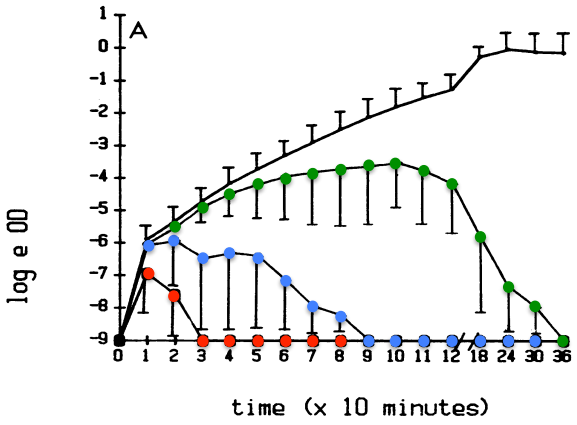

Figure 6.6 Growth curves of *E. coli* exposed to ampicillin for 6 hours at 0 (no symbol) 16 (green) 64 (blue) 256 μg/ml (red), published by Yourassowsky *et al.* [160]. Coloured symbols have been superimposed on original symbols for clarity. Wavelength used in OD measurements not specified in [160].

[160]. The researchers refer to their OD measurements as 'growth curves' and their CFU measurements as 'killing curves'.

Lysis (the breaking down of a cell) causes an immediate drop in OD whilst other mechanisms of cellular death do not. Thus macroscopic, population based measurements of OD and CFU, when compared, are able to give some information on antibiotic mechanism. The bactericidal, non-lytic, activity of daptomycin has been displayed using a comparison of CFU to OD measurements [161]. OD of the culture remained constant while CFU counts dropped 1000×. Note that the drop in OD is an underestimation of the number of cells lysed as, depending on the mechanism, significant fractions of the cell remain [162].

In the following chapters the measurement of density of cells with time is referred to as a 'density curve' and the method used is always stated. CFU are compared to OD measurements of cells in a sub-MIC concentration of pexiganan in section 8.3.3.

6.2.5 Limitations of the MIC measurement

In researching the MIC of pexiganan, its usefulness as a threshold is being evaluated. Limitations of the MIC assay for antibiotics, both as a precise and accurate measurement, and as a useful threshold, are well recognised and often discussed [126, 153, 163].

Some researchers argue that the principle problem with MIC techniques are that they are imprecise [163]. The precision in the standardised methods is limited by the two-

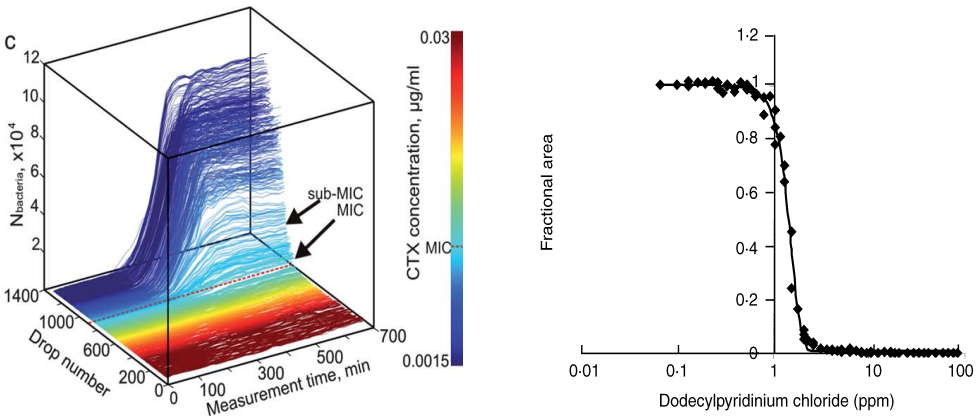

Figure 6.7 Data collected during a MIC assay and an example of how it can be used to establish a more accurate MIC. (a) *E. coli* grown in a gradient of cefotaxime concentrations corresponding to a colour mapping [164]. (b) Inhibition profile of *Staphylococcus aureus* against dodecylpyridinium chloride; experiments (symbols), fitted Gompertz function (line) [163].

fold dilutions used, returning a MIC with a corresponding negative uncertainty of half its value. One strategy in approaching this problem is to increase the number of concentrations tested easily to obtain fine concentration steps over a large range *e.g.* using a millifluidic droplet analyser (MDA) (Figure 6.7(a)) [164], as I do in section 8.2.5.

A second approach is to further analyse the quantitative growth information at sub-MIC concentrations, often automatically collected but disregarded [163]. Figure 6.7(a) is an example of sub-MIC growth curves of *E. coli* in cefotaxime, collected with an MDA. Lambert *et al.* [163] suggest plotting the fractional area under each growth curve against antibiotic concentration, returning an inhibition profile such as is shown for dodecylpyridinium chloride against *Staphylococcus aureus* in Figure 6.7(b). The shape of inhibition varies between antibiotics, and is shown for pexiganan in section 9.1.1. By fitting a modified Gompertz function [165, 166], an accurate and reproducible MIC can be deduced, as well as a measurement of the concentration below which growth is normal (the NIC).

As is seen in this study, the conditions of the MIC assay are critically important to obtaining a reliable result. Schuurmans *et al.* [126] showed that small variations in experimental protocol could change the MIC obtained by a factor of 8 for some antibiotics. By observing the density of bacteria with time at each concentration during a MIC assay, they concluded that the length of measurement was critical in reproducing a MIC. The MIC measured for tetracycline with *E. coli* after 16 hours is 4

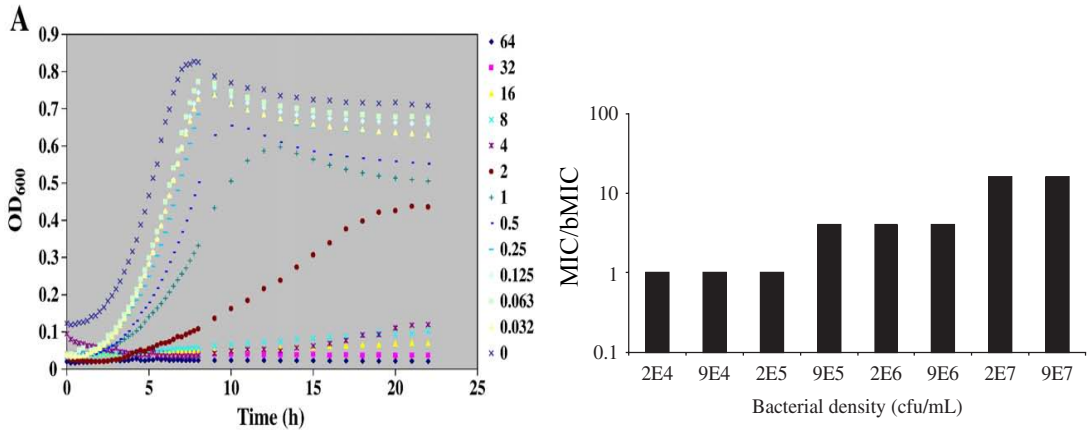

(a) (b)

Figure 6.8 Example of sub-MIC growth curves and the inoculum effect. (a) Growth curves of *E. coli* from a MIC assay of tetracycline, published by [126]. Concentrations of tetracycline in the wells of a 96-well plate are shown in μg/ml in the legend. (b) Relative MIC (to the bMIC= the MIC at 5×10^5 cells/ml) against inoculum size for *S. aureus* in daptomycin [155].

times below that measured at 24 hours (Figure 6.8(a)). Other factors to be taken into consideration were the induction of resistance in the case of *P. putida* in enrofloacin, and morphological changes of bacteria affecting an OD reading. To interpret the results of each MIC measurement, a knowledge of the mechanism and how this influenced the OD reading with time, was needed. Schuurmans *et al.* concluded that while trends in MIC reported from the same protocol are real, the comparison of absolute values between studies are untrustworthy, a sentiment also stated in [153].

The use of the MIC in the PK/PD index has been criticised as it does not take other pharmacodynamic factors, able to alter the course of treatment, into account. These factors include; the functional form of the time-kill curve, persisters, biofilms and post antibiotic effects [156]. An *in vitro* understanding of MIC estimation may not translate to the complex, un-controlled conditions *in vivo*. In an infected host the bacteria may be in a different physiological state, they may be part of a physical structure such as a biofilm and their environmental conditions may differ markedly from those in a standardised MIC measurement [155].

Inoculum effect

One of the primary concerns, related to the use of *in-vitro* MIC values in *in-vivo* therapeutics, is that a population of pathogens in a host is not necessarily of the same density as the standard inoculum tested in MIC assays. MICs are measured at $\sim 10^5$

cells/ml and many deep-seated infections, including bacterial meningitis, can reach densities of $10^7 - 10^9$ bacteria/ml [167]. In some cases high inocula return higher MICs than low inocula. This has been termed an 'inoculum effect (IE)'; the decline in efficacy of an antibiotic with the increase of bacterial density. Inoculum effects have been noted since the early days of antibiotics and occasionally the magnitude of the effect for an agent is included in the files considered for clinical testing [155]. Animal model experiments have supported the finding of IEs *in vitro* [167].

IEs have been measured for β-lactams, glycopeptides, amino glycosides, macrocodes, quinolones and others [168]. There is some understanding of why IEs are seen for antibiotics which are known to be actively degraded by the pathogens being attacked, although some researchers argue that the results are a measurement artifact and have little clinical relevance [169]. For example, β-lactam antibiotics show a pronounced IE when used against extended-spectrum β-lactamase (ESBL) producing bacteria. It is thought that either the release of the enzyme from alive cells or liberated enzyme from dead cells can break down the antibiotic, lowering the effective concentration [170].

E. coli are not known to actively break down pexiganan. Recent publications [155, 168] have addressed the cause of observed IEs for antibiotics not known to be actively broken down by bacteria. Of particular relevance to this thesis, a study by Udeku *et al.* [155] addressed the cause of the IE of six antibiotics on *S. aureus* and discussed the consequences of the density effects on a treatment regimen using a PK/PD antibiotic treatment mathematical model.

The IE seen with four of the six antibiotics, linezoid, gentamicin, oxacillin and ciprofloxcin, was attributed to a decrease in amount of antibiotic available per cell at higher inoculum levels. The IE for the other two, daptomycin (Figure 6.8(b)) and vancomycin, was attributed to a density dependent reduction in the amount of antibiotic available over time due to denaturing enzymes or binding of the antibiotic to cell structure. After six hours incubation with 5×10^8 cells/ml, no biologically effective daptomycin or vancomycin was retrieved from samples. Udekwu *et al.* note that the two causes identified are not mutually exclusive, it is possible that in some cases both are acting. The study was not extended to investigate the mechanisms responsible for these causes, but the researchers mention that their results were unexpected given the enormous number of antibiotic molecules per bacterium in all samples.

From the modelling results, Udekwu *et al.* concluded that, if a dosing regimen was based solely on the conventional MIC (a PK/MIC index), without taking density effects into account, the treatment could fail. Instead of regimens based on PK/MIC indices,

density dependent MICs should be employed as the denominator. They indicated that, although both IE causes ('per cell' or depletion) lead to similar magnitudes of effect, if there was knowledge of which cause dominated, treatment protocols could be adjusted. Accordingly, as part of this study, the IE of pexiganan is measured and it is determined which of these two mechanisms is the cause. The IE of pexiganan is quantified (section 8.2.6), improving on previous reports of the IE, of which Figure 6.8(b) is the most quantitative.

Unsuitable antibiotic treatment protocols, on occasions due to inappropriate use of the MIC, drive antibiotic resistance by exposing bacteria to sub-lethal concentrations. All previous research on the MIC measurement, its meaning for a given agent, whether it displays an IE and corresponding weaknesses, has been on small molecule antibiotics. There is room for an investigation of these simple but heavily used measurements for an antimicrobial peptide, attempted in this thesis.

6.3 Antimicrobial peptides and pexiganan

6.3.1 Antimicrobial peptides

In the second part of this introduction, the focus is shifted to antimicrobial peptides (AMPs). AMPs are defined as being $12 - 50$ amino acids in length, almost all are cationic (on the order of +2 to +9) and contain >30% hydrophobic residues (such as Leu, Ile, Val). These properties allow them to form ampiphatic structures on contact with a membrane, with one face containing a cluster of positively charged residues and the other being hydrophobic. AMPs are typically categorized according to their secondary structures into four groups [171]; α- helical, β- sheet, extended conformation and looped peptides. Almost every positively charged, hydrophobic peptide has the ability to kill a broad spectrum of microbes when tested in a buffer solution [172].

Antimicrobial peptides, sometimes referred to as 'natures antibiotics' [172], are found distributed widely in plants, insects, mammals and bacteria. Consequently, they are believed to have aided the evolution of multicellular organisms both by providing the initial line of defence against infection and by playing a role in innate immune responses. Despite microbes being exposed to AMPs for at least 10^8 years, they have remained effective *i.e.* it is believed that bacteria have not evolved resistance. This may be because organisms express a wide range of different AMPs, with the AMP cocktail varying greatly even between species that are closely related. Also, commonly, there

are several different AMPs with differing modes of action at a single infection site. Alternatively, it has been claimed that the target of AMPs (the negatively charged membrane) is a bacterial 'achiles heel', as its composition is costly to change [173].

With the realisation that the golden age of the traditional small-molecule antibiotics (referred to previously and hereafter as simply 'antibiotics') was ending and drug resistant pathogens were on the rise, research into AMPs began in the 1960s. Popularly, research is thought to have begun later as the well-known cecropins were first described in 1981 and the magainins in 1987 [174]. As of october 2013, 2308 natually derived AMPs have been entered into the Antimicrobial Peptide Database [129]. Although two peptides have been in use as topical treatments (polymyxin B and gramicidin S) and one as food additive (lantibiotic nisin) for a long time [172], the intense period of modern research has disappointingly not resulted in any novel AMP anti-infection therapeutics. Several peptides have appeared promising and been developed for application, but to-date none have been approved.

AMPs are present in any likely sites of infection such as the mouth and mucus. Interestingly, no single AMP is found in the body at levels as high as are required to eradicate a population *in vitro* (their MIC). There are two possible reasons for this, that they act in addition to other peptides and that they are produced locally at high concentrations only when the site is infected [174]. The selective targeting of prokaryotic cells with limited toxicity towards red blood cells and other human cells is attributed to differences in their outer membranes. Mammalian eukaryotic cells have less negatively charged lipids on their surface, their membrane potential is lower and they contain more cholesterol, all factors which reduce their interaction with AMPs. Haemolytic activity at high concentrations has been attributed to hydrophobic interactions between the peptide and eukaryotic membranes [125].

AMPs are believed to accumulate at negative bacterial membranes due their net positive charge [175]. Their mechanism of action once located at the membrane is a controversial area of research, with several complex models developed to describe subsequent events. Pore-forming peptides are believed to create holes with water cores in the bacterial membrane through a variety of mechanisms, eventually leading to membrane lysis [175]. These consist of the toroidal pore (described in Figure 6.9), barrel stave (parallel insertion of the peptide to the lipid bilayer normal), micellization (lipid encompassed peptides leading to membrane degradation) and the carpet model (destabilisation of the membrane). Alternatively, others traverse the lipid bilayer to interfere with inter-cellular processes by binding to proteins or nucleic acids. A third group interact with and inhibit the cytoplasmic membrane actions thus preventing cell-

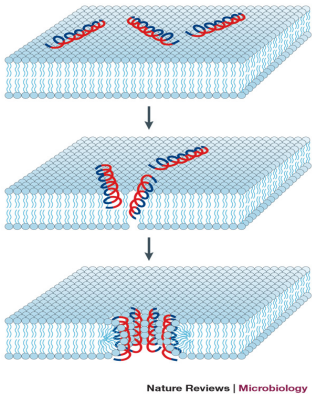

Figure 6.9 Schematic of the toroidal pore mechanism, from [175]. Peptides attached to the membrane aggregate and induce curvature of the lipid layer, creating a pore lined with both peptides and lipid head groups. Hydrophobic regions of the peptides are coloured blue.

division. For detailed reviews of on-going research into the mechanisms of AMPs, see the reviews [175] and [176].

This thesis carries out a study of the pharmacodynamic properties of an AMP. The discovery and synthesis of novel peptides have taken precedence over pharmacodynamical studies of AMPs, regarded as one of the areas in need of future research [171]. Additionally, there have been few formal pharmacokinetic studies to determine their distribution, half-life or mechanism of clearance in the body, unlike conventional antibiotics which have been optimised for these roles [124].

One of the primary obstacles to the development and testing of AMP therapeutics is their susceptibility to proteolysis. All clinical trials so far have used topical creams to apply to infections on the surface rather than internally. The systemic antibiotic market is more lucrative [172], but the digestive tract contains the proteases trypsin, pepsin and chrymotrypsin which the peptides would be exposed to if administered orally [171]. There is current research into the delivery of systemic doses directly to the site of an infection via injectable hydrogels [177]. In addition, some bacteria are known to produce proteases which degrade AMPs, enhancing their chances of survival [171, 178].

Two *in vitro* studies have highlighted the importance of this area of research, and are of relevance to the findings presented in this thesis. Ulvatne *et al.* [179] compared the MIC of Lactoferricin B on *E. coli* and *S. aureus*, in the presence and absence of a protease inhibitor cocktail. They found that the MIC was substantially reduced by the synergistic action of several groups of bacterial proteases inhibitors. In a separate study,

Schmidtchen *et al.* [180] found that proteases from the human pathogens *E. faecalis*, *S. pyogenes* and *Proteus mirabilis*, at concentrations typically found in overnight cultures of each, could degrade LL-37, in some cases within 30 min. The peptide was incubated with sterile wound fluid and *P. aeruginosa* previously infected wound fluid, which were found to have no effect and to result in complete degradation of the peptide respectively.

Finally, evolution experiments [181] have suggested that the assumed unlikelihood of evolved resistance to AMPs could be unfounded. Although molecular mechanisms of resistance had been identified as necessary in the action of some pathogens [182], and resistant bacteria had been constructed in the lab; previous to 2006 laboratory evolution had not produced resistance [173]. Perron *et al.* (2006) investigated the continued exposure of six lines of *E. coli* and *P. fluorescens* to an increasing concentration of a single peptide (pexiganan) for $600 - 700$ generations; a longer and more clinically relevant scenario to previous studies. The selected descendants had a MIC $\sim 10\times$ higher than the original bacteria, indicating rapid repeatable inheritable resistance. The researchers argue that in nature, subsequent generations are exposed to a wide-range of different stresses unlike in clinical settings where it could easily become advantageous to trade fitness with AMP resistance.

Before its use as an antimicrobial, bacteria had been exposed to penicillin in the soil for millennia. Yet they had not evolved the levels of resistance developed under clinical exposure to sub-lethal concentrations for extended periods of time. Given the reliance of our natural defences on AMPs, it is crucial that the mistakes of the antibiotic era are not repeated with AMPs [183], risking a situation worse than a return to pre-antibiotics.

6.3.2 Pexiganan

Pexiganan was chosen as the AMP of interest for this study as it is one of the most thoroughly researched AMPs to date. Pexiganan or MSI-78 is a synthetic analogue of magainin2, produced by Zasloff and co-workers [184]. In 1987 magainin1 and magainin2 were co-discovered by researchers conducting research on *Xenopus laevis*, the African clawed frog. They noticed that incisions on the frog's legs remained infection-free in water containing high levels of microbes [185, 186] leading to the extraction of the two AMPs from their skin. Pexiganan followed research into the effect of length, helical content and systematic amino acid substitutions on activity.

Pexiganan was entered into clinical trials as a topical cream treatment of diabetic foot ulcers. In phase 3 trials it returned clinical cure in 90% of patients. It was denied

Magainin 2: GIGKFLHSAKKFGKAFVGEIMNS
MSI-78: GIGKFLKKAKKFGKAFVKILKK-NH_2

(a)

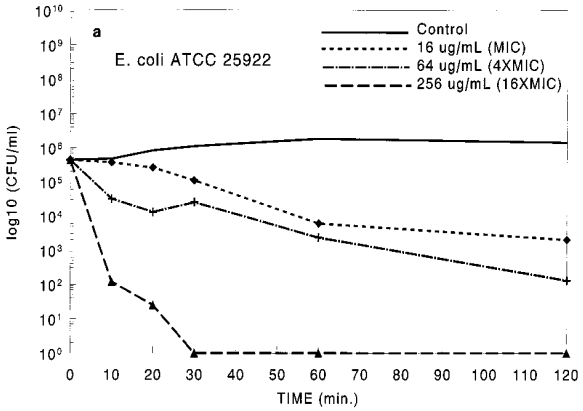

(b)

Figure 6.10 (a) Amino acid sequences of magainin2 and pexiganan/MSI-78 from [184]. (b) Time-kill curve of pexiganan on *E. coli* from [189].

approval by the FDA as this result was equivalent to treatment with oral ofloxacin, a therapeutic already in use. The two multi-centre, randomised, double-blind, phase 3 trials are described in detail in [187, 188]. Advances in peptide manufacturing, better understanding of foot ulcers and a synergistic capability with beta-lactams mean there remains a chance of the approval of pexiganan in the future [184].

The 23 amino acid sequence of pexiganan is shown in Figure 6.10(a). It displays bactericidal antimicrobial activity against gram-positive, gram-negative, aerobic and anaerobic bacteria [189]. *In-vitro* MIC estimations have returned MIC values of $16 - 32\mu$g/ml ($6.4 - 12.8\mu$M) for 100% of *E. coli* strains [189, 190]. Importantly, MIC values reported for 100% of MRSA strains tested (64μg/ml) [190] are below concentrations required for 100% hemolysis (250μg/ml) [191]. Additionally, there were no side effects of treatment during the clinical trials illustrating low toxicity/ haemolytic activity at these concentrations [184].

As part of the work presented in this thesis, time-kill curves are measured for pexiganan. This builds on work from two previous studies [189, 191]. Both performed plate counts with time at pexiganan concentrations of either the MIC or at higher multiples of the MIC. In [189] the killing rate of *E. coli* at 16 (MIC), 64 and 256μg/ml in cationically adjusted (levels unstated) MHB was concentration dependent for the first 120 min after peptide addition, but subsequent times were not monitored (Figure 6.10(b)). An initial inoculum size of $\sim 5 \times 10^5$ bacteria/ml was reduced to zero CFU within 30 min

by 256μg/ml. In [191] a single concentration of 20μM (50μg/ml) showed the reduction of *E. coli* CFU from 10^6 to 0 in 30 min in 2× TY medium. Despite the fact that most researchers measuring the MIC of pexiganan will routinely collect OD measurements of sub-MIC bacterial growth, they have not been reported in the literature to date.

The majority of previous work on pexiganan has been on its mechanism of action rather than its pharmacodynamics (the subject of this thesis). Gaining an understanding of the action of an AMP has typically involved research into its secondary structure, its topology in membranes and mechanistic studies [184]. There is no single technique capable of identifying the mechanism of an AMP, rather a picture is built up using many different techniques [175]. The techniques which can be used to probe bacterial cells are limited to those which either, do not interfere with the cells (microscopy and AFM) or only interfere after cell death (SEM). Consequently, the majority of research into the molecular details of AMP mechanism has been on model membranes.

Circular dicroism studies have shown that pexiganan is unstructured in solution, but α-helical when lipids or detergents are present [192]. It has also been suggested that pexiganan self-associates to form dimers in the presence of multilamenar vesicles [193] and when solubilized in dodecylphosphocholine (DPC) micelles [194]. Solid-state NMR on fluid and physiologically relevant lipid bilayers shows that pexiganan is oriented near the surface of the membrane, perpendicular to the bilayer normal [192, 195] ruling out the barrel- stave mechanism of pore formation [184]. Mechanistic studies have employed a wide-range of biophysical techniques to come to a consensus that pexiganan forms toroidal pores in bacterial membranes and that this is its mode of antibacterial action [184, 196] (described in Figure 6.9). NMR and DSC studies on lipid bilayers have shown that on incorporating pexiganan they develop positive curvature strain [192, 195].

Pexiganan causes time and concentration dependent membrane thinning of lipid bilayer and vesicles both before the formation of pores and at lower concentrations than pores are seen [197]. POPC/POPG lipid vesicles leak their contents after pexiganan addition, with maximal effect after 5 min [192]. Leakage at 5 min was linearly dependent on concentration in the narrow range of concentrations studied ($0.2 - 1.2\mu$M).

Only two studies have included mechanistic research on live bacteria, *E. coli* in both cases [192, 198]. Ramamoorthy and co-workers measured the membrane disruption of *E. coli* in buffer containing pexiganan by measuring the uptake of the fluorescent molecule ANS. Maximum ANS uptake, indicating outer membrane disruption, was at 5 min after the addition of the peptide, and was concentration dependent. Membrane disruption occurred at concentrations below the MIC measured (no data was shown for

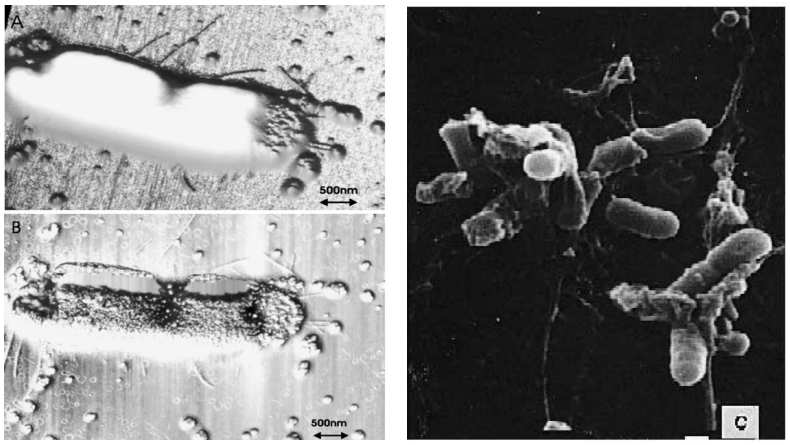

(a) **(b)**

Figure 6.11 AFM and SEM images of *E. coli* treated with antimicrobial peptides. (a) (A) Topology and (B) phase atomic force microscopy of *E. coli* treated with magainin2 amide at a concentration above a 50% inhibition of growth (exact concentrations not stated) [200]. (b) Scanning electron microscopy published in [199], showing *E. coli* exposed to magainin2 for 30 min (0.1nmol/10^6CFU).

concentrations above the MIC). This caused the researchers to conclude that disruption was not necessarily sufficient for antimicrobial action, despite the measurements having been made in different buffers. Pius *et al.* [198] incorporated ^{2}H labels into *E. coli* in order to use NMR to study the interactions of pexiganan with intact *E. coli*. Again, they found that the outer membrane is disrupted at sub-lethal concentrations and that the majority of the peptide does not even reach the inner membrane.

In spite of the interest in pexiganan, there have been no AFM or SEM images illustrating the effect of pexiganan on bacteria rather than bilayers. Figure 6.11 shows images of magainin2 amide and magainin2 respectively acting on *E. coli* [199, 200], as examples of the capabilities of a peptide that that has the same toroidal pore forming action in lipid vesicles as pexiganan. Below a concentration required for 50% inhibition of growth, surface bound vesicles were seen using AFM, while above this concentration, deep lesions, vesiculation, collapse and inner membrane withdrawal were all seen. Electron microscopy showed similar results [199]. But [200] also demonstrated that the damage caused by three different peptides (magainin2, melittin and PGLa) was markedly different, so it must not be assumed that pexiganan behaves identically to magainin2.

It has been suggested that one of the bacterial resistance mechanisms against magainins is due to proteases located on the membrane surface [201]. Gottler *et al.* investigated the susceptibility of pexiganan to lysis by trypsin and chemotrysin using reverse phase

HPLC [202]. They found that the peptide was completely degraded within 30 min of incubation with either protease, both when structured in the presence of liposomes, or unstructured. To improve the peptide's stability without losing its antimicrobial properties they synthesized a fluorous analogue of pexiganan, fluorogainin-1 by replacing two amino acids with fluorous amino acids. Fluorogainin-1 took more than 10 hours to be degraded by the same proteases when structured. A comparison of the MIC values measured for both peptides against *S. aureus*, known to resist AMPs by secreting proteases, showed that fluorogainin-1 had a lower MIC than pexiganan.

6.3.3 Problems in the AMP field of study

Integrating biological and mechanistic studies

A secondary aim of the study presented in this part of the thesis is to provide population and single cell measurements of pexiganan action on live bacteria, for comparison with mechanistic studies. There have been fascinating reviews [203, 204] and perspectives [125] comparing biophysical studies with biological studies of AMPs. These have been driven by the feeling that the two strands of research have not been integrated. One of the reasons for this has already been mentioned, much of the biophysical characterisation has taken place in model systems such as lipid vesicles, rather than in bacteria. It is not known how closely the two mechanisms of action overlap [203].

In a table published in [203] (Figure 6.1) Wimley quantitatively compares a typical MIC assay with a typical synthetic large unilamellar vesicle experiment. In both experiments peptides are effective at μM ranges, which would lead to 1×10^3 peptides/vesicle or 1×10^9 peptides/cell. Peptide to lipid ratios are calculated (given some assumptions) to roughly 10^4 times different between the two systems, despite action being measured at the same concentration. The two experiments are carried out in entirely different regimes.

It is not physically possible for 100 peptides (see Figure 6.1) to be bound to a single lipid on a bacterium. Rather this number suggests that peptides bind to other cellular components such as lipopolysaccaride and DNA. These calculations indicate that it is safe to assume that at an active concentration the membrane is completely saturated with peptides, also concluded by Melo *et al.* [125]. Interestingly, concentrations this high are necessary for activity. If the peptide concentration is reduced by one order of magnitude there is no longer any antimicrobial action (sub-MIC) despite there still being 10^8 peptides per cell.

TABLE 1. Statistics of peptide and lipid stoichiometry in vesicle permeabilization and microbe sterilization assays calculated for typical experimental conditions[a]

Property	Large unilamellar vesicle	*E. coli* sterilization assay
Dimension	0.1 μm diameter	1 μm × 2 μm diameter
Aqueous volume	10^{-19} L	10^{-15} L
Number of lipids	100,000 per vesicle	25,000,000 per cell
Typical concentrations	500 μM lipid	10^5 cells mL^{-1}
	1×10^{12} vesicles mL^{-1}	0.004 μM lipid
	5 μM peptide	5 μM peptide
Relative peptide	1×10^3 peptides per vesicle	1×10^9 peptides per cell
Total peptide:lipid	1 peptide:100 lipids	1000 peptide:1 lipid
Bound peptide:lipid	1 peptide:200 lipids	100 peptides:1 lipid

[a]Bound peptide to lipid ratios are conservative estimates based on direct, experimentally measured binding (see text).

Table 6.1 Table from [203] presenting peptide and lipid statistics from typical vesicle permeabilization and biological sterilisation assays.

Wimley [203] is critical of many of the conclusions drawn from experiments carried out on vesicles. In his opinion areas of concern are the infrequent reports of vesicle aggregation on addition of peptide, the scarce evidence that pore-forming AMPs form actual water-filled transmembrane pores and 'the enigma of partial transient release'. The collation of these features lead Wimley to conclude that vesicle permeabilization is driven by non-equilibrium events and that overall membrane disruption is a more likely mechanism than stable pore formation. Whether these conclusions are relevant for biological systems is not commented upon, possibly due to the small number of temporal peptide action studies, to which this thesis hopes to contribute.

There have been some single cell experiments reported that bridge the gap between biological and biophysical studies. Gee *et al.* [205] measured the timescale of GFP fluorescence leakage from an *E. coli* in the presence of a melittin derivative (judged to be a pore former in model membranes). Fractional fluorescence of GFP in the cytoplasm decreases rapidly for the first ∼25 mins, as fractional fluorescence from melittin increases at a corresponding rate, and then plateaus. The fractional fluorescence of pores, measured separately to cytoplasmic leakage, did not change from time 0 onwards. The researchers conclude that that cytoplasm is not lost by permanent pore formation but either through membrane disruption or by transient pores which are a kinetic intermediate species, forming and closing at a similar rate.

In another interesting single cell experiment, Sochacki *et al.* [206] used time-resolved fluorescent microscopy of *E. coli* in the presence of LL-37 to enable them to correlate the degree of LL-37 binding, its spatial distribution, permeabilization of the membranes and the halting of growth. Despite the relevance and usefulness of measurements of this nature, it is unclear how they relate either to MIC measurements or to the proposed

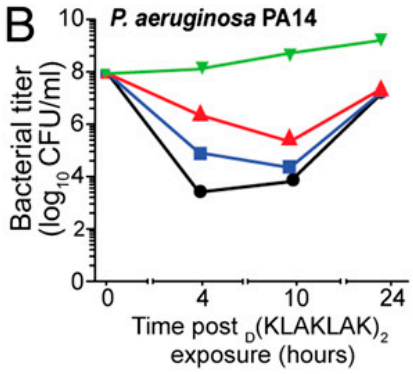

Figure 6.12 An example of time-kill curves showing regrowth. *P. aeruginosa* PA14, exposed to MIC (red), 2× MIC (blue) and 4× MIC (black) concentrations of $_D$(KLAKLAK)$_2$. From [207].

carpet or toroidal pore mechanisms of LL-37 action. For instance it is surprising that few cells stopped growing at the MIC, but all cells stopped growing at 4×MIC, despite the numbers calculated in Table 6.1 suggesting that both concentrations studied should be able to result in complete membrane saturation. Quantitative observations linking length scales are crucial in the future development of the field of AMP action. Single cell experiments are reported in this thesis to link population measurements to pexiganan action on individual bacteria.

Pharmacodynamics of AMPs

Biological action studies into AMPs show concerning trends in the literature, the validity of which this project hoped to investigate. Firstly, the MIC is often interpreted as the threshold for bactericidal AMP action [125]. One example comes from research into pexiganan. Pius *et al.* [198] found that membrane disruption was not an indication of cell death, as it occurred at 'sub-lethal concentrations' defined as concentrations below the MIC. A MIC measurement is defined as the concentration at which no growth is observed in a time period. For some antibiotic-bacteria combinations the MIC may well be the threshold of action, however there has been no study proving that this is the case for AMPs in general or pexiganan specifically, and until verified, this assumption could lead to the mis-interpretation of data. A specific objective of the study presented here was to attempt this verification.

Secondly, time-kill studies are often (not always) monitored only for a short period of time (a few hours in contrast to 24 hours for a MIC assay), at MIC concentrations and above, and the full implication of the results is little discussed. Partial killing is a topic often discussed in the literature on small molecule antibiotics, and has been attributed

to persisters, but it is unclear if this explanation is applicable to AMPs. Regrowth at concentrations which initially reduces cell numbers [199, 207, 208] typically occurs at long times (not always, seen after 30 min in [199]), sometimes only recorded by a single time point at the lowest concentration tested (an example is shown in Figure 6.12). There is no consensus on reasons for regrowth. It has been dismissed as being likely due to a decrease in phenotypic susceptibility to the peptide [207], although no explanation for why a phenotypic tolerance develops is proposed. Two magainin derivatives MSI94 and MSI93 degraded sufficiently in the media over a 24 hour incubation period that this was deemed to be the cause of regrowth [209].

Finally, there has been little discussion of explanations for peptide inoculum effects (IE) observed for some AMPs, but not for others [210]. Casteels *et al.* [211] comment that an IE for apidaecin-type antibacterial peptides exists against some bacterial strains, but not against all. They postulate that the IE is due to non-selective binding to the surfaces of large numbers of cells, but do no experimental work to support this hypothesis. The magnitude of the AMP IE can be substantial; the MBC of Lactoferricin B against *E. coli* went up with the initial concentration of *E. coli* from $\sim$10 mg/L at 10^4 cells/ml to 120 mg/L at 10^8 cells/ml [212]. An IE for pexiganan has not been reported, but magainin derivatives MSI-94 and MSI-93 showed an increased rate and extent of bactericidal activity with decreasing inoculum of *P. aeruginosa* [209].

Chapter 7

Methods: Pexiganan action on growth

In this chapter the methods used in the study of the growth of *E. coli* in a suspension containing pexiganan are described.

7.1 General experimental procedures

7.1.1 Culture of bacteria

E. coli MG1655 was the primary strain of bacterium used. MG1655 is a laboratory K-12 derivative, maintained with minimum genetic manipulation [213]. Two fluorescent *E. coli* strains were also used; RJA002, a derivative of parent strain MG1655, contains a chromosomal insertion of a yellow fluorescent protein (YFP)/Chloramphenicol resistance cassette [214] performed previously in our lab by L. Black, and K-12 derived BW25113 from the Keio collection contains plasmid pWR20, carrying enhanced green fluorescent protein (GFP) and kanamycin resistance [215].

E. coli strains were stored in frozen aliquots at $-80°$C and streaked onto plates of Mueller Hinton Broth (MHB) agar which were kept for one week. According to the guidelines published for MIC experiments in [153], roughly 5 colonies were touched and placed into 5ml of MHB. Cultures were incubated at 37°C and 200 rpm until the OD indicated they were in late exponential phase. These cells were then diluted to the desired density in fresh MHB, without being washed, ready for inoculation.

Mueller Hinton Broth (MHB) is the medium of choice for antibiotic susceptibility testing [153]. It is composed of beef infusion (2 g/L), Casein Hydrolysate (17.5 g/L) and starch (1.5 g/L). MHB was prepared by dissolving 21g/L of powdered MHB (Oxoid) in distilled water and autoclaving. MHB was converted into a solid medium by adding 10 g/L of powdered agar (Oxoid) prior to autoclaving.

MHB can be cationically adjusted to $20 - 25$ mg/L Ca^{2+} (from 2.7079 mg/L) and $10 - 12.5$ mg/L Mg^{2+} (from 3.644 mg/L) to result in 2+ ion concentrations which more accurately resemble physiological conditions [153]. The divalent cations Mg^{2+} and Ca^{2+} ions are potent inhibitors of peptide action [172] due to the stabilisation of lipopolysaccharide by the divalent cations [216, 217]. In this study, pexiganan was found to be ~ 4 times less effective in cationically adjusted MHB, but I decided to continue using un-adjusted MHB to conserve peptide stocks. This was deemed reasonable as the aim was not to measure the precise concentration effective for a particular application and many researchers actively advise against adjustment [153].

The optical density (OD) of bacterial cultures was measured using a Cary spectrophotometer at 600 nm. OD measurements of exponentially growing *E. coli* MG1655 in MHB were calibrated to colony forming units (CFU) by plate counting, to give OD$= 1 = 5 \times 10^8 \pm 1 \times 10^8$ cell/ml. The spectrophotometer's lowest limit of detection is $\sim 5 \times 10^5$ cell/ml.

7.1.2 Preparing antimicrobial agents

Pexiganan was synthesised at the National Physics Laboratories (NPL) and posted in powder form. Stock solutions at 2mM were prepared by dissolving peptide in sterile water and stored at -20°C. Stocks were defrosted immediately before use and some of the solution was removed, before they were re-frozen. No difference was observed between the activity of a freshly prepared stock and one which had been frozen. Other peptides used included, amhelin, magainin and PR-39, also synthesised at NPL, which were prepared identically to pexiganan.

Solutions of kanamycin were filter sterilised and stored at -20°C. Once defrosted for use they were kept at 4°C for 1 week.

Poly-L-lysine (Sigma Aldrich) was purchased at 0.1% (w/v) in water (M_W=150,000-300,000) and stored at 4°C.

7.2 Optical Density measurements in a multi-well plate reader

7.2.1 Sample preparation: Setting up a multi-well plate

A FLUOstar Optima (BMG Labtech) plate reader measured the optical density at 600 nm of 96 test cultures in a multi-well plate. Flat bottomed, polystyrene, 96-well plates (Greiner), with cylindrical wells containing 200μl of suspension were used. Lids covered the plates, allowing air flow. It was checked that the bioactivity of the peptides was not affected by the use of polystyrene plates instead of polypropylene plates. Previous research has suggested adhesion of AMPs to polystyrene [217].

In most cases the protocol followed for plate preparation was to first pipette the desired volume of MHB into the well, followed by peptide, to make up a total volume of 190μl. Then 10μl of prepared bacterial suspension was added to the well to result in a total volume of 200μl, and ensure the required $t = 0$ min inoculum size $N(0)$ and peptide concentration $P(0)$ in the well. As the environmental conditions (temperature, shaking, volume) were kept constant, the parameters changed were the initial density of bacteria $N(0)$ and the initial concentration of pexiganan $P(0)$. A number of wells in each plate always contained 200μl of MHB alone to check for contamination. If these wells grew, the data from the plate was discarded.

After inoculation, the plate was immediately placed in the plate reader, pre-heated to 37°C. The OD of each well was measured every 5.21 min for 24 hours, with 220 seconds of shaking at 200 rpm in between measurements.

The detection limit of the plate reader is $\sim 2 \times 10^7$ cell/ml; far less sensitive than the Cary single read spectrophotometer. This has been reported as typical for plate readers [218, 219]. It was verified that OD measured in the plate reader was linear with cell density up to OD=1 and, once blanked with the OD measured for MHB alone, could be calibrated to N (density of bacteria) using the same calibration as for the single read spectrophotometer (albeit with a larger propagated uncertainty of $\pm 1.1 \times 10^8$ cell/ml).

Varying $N(0)$ in a well

In order to vary the inoculum size $N(0)$ (the density of bacteria N at $t = 0$ min, expressed in cell/ml or cell/well) in a well, the bacterial culture, grown in the incubator,

was diluted (using 5× or 10× serial dilutions) to the required density. The suspension was then vortexed, before 10μl was added to each well. Inoculum sizes in the range $5-2.5\times10^7$ cell/ml or $1-0.5\times10^7$ cell/well were achieved with this method. To achieve a higher $N(0)$ of 2.5×10^8 cell/ml whilst still inoculating late-exponential cells, 100μl of OD=1 in MHB was added to the well. Additionally, in one case, a serial dilution method was used to result in a different $N(0)$ in each of the 96 wells.

Single cells in wells: For researchers studying the adaption time of single bacteria to different environmental conditions, as is done in this study for pexiganan, there is a well established method of working with ~ 1 bacterium per well, sometimes called the dilution method [220].

The culture is diluted to the density required to result in 1 cell/well (5 cells/ml) after inoculation (100 cell/ml, if 10μl is added). However, when $N(0)$ is this low, small differences in the density of the inoculum can result in observable variation between experiments. Therefore an alternative method of verifying the $N(0)$ used is necessary. As $N(0)$ is reduced, the likelihood of a well not growing due to the absence of bacteria increases. This allows a calculation of the mean number of cells per well at $t = 0$ in those that grow, using the equations below, reproduced from [219].

It can be assumed that the number of cells per well follow a poisson distribution;

$$P(N(0) = k) = exp(-\rho)\rho^k/k! \tag{7.1}$$

where,

$$\rho = -ln(W/W_0). \tag{7.2}$$

The fraction of empty wells (W/W_0) can be used to calculate the expected value and variance ρ of this distribution. The mean number of cells per *growing well* ρ^+, follows a truncated poisson distribution and is given by the equation;

$$\rho^+ = \rho/(1 - e^{-\rho}). \tag{7.3}$$

The variance of the truncated poisson distribution is,

$$Var = \rho^+ - (\rho^+)^2 e^{-\rho}. \tag{7.4}$$

At an average of 1 cell/growing well, 10% of the wells grow. It is impractical to collect

data with so few wells growing, so it is usual to work in the range of 50%-75% of wells growing [144]. At 75% growing, ρ =1.38 and ρ^{+}=1.85, meaning that 34% of wells contain 1 cell, 24% of wells contain 2 cells and 11% of wells contain 3 cells at $t = 0$.

Varying $P(0)$ in a well

In order to vary the concentration of pexiganan $P(0)$ in a well, the volume of the peptide stock added to the medium was varied. Volumes added were kept within the range $3 - 20\mu$l by diluting the stock $10\times$ in sterile water if required. Peptide was pipetted separately into $8 - 12$ wells of the plate and then additional concentrations created by a $2\times$ serial dilution (described below for MIC assays). When serial dilution was not possible, the peptide was added to a larger volume of MHB in a test tube, mixed by inverting the tube, and then pipetted into wells.

Brief exposures to pexiganan

Pexiganan concentrations between 0.1 and 10μM were added to 1 ml of *E. coli* MG1655 at OD=0.5 for a time-period of $1 - 15$ min. The suspension was then serially diluted and roughly half of the wells of a 96 multi-well plate inoculated with ~ 1 cell/well. This resulted in a negligible $P(0)$ in the well. An identical control suspension underwent the same protocol, without the addition of pexiganan, and inoculated the remainder of the wells.

7.2.2 Minimum Inhibitory Concentration (MIC) measurements

MIC assays are a specific way of preparing a multi-well plate to test the same $N(0)$ against a range of peptide concentrations $P(0)$. The MIC of pexiganan was determined by the broth micro dilution method, using the protocols outlined in [153], with some adaptions.

A volume of 190μl of MHB was added to each well in a plate except for the first row of 8 wells. These wells were prepared with 380μl of medium containing peptide at the highest test concentration. This concentration was serially diluted in $2\times$ dilutions by removing 190μl from the first row, pipetting it into the second, mixing well with the pipette, removing 190μl into the third, and so on until the row before last. The final row was left without peptide as a 0μM control. The culture of bacteria was then removed from the incubator and diluted to OD=0.02 (1×10^7 bacteria/ml). Ten μl

of the bacterial solution was added to each well to obtain a concentration of 1×10^5 bacteria/well or 5×10^5 bacterial/ml, beginning with the lowest peptide concentration. MICs performed at this standard inoculum level will be referred to as the baseline MIC or bMIC [155]. The three *E. coli* strains used in this investigation had the same bMIC within uncertainty.

When a more precise measurement of the MIC was needed a linear concentration range was used. This was more time consuming as the pexiganan concentrations required were prepared in test tubes and then pipetted into the wells.

The MIC was defined to be the lowest concentration of peptide to result in no detectable growth at 24 hours *i.e.* to have an OD of equal to or lower than than at $t = 0$. At this inoculum level, the OD at $t = 0$ min is that of MHB given that $N(0)$ is too low to detect. There was some noise in the background OD, but not enough to influence the decision of whether growth had occurred.

7.3 Millifluidic Droplet Analyser (MDA)

A Millifluidic droplet analyser at the ESPCI Paris measured the fluorescent signal of *E. coli* RJA002 contained in millifluidic droplets of MHB. The MDA was used in collaboration with Jean Baudry and Denis Cottinet (who operated the MDA for each experiment) in the 'Laboratoire collides et material divides' group.

The MDA and the procedure for its use are described in detail in [164]. In summary, 100 nL mini incubator droplets were produced by accurately mixing MHB, bacteria in MHB and pexiganan in MHB, using precision syringe pumps. By programming the pumps, the desired peptide concentration and $N(0)$ can be achieved in each droplet. Green fluorescent markers were added to the antibiotic solution to act as a marker of concentration. The droplets were then dispersed in a continuous HFE oil with surfactant (0.006% of highly biocompatible tri-block copolymer) phase in a 1D train down a tube. Mineral oil droplets act as spacers. When enough droplets had been produced, some were removed from each end of the train and a mineral oil plug was inserted.

To observe the density of cells in each incubator with time, the train of droplets was passed back and forth in front of a detector. This is done by injecting oil into the tube at a steady rate, passing each droplet in front of a fixed point detector once every $\sim 7 - 8$ min. Droplets are numbered in order not to lose track of each individual

droplet for analysis. The detector, equipped with a photomultiplier tube, measures the fluorescent signal (in Volts (V)) from each drop, excited by $\sim$ 490 nm light, focused by 20$\times$ objective and passed through an emission filter ($\sim$ 525 nm). In the range of bacteria concentrations used, density is related linearly to fluorescent signal [164]. The detection limit is $\sim$2000 cells/drop, or 2 $\times 10^7$ cells/ml, the same limit measured for the plate reader.

The bacterial culture was grown as for experiments conducted in the plate reader and then diluted to a density for injection which resulted in the desired number per droplet. The growth conditions in the MDA differ from those in the plate reader. Although the droplets are kept at 37°C, they are not shaken, oxygen supply is likely to be limited and there are no hard surface walls.

A linear $\sim 1-2\mu$M step of concentrations between 0 and 20μM was used. Roughly 30 replicate droplets were incubated at each concentration. In reality, when implementing the method described above, droplet volume and hence $N(0)$ was more variable than hoped for. Due to time limitations the method was not improved upon, but despite these problems, the results collected add information to this study.

7.4 Data analysis: Detection times

Detection times were used to analyse the turbidity data collected in the plate reader and the MDA. The chosen detection time T_{det} for analysis was defined to be the time required for a population of *E. coli* to reach OD=0.12 above the background of MHB, and will be referred to as $T_{0.12}$. In the plate reader this turbidity change corresponded to a density of $N_{0.12} = 2\times10^7 \pm 0.4\times10^7$ bacteria/well, $\sim 5\times$ above the detection limit of the instrument. Likewise, the chosen detection time for analysis of data collected in the MDA was a difference in fluorescent signal above the blank of 0.12. The corresponding bacterial density is unknown, but was not required for the observations made.

Raw data from the plate reader or the MDA was imported into Igor Pro. The growth curves were plotted and blanked using the first or third time-point (see results), provided that $N(0)$ was below the detection limit. The $T_{0.12}$ was chosen to be the first time-point above the $N_{0.12}$, found using a script written for Igor Pro by Vincent Martinez.

7.5 Time-kill density curve ($N(t)$)

7.5.1 Plate count (CFU) method

E. coli MG1655 were grown following the same protocol as for MIC assays and diluted to either 5×10^5 cell/ml or 2.5×10^8 cell/ml in either PBS (Phosphate buffered saline) or MHB. If PBS was the medium of choice then cells were washed twice (centrifugation for 5 min at 3000 rpm) before dilution. Three ml of the suspension was placed in two tubes (Greiner, polystyrene, 50ml). Pexiganan was added to one of the tubes at $t = 0$ and both placed in an incubator at 37°C and 200rpm. A 100μl sample was removed from both tubes 1 min after the peptide addition, and diluted in 10$\times$ dilutions of PBS. A range of dilutions, depending on the anticipated density, were spread onto MHB agar plates in triplicate. No more than 5 samples were removed, resulting in a maximum volume reduction of 500μl to the total volume, (17%). This is above recommended levels and would be amended in any future studies. The agar plates were incubated at 30°C for 16 hours before the colonies were counted manually and density of cells N_{CFU} in cell/ml calculated.

It is recommended that CFU are in the range $\sim 30 - 300$ per agar plate, depending on the bacterium plated [221]. Due to variation in the $N(t)$ curves and limited resources, the optimum dilution was not always plated. If the CFU fall outside these limits the advice is to disregard the plate. The uncertainty in this measurement and the rationale for these limits are reviewed in [221]. The upper limit advised is due to competition for space and nutrients between colonies leading to miscounting. The lower limit is due to experimental studies showing poor accuracy at low counts. This is derived from the fact that if the counts follow a Poisson distribution (random sampling from a homogeneous suspension) then the width of the distribution approaches the mean as the counts reduce. In this study, rather than disregarding counts below 30 CFU, they are plotted with their poisson error. Otherwise valuable information would have been lost.

Averages and standard deviations of replicate plates were calculated and compared to the propagated poisson uncertainty. For lower counts the poisson uncertainty was often larger than the standard deviation and as the counts increased the situation was reversed. This suggests that the true estimation of the uncertainty of a single plate count is larger than poisson, as has been noted before [222], as it incorporates errors due to dilution and the plating process. With further work a more accurate error on a single plate count could be estimated, but for the purpose of this study the larger of the

two errors calculated is quoted alongside the average. More finesse would be unlikely to change the appearance of the plots shown.

7.5.2 Comparing OD to CFU

E. coli MG1655 were prepared as above with $N(0)= 2.5 \times 10^8$ cell/ml and $P(0)=10\mu$M in MHB. At each time-point 100μl was removed from the tube and diluted $10\times$ in MHB in a sterile 1 ml cuvette for optical density measurement. After the measurement, 100μl of this sample was removed from the cuvette and diluted in $10\times$ serial dilutions in eppendorfs for plate counting.

7.6 Resistance and effective residual concentration assays

7.6.1 Testing resistance

A MIC assay performed in a multi-well plate resulted in growth in wells at 5μM and 2.5μM pexiganan. The plate was removed from the plate reader after $\sim$1000 min, as these populations both approached the stationary phase. A well was grown from a single cell inoculum at 0μM in the same plate, as a control in the same phase of growth. Bacteria were removed from each of the three wells and diluted in MHB. Each was used to inoculate ($N(0) = 5 \times 10^5$ cells/ml) four replicate MIC assays ($0 - 20\mu$M of pexiganan) in a second multi-well plate.

7.6.2 Effective residual concentration

Two experiments were conducted to probe levels of residual peptide after incubation with and without bacteria. A culture of *E. coli* MG1655 were grown in MHB as already described and diluted to the densities specified below. Similar experiments were conducted in [155] to test the residual antibiotic concentrations in cultures of *S. aureus*.

Experiment A: A multi-well plate was prepared containing;

(a) 3 replicate MIC assays testing 40, 20, 10, 5, 2.5, 1.25μM at $N(0) = 2.5\times10^7$ cell/ml.

(b) 3 replicate MIC assays testing 40, 20, 10, 5, 2.5, 1.25μM at $N(0) = 5\times10^5$ cell/ml.

The plate was placed in the plate reader at 37°C and 200 rpm for 24 hours. Wells which did not show growth above the detection level after incubation were transferred into a second sterile plate and re-inoculated with 5×10^5 cell/ml. The plate was incubated for another 24 hours in the plate reader, reading the optical density of each well every 5.21 min.

Experiment B: Two separate tubes containing 5 ml of bacterial suspension each were prepared;

(a) $N(0) = 5 \times 10^6$ cells/ml with $P(0) = 40\mu$M pexiganan.

(b) $N(0) = 0$ cells/ml with $P(0) = 40\mu$M pexiganan.

Samples were incubated at 37°C and 200 rpm for 18 hours. One hundred μl was removed and spread onto an agar plate to check for surviving bacteria. The suspensions were then filtered (0.22 μm) to remove any survivors and the supernatant used as media in a 96 multi-well plate MIC assay. A fresh culture of MG1655 was grown for inoculation. Four MIC assays were prepared in the plate (replicated twice):

1. $N(0) = 5 \times 10^5$ cells/ml with supernatant from (a), diluted in 2× serial dilutions with MHB.

2. $N(0) = 5 \times 10^5$ cells/ml with supernatant from (a) with an additional 20μM of pexiganan added, diluted in 2× serial dilutions of MHB.

3. $N(0) = 5 \times 10^5$ cells/ml with supernatant from (b) diluted in 2× serial dilutions with MHB.

4. $N(0) = 5 \times 10^5$ cells/ml with MHB and $P(0) = 20\mu$M pexiganan, diluted in 2× serial dilutions in MHB (standard MIC assay).

The plate was incubated for 24 hours in the plate reader and growth curves plotted.

7.6.3 Sonication

In order to create a suspension containing lysed bacteria in which to test pexiganan efficacy, a sonication technique was used. Ten ml of *E. coli* MG1655 were grown in MHB to late-exponential phase. The culture was transferred to 14 ml polyproylene round-bottom tubes (Falcon) and placed in a 1L beaker of compact ice. The sonicator and surrounding area were wiped with ethanol. The beaker was placed on the sonicator shelf with the probe inside the tube. The shelf was adjusted such that the probe did

not touch the sides of the tube and its tip was $\sim$ 1 cm away from the bottom of the tube. The sample was sonicated at amplitude 11 in 10 pulses of 30 seconds with 2 min resting on ice between each sonication.

Plate counts before and after sonication showed that 99.98% of cells lost viability during the procedure. Furthermore, the culture appeared less turbid after sonication than before. To remove the surviving cells the suspension was filtered (0.22 μm). The supernatant was used to prepare 4 replicate MIC assays (0μM-20μM) in a multi-well plate. Two MIC assays in fresh MHB were prepared alongside as a control. All wells were inoculated with a fresh culture of MG1655 grown in MHB, to result in an $N(0) = 5 \times 10^5$ cells/ml.

7.7 Single cell microscopy

7.7.1 Times to first division

In this study bacteria were placed on agar to image their time to first division after exposure to pexiganan. The protocol followed for imaging growing MG1655 on an agar pad was adapted by Diarmuid Lloyd from [223]. Agar (0.2 g) was added to 10 ml of MHB in a 35 ml tube. The mixture was microwaved on a low heat, stopping every 30 seconds to observe whether the agar had melted, turning the solution clear. An adhesive Gene Frame (Thermo Scientific) was stuck to a microscope slide and 500μl of warm agar solution pipetted into the frame. Another glass microscope slide was placed gently onto the frame as soon as the agar was in place, before it solidified. The slides were prepared up to an hour in advance with the agar remaining covered to prevent evaporation.

E. coli MG1655 were adjusted to OD=0.5 and pexiganan added at the required concentration (controls had no peptide added). The solution was mixed and left for an incubation period. A range of peptide concentrations ($0.1 - 5\mu$M) and incubation times ($1 - 15$ min) were tested in order to capture a situation resulting in a significant proportion of the initial cells both dying and surviving to divide. The data shown in results is from 3μM pexiganan incubated for 3 min.

While the bacterial suspension incubated on the bench, the microscope slide was removed from the agar, leaving a flat clean surface. A scalpel was used to trim around the edges of the frame and remove sections of the agar to leave two agar strips beside oxygen reservoirs. After 3 min, 1μl of the bacterial solution was pipetted onto the agar

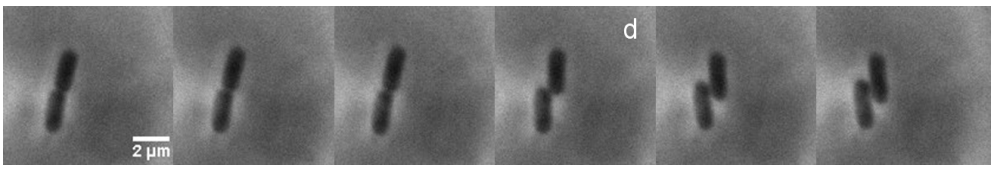

Figure 7.1 Phase contrast time-course of an *E. coli* bacterium undergoing division on MHB agar. Images taken 1 min apart moving from left to right. The time-point chosen to represent division is labelled with a d.

pad. The slide was tilted in order than the liquid spread out down the pad. Within 4.5 ± 1.0 min all residual liquid disappeared, in part due to absorption into the pad, but primarily due to evaporation [223]. When liquid could no longer be seen, the plastic cover was removed from the frame and a glass cover slip was gently placed onto of the agar and stuck down firmly to the frame. The sample was transferred to a inverted microscope (Nikon TE300 Eclipse), pre-heated in a temperature controlled box to 37°C. The bacteria were located and the acquisition started. It took between 6 and 10 min to begin acquisition from the adhesion of the cover slip. Images were recorded for ~ 2 hours.

Phase contrast images were taken with a CoolSNAP HG^2 CCD camera (Photometrics), of $12 - 14$ fields of view, using a 100X PH3 oil immersion objective. The software Metamorph controlled the stage to move between the fields of view (xy plane) and enabled auto focussing in the z plane. One image of each field was acquired every minute allowing a determination of the TTFD to ± 0.5 min. Given the uncertainty in deciding when the first division takes place, this uncertainty is insignificant. Image J was used to inspect the images and to save them as time courses. The time to first division (TTFD) was determined by eye to be the time at which the daughter cells change orientation, illustrated in Figure 7.1. Niven *et al.* [224] state that this is the time at which there is sufficient flexibility at the point of attachment to allow movement.

It was straightforward to distinguish living cells from those which were dead. A bacterium was deemed to have lost viability and hence be dead if it did not grow, divide and it gradually lost contrast in the images over time. Some samples were observed the following day to verify that cells showing these features had not recovered.

No thorough investigation into the location of the peptide after liquid evaporation was conducted. Changing negatively charged agar for neutral agarose, did not change the results. Both agar and agarose have pore sizes of $\sim$ 100nm, allowing the peptide to diffuse fairly freely. Therefore, it is likely that peptide deposited on the agar during evaporation of the liquid diffuses into the agar gel, establishing a concentration which is

too low to effect further generations of bacteria on the surface. However during the ~ 5 min of evaporation it is likely that the initial cells are exposed to higher concentrations than added to the original suspension. No quantitative comparisons should be made between pexiganan concentrations used in this protocol and in other protocols.

7.7.2 Tunnel chamber

A tunnel chamber was used to allow single cell observations to be made during the addition of pexiganan to their growth medium. The chamber allowed the exchange of media after bacteria growth had begun. Tunnel slides were prepared from assembling coverslips as described in [215]. Scotch double sided tape was stuck onto a microscope slide in two strips, 3 mm apart. A coverslip was placed ontop of the tape and a plastic pipette tip used to press on the tape, ensuring complete adhesion of slip to tape. This created a tunnel chamber of size $\sim 3 \times 20 \times 0.1$ mm.

Ten μl of 1% (w/v) Poly-L-lysine was pipetted into the chamber, the slide inverted and left for 3 min. Unbound polymer was removed by washing through 200μl of LB. Small (4cm×4cm) squares of kitchen roll were used to suck the media through the chamber. Note that in [215] the growth medium of the bacteria is used to remove unbound polymer. However, washing with MHB instead of LB reduced subsequent binding of cells to the coverslip and caused dirty streaks seen under the microscope. It is likely that components in the MHB bind to the positive polymer, requiring LB to be used for this step.

E. coli BW25113, a non-motile strain containing an EGFP plasmid, was grown in MHB to OD=0.5. After removal from the incubator the culture was used in sample preparation for up to 2 hours. Cells were concentrated 5× using centrifugation, immediately before 10μl were inserted into the tunnel. The slide was inverted and incubated for 7 min. Unbound cells were then washed out of the tunnel with 100μl of MHB. Droplets of MHB were placed at either end of the tunnel to slow evaporation from the open ends.

Cells were observed in phase contrast and fluorescence using a Nikon E800 upright Microscope. The microscope and the surrounding environment were pre-heated to 37°C. After the tunnel slide was placed on the stage, a field of view containing a minimum of 5 flat (adhered to the cover slip along the whole of the cell body) cells was found. Micro Manager multidimensional acquisition software was used to record images taken with QImaging Retga 2000R CCD camera every 20 seconds. Light was shuttered

in between image acquisition to reduce photobleaching. The fluorescent channel used was YFP (excited at $490-510$ nm) rather than GFP (excited at $450-490$ nm), as GFP was found to significantly slow the growth of the *E. coli* within minutes. Autofocus in phase contrast channel, maximising the sharpness of the edges, was used to maintain a constant z position.

An eppendorf containing MHB and pexiganan at the desired concentration was placed inside the heat controlled box. After $5-10$ min of recording images, it was checked that the cells were growing. Then, without disturbing the stage or touching the pipette to the microscope slide, 30μl of peptide solution was dropped onto the slide, at the opening of the tunnel. From the other side, a square of tissue was used to draw the solution through the tunnel, until very little liquid was left where dropped. Often some cells were washed out of the field of view, and occasionally the focus had to be found manually once more before the autofocus could locate the cells. Images were recorded for 30 min to 1 hour after peptide addition, depending on observations.

For cell volume measurements, data analysis of fluorescent images followed [215], using Labview scripts developed by T. Pilizota. Analysis was only performed on cells which appeared flat on the coverslip, and remained stuck throughout the media exchange. The long axis of a flat cell is aligned horizontally with the image axis. A rectangle is then chosen around the cell and a second smaller rectangle chosen as a background inside the first. The mean intensity of the background rectangle is subtracted from all pixels in the cell rectangle. Pixel values were then normalised and any pixels with intensity 30% of the difference between the minimal and maximal value in that frame was deemed to be part of the cell cytoplasm. For each frame, the number of pixels above this threshold is recorded. Cell volume traces were normalised to the number of pixels at $t = 0$, taken to be the first frame recorded.

The fraction of lysed cells in a field of view was judged by eye. Lysis was assumed to correspond to a rapid drop in fluorescent signal, and a cell was deemed lysed when it no longer displayed any fluorescent signal above the background. Time-lapse images were constructed of stacked phase contrast (grey channel) and fluorescent images (yellow channel). A section, usually 1/4 of the field of view was selected and at every third frame after peptide addition ($t = 0$) the number of cells appearing black rather than yellow was counted. At later times the frame interval between counting was increased. The contributions from all 4 sections of the field of view were accumulated and the number lysed at each time point normalised to the total number of cells.

Chapter 8

Results: Pexiganan action on growth

8.1 *E. coli* growth

Before interpreting the results of pexiganan susceptibility tests, bacterial growth in the absence of peptide must be understood. The following sections present an example of the *E. coli* growth curve and analysis of its parameters using detection times. Additionally, section 8.1.3 includes a verification of the method used to obtain single cells in wells.

8.1.1 The growth of *E. coli* in a well

To understand and characterize the population growth of *E. coli* MG1655 in MHB, a single plate was prepared by serial dilution with planned inoculum sizes ($N(0)$) ranging from 5×10^6 to 7 cells/well. One of the resulting 24 hour growth curves, from $N(0)$= 5×10^4 cell/well = 2.5×10^5 cell/ml, is shown in Figure 8.1.

The data is presented in four different ways to aid understanding. Figure 8.1(a) shows the raw OD data as well as its linear conversion to N on the righthand axis, (b) shows the same data having been blanked with the OD measured at $t = 0$ (OD of MHB). Once blanked, OD-OD(0) is directly related to N, shown on the righthand axis. In (c) the data is plotted as ln of the un-blanked, normalised data (ln(OD/OD(0))), and in (d) as ln of blanked data (ln(OD-OD(0))). Taking ln of the blanked data demonstrates

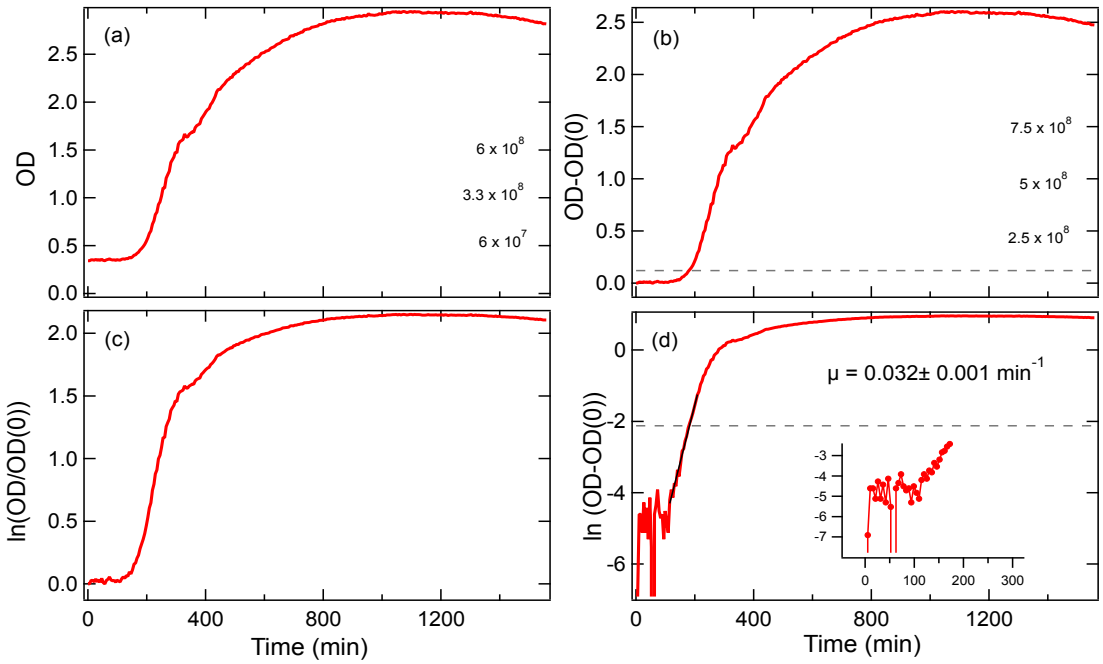

Figure 8.1 *E. coli* growth curve in MHB. (a) Raw OD data, (b) blanked OD data, (c) normalised OD data, and (d) ln of blanked data, with time for an inoculum size of N(0)= 5×10^4 cell/well growing in 200μl of MHB at 37°C. The inset in (d) is a magnification of the main plot between $t = 0$ and $t = 300$ min.

that the OD is increasing exponentially from the moment it is detected to be above the noise. The region around the time of detection is shown more clearly in the inset.

Growth is detected first at $\sim$ 115 min, and is exponential until $\sim$ 210 min. Culture growth is diauxic; at $\sim$ 325min the bacteria appear to enter a brief stationary phase, presumably on the depletion of a metabolite, but then adapt and resume growth to enter a permanent stationary phase $\sim$ 200 min later. A best fit line to the exponential section of the curve gives a growth rate of $\mu = 0.032 \pm 0.001$ min^{-1}, the value of which is discussed in the next section. The lag time λ (see Figure 6.1 for definitions of μ and λ) is hidden below the detection level, there is no visual information about it.

The chosen detection level of OD-OD(0)=0.12 is shown as a dashed line on (b) and (d). The $T_{0.12}$, the time at which the growth curve intersects the dashed line, lies between two data points, t = 177 and 182 min. Therefore, the $T_{0.12}$ quoted for this growth curve is 182 min. Uncertainty in this measurement, estimated at $\pm$10 min, is derived from the OD reading at this point and at $t = 0$, and the decision to chose the later point rather than a value in between.

Given that it takes an initial inoculum of 5×10^4 cell/well 182 $\pm$10 min to reach a density of 2×10^7 cell/well growing at a μ of 0.032 min^{-1}, λ can be calculated to

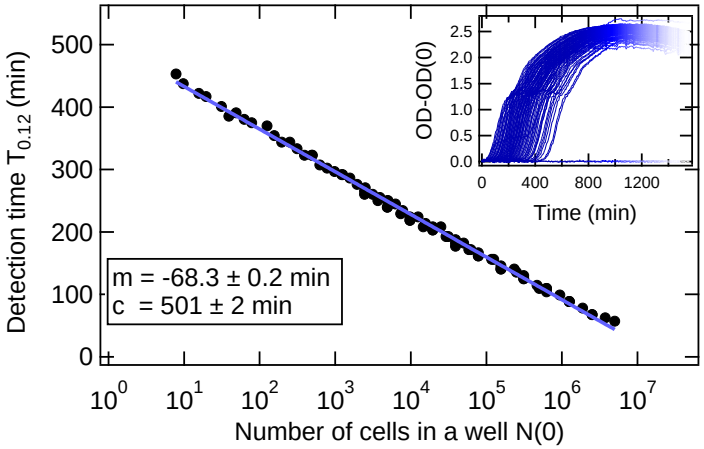

Figure 8.2 Detection times for growth in MHB. Time taken for each curve shown in the inset to reach OD=0.12, plotted against corresponding inoculum size on a log scale. Best fit line fitted by Igor Pro returning gradient (m) and intercept (c).

be -5 ± 12 min. A negative lag time is not meaningful, but without a more precise measurement can be interpreted as exponential growth from inoculation, within error.

Although a single growth curve can return μ and λ, an alternative measurement is obtained from multiple curves, demonstrated by the next section.

8.1.2 Growth rate and lag time

The inset of Figure 8.2 shows the growth curves from every well in the plate prepared with a range of inoculum sizes, each representing initiation from a different inoculum level. The curves are congruent; the growth rate and stationary levels are similar in every well. As $N(0)$ is reduced, the time to detection is increased, as expected. Each curve could be analysed separately as above, and μ and λ averaged. Instead, the $T_{0.12}$ for each curve is plotted against its inoculum size $N(0)$ in a singe plot, for a more reliable measurement.

The fitted line (Igor Pro) intercepts the x axis at $2.1 \times 10^7 \pm 0.1 \times 10^7$ cells/ml which is the density of cells at OD-OD(0)=0.12, agreeing with plate counts within error. The specific growth rate is calculated from the gradient m as $\mu = ln(10)/m = 0.0337 \pm 0.0002$ min^{-1}, giving a population doubling time of 20.6 ± 0.1 min. It is known that *E. coli* are able to double within $\sim$ 20 min in a rich medium at 37°C [225], but this rapidity confirms that growth conditions are favourable in the plate reader.

The y axis intercept is the expected time taken for a single cell to grow to $T_{0.12}$,

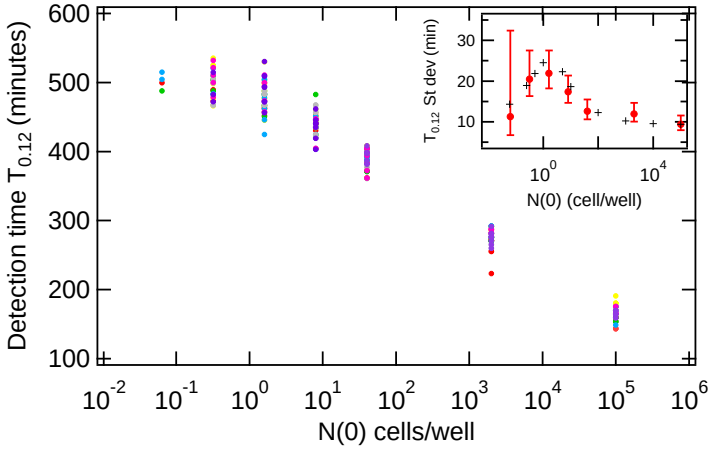

Figure 8.3 Variation in detection times for *E. coli* in MHB. Detection time plotted against $N(0)$ on a log scale for 56 replicates of 7 different inoculum sizes between $N(0) = 1 \times 10^5$ and 0.064 cell/well. Colour represents one plate containing 8 replicates of each inoculum. Inset: The measured (red) and predicted (black) standard deviations of detection times, at each $N(0)$ on a log scale. Error bars plotted are 95% confidence intervals.

measured to be 501 ± 2 min. Theoretically if a single cell were to grow exponentially at the growth rate measured, without any lag time, until the population was at the $N_{0.12}$, this would take 500 ± 3 min. Comparing these two values confirms that the population lag time is too short to be measured with growth curves. All points lie on, or close to, the best fit line, indicating that λ remains independent of $N(0)$ down to $\sim$ 7 cell/well. It is reassuring that the time spent at room temperature, being prepared for inoculation, does not result in a significant adjustment time, or heterogeneity in single cell cell adjustment times.

8.1.3 Variation in detection times

The previous section measured detection times, but their variability for a single $N(0)$ was not explored. The variation in detection times contains information on the experimental set-up and further information on heterogeneities within the bacterial population.

Fifty six replicates of 8 different $N(0)$'s, between 1×10^5 and 0.064 cell/well were performed over 7 different plates (8 replicates of each dilution in each plate). The resulting detection times are plotted against $N(0)$ in Figure 8.3. Even at an $N(0)$ of 1×10^5 cell/well there is a considerable range of detection times, returning a standard deviation of $\sim$10 min. This variation is attributed to uncertainty in the inoculation size, pipetting errors, variability in environmental conditions between days and noise

in the plate reader's measurement of OD [144]. Note that at the time of these measurements, more noise was experienced in results from the plate reader than for the other experiments discussed in this chapter. This does not influence the observations made.

At $N(0) = 1{\times}10^5$ cell/well, poisson number fluctuations in $N(0)$ (scaling as $\sqrt{N(0)}/N(0)$) would be expected to add 0.09 min only to the standard deviation of detection times, not a significant contribution. As $N(0)$ decreases, the contribution of number fluctuations increases until $N(0) \sim 1$, and then it decreases for lower inocula. Assuming the sources of variation are additive [144], this contribution can be added to the 10 min measured at high inoculum (plotted in the inset of Figure 8.3). The predicted standard deviation lies within the confidence interval of the measured values, at all inoculum levels. Therefore, the increased variation in detection times at low inoculum levels is interpreted as being due to fluctuations in $N(0)$ only, with the contribution from single cell heterogeneity being too small for measurement.

If the $N(0)$ is diluted below an average of $\sim$ 1 cell/well (the cell density in the 10μl of culture inoculated is below 100 cell/ml) then the average $T_{0.12}$ ceases to be further lengthened and this $T_{0.12}$ is taken to be that of a population beginning with a single cell. The four detection times obtained at the lowest inoculum level are clustered around 500 min as expected, further evidence that, unlike in the case of *Listeria monocytogenes* [137, 143], single cell heterogeneity neither lengthens or increases variation in the population lag time measured at low inocula. The population is homogeneous without measurable differences in single cell lag times and growth rates.

This experiment also provided a verification of the procedure used for obtaining small inoculum sizes of $\sim$ 1 cell/well and checked the calibration of OD to N used. At a prepared inoculum level ($N(0)_{dil}$) of 0.064 cells/well, 4 out of the 56 wells inoculated show growth. The average number of cells per well ρ is calculated from the fraction of non-growing wells (52/56) to be 0.074. This is within 95% confidence interval of the number expected by dilution, given only 56 replicates. The average number of cells *per grown well* ρ^+ is 1.03. At this inoculum level 96% of growing wells contain 1 cell, 3.5% contain 2 cells and 0.08% contain 3 cells.

The same calculations performed for the inoculum levels 5$\times$ and 25$\times$ above $N(0)_{dil} =$ 0.064 cells/well are shown in Table 8.1. At an $N(0)_{dil} = 0.032 \pm 0.06$ cell/well, the ρ calculated does not agree with $N(0)_{dil}$ within its 95% confidence level. A possible explanation for the discrepancy is that the uncertainty in $N(0)_{dil}$ quoted is derived from the calibration of OD to CFU, and neglects additional uncertainty from the dilution

Table 8.1 Comparing the inoculum size expected from dilution to that calculated from counting the number of growing wells.

$N(0)_{dil}$	Unc $N(0)_{dil}$	Frac growing wells	ρ	CI_{95} ρ	ρ^+	CI_{95} ρ^+
0.064	$\pm$0.01	0.071	0.074	0.02-0.19	1.03	1.00-1.10
0.32	$\pm$0.06	0.52	0.73	0.49-1.03	1.41	1.27-1.60
1.60	$\pm$0.30	0.84	1.83	1.27-2.47	2.18	1.76-2.70

procedure. Otherwise, the calculations are further verification that the calibration (OD to N) is accurate and the inoculation method works as it should.

8.2 Determination of the Minimum Inhibitory Concentration of pexiganan

Having developed an increased understanding of bacterial growth in a well, the study moves on investigate the Minimum Inhibitory Concentration (MIC) of pexiganan. A MIC assay was performed to test 2$\times$ increments of pexiganan between $0-10\mu$M against an inoculum size of $N(0) = 5 \times 10^5$ cell/ml MG1655 *E. coli* (bMIC). The plate was set up to allow 12 replicates, shown in Figure 8.4.

8.2.1 End-point results

The MIC is determined by the end-point results after 24 hours, shown diagrammatically in Figure 8.4(a). Dark yellow indicates wells which had grown to $\sim 10\times$ the OD of MHB and light yellow shows wells that had an OD slightly above that of the control at 24 hours. A photograph of the plate after an additional 48 hours at 37°C after the 24 hour endpoint, shows clearly the turbid wells in which growth has occurred, and those which appear the same as the MHB controls (Figure 8.4(b)).

To interpret these results according to the guidelines [153], each column represents a MIC measurement. Therefore, a MIC of 2.5μM was measured 5 times and MIC of 5μM measured 4 times. In three columns the bacteria grew in 5μM, but did not in 2.5μM. The guidelines would suggest ignoring these results (these columns of the plate), and attributing them to pipetting mistakes, but this pattern is often seen in repeats of this assay, suggesting that its origin lies elsewhere.

When replicates of MIC assays are prepared in the same plate, a more useful interpretation of the results may be that 12/12 wells grew at 1.25μM, 4/12 wells grew

	1	2	3	4	5	6	7	8	9	10	11	12
A	MHB	MHB	MHB	MHB	MHB	MHB	MHB	MHB	MHB	MHB	MHB	MHB
B	10	10	10	10	10	10	10	10	10	10	10	10
C	5	5	5	5	5	5	5	5	5	5	5	5
D	2.5	2.5	2.5	2.5	2.5	2.5	2.5	2.5	2.5	2.5	2.5	2.5
E	1.25	1.25	1.25	1.25	1.25	1.25	1.25	1.25	1.25	1.25	1.25	1.25
F	0.63	0.63	0.63	0.63	0.63	0.63	0.63	0.63	0.63	0.63	0.63	0.63
G	0.31	0.31	0.31	0.31	0.31	0.31	0.31	0.31	0.31	0.31	0.31	0.31
H	0	0	0	0	0	0	0	0	0	0	0	0

(a)

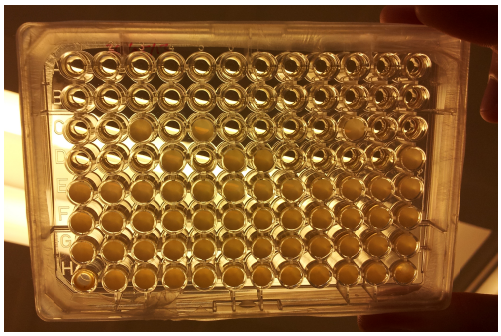

(b)

Figure 8.4 End-point MIC results. (a) Table representing the setup of the plate for 12 replicate MIC assays. The number in each 'well' is the concentration of pexiganan present in the 200μl. The wells labelled MHB were not inoculated. Dark yellow indicates an OD $\sim 10\times$ above that of MHB at 24 hours. Two wells which began showing growth within an hour of the 24 hour cut-off are shaded in light yellow. (b) Photo taken of the same plate after 72 hours at 37°C.

at 2.5μM, 3/12 at 5μM and 0/12 at 10μM, given that there is no link between the tests in a single column except that they were subject to the same serial dilution of peptide. To miss a well in the serial dilution, or to miss-stir a well in this experimental situation (with multiple replicates prepared with a multi-well pipette), is extremely unlikely. The guidelines cater for several bacteria/antibiotic combinations in one plate, where perhaps only two replicates of each condition would be run; a situation where a mistake could occur.

Previous measurements of the MIC of pexiganan against *E. coli* have been in the range $6.4 - 12.8\mu$M [189, 190]. The results were within one concentration step of these values and the variation within the results were at a typical level [154]. However, the difference in MIC measured of a factor of 4 within 12 replicates, using the same pexiganan stock and the same bacteria, warranted further investigation. As it seemed unlikely that experimental variation in the set-up could lead to this outcome, inherent variation could be a property of the bacteria-peptide system, an understanding of which would be valuable to an interpretation of the MIC.

Note that the plate shown is one example of an outcome from these experiments. The features seen appear frequently, but not always. For example, it is possible to obtain a plate of 12 replicate MIC values which are exactly the same.

8.2.2 Growth curves and detection times from the plate reader

A practical and informative method of further investigating a MIC measurement is to inspect the growth curves recorded at sub-MIC concentrations. Plots of sub-MIC growth curves are shown in Figure 8.5 for the plate setup in Figure 8.4. The growth curves from the 0μM wells are as expected for $N(0) = 1\times10^5$ cell/well. When pexiganan is added to the wells, the growth curves are influenced in a concentration dependent manner. However, at all concentrations the specific growth rate of the population are indistinguishable from that in 0μM. This is shown most clearly in Figure 8.5(d).

The most striking feature of the growth curves is that there is a concentration dependent lengthening of detection times. At low concentrations of 0.31μM pexiganan the detection time measured is $\sim$ 10 min longer. At 0.62μM of pexiganan the detection time is later still by 30 min, and there is more variation in detection times between replicates. At 1.25μM all 12 replicate wells grow but there is a drastic change to the growth curves: the population takes far longer to reach a detectable level. The noise in the detection times increases enormously, with replicates being detected as much as 400 min apart. At higher concentrations of pexiganan than 1.25μM some of the replicate wells do not grow *i.e.* they do not reach a detectable level within 24 hours. Those that do grow have longer detection times again.

Interestingly, but of less relevance to the MIC, trends in the diauxic lag and N_{max} (the stationary level) are also seen. The brief diauxic lag is less prominent when pexiganan is present and N_{max} is slightly higher.

As the main effect of the peptide is to lengthen the detection time, plotting $T_{0.12}$ for each growth curve is a natural way of looking at the effect of peptide on a large number of growth curves. The chosen OD=0.12 detection level is shown in Figure 8.5(b) and (d). It is above any noise in the baseline level and within the exponential growth phase of every curve. Figure 8.5(c) shows the time at which each curve reaches this level against concentration of pexiganan. If data had been collected for longer time period, there would have been two additional $T_{0.12}$ at longer times for 5μM, as two wells began to show growth at $\sim$ 1500 min. The growth becomes apparent when plotted as in Figure 8.5(d).

Implications of these findings are discussed after results for four other inoculum sizes are shown.

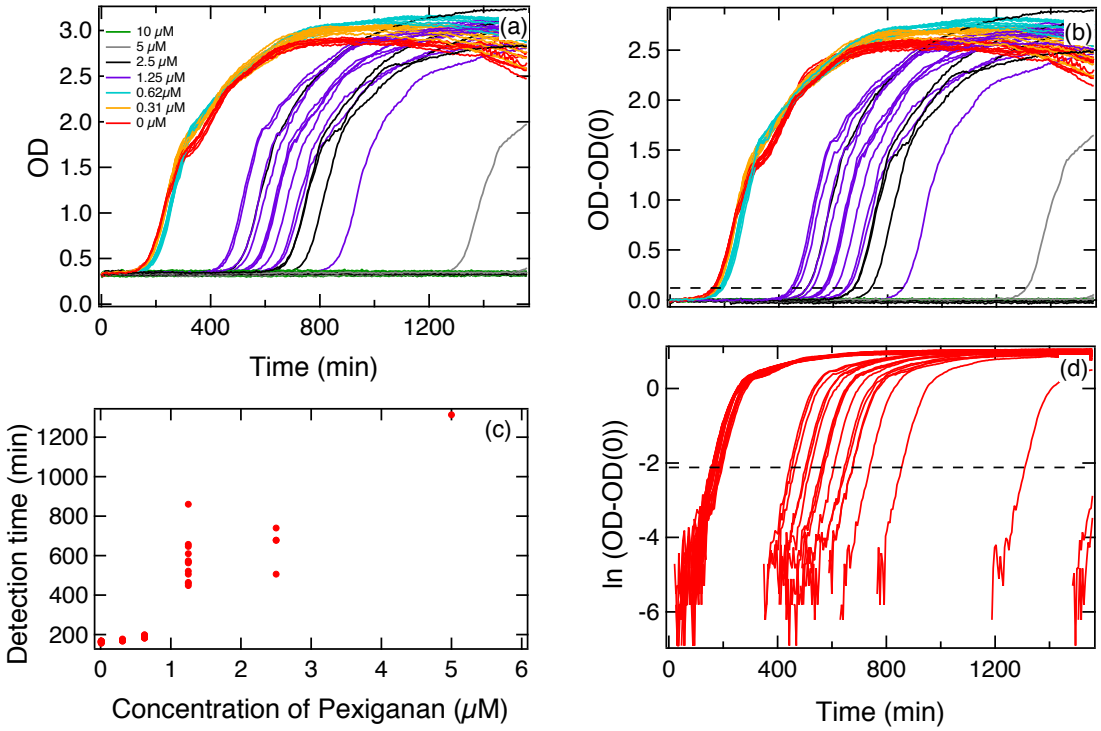

Figure 8.5 *E. coli* growth curves from 12 replicate pexiganan MIC assays and their detection times. (a) Raw OD data against time. Each colour represents OD in a well at a concentration of pexiganan specified by the legend. (b) The same OD data blanked by OD (t=0). (c) The $T_{0.12}$ plotted against concentration of pexiganan. (d) ln of the blanked OD. All data points before the visually judged point of growth detection have been deleted to ease interpretation. The detection level is shown by a dashed line on (b+d).

8.2.3 Detection times for four different $N(0)$s

As the inoculum effect is one of the primary concerns in the use of the MIC measurement, it was decided to repeat the test with other $N(0)$s. Figure 8.6(a) shows detection time data for MIC assays using 4 different inoculum levels. Note that $P(0)$ is now plotted on a log scale and 0μM is plotted at 0.01μM. The data presented for $N(0) = 5 \times 10^5$ cell/ml is that presented in the previous section, in addition to the data from one other plate with 8 replicates, testing additional low peptide concentrations. Data from 8 replicate assays with $N(0) = 2.5 \times 10^7$, $N(0) = 5 \times 10^3$ and $N(0) = 5$ cell/ml ($N(0) \sim 1$ cell/well) show a changing MIC with inoculum size.

Again, sub-MIC growth curves (not shown) did not display any variation in their specific growth rate at any $N(0)$. At $N(0) = 2.5 \times 10^7$ cell/ml, similar trends in N_{max} and diauxic lag as for $N(0) = 5 \times 10^5$ cell/ml were seen. For both lower inoculum sizes the diauxic lag feature was independent of pexiganan concentration and for $N(0) \sim 1$ cell/well, no change in N_{max} was apparent. At $N(0) = 10^3$ cell/well the stationary

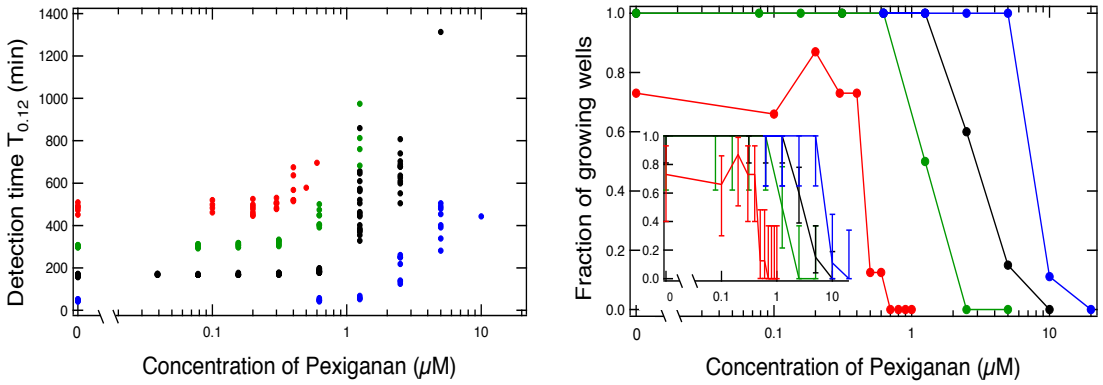

Figure 8.6 MIC assay detection times and fraction of growing well results for four inoculum sizes. (a) The $T_{0.12}$ detection times and (b) the proportion of growing wells against pexiganan concentration, for $N(0) = 2.5 \times 10^7$ (blue), $N(0) = 5 \times 10^5$ (black), $N(0) = 5 \times 10^3$ (green) and $N(0) = 5$ cell/ml (red).

level remains unaffected until pexiganan concentrations of 1.25 and 2.5μM. These trends were not further investigated experimentally, although an explanation is proposed in Chapter 9.

Below $\sim 0.3\mu$M, pexiganan does not affect the detection times of any of the *E. coli* populations, regardless of their $N(0)$. However, by $\sim 0.5\mu$M the $T_{0.12}$ have visibly lengthened for all inoculum levels except for the highest. It only requires a concentration rise to $0.7 - 1\mu$M to ensure that none of the wells grow when $N(0)$ is ~ 1 cell. At the higher inoculum sizes, the detection times lengthen further, requiring $1.25 - 2.55\mu$M to ensure no $N(0) = 10^3$ wells grow, $5 - 10\mu$M to ensure that no $N(0) = 10^5$ wells grow and $10 - 20\mu$M to ensure that no $N(0) = 10^7$ wells grow. As $N(0)$ is increased the $T_{0.12}$ at the concentrations immediately below the MIC become longer and more noisy. This effect is less pronounced (the detection times are not extended by as long) at $N(0) = 10^7$ cell/well compared to the two inoculum levels below this. The patterns in detection times described are reproducible and indicate differing population dynamics in pexiganan for different cell densities.

Figure 8.6(b) plots the proportion of replicate wells which grew against the concentration of pexiganan on a log scale. Given that the number of replicates completed was low, statistics are poor and 95% confidence intervals plotted are large (inset). Having said that, the trends are clearly visible. The fact that the MIC is not a straightforward threshold, but that there is a inoculum dependent range of concentrations in which the population might not grow in 24 hours, is very interesting. This result is directly relevant to clinical research and has the potential to influence the protocol used for

measuring MIC assays. The range of pexiganan concentrations over which an inoculum size of ~ 1 cell has a chance of either growing or not growing is small, compared to that for a larger inoculum size, perhaps hinting at reasons for the variation observed.

8.2.4 Relevance of these results for MIC assays

Simply by observing the patterns witnessed in these growth curves it is possible to draw significant conclusions of relevance for the measurement of the MIC of pexiganan. Clearly the time of measurement, for example 18 hours compared with 24 hours, is critical and can alter the result by at least a factor of 2. It is fortuitous that the majority of the wells that do not show growth at 24 hours, never grow. This was inferred from observing plates days later, as in the photo. Assuming the effect of pexiganan is primarily bactericidal, the MBC of pexiganan is inferred to be equal to or $2\times$ higher than its MIC, as was measured in previous research [189]. If a shorter time-span had been chosen for the MIC measurement, there would be a larger discrepancy between the two values.

At concentrations one dilution step below those never exhibiting growth, there is significant variation in the detection times of any growth curves. Given this variation, the fact that some wells do not show growth within 24 hours at this concentration, while others do, becomes less surprising than if the curves had not been observed. One replicate of each concentration could lead to confusing results, for example with a well at 1.25μM growing, one at 2.5μM not growing and one at 5μM growing. In the context of many replicates whose growth curves contain inherent variation, this is less likely to be interpreted as a laboratory mistake, and more likely to be interpreted as a feature of the population dynamics.

Findings thus far have indicated that the pexiganan MIC measured in the plate reader is not a simple threshold concentration, that sub-MIC growth curves display interesting features and that the MIC displays an inoculum effect. Before explanations for these results are explored further, a verification that these features are not specific to the precise experimental set-up is required. Although most researchers would measure a MIC by monitoring turbidity in a plate reader, other modern techniques that allow greater flexibility are under development, one of which is the Millifluidic Droplet Analyser (MDA).

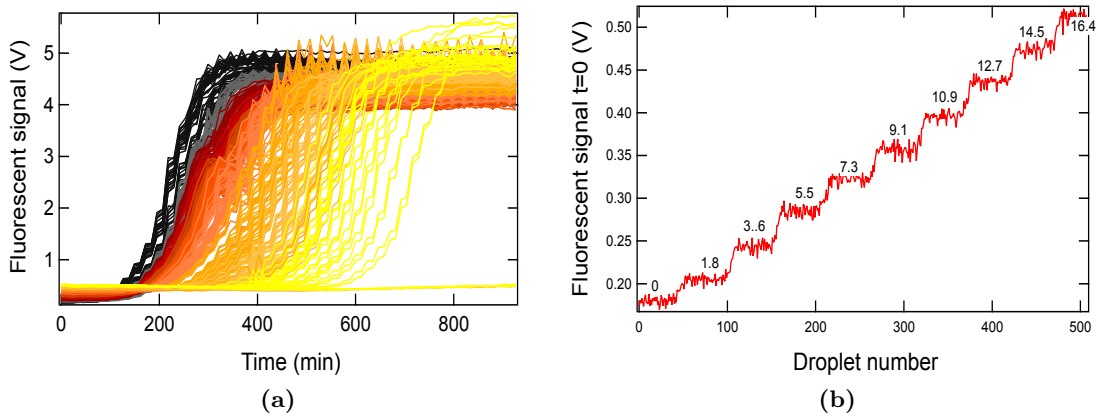

Figure 8.7 *E. coli* growth curves from pexiganan MIC assays in the MDA. (a) Raw fluorescent signal with time in droplets. The concentration of pexiganan in the droplet is indicated by the colour of the curve; low= black, high= yellow. (b) Fluorescent signal *vs* droplet number at $t = 0$, showing the linear increases in pexiganan concentration, values of which are written above the step in μM.

8.2.5 Growth curves and detection times from the MDA

There was the opportunity to collaborate with researchers from the ESPCI, Paris to use an alternative density measurement to the plate reader. MIC assays were conducted in a Millifluidic Droplet Analyser (MDA), see section 7.3, measuring fluorescent signal rather than optical density.

In Figure 8.7(a) the 508 growth curves resulting from a MIC experiment covering the pexiganan concentration range $0-16.4\mu$M in linear steps are shown. It was decided not to use a continuous concentration gradient as with cefotaxim in [164] (Figure 8.5(a)) as variation had been observed to play a role, requiring replicates of a single concentration to confirm. The concentration of pexiganan present in each droplet is determined from the fluorescent bead signal of the droplet at $t = 0$ min, while the concentration of bacteria is below the detection limit (Figure 8.7(b)). Each resulting growth curve is coloured according to the pexiganan concentration of the droplet. At the highest concentration of 16.4μM, some of the droplets do not show any growth within the time span of 800 min. Unfortunately the peptide concentration wasn't extended high enough to result in no growth in any replicate droplets.

Broadly speaking, the growth curves look similar to those obtained in the plate reader. The bacteria are in exponential phase at the detection level, and their detection time is dependent on the pexiganan concentration. The signal is too noisy to comment on whether trends in diauxic growth are present. N_{max} was observed to be a function of droplet number, even at 0μM. An exponential fitted to five 0μM curves for ~ 8

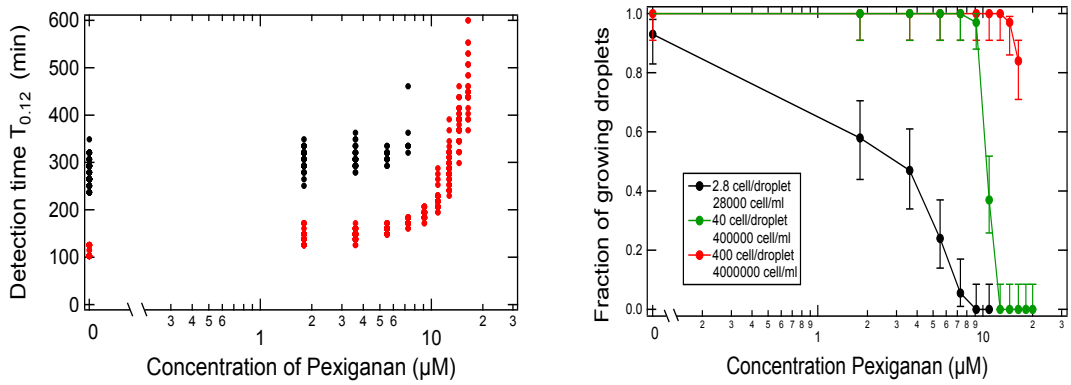

(a) **(b)**

Figure 8.8 MIC assay results from the MDA. (a) The Detection times and (b) the proportion of growing droplets against pexiganan concentration, for the inoculum sizes shown in the legend. 0μM is plotted at 0.1μM.

time points after detection returned μ=0.034±0.003 min^{-1}. The growth rate is within uncertainty of that measured in the plate reader, suggesting that conditions in the MDA are more favourable for growth than anticipated (see section 7.3). $N(0)$ was calculated from the detection time at 0μM to be $\sim$ 400 cell/drop.

Figure 8.8 shows the proportion of droplets growing at each peptide concentration in 3 separate MIC experiments. Again, $N(0)$ is calculated from the detection time at 0μM. For the lowest inoculum of 2.8 cell/growing drop, $N(0)$ is also calculated from the proportion of growing droplets at 0μM, and the two calculations agree (growth is detected $175-225$ min, $N(0)=2$ cells/drop would take 203 min to reach a detectable level, and $N(0)=3$ cells/drop would take 191 min). As previously, the pexiganan MIC is a $N(0)$ dependent range of concentrations.

The detection time patterns for two of these experiments (the signal unfortunately contained too much noise to plot detection times at $N(0)=40$ cell/droplet) are shown in Figure 8.8(b). The pattern of lengthening detection times mimic those seen already. The range in $T_{0.12}$ at 0μM is larger for the smaller inoculum as expected, and they are only lengthened by $\sim$ 100 min at concentrations immediately below those resulting in complete no-growth. At the higher inoculum, the $T_{0.12}$ are affected over a broad range of concentrations and can be lengthened by up to 500 min.

The MICs measured are consistent with those measured in the plate reader for similar $N(0)$ densities, rather than numbers. For the higher inocula this is an intuitive result confirming there is a density inoculum effect, but for single cell levels this is surprising. For a single cell in a 200μl well ($N(0)=5$ cell/ml), there must be a $P(0)$ of $\sim 0.7\mu$M to result in no growth of any replicate, whereas single cells in droplets ($N(0)=3\times10^4$

cell/ml) require 9μM to ensure no droplet grows (although growth is affected below 2μM). The *amount* of peptide present in the total volume is important, as well as the *concentration* of peptide. A speculative explanation is offered in the next section.

In summary, the experiments in the MDA reinforce the conclusions from the plate reader assays. Specifically, they reproduce the main feature in $N(t)$ seen at sub-inhibitory concentration of pexiganan; the lengthening of the detection time. As μ is constant, Equation 6.3 suggests that this is due to a lengthening lag time λ. But, as pexiganan is a bactericidal agent, it is possible that the lengthened detection times are due to reduced viability at short times rather than an extended lag phase. In order to explore whether either of these suggestions, or a combination of both are taking place, measurements of the whole $N(t)$ curve were made, and are presented after further inspection of the IE measured.

8.2.6 Inoculum effect

A striking feature of the results from the plate reader and the MDA is the inoculum effect (IE) displayed, summarised by Figure 8.9. Additional results from the plate reader at different inoculum levels to those presented already have been incorporated (black). As replicate wells and droplets showed that the MIC is not a straightforward threshold, the concentration at which no replicates grow is plotted. As a verification, IE results collected using a single pexiganan stock over only 2 days of experimentation, completing between 2 replicates (highest inoculum requiring a lot of peptide) and 5 replicates (lower inoculum levels) at each inoculum level are also plotted (grey).

When MIC results are plotted as a log-log plot in Figure 8.9, the plate reader results fall on a straight line against pexiganan concentration, indicative of a power law, down to $\sim$ 1000 cells/ml, below which the MIC is constant. When $N(0)$ is plotted in units of number/ml rather than a number per well/droplet (inset), the limited MDA data (red) almost collapses onto the same line. One data point, at the lowest $N(0)$ measured, disagrees.

Deviation of the MDA results (red) from the power law at low inoculum levels replicates the pattern observed in wells, and may suggest a reason for the difference in single cell MIC between wells and droplets. If peptide adheres to all surfaces, and is assumed to form a single layer, as has been observed for other cationic polymers and peptides [226], then it would require on the order of $\sim 10^{13}$ molecules in a well before some peptide remained in the bulk. There has been evidence of antimicrobial peptides adsorbing to

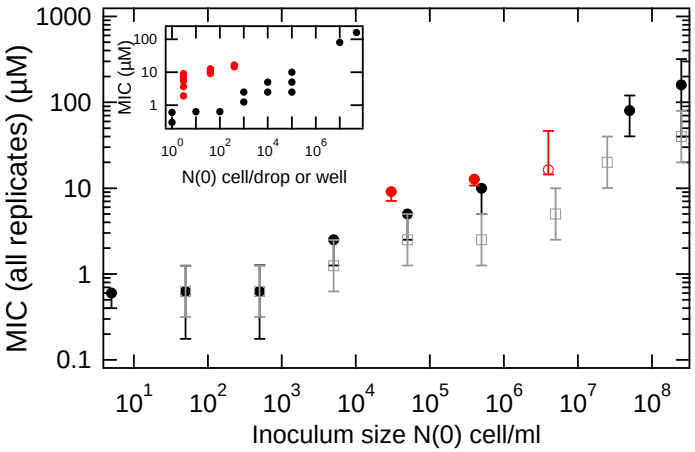

Figure 8.9 Inoculum effect of the *E. coli*-pexiganan MIC. The concentration of pexiganan at which no replicate grows (MIC(all replicates)) for a given inoculum size $N(0)$ in units of cell/ml from the plate reader (black), from the plate reader using a single pexiganan stock (grey) and from the MDA (red). Error bar of minus one dilution step. IF only one MIC assay was performed at the $N(0)$, it is plotted with an error bar of *plus* one dilution step, *minus* two dilution steps. Inset plots every pexiganan concentration at which one replicate has not grown for a given inoculum size expressed in cell/compartment. Note: the time-span of the MDA experiments varied between 900 and 1100 min. At the highest $N(0)$ used in the MDA the concentration range was not extended high enough so although the pexiganan concentration at which no replicates grew is indicated, it was not measured (empty data point).

polystyrene [227], oil [228] and the air-water interface [226, 229]. The surface to volume ratio is 10× higher in a droplet, thus it would be expected that 10× more peptide would be needed to achieve the same bulk concentration, approximately what is measured.

Despite this explanation being speculative, it would also explain why more peptide is required to kill a larger number of bacteria, as is seen in Figure 8.9. If no adherence to the surface occurs, with 10^{14} peptide/well at 5μM there is enough to provide 10^9 molecules per bacterium at 10^5 cell/ml or 10^6 molecules per bacterium at 10^8 cells per ml. These are both peptide levels which can support peptide to lipid ratios representing complete saturation [125], so it is difficult to see why for one inoculum size (10^5 cell/ml) this concentration represents the MIC whilst for the higher inoculum size it is $>$ 10× below the MIC. However, if surface effects remove much of the peptide from the bulk, or much of it is lost in adherence to appendages of the cell wall, then perhaps the active concentration per bacterium is reduced sufficiently to require further peptide to be added at higher inocula.

This hypothesis links to work by Udekwu *et al.* [155], where this IE mechanism is described as a decrease in antibiotic concentration per cell with increasing inoculum. The researchers comment on the un-intuitive nature of this explanation given the enormous number of molecules in their suspensions, but believe probabilistic or

physiological reasons could result in a large number being needed to affect each cell. If a 'per cell' effect was the IE mechanism responsible, either here or in previous work, a power of 1 would be expected for the inoculum effect; for every bacterium added, a proportional extra amount of peptide would be required. Fitting a power law to the results in Figure 8.9 returns a power of 0.43±0.01 (black) and 0.32±0.01 (grey), both far below 1. This suggests that the cause of the IE is more complex than this simple hypothesis.

Given that the MIC is the concentration at which no regrowth is observed at 24 hours, the IE measured may be a complex function of the population dynamics of *E. coli* in a suspension of pexiganan and its causes. Further experiments undertaken and presented in subsequent sections attempt to address whether this is the case. Time-kill curves, peptide depletion assays and single cell experiments are discussed before finally, section 8.6 returns to the implications of their results for MIC measurements and the IE.

8.3 *E. coli* density curve in the presence of pexiganan

As stated in the section before last, measurements of the whole density curve $N(t)$ were needed to complement the sub-MIC growth curves measured in the plate reader. It was hoped that density curves would establish whether lengthened detection times were due to an increased adaption time or early time cell death, and provide a comparison to previously published time-kill curves. Motivated by the need to measure $N(t)$, two methods were implemented: CFU were obtained by plate counting and OD measurements were collected by raising $N(0)$ above the detection limit. As pexiganan is thought to cause cell lysis [184], it was hypothesised that OD measurements would match CFU closely. Two inoculum sizes ($N(0)$s) are compared in this section; $N(0) = 5 \times 10^5$ cell/ml was chosen to be the lower inoculum as it is the density for bMIC assays [153] and $N(0) = 2.5 \times 10^8$ cell/ml was chosen as a higher inoculum as it represents a high enough OD to be monitored in the plate reader.

8.3.1 Plate count curves

CFU in MHB

Density curves $N(t)$ measured with CFU counts ($N(t)_{CFU}$) for the smaller inoculum size of $N(0) = 5 \times 10^5$ *E. coli*/ml, in MHB at 37°C (the same conditions as the MICs reported), are shown in Figure 8.10(a). Data was collected for the first $\sim$ 200 min

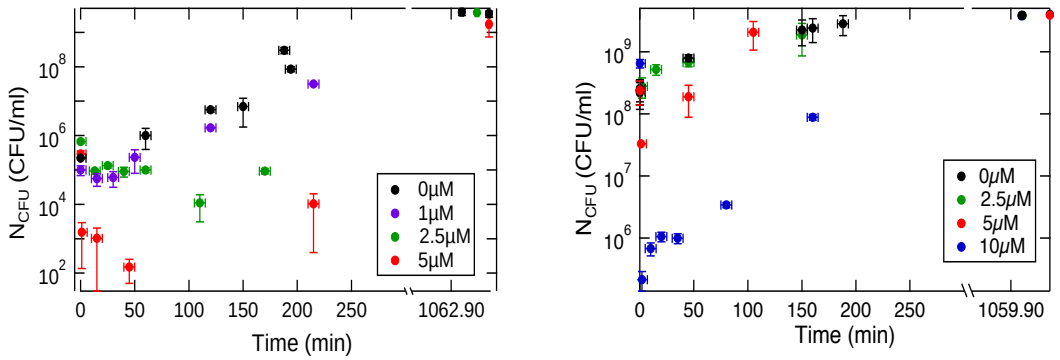

(a) (b)

Figure 8.10 Density curves (CFU) in MHB. $N(t)_{CFU}$ for values of $P(0)$ shown in the legend. (a) $N(0) \sim 5 \times 10^5$ cell/ml in MHB. (b) $N(0) \sim 2.5 \times 10^8$.

and then, in some cases, once the following day. With no pexiganan present, the population grows exponentially, at a growth rate within uncertainty of that already quoted, remaining in this phase of growth for the duration of the first 200 min.

Pexiganan was added at $t = 0$ min to concentrations of $P(0) = 1$, 2.5 or 5μM. At 1μM the sample shows a slight drop in N_{CFU} within the first 100 min and then growth at a similar rate to at 0μM. At 2.5μM N_{CFU} drops at early times, but the lowest value measured does not come immediately. Rather, although the largest drop in N_{CFU} is immediately, N_{CFU} then continues to drop gradually for roughly 100 min before regrowth occurs. This is also apparent at 5μM. For all samples measured the next day, regrowth had completed to the same density within uncertainty. At 10μM no CFUs were recorded, and the suspension was not turbid the following day; all of the cells were unviable by $t = 2$ min.

A replicate sample at 1μM showed some variation to the curve shown, but growth also lagged behind the control by $\sim$ 50 min in reaching 10^7 cell/ml. A replicate at 2.5μM did not agree with the plotted curve, dropping two orders of magnitude rather than one. Contrary to indicating that experiments are irreproducible, this is as expected from the detection times measured at 2.5μM which showed large amounts of variation, and even on occasion no growth within 24 hours. A replicate measurement in 5μM resulted in no viable counts by 5 min.

From these results it is clear that the main cause of the lengthened detection times seen in section 8.2.2 is an early-time drop in the density of viable cells. The higher the peptide concentration, the further the drop and the longer it takes for regrowth to occur, lengthening the time taken to reach the detection level. There are pexiganan

concentrations at which cell numbers are reduced to low levels before regrowth, leading to some populations surviving and others being eradicated (the cause of the ill-defined MIC observed).

CFUs were counted for a larger inoculum size of $N(0) \sim 2.5\times10^8$ cell/ml with $P(0)$=2.5, 5 or 10μM (Figure 8.10(b)). For this $N(0)$ the MIC was measured to be $80-160\mu$M. At 0μM and 2.5μM N_{CFU} follow the growth curve expected in the absence of peptide, entering post exponential phase soon after inoculation, and are indistinguishable from each other. At 5μM and 10μM by $t = 2$ min, N_{CFU} has fallen 1 order of magnitude and 3 orders of magnitude respectively. In both cases growth resumes within the timescale of the following measurement, at the maximum growth rate of *E. coli* in MHB within uncertainty, until they pass out of exponential phase. The next day all assays contain the same stationary phase density of cells.

The $N(t)$ curves presented show pexiganan concentration dependence and inoculum density dependence. Some features are as expected from published killing kinetics [189] at above MIC concentrations. As the concentration of pexiganan is increased, the death rate at early times increases and the surviving fraction after death decreases. There is no measurable lag before killing begins. A low concentration of pexiganan, able to effect a low $N(0)$, is seemingly unable to influence higher $N(0)$, a finding expected from the MIC measurements. However, additionally, there are unexpected changes to the shape of the $N(t)$ curve; at a higher inoculum the period of net bacterial death is confined to much earlier times than for the lower inoculum. This feature suggests an explanation for the lesser lengthening of detection times at high inoculum sizes compared to at lower inoculum sizes (Figure 8.6), discussed further in section 8.6.2. The primary feature of the curves observed is independent of the $N(0)$ and $P(0)$; if complete death is not achieved, regrowth occurs, a feature not reported previously.

CFU measurements count the bacteria able to form colonies at a given time. It is a subtle point, but worth making, that depending on the definition of alive, this is not quite the same as the number of alive bacteria at time t, but is the number of bacteria which will manage to divide successfully in the future. Nevertheless the peptide works impressively fast, especially at high $N(0)$ and $P(0)$.

There are limitations to this measurement technique. Although large disagreements between replicates are being attributed to a real feature of the density curve, experimental uncertainties contribute. Given the labour intensive nature of the measurements, to do a study of the differences between replicates would be difficult.

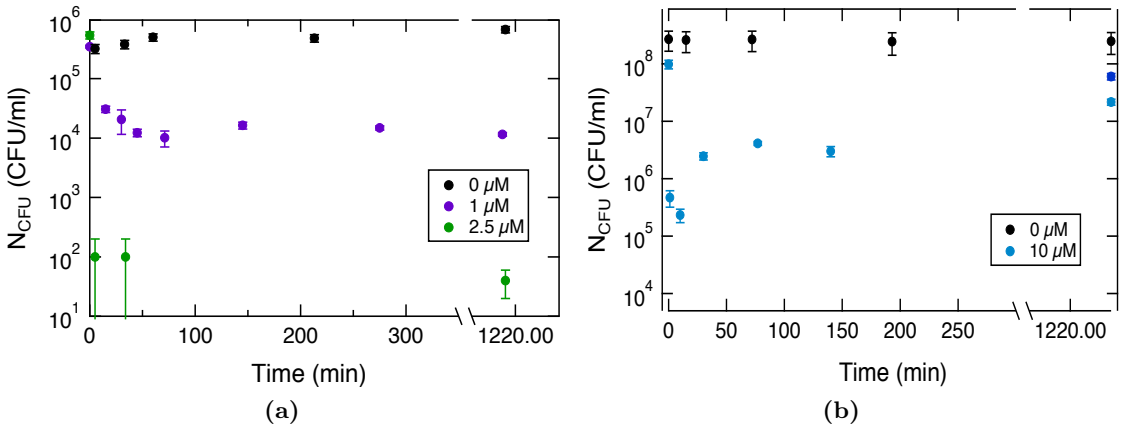

Figure 8.11 Density curves (CFU) in PBS. $N(t)_{CFU}$ for values of $P(0)$ shown in the legend. (a) $N(0) \sim 5 \times 10^5$ and (b) $N(0) \sim 2.5 \times 10^8$ cell/ml in PBS.

CFU in PBS

In order to further explore these density curves, a selection were repeated in PBS to remove the contribution of growth *i.e.* to observe death only (Figure 8.11). In the absence of pexiganan the density of *E. coli* remains constant in PBS for $\sim$ 24 hours.

At the higher inoculum level of $N(0) \sim 2.5 \times 10^8$ cell/ml, with $P(0) = 10\mu$M (Figure 8.11(b)), the immediate drop in CFU is of a similar magnitude to that in MHB ($\sim 10^3$), and is reproducible within an order of magnitude (not shown). At the lower inoculum of $N(0) = 5 \times 10^5$ cells/ml, 1μM and 2.5μM of pexiganan cause a greater drop (2 and 4 orders of magnitude respectively) (Figure 8.11(a)) than in MHB ($\sim$ 20% and 2 orders of magnitude respectively), and increases the variation between replicates (not shown).

Once a sufficient quantity of cells have died in the suspensions some regrowth can occur, this is seen most clearly in Figure 8.11(a), where a large number of cells (not only a large proportion of the cells), 9.99×10^7 cell/ml, become unviable before $t = 5$ min. Unfortunately, this confuses the interpretation of these experiments at later times, but should not influence observations at early times.

Unlike antibiotics which affect growing cells more than non-growing cells, these results suggest that pexiganan may not distinguish between them. To show this conclusively, the experiment would have to be repeated with cells grown to stationary phase instead of exponential phase [158]. However, the aim here was to use the same cells are are inoculated into MHB, to observe whether death is able to progress further when growth is not present, as would be expected if the death rate was competing with an independent growth rate. This was confirmed for the lower inoculum but not for the

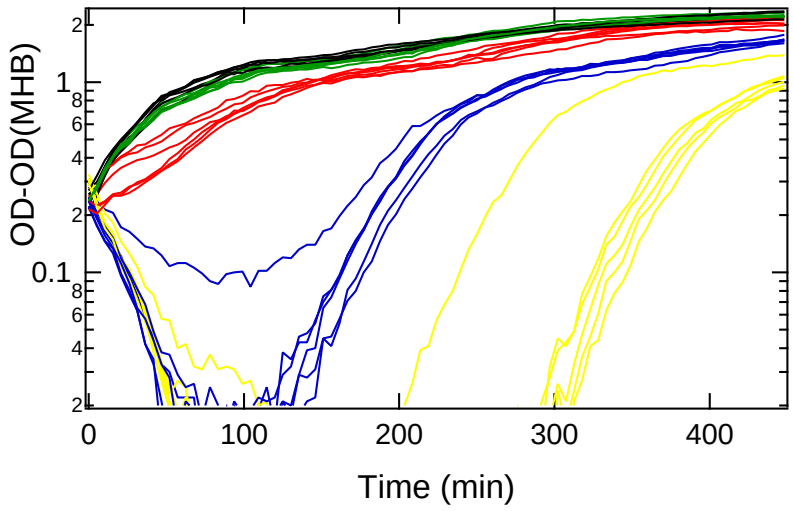

Figure 8.12 Pexiganan concentration dependence of the density curve (OD) in MHB. OD with time in 5 replicate wells (MHB), with pexiganan concentrations 0μM (black), 2.5μM (green), 5μM (red), 10μM (blue) 20μM (yellow).

higher inoculum.

8.3.2 OD results

Optical density measurements were made in the plate reader to allow frequent data acquisition of multiple replicate samples in MHB. The cells are in the late exponential phase as they are inoculated at $N(0) = 2.5 \times 10^8$ cell/ml, but Figure 8.12 demonstrates that there remains no lag time at 0μM. Five replicate curves are shown at each concentration of pexiganan tested.

At the lowest concentration, 2.5μM, the population follows a similar growth curve to at 0μM with little variation between replicates. As the concentration increases to 5μM, the net growth rate of the population is slowed with respect to the control for the first $\sim$ 100 min and replicates become more noisy, with a 30 min range in time taken to reach OD=0.9. At 10μM the OD first decreases, before plateauing and increasing again at a similar maximum growth rate to at 0μM. Likewise at 20μM, but the OD takes longer to begin increasing again. The time taken to regrow becomes even more erratic at 20μM, showing a $\sim$100 min range in time to regrow to OD=0.9, rather than a $\sim$ 40 min range at 10μM. This replicates the increase in variation with peptide increase seen in detection times at lower $N(0)$ and $P(0)$.

Unfortunately, the OD of wells at 10μM and 20μM dropped below the detection limit, resulting in an unchanging OD measurement for some of the time. It is likely the OD

dropped beyond this, but measuring it was not possible.

8.3.3 Comparing OD to CFU

The density curves in MHB were performed with both methods and can be compared. N_{OD} and N_{CFU} agree that 2.5μM does not cause a measurable affect on $N(t)$. At 10μM pexiganan N_{OD} drops initially and then regrowth, at the same maximum growth rate as the control, is observed. Both methods show the regrowth 'lagging' $\sim$ 200 min behind the population at 0μM. Likewise at 5μM, growth 'lags' behind the control by $\sim$ 50 min. However, between $t = 0$ and the recovery of growth at its maximum rate, there are large discrepancies between the measurements at both 5μM and 10μM. Instead of causing an immediate drop in viable cells, OD measurements suggest that 5μM reduces the net growth rate of the population at early times, and there is no evidence of a 3 orders of magnitude drop in viability immediately after the addition of 10μM, as seen by CFU.

In order to directly compare the two methods, small volumes of a sample ($N(0) \sim 2.5 \times 10^8$ cell/ml and 10μM of pexiganan) were removed for measurements in the single read spectrophotometer and then plated for CFU counts (Figure 8.13). OD readings were converted to a cell density (N_{OD}) using the calibration for *growing* MG1655 in MHB.

At $t = 0$ the two methods should agree, as CFU define the calibration of OD to N_{OD}. The fact they differ is believed to be due to the slight time delay between measuring the OD and completing the plate count, over which the bacteria continued to grow. In red, N_{OD} shows a gradual decrease in OD after peptide addition, which bottoms out at 1×10^8 cells/ml after roughly 40 min. By 150 min N_{OD} is beginning to increase again. The black data points (N_{CFU}), already described above, differ significantly at early times. At 150 min N_{OD} and N_{CFU} agree.

Disagreement between the methods indicates that during this time-period there are non-viable cells which have not undergone lysis. By subtracting N_{OD} from N_{CFU} the fraction of non-viable, but un-lysed cells can be calculated and plotted against time (Figure 8.13(b)). A significant proportion of cells lose viability within minutes and then undergo lysis at later times. The fraction of non-viable, un-lysed cells decreases for $\sim$ 50 min and then bottoms out for $\sim$ 100 min (although at $t = 150$ min OD and CFU are within uncertainty of agreeing, therefore the number of non-viable, un-lysed cells is within uncertainty of 0). A quantitative interpretation of this plot relies on the

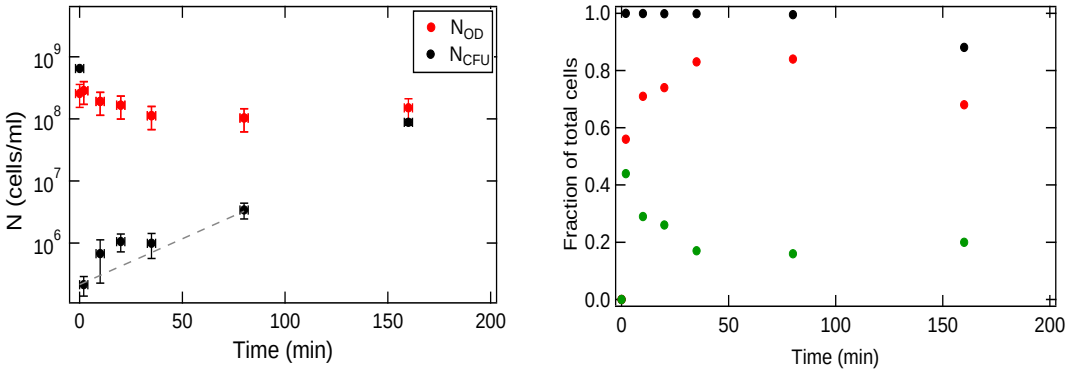

(a) (b)

Figure 8.13 Comparing OD to CFU measurements of *E. coli* in MHB with added pexiganan. (a) N_{OD} and N_{CFU} for $N(0) \sim 2.5 \times 10^8$ and $P(0) = 10\mu$M. Grey dashed line represents growth at $\mu = 0.034\text{min}^{-1}$. (b) The fraction of total cells non-viable (black), lysed (red) and non-viable but unlysed (green).

assumption that changes in OD are directly related to changes in the number of lysed cells, which cannot be justified. However the main qualitative features are believed to be real as it is unlikely that the lysis of all but 10^5 cells/ml would not result in an OD drop much larger than is seen.

These observations do not contribute to the primary aim of this study, but do address the secondary aim. The finding that pexiganan is able to reduce viability *before* causing cell lysis constrains the proposed mechanism of action of this peptide.

8.3.4 Discussion of the $N(t)$ curve

Experiments which follow in sections 8.4 and 8.5 aim to answer questions arising directly from the $N(t)$ curve.

The first pressing question, addressed by the next section, is: why do the bacteria regrow? Suppose one visualises the experiment as a competition between *E. coli* and pexiganan. At concentrations where the peptide is winning emphatically at the beginning, the *E. coli* manage to recover and go on to win at later times. There are two possible explanations for this population regrowth. The bacteria could be developing resistance to the peptide due to either genetic mutations, the development of phenotypic tolerance or a resistant sub-population. The second possibility is that the concentration of pexiganan is reducing over time. In fact, similar growth curves are shown in the literature for assays in which antibiotics are diluted over time to simulate the natural dilution process in the body [230].

The second question arising from these results is: does pexiganan have any effects other than death on the growth of *E. coli*? As the majority of the population are dying, do the survivors continue to divide normally, or is their growth inhibited, recovering at later times? This is identical to asking, when a reduced net growth rate is seen (for example at low $N(0)$ after the drop in N_{CFU}, at the initial stages of recovery), is it due to a reduced doubling rate or a death rate acting alongside a faster growth rate? The rapid recovery of the growth rate at high inoculum levels already indicates the answer to these questions, however section 8.5 attempts to confirm this indication with single cell measurements.

8.4 Regrowth explanations

8.4.1 Resistance

The first hypothesised explanation for the regrowth observed is that genetic or phenotypic resistance to the peptide is acquired. Four replicate MIC assays were performed using bacteria which had grown in 0μM, 2.5μM and 5μM pexiganan the previous day. There was no systematic difference in the MICs measured, indicating that the cells had not become any more tolerant to pexiganan during regrowth. This verifies that resistance by genetic mutation, allowing a resistant population to regrow, has not taken place. Given the speed of regrowth under certain conditions, this was already an unlikely scenario.

Phenotypic tolerance cannot lead to net regrowth in a constant concentration of antibiotic agent. Cells with a phenotypic, rather than genetic, advantage divide and grow to create a population with the same makeup as the original before the antibiotic was applied. The peptide would continue to kill all the susceptible daughter cells, maintaining at best a net growth rate of 0. Furthermore, the fact that the fraction of cells which die changes with $P(0)$ suggests that it is not a fixed sized, slow-dividing sub-population that survives.

8.4.2 Depletion of peptide

The second hypothesised explanation for the regrowth observed is that the peptide is depleted or deactivated with time. MIC assays using pre-incubated peptide indicate that the activity of pexiganan degrades by a factor of $2-4$ during 24 hours in MHB at

37°C. However, this is a small contribution compared to what was found when bacteria had also been in the solution.

Experiment A described in the Methods section 7.6.2 returned a MIC of $P(0) = 10 - 20\mu$M for $N(0) = 2.5 \times 10^7$ cell/ml. Wells which did not show growth (*i.e.* wells at 10, 20 and 40μM) were re-inoculated at $N(0) = 5 \times 10^5$ cell/ml. The next day growth was observed at all of these concentrations.

A MIC of $P(0) = 2.5\mu$M was recorded for the lower $N(0)$ of 5×10^5 cell/ml. Re-inoculation of un-grown wells (*i.e.* wells at 2.5, 5,10, 20 and 40μM) with $N(0) = 5 \times 10^5$ cell/ml, resulted in next-day growth at $P(0) = 2.5, 5$ and 10μM, but not at 20 or 40μM. At 10μM the detection times of the resulting growth curves were lengthened in comparison with the control, indicating that the peptide had retained some activity.

These results demonstrate that the peptide is de-activated by the process of killing or interacting with *E. coli*. The greater the number of killed bacteria, the greater the reduction in peptide activity; when the eradicated population size is low enough, the solution still contains active peptide the following day. The greater $P(0)$, the higher the likelihood of remaining peptide after incubation with bacteria.

The second experiment described in the Methods section, Experiment B adds some quantification to the depletion. An assay containing $P(0) = 40\mu$M and $N(0) = 5 \times 10^6$, after being filtered to remove any surviving bacteria, no longer had any measurable effect on the growth of a new *E. coli* inoculum. The activity of the peptide had been reduced >16×. When an additional 20μM of pexiganan was added to the solution and serially diluted with MHB it resulted in a MIC 4× greater than that of a control (normal MIC assay). Not only has the original peptide been depleted, but additional peptide has less activity in this solution than in MHB.

Following these findings, a suspension containing the filtered remains of $\sim 10^8$ sonicated cells/ml was used to set up a MIC assay, rather than MHB. Even at the highest concentration of pexiganan tested (20μM), there was no effect on the growth curves of an inoculum of $N(0) = 5 \times 10^5$ cell/ml, suggesting a reduction in the antimicrobial action of the peptide of $> 10 - 20\times$.

There are two probable explanations for these results. Firstly, pexiganan may bind to cellular components, exposed after lysis, such as anionic DNA. It is known that when lysis occurs there is an increase in free DNA [231]. Additionally, physical proteomics have found that the mean charge of an *E. coli* protein is negative [232]. Secondly, it could be that proteases released by lysis degrade the peptide. Trypsin at 1.25%

causes 40% degradation of pexiganan within minutes, and causes complete degradation within 30 min [202]. Whether proteases are able to cleave pexiganan this rapidly at the concentrations released from the cell is unknown. As the main focus of this project was to probe the time-dependent effect of pexiganan on a population of *E. coli*, an investigation into the cause of peptide depletion was not pursued.

8.5 Single cell measurements

The section before last (section 8.3), on density curves, demonstrated that pexiganan is bactericidal over a range of concentrations. However, simply because an antimicrobial agent is bactericidal does not necessarily mean that is does not additionally cause bacteriostatic contributions to growth. For example, a recent publication [233] showed that when isoniazid was added to a colony of growing *M. smegmatis*, some died while others continued to grow at a much reduced growth rate to previously. When the isoniazid was removed, the growth rate of those surviving recovered, not immediately, but within a division time later (10 hours). The objectives of this section are to;

- Probe whether the growth rate of surviving *E. coli* under pexiganan exposure is influenced by the peptide, and to
- Investigate whether survivors required a recovery period to resume normal growth on the removal of pexiganan.

Four experiments were conducted towards these objectives. The first two presented use the indirect dilution method. The second two experiments use microscopy as a direct method of observing cells. For clarity the four experiments conducted are listed below:

1. Dilution method. OD measurements of wells with $N(0) \sim 1$ and $P(0) = 0.5\mu$M.
2. Dilution method. OD measurements of wells with $N(0) \sim 1$ and $P(0) = 0\mu$M. Cells exposed to $0.1 - 1\mu$M for $5 - 45$ min before inoculation.
3. Microscopy: Agar pad. The time to first division of cells exposed to $P(0) = 3\mu$M at $N(0) = 2.5 \times 10^8$ cell/ml, before placement on agar for imaging.
4. Microscopy: Tunnel chamber. Growth, death and lysis of cells at $N(0) \sim 10^8$ cell/ml adhered to a coverslip, on the introduction of pexiganan ($5 - 40\mu$M) into a liquid medium.

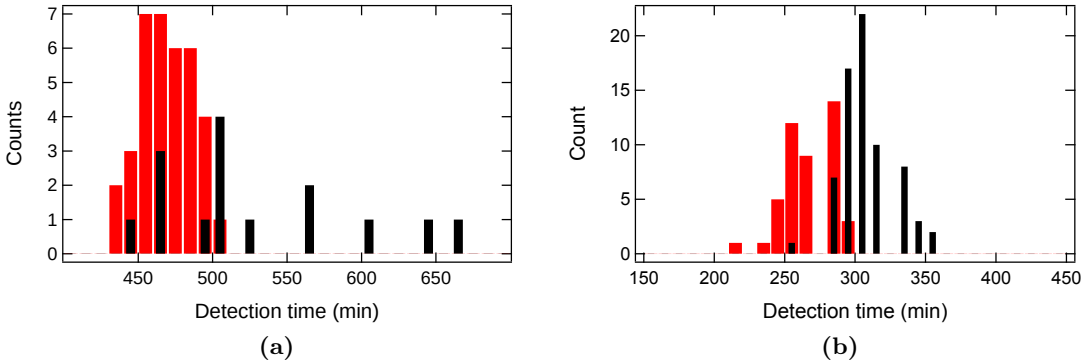

Figure 8.14 Histogram of single cell detection times in pexiganan, (a) from wells at 0μM (red) and 0.5μM (black), (b) from droplets at 0μM (red), 4μM (black).

The results from all four experiments are presented below in the order listed. Microscopy provides many interesting observations and images, some of which are shown as they may be of relevance to mechanistic studies. Finally, the totality single cell data is discussed.

8.5.1 Dilution method (experiments 1 and 2).

The dilution method, introduced and detailed in sections 6.2.2 and 7.2.1 respectively, gives indirect information on the single cell adjustment time. Experiment 1 inoculated small numbers of cells into the wells of a 96 well plate. Thirty wells contained 0.5μM pexiganan, chosen from Figure 8.6 (a) as being a concentration which affects detection times without resulting in complete death. The remainder of the wells contained no pexiganan for a comparison of the growth of the same $N(0)$ dilution, with no peptide present.

There was an average of 1.73 cells/growing well at 0μM and the distribution of detection times spanned a period from $\sim 430 - 510$ min (Figure 8.14(a) (red)). At 0.5μM, the was an average number of cells/growing well of 1.24, consistent with some of the cells dying at this concentration. Despite limited data, the histogram of detection times at 0.5μM (black) indicates that the peptide lengthens detection times. Not only has it reduced $N(0)$ which would have resulted in the detection times being at the latter end of the control distribution, but detection times are seen up to 160 min later than the last at 0μM. Figure 8.14(b) shows a similar distribution shift measured in the MDA at 4μM.

At first glance it appears that these results are evidence of an increased single cell adjustment time due to pexiganan. The histograms appear similar to those shown

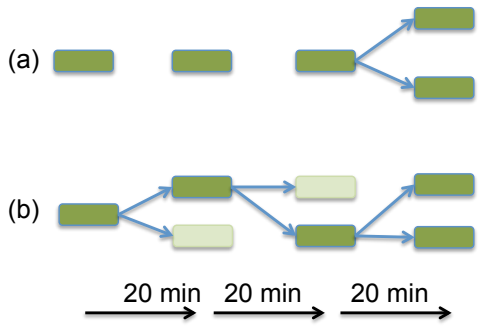

Figure 8.15 Schematic representing the two possible explanations for the extended detection times in the presence of pexiganan discussed in the text. Green rectangles represent viable cells whereas clear rectangles represent dead cells. Black arrows show the passage of time while blue arrows indicate cell division. (a) Cell requires time to adjust before first division. (b) Early time death due to the peptide is at a similar rate to growth.

for preservatives known to increase single cell lag time [143, 148]. Further thought suggests a second possibility (Figure 8.15). If the bacteria continue to grow at their normal growth rate, with no adjustment time, but the peptide present is killing at a rate similar to this, then once the first cell has successfully divided (which must have occurred, to ever witness growth in the well) the daughter cells remain at risk. If one of the daughters dies and the other survives to create a normal population, the detection time has already been increased by $\sim$ 20 min. Whether this type of competition can continue long enough to increase the T_{det} by 150 min, is difficult to know.

The same procedure was followed for cells only exposed briefly to pexiganan (experiment 2) to probe recovery from exposure. While at $N = 2.5 \times 10^8$ cell/ml, pexiganan was added to the suspension for $5-45$ min. The suspension was then diluted and inoculated into wells, using the same dilution as for the unexposed control. The dilution is so large ($\times 10^7$ to obtain $\sim$ 1 cell/well) that the concentration of pexiganan in the wells after inoculation is negligible, presumably leaving subsequent offspring unaffected by pexiganan in the medium. Figure 8.16 plots histograms for a range of concentrations (between 0.1μM and 1μM) and exposure times ($5-45$ min). No data was collected for exposure to 2.5μM or 5μM, as no wells grew.

Statistics are poor for each individual set of conditions. However, all conditions showed a reduced proportion of wells growing compared to the control. The distribution of detection times is within those of the unexposed cells for all conditions except 1μM of pexiganan for 15 min. This condition was repeated in a 384 well plate in order to confirm that under this condition there are a small number of wells with detection times outside those of the control distribution. This observation would require further work to become conclusive evidence of the cells needing to adjust after exposure to the

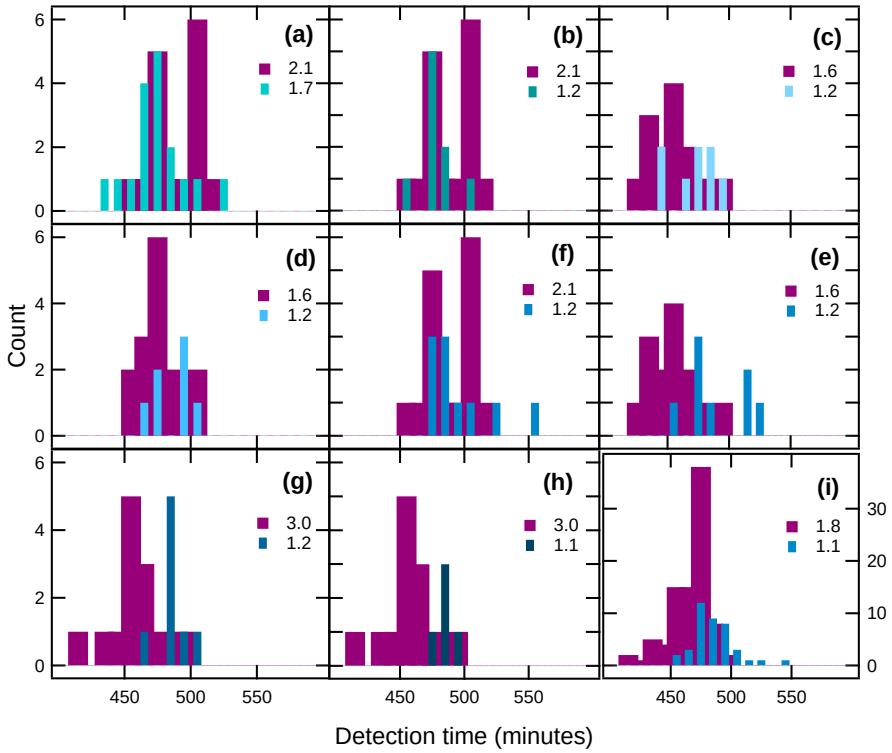

Figure 8.16 Histograms for cells exposed to peptide before being diluted to ∼1 cell per well. Unexposed corresponding control histograms recorded in the same plate are shown in purple. Exposure concentration and time, (a) 0.1μM, 15 min. (b) 0.5μM 15 min, (c-i) 1μM for (c) 5 min, (d) 10 min, (e+f) 15 min (g) 30 min (h) 45 min (i) 15 min, and then diluted into a 384 well-plate. The calculated average number of cells per growing well is shown in each legend.

peptide.

The primary conclusion from comparing Figure 8.14 and Figure 8.16 is that brief exposure to pexiganan influences the detection time distribution significantly less than continued exposure. This finding suggests recovery from exposure is rapid, but is unable to conclusively separate the two scenarios presented in the cartoon (Figure 8.15).

8.5.2 Microscopy: The effect of pexiganan on the times to first division (experiment 3).

Microscopy was used to directly observe *E. coli* on agar after exposure to pexiganan. The indirect dilution method detection time distributions are subject to the amplification of small uncertainties through extrapolation [220, 234] and do not return any information on non-dividing or dead cells.

Defining the lag time of a single cell dividing on agar is not straightforward. The time

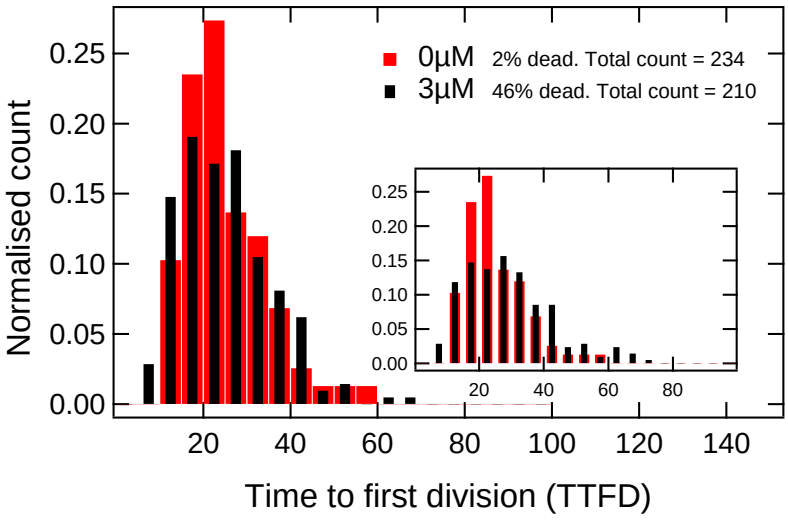

Figure 8.17 Normalised histogram of times to first division (TTFD) for bacteria on agar. Unexposed to pexiganan (red) and exposed to 3μM of pexiganan for 3 min (black). Inset shows the same plot if time to second division is counted for all first divisions resulting the death of a daughter cell.

to first division is a measurable quantity, thought to be the sum of the lag time and the first generation time [220, 235]. The conditions chosen for the data set shown (Figure 8.17) resulted in a sufficient number of cells dying to prove peptide effect, whilst a sufficient number survived to collect meaningful data.

Firstly, *E. coli* diluted to OD= 0.5 and left on the bench for 3 min before being placed on agar, without pexiganan addition, were imaged as a control. Two hundred and thirty four cells were visible in the field of view, 2% of which did not grow and appeared dead. The times to first division (TTFD) were recorded and are plotted as a histogram in Figure 8.17. Controlling for the time to image acquisition results in there being no data collected in the first 9 min.

The TTFD is distributed over $\sim$ 50 min, due to cells being placed on to the agar at different stages of the growth cycle and heterogeneities in lag or generation time. As expected, the distribution is narrower than the single cell detection time distribution, which incorporates uncertainty from $N(0)$.

No detailed study of second division times was conducted, but it was noticed that they are shorter and more homogeneous than first division times, as expected from [235]. Crudely, assuming that cells divide exponentially at their maximum growth rate after their first division would result in an estimated population lag time (λ, defined in Figure 6.1) of $\sim$ 10 min. A more sophisticated measurement of λ would rely on measuring the generation time distribution and stochastically simulating the resulting

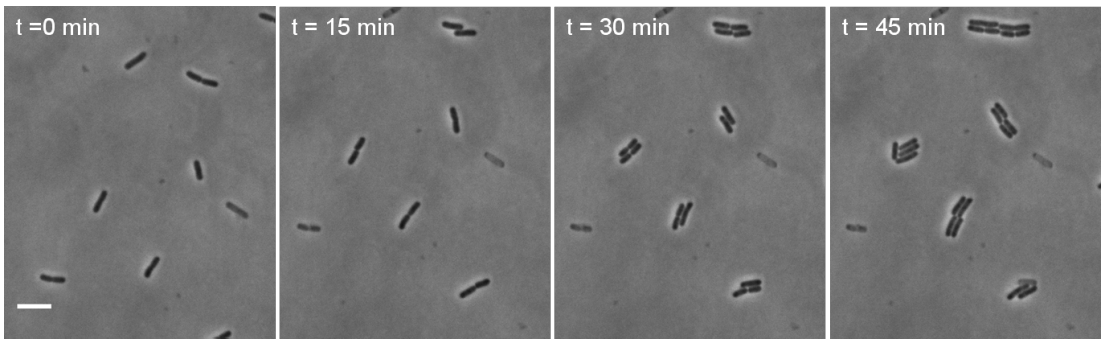

Figure 8.18 Time-lapse phase contrast microscopy of cells exposed to 3μM of pexiganan for 3 min before being placed on MHB agar. The time since beginning image acquisition is shown on each frame. The agar drifts within the first 15 min, changing the position of cells within the frame. Scale bar= 5μm.

populations [218]. A measurable population lag time suggests that inoculation onto an agar medium using this method affects the cells more than inoculation into bulk medium, where λ was negligible.

On exposure of the *E. coli* to sufficient concentrations of pexiganan before placement onto the agar, a proportion of the cells never undergo division. Some of the cells are deemed to be dead by the time the first image is acquired, appearing to have less contrast from growing cells, but others grow initially and then stop at later times. Some cells lyse suddenly, losing contrast in the space of a minute, whereas others fade over time. Those which survive divide and form colonies, see Figure 8.18.

Interestingly, 29% of those which grow and divide undergo subsequent death of a daughter cell (referred to as 'division before death'). Sometimes a cell undergoes two divisions before a daughter dies. On a close inspection of all samples not exposed to pexiganan, division before death does occur in the controls. However, it is not seen often. Division before death was seen frequently in all samples exposed to pexiganan. An example is shown in time-lapse images in Figure 8.19.

The histogram shown in black (Figure 8.17) is the TTFD for cells which were exposed to 3μM of pexiganan for 3 min before being put onto the agar. Forty seven percent of cells died and never underwent a first division. The TTFD for the 245 cells which survive to undergo division have a similar distribution to unexposed cells. The distribution is slightly wider, with more cells dividing at later times, but the effect is small, within the noise of repeating control measurements. If the division times of all cells resulting in the death of one of the daughters are changed to their second division time (the time at which there are two cells that will both survive), then the resulting distribution is shown in the inset of Figure 8.17. Despite only shifting the distribution slightly,

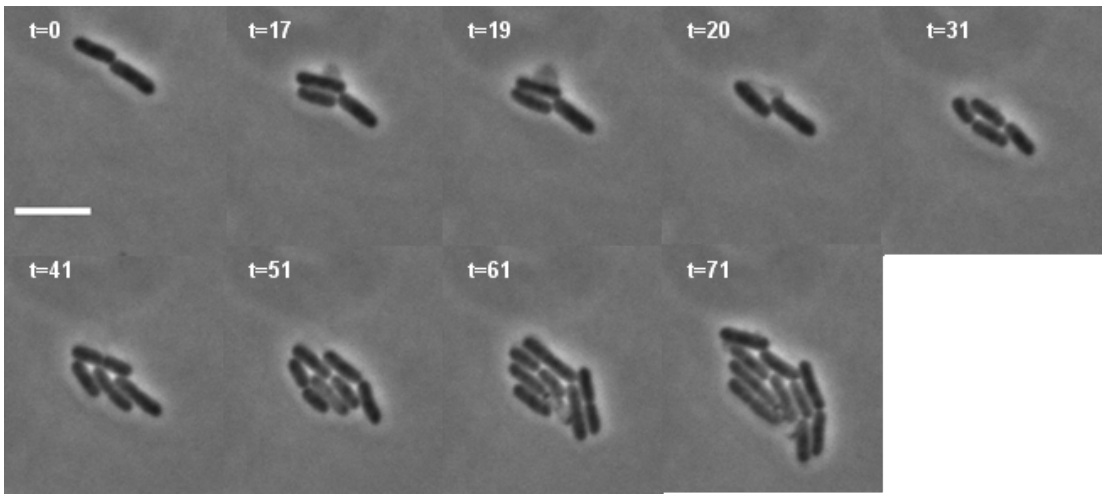

Figure 8.19 Phase contrast time-lapse of colony growth after the exposure of the initial cells to 3μM pexiganan for 3 min. Both original parent cells grow after being placed on the agar, but 17 min after beginning recording a large bleb forms above one. This expands for 4 min and then the cell lyses, leaving only a faint outline of the original cells wall. The daughter cells of the other parent continue to grow and each divide. At ∼42 min one of the 4 cells stops growing and over the next 15 min fades. The time after the beginning of recording is shown in min. Scale bar= 5μm.

there are now some division times which occur $\sim 10 - 20$ min after the longest of the unexposed cells, potentially explaining the longer detection times in Figure 8.14.

Dark shadows are sometimes seen next to cell bodies before lysis, assumed to be blebs. Membrane blebbing, also called membrane bulging, membrane vesicles, or membrane micellisation, occurs when the membrane deforms outwards and then pinches in on itself. An example of blebbing is shown in phase contrast in Figure 8.19. Fluorescent *E. coli* BW25113 expressing a GFP plasmid was used to demonstrate cytoplasmic content to the blebs (Figure 8.20). The images taken of blebs appear similar to those taken by Yao *et al.* [236] of *E. coli* treated with beta-lactams, before lysis. These researchers showed that *E coli* treated with cefsulodin underwent two rounds of division before bulge formation and lysis began, with some bulges showing no membrane gaps. These features were observed with pexiganan (Figure 8.20). AMPs have commonly been seen to induce blebbing at sufficient concentrations [207, 208], but the features are usually smaller than those imaged here.

In conclusion, the peptide does not have an effect on the times to first division. The populations monitored in Figure 8.17 (after controlling for the number of counts and difference in times to acquisition) would reach 2×10^7 cells within 1 min of each other *i.e.* they have the same λ within error. Again, the conclusion is that the peptide results in death or leaves the growth of single cells unaffected. Recovery from exposure is

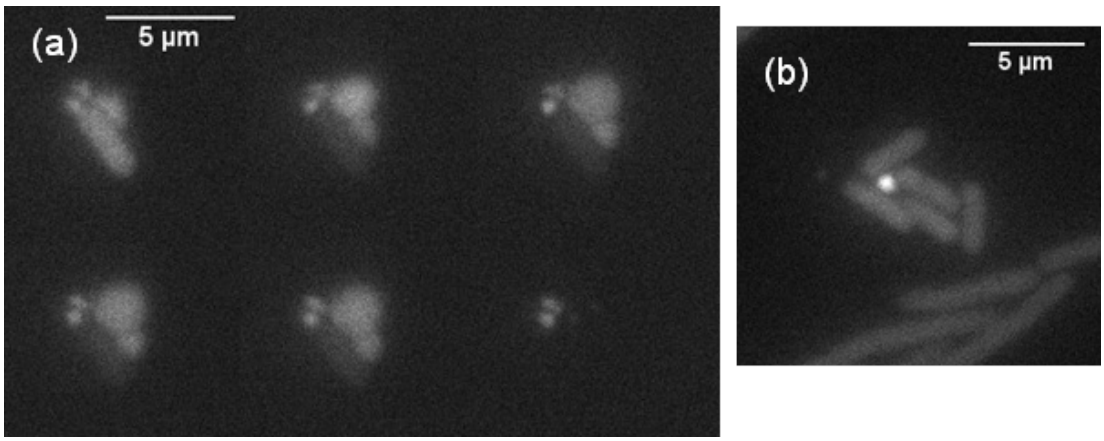

Figure 8.20 Fluorescent GFP images of *E. coli* on agar as examples of interesting blebs. (a) The first image is of 85 min after the cell was exposed to 10μM pexiganan. Three blebs are seen next to the cell body. Five min later the body of the cell loses its fluorescent signal, but the blebs do not. Twenty five min later two blebs lose their signal leaving two remaining. The time between subsequent images is 5 min. (b) Ninety three min after beginning to record, cells exposed to 5μM have formed colonies, but there are bright fluorescent blobs sitting next to cells. It is not always obvious which cell they are associated with.

immediate, reiterating what was found indirectly. The weakness of placing the bacteria on agar is that the likely drop in pexiganan concentration is not controlled or monitored. There remains the possibility that cells under constant exposure to pexiganan grow more slowly.

8.5.3 Microscopy: Single cell measurements during pexiganan exposure (experiment 4).

A tunnel chamber was used as a method of monitoring single cells under exposure to pexiganan. Cells were attached to a cover slip using poly-L-lysine and their growth in MHB monitored for $\sim$ 10 min before the medium was exchanged for MHB containing peptide. The results obtained for a set of samples using the same bacterial culture and pexiganan stock (concentrations between 0 and 40μM) are described in three ways: observations of the reconstructed time-lapses with the fluorescent channel superimposed on the phase contrast, volume traces of 5 example cells to reinforce these observations (shown for 0μM and 10μM), and fraction of lysed cells at each time-point.

Bacterial growth in a tunnel chamber

In MHB only, with no peptide present, 100% of the cells in the field of view grow and divide. It is not possible to compare their growth to the situation with no poly-L-lysine

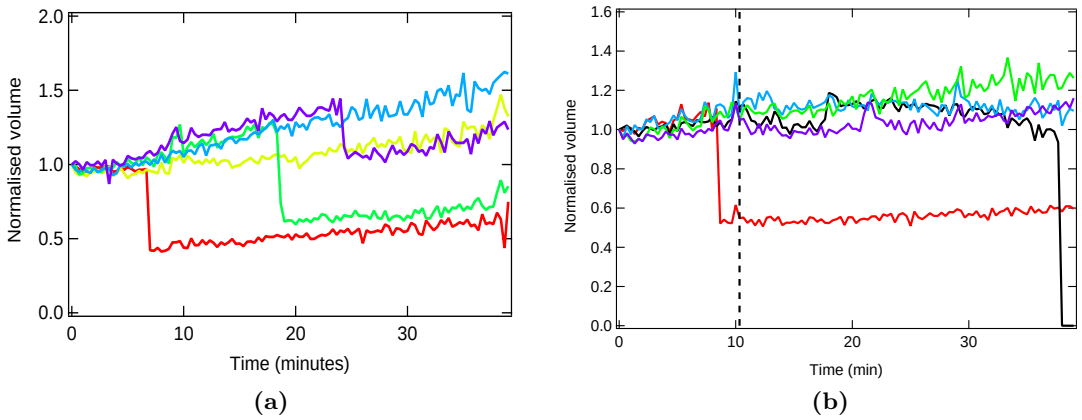

Figure 8.21 Volume traces of 5 representative cells in the tunnel chamber. Growing in (a) MHB and (b) MHB with 10μM pexiganan added at the dashed line.

present, as cells would not adhere to the surface. High levels of poly-L-lysine on surfaces are known to impede the growth of gram negative bacteria [237].

Figure 8.21(a) shows five normalised cell volume traces at 0μM pexiganan. There is an adjustment period of $3-4$ min before the cell volume begins increasing linearly. Note that this adjustment period was not always observed, it may have been dependent on the amount of time taken to locate and focus the cells after sample insertion into the microscope. The rate of volume increase varies between cells at early times, but after 25 min appears similar. Division can occur unseen in the traces if the daughter cell remains adhered to the slip and within the analysis box. However, sometimes cell division is seen as a sudden drop in area when one of the daughter cells detaches from the surface and moves away into the bulk fluid. For example, the purple trace tracks a situation in which a cell divides at early times, and both daughter cells contribute to the increasing volume measured until they both divide and one of these four daughter cells floats away at $t = 24$ min.

Interestingly, cells do not grow to twice their volume before dividing. For cells which undergo two divisions in the 40 min of observation it is clear that daughter cells are significantly shorter than those initially adhered to the glass. This emphasises the fact that, as recording began only minutes after the sample was placed in the microscope at 37°C, the cells are transitioning to this new environment during the measurement.

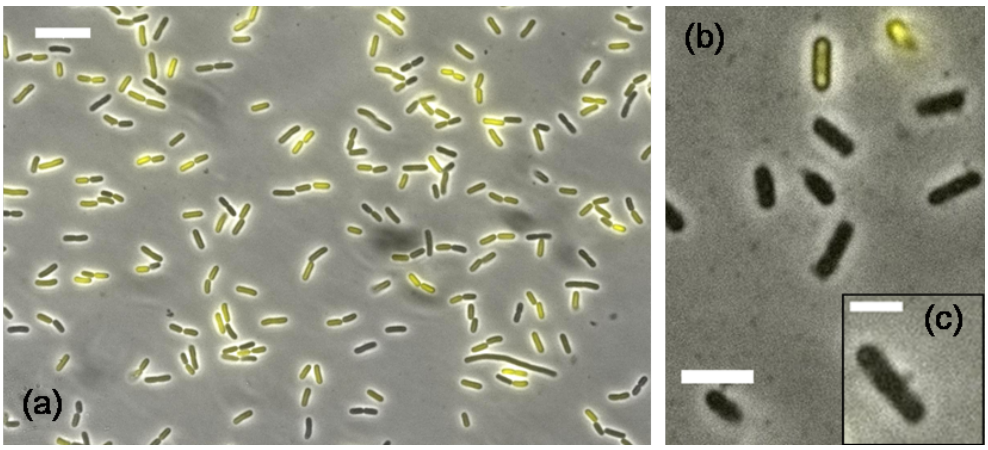

Figure 8.22 Composite YFP and phase contrast of cells in the tunnel chamber. (a) A proportion of cells have lost their fluorescent signal 100 seconds after the addition of 20μM pexiganan, and (b) dark shadows next to cell bodies and debris accumulation on the slide 30 min after the addition of 20μM pexiganan. (c) An example of a dark shadow or bleb in a phase contrast image, 30 min after addition of 10μM pexiganan. Scale bars = (a) 10μm, (b) 4μm and (c) 2μm.

Pexiganan introduced into the tunnel chamber

After the addition of 5μM of peptide to the media, the cells continue to grow. A second identical exchange of media caused one cell to stop growing immediately. Volume traces (not shown) confirmed these observations but were not informative enough to allow a comment on whether there were slight changes to the growth rate following peptide addition.

The situation changes dramatically when the concentration of peptide is increased to 10μM. By $\sim$ 30 min after the addition of the peptide, 7% of cells have completely lost their fluorescent signal, 7% of cells have stopped growing but still have a fluorescent signal, and the remaining 86% continue to grow. A sudden drop in fluorescent signal is assumed to correspond to lysis of the cell resulting in the leakage of intracellular materials. Fluorescent signal from the cytoplasm is known to drop within seconds of lysis [238]. The first lysis occurs 2 min after peptide addition (evidence shown in the next section on the lysis analysis). Post-lysis, two of the cells show shadows next to their bodies, assumed to be blebs, visible in phase contrast (example shown in Figure 8.22).

Volume traces (Figure 8.21(b)) support these observations, showing growth halt and then sudden lysis (black trace), growth halt (light blue trace) and growth continuing at a similar rate. From the volume traces it appears as if cells may spend $\sim$10 min adjusting to peptide addition before resuming growth. As this was only seen in one

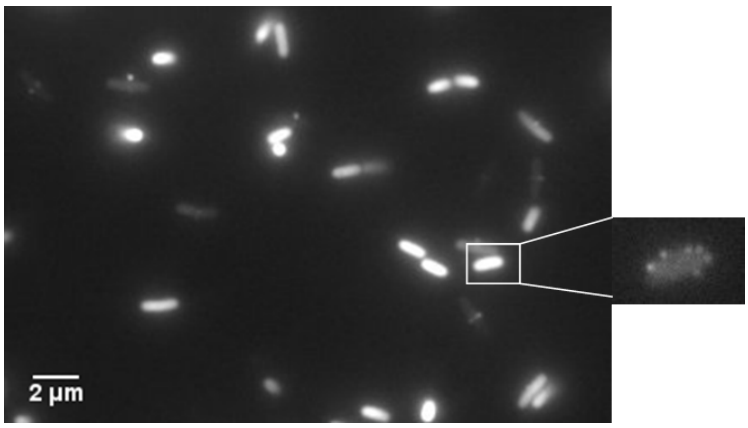

Figure 8.23 YFP image taken 140 seconds after the addition of 20μM pexiganan to the media. Several cells show accumulation of fluorescent signal at the septis. One cell is shown magnified, 8.6 min after peptide addition, with 6 fluorescent dots distributed around its body.

other sample, and similar features have been observed in controls (media exchanged for MHB only), this apparent lag would require more work to confirm. Additionally, the traces are too noisy and prone to error to judge small changes in growth rate after peptide addition to be real. With further work, this method could provide a means of monitoring small changes in adjustment time and growth rate, but here it has been shown that if there are changes, they are small and within current error. Most importantly, at concentrations where pexiganan is able to kill and lyse some cells, others keep growing at a similar rate to previously, a result suggested by the previous single cell measurements.

When the peptide concentration is doubled again to 20μM, all bacteria stop growing immediately, and some cells have lysed by 1 min. Thirty min after addition 78% of cells retain no fluorescent signal, and the coverslip surface appears to be more dirty (Figure 8.22(b)). Some cells show bright fluorescent areas outside the cell body before lysing (Figure 8.23) and most cells have shadows (blebs) after they lose their fluorescent signal.

Similarly, at 40μM all cells stop growing immediately and lysis begins 1 min after peptide addition. The proportion of cells without any fluorescent signal by 30 min is greater, about 90%. Pre-lysis, blebs are seen in the fluorescence images for most cells, often at the septis of cells which have begun to divide, but also seen at all other positions around the cell (Figure 8.24). Again, post-lysis, blebs can be seen in phase contrast and the coverslip gradually accumulates debris. Volume traces show lysis at varying times after peptide addition and volume fluctuations before lysis.

As with the experiments conducted on agar, no cell which had obviously stopped

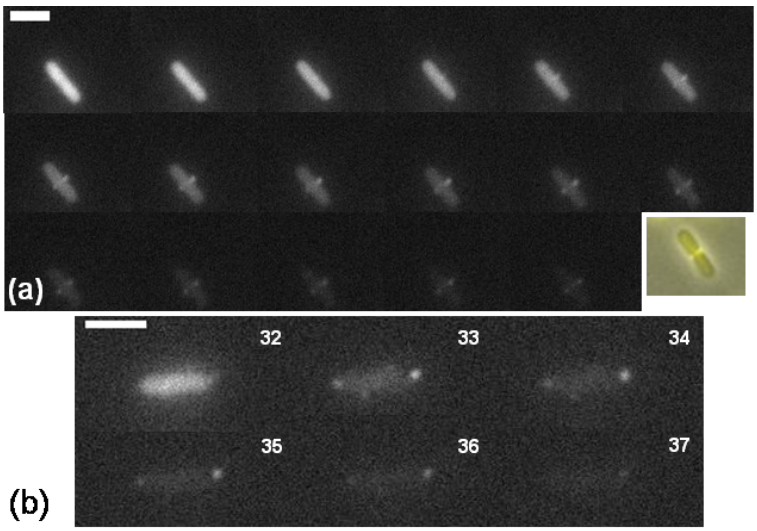

Figure 8.24 YFP images of cells in the tunnel chamber. (a) Formation of blebs at the septis under exposure to 40μM pexiganan. The first frame shown is 20s after peptide added, and each subsequent frame is 20s later than the last. Final image is composite of YFP and phase contrast images, 140 s after addition. (b) Formation of blebs at the ends of a cell body at 20μM pexiganan. Time after peptide addition is shown in min at the top of each frame. Scale bars= 3μm.

growing was ever seen to resume growth. However, most samples were only observed for $40 - 60$ min in total. As the samples were held at 37°C, evaporation from the end of the tunnels progressed rapidly and prevented observation of the samples for longer time periods.

Lysis analysis

The fraction of non-fluorescent cells was counted by eye with time from the addition of pexiganan ($t = 0$ min). The dynamics of cell lysis differ between 20 and 40μM (Figure 8.25). The lysis rate is similar, within uncertainty, for the first 5 minutes at ~ 0.1 fraction per min. After this, lysis continues, with the rate gradually slowing at 40μM until data acquisition stops at 20 min. At 20μM the lysis rate reduces markedly to ~ 0.0043 fraction per min at $t \sim 6$ min. Only 7 cells lyse at 10μM, not providing good enough statistics to allow comments on dynamics.

At both 20μM and 40μM, all cells have stopped growing, and as they never recover, are therefore dead. Thus a plot of the fraction of fluorescent cells (1- the data shown in Figure 8.25) with time would show the number of dead, unlysed cells. Population measurements comparing CFU to OD demonstrated that all dead cells do not immediately undergo lysis, many still scattered light. These measurements have

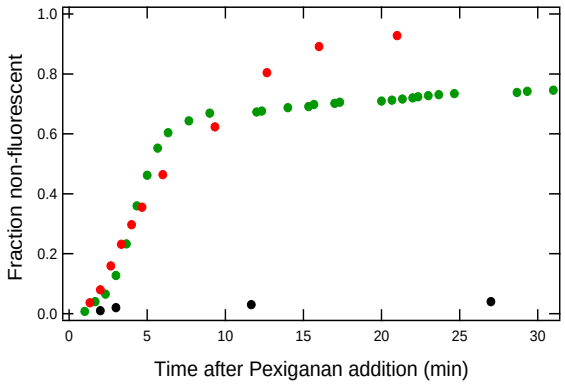

Figure 8.25 The fraction of cells within a tunnel chamber to have lost their fluorescent signal with time after pexiganan addition. Judged from one field of view at 40μM (red), 20μM (green) and 10μM (black).

confirmed that finding on a single cell level by showing that many cells which have stopped growing retain their fluorescent signal.

The density of *E. coli* in the tunnel chamber is $1\pm0.8\times10^8$ cell/ml, so 100% death would be expected to occur at a MIC of $20-80\mu$M (Figure 8.9). Broadly speaking, these results agree if 40μM is interpreted as the concentration at which 100% death occurs every time. That being said, a more quantitative comparison to Figures 8.10 and 8.12, for which $N(0)$ was similar to in the tunnel chamber, indicates discrepancies. At 5μM the resulting growth curves grow roughly 35 min after the control, this cannot be explained by the 2% death observed in the tunnel chamber. At 10μM the growth curves lag $\sim$200 min behind the control, suggesting only 10^5 cells/ml survived the addition of peptide *i.e.* 0.1%. Therefore, no (or a very small number of) cells would be expected to be seen surviving in the tunnel chamber at or above this concentration. In summary, pexiganan was marginally less active than expected in the tunnel chamber.

The experimental situation in the tunnel chamber is not identical to in a well or a larger test tube. The cells observed are all attached to the surface with poly-L-lysine, itself known to have bacteriostatic and bactericidal effects [239] (see section 8.7). It is not known whether the proximity to poly-L-lysine influences the interaction with the peptide. Instead of being uniformly distributed in the media, all of the cells are close to each other (on both surfaces) with a reservoir of media next to them. When these factors are considered it becomes less surprising that quantitatively there are small differences between these results and measurements in bulk media.

Finally, samples which resulted in complete death in the field of view positioned in the centre of the tunnel, still had living, growing cells at the edges, next to the tape (Figure

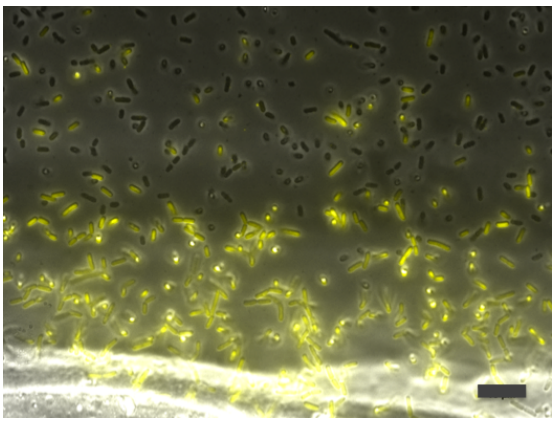

Figure 8.26 Composite YFP and Phase contrast image of a field of view next to the tape. Taken 30 min after the addition of 20μM pexiganan. Within $\sim$ 50μm of the tape there are are a greater proportion of cells which retain their fluorescent signal. Scale bar= 10μm.

8.26). These images highlight the need to measure MIC in the environment of interest as some environments may have the ability to protect cells at short times.

8.5.4 Conclusions from single cell results

Single cell measurements have shown conclusive evidence that recovery from pexiganan exposure is rapid. As it has already been established that the pexiganan concentration drops as a result of cell death, single cell response to a drop in peptide concentration is of relevance to this study. However, achieving the first objective of the section (to establish whether the growth of surviving bacteria under constant pexiganan exposure is effected) proved more difficult.

Indirect measurements show detection times from populations initiated from single cells influenced greatly by the presence of the peptide. Direct measurements in the tunnel chamber could not prove whether this was due to a slowed single cell growth rate, or to a death rate competing with the growth rate (the two scenarios of Figure 8.15). Although peptide is not manually removed in experiment 4, its concentration would be expected to drop due to cell death. For the example shown at 10μM in the tunnel chamber, 14% of the bacteria die immediately, representing a density of $\sim 10^7$ bacteria/ml. From the previous section, it is known that this magnitude of cell death results in a drop in pexiganan concentration. When a single cell is placed in 0.5μM in a well, no scenario would result in the concentration of pexiganan dropping at early times.

The tunnel chamber provided a third method (after CFU and OD) of probing the short-

term characteristics of the *E. coli* density curve in pexiganan. The advantage of its use over population measurements (CFU, OD and motility in the next chapter) is that direct observation delivers additional information, such as bleb formation. Moreover, data was collected every minute, delivering far more resolution with time than possible with the population measurements.

To conclusively measure growth rates or recovery times of *E. coli* in an unchanging concentration of pexiganan, the tunnel chamber protocol would require improvement to allow longer measurements and less noisy volume traces. A modification to allow constant media flow rather than a single exchange would remove the effect of pexiganan depletion.

8.6 Modelling the experimental results

To reiterate the results of the last two sections: in immediately sub-MIC concentrations of pexiganan some cells die while others continue to divide normally. Bacterial death reduces the effective concentration of peptide, allowing net bacterial regrowth. These findings suggest that the main contribution to population dynamics is determined by a competing growth rate and death rate. The following section constructs a simple deterministic model of bacterial growth subject to a death rate due to a depleted agent. It discusses how this simple interpretation of the experimental results alone could, at least partially, explain the results of the density curves, the inoculum effect and detection time patterns.

8.6.1 Shape of the $N(t)$ curve

The number of living bacteria N is assumed to grow exponentially with time, at a growth rate of $a = 0.034$ min^{-1}. Changes in N with time are modelled by;

$$\frac{dN}{dt} = aN - \frac{dB}{dt} \tag{8.1}$$

where B is the number of dead cells. Death is modelled as linear in N and its rate $D(P)$ is peptide number P dependent.

$$\frac{dB}{dt} = D(P)N. \tag{8.2}$$

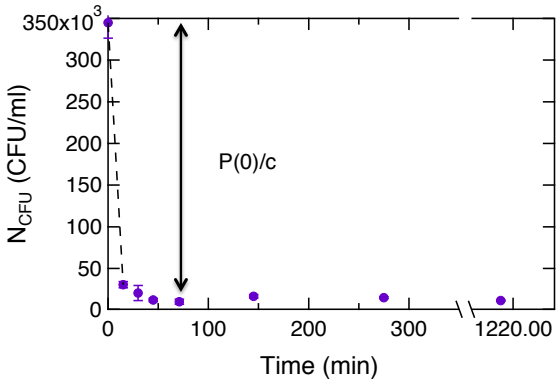

Figure 8.27 Calculating b from a density curve in PBS at 1μM pexiganan.

The death rate is chosen for simplicity to be linearly related to P;

$$D(P) = \frac{bP}{c}, \tag{8.3}$$

with it requiring c peptides to kill one cell, and a death constant b. For every bacterium which is killed, c amount of the peptide becomes inactive for further use,

$$P(t) = P(0) - cB(t). \tag{8.4}$$

The final system of differential equations to solve is therefore;

$$\frac{dN}{dt} = aN - \frac{bPN}{c}, \tag{8.5}$$

$$\frac{dP}{dt} = -bPN. \tag{8.6}$$

The amount of peptide remaining, in units of 'amount required to kill a bacterium', $P(t)/c$, was not allowed to drop below 1. Below this the death rate $D(P)$ drops to 0. An approximate value for b was inferred from the time-kill curve shown in Figure 8.27. In PBS $a = 0$, thus,

$$\frac{dN}{dt} = -\frac{bPN}{c}. \tag{8.7}$$

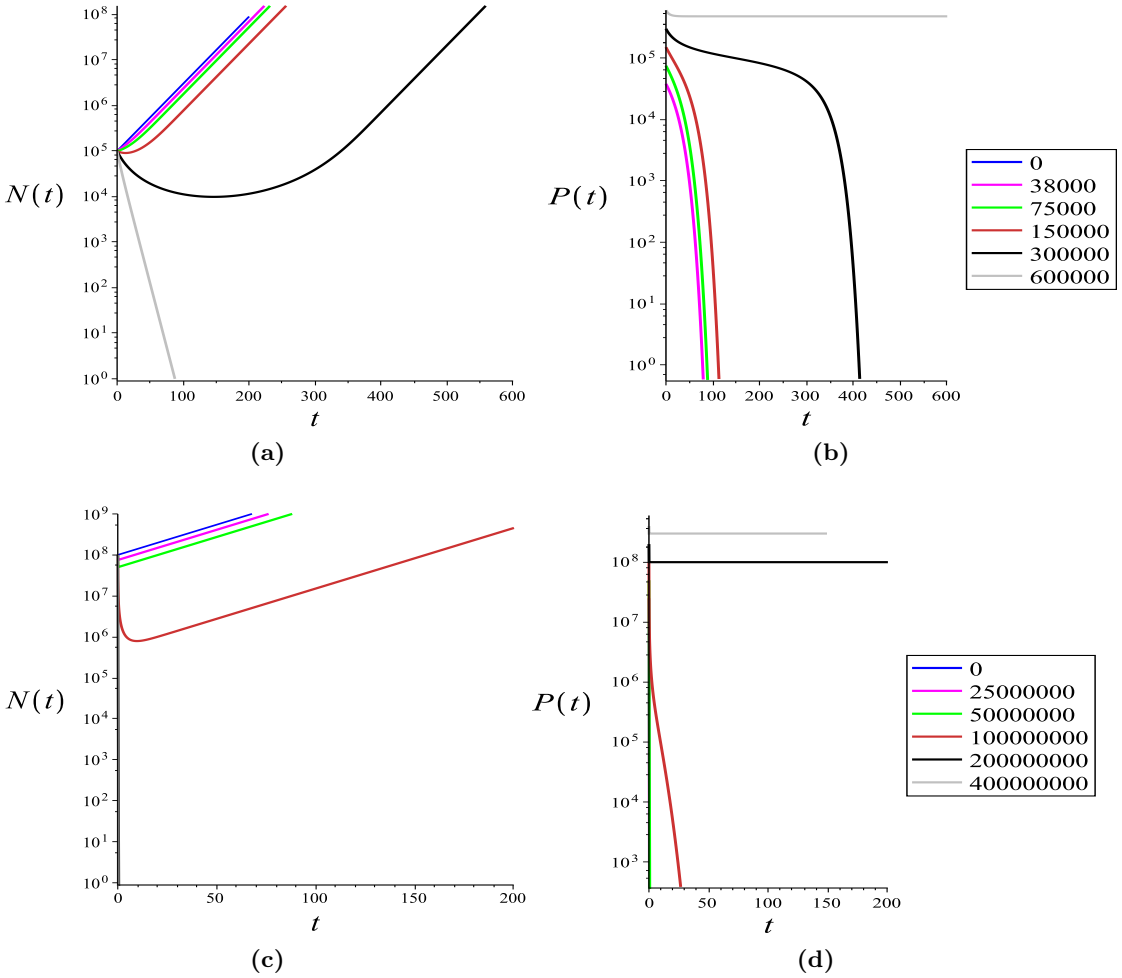

Figure 8.28 Simulated density curve from the deterministic model. (a) $N(t)$ and (b) $P(t)$ for $N(0) = 1 \times 10^5$. (c) $N(t)$ and (d) $P(t)$ for $N(0) = 1 \times 10^8$. $P(0)/c$ shown in the legend.

At very short times $N(t)$ is approximated by,

$$N(t) = N(0)e^{-\frac{bP(0)N}{c}} \sim N(0)\left(1 - \frac{bP(0)}{c}\right). \tag{8.8}$$

Fitting a straight line through the $t = 0$ and $t = 2$ min time points gives $N(0)bP(0)/c = -2 \pm 1 \times 10^4$ min^{-1}. $P(0)/c$ is estimated as $\sim 3.3 \pm 0.2 \times 10^5$ by calculating the total number of killed cells from $N(0)$ and the lowest value N reaches N_{min}. Therefore b is calculated to be $2 \pm 1 \times 10^{-7}$min^{-1}. Following this procedure for each of the density curves performed in PBS (Figure 8.11) yielded values of b between 10^{-6} and 10^{-8} min^{-1}.

The differential equations were numerically simulated by Maple with $c = 1$ (scaling $P(t)$ to manageable numbers) and $b = 3.4 \times 10^{-7}$ min^{-1} (chosen to be 5 orders of

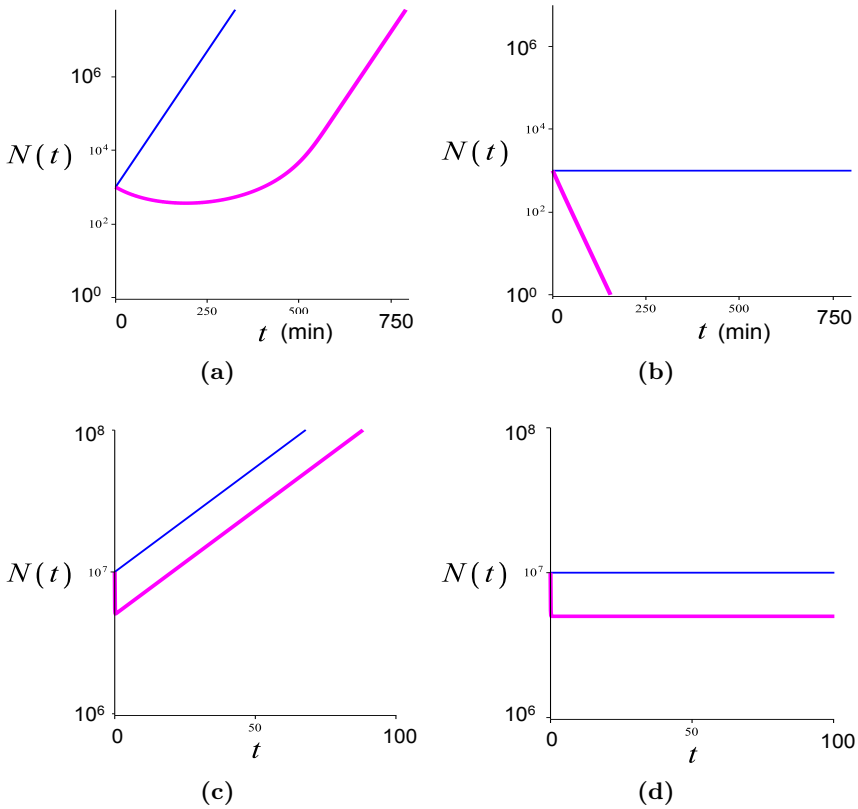

Figure 8.29 Comparing simulated density curves with and without growth for a high and low inoculum. N against t for (a+b) $N(0) = 1 \times 10^3$ and $P(0)/c = 14000$ (pink), $P(0)/c = 0$ (blue), (c+d) $N(0) = 1 \times 10^7$ and $P(0)/c = 5000000$ (pink), $P(0)/c = 0$ (blue). In (a+c) $a = 0.034$ min^{-1} whilst in (b+d) $a = 0$ min^{-1}.

magnitude lower than a). Two values of $N(0)$ were chosen for comparison and $P(0)$ varied in 2× increments over a range below those that lead to population eradication (Figure 8.28).

As $P(0)$ is increased, growth of $N(t)$ is impacted at short times, followed by growth at its maximum rate once $P(t) < 1$. The higher initial population size requires higher values of $P(0)$ to significantly change $N(t)$ compared to the control at $P(0) = 0$. At high $N(0)$ the initial drop in $N(t)$ and $P(t)$ is much faster than at lower $N(0)$, where the drop in $N(t)$ is more gradual and regrowth slower to reach its maximum rate. These features were seen experimentally in section 8.3.1. Returning to the model, for a $P(0)$ 2× below that which leads to $N = 0$, $P(t)$ drops rapidly at early times, then its rate of depletion slows as the death rate matches the growth rate before growth exceeds death, rapidly depleting the remaining $P(t)$.

When growth in the model is removed ($a = 0$), the magnitude of the drop in $N(t)$ for a given $P(0)$ at high $N(0)$ is similar to when $a = 0.034$ min^{-1} (Figure 8.29 (c+d)). At

lower $N(0)$ the drop is larger when growth is absent than when growth is present, as net death acts over a greater time period (Figure 8.29 (a+b)). Section 8.3.1 demonstrated this feature experimentally.

To investigate the inoculum effect (IE) predicted by the model it is possible to solve the differential equations to obtain an analytic IE expression. Using Equations 8.5 and 8.6,

$$\frac{dN}{dP} = \frac{\dot{N}}{\dot{P}} = \frac{1}{c} - \frac{a}{bP}, \tag{8.9}$$

which integrates to

$$N(t) = \frac{P(t)}{c} - \left(\frac{a}{b}\right) \ln P(t) + k. \tag{8.10}$$

The constant k can be determined from initial conditions $P(0)$ and $N(0)$, giving,

$$N(t) = \frac{P(t)}{c} - \left(\frac{a}{b}\right) \ln P(t) + \left[N(0) - \frac{P(0)}{c} + \left(\frac{a}{b}\right) \ln P(0)\right]. \tag{8.11}$$

N_{min} will occur when $D(P) = a$, or $P(t) = ac/b$,

$$N_{\min} = \frac{a}{b} - \frac{a}{b} \ln \frac{ac}{b} + N(0) - \frac{P(0)}{c} + \left(\frac{a}{b}\right) \ln \left(\frac{P(0)}{c}\right). \tag{8.12}$$

If $N_{\min} \leq 1$ the population is eradicated. When $N_{min} = 1$, $P(0) = P(0)_{MIC}$; the initial peptide concentration at which the population just survives for a given $N(0)$. Thus, setting $N_{min} = 1$ and rearranging to,

$$N(0) = -\frac{a}{b} + \frac{a}{b} \ln \frac{ac}{b} + \frac{P(0)_{MIC}}{c} - \frac{a}{b} \ln P(0)_{MIC} \tag{8.13}$$

gives a plot of the IE (Figure 8.30(a)) when the highest $P(0)_{MIC}$ solution for every $N(0)$ is plotted. There are no analytic solutions to Equation 8.13 for $N(0) < 10$ at $b = 3.4 \times 10^7$ and $c = 1$. However, by simulating $N(t)$ at each $N(0)$ for $P(0)$ increasing in $2\times$ increments over the range $5000 - 10240004$ and plotting the first concentration which leads to no net growth in a given time-period (in this case chosen to be 500 min), the first $P(0)$ above $P(0)_{MIC}$ can be established for the full $N(0)$ range (Figure 8.30(b)).

At the limit of small inoculum sizes, $N(0) = 1$, the $P(0)_{MIC}$ plotted is the number of peptides at which the death rate exceeds the growth rate ($P(0) = ac/b$). As $N(0)$ increases, depletion of the peptide begins to play a role in the determination of $P(0)_{MIC}$, increasing it with respect to $P(0) = ac/b$. In other words, more peptide is required than

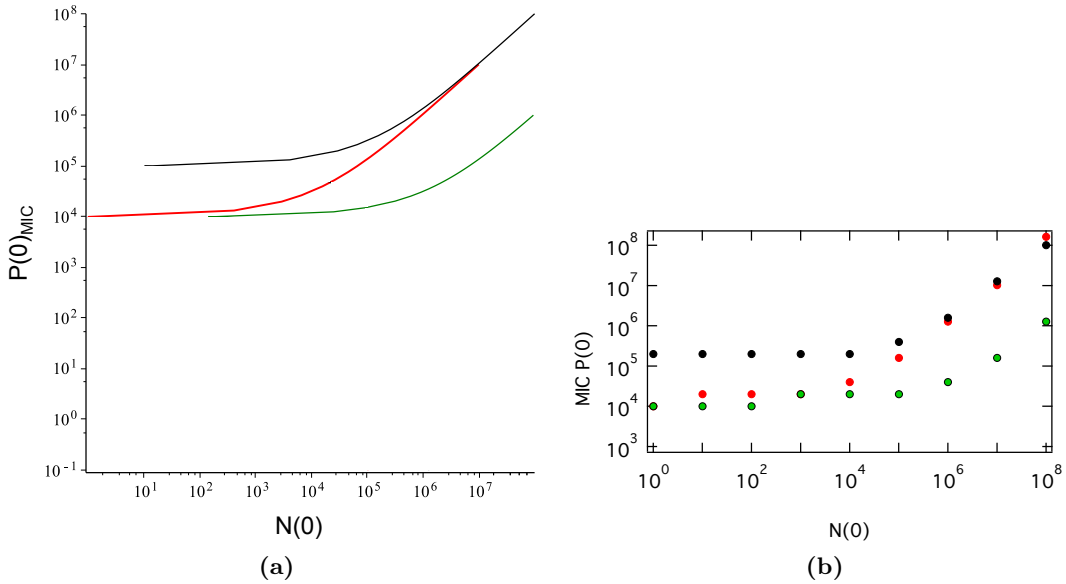

Figure 8.30 The inoculum effect of the simulated model. (a) Solutions to equation 8.13. (b) The first value of $P(0)$ in the range 5000 to 1024000 (increasing in 2× increments) to show a net reduction in N over 500 min, plotted against $N(0)$. (black) $b = 3.4 \times 10^{-7}\text{min}^{-1}$ and $c = 1$ (red) $b = 3.4 \times 10^{-6}\text{min}^{-1}$ and $c = 1$ (green) $b = 3.4 \times 10^{-8}\text{min}^{-1}$ and $c = 0.01$.

is necessary to ensure that the death rate is higher than the growth rate at $t = 0$. At high $N(0)$ depletion of the peptide occurs at early times, therefore $P(0)_{MIC}$ is simply the concentration at which the number of peptides $P(0)/c$ becomes greater than the number of cells $N(0)$. In this regime, the IE is described by a power law with power=1. The $N(0)$ at which this term begins to dominate depends on the values of a, b and c, illustrated in Figure 8.30.

8.6.2 Comparison with experimental results

Qualitatively the model predicts the experimental features seen in time-kill curves and the IE. However, quantitatively there are discrepancies. For a given $N(0)$ the transition from an unaffected population to complete death of the population is over a narrower concentration range than observed experimentally. Further work on the model would adjust the death rate dependency on P, to investigate whether this lead to better agreement. It is likely that there is a threshold concentration of peptide, above which death is no longer accelerated. Researchers modelling pharmacodynamics have used a Hill function to describe the rate of death with antibiotic concentration [240]. Additionally, peptide action is over a shorter period of time. This may indicate that experimentally, not all the peptide required to kill a cell is depleted as a consequence of its death. Simulating the model with an additional multiplying constant in Equation

8.6 is able to adjust the action timescale.

The IE measured experimentally had a similar shape to that predicted by the model, indicating that for low inoculum sizes it is the concentration of peptide in the medium which determines the MIC measured, whereas for high inoculum sizes the amount of peptide in the medium begins to play a role. However, the power law measured experimentally is described by a power of < 0.5, unlike in the model. To influence the power law predicted by the model a population size effect would have to introduced, for example a b or c which is dependent on N.

Experimentally, a power law of < 1 suggests that as the population size increases it requires the addition of less peptide than expected from the model to achieve population eradication. Either larger populations are more susceptible to the peptide, requiring less peptide per cell to be killed than smaller populations, or the peptide is depleted less efficiently by large numbers of cells dying. Biological population effects of this nature are known to exist, for example quorum sensing, but usually it is advantageous for the cells to be in a larger population, contrary to this case. The other possibility is that physical effects are responsible, such as aggregation (see section 10.5), allowing peptides to aversely influence more than one cell at high densities by bridging cells [241]. Finally, experimentally, more replicates at the highest inoculum levels are needed, where the number of replicates completed was small. With more replicates it is possible that at the highest inocula the MIC would move up a factor of 2, displaying the increasing gradient shown in the model. It is possible that experiments are represented by the modelled regime before a power law of 1 is reached.

There is a threshold concentration below which the peptide has no effect on the bacteria, unable to kill a single non-dividing cell, measured to be $\sim 0.5\mu$M experimentally, but not included in the model. To rescale the experimental IE data to account for this 0.5μM could be subtracted from each concentration. However, this only increases the power fitted marginally (from 0.32 to 0.36 for the grey data in Figure 8.9).

The above model represents the simplest representation of the experimental situation, without incorporating any of the subtleties or complexities known to exist for growing bacteria in antibiotic agents (*e.g.* persisters). Nevertheless it captures the main features of the $N(t)$ curve and aides understanding of the data collected. If future research were to show an effect of pexiganan on the growth rate of surviving *E. coli* then a could be made a function of $P(t)$.

Understanding of the growth curves and detection time patterns observed in section 8.2 follow from the increased understanding of $N(t)$. All sub-MIC growth curves displayed

the same maximum growth rate, as once above the plate reader detection level the influence of the peptide is over. The detection time is influenced if a substantial number of cells were killed at early times. At $N(0) = 10^3 - 10^5$ cell/well the detection time can be lengthened enormously at immediately sub-MIC $P(0)$ by many cells being killed over a prolonged period of time. When $N(0)$=1 cell/well and $P(0)$ is immediately sub-MIC, detection times are not lengthened by as much time, as at $t = 0$ the growth rate roughly equals the death rate; population dynamics do not begin with a lengthy drop in cell number. At high inoculum sizes of $N(0) = 10^7 - 10^8$ cell/well, net death is rapid and confined to early times. If, after 10 min, only a single cell remains alive, diving normally, then $T_{0.12}$ of the population would be within 515 min. The limited number of MIC assays done at inoculum levels this high have not shown any detection times over 600 min, significantly shorter than for intermediate inoculum sizes.

A striking feature observed throughout the experimental work was variation between replicates, a feature that a deterministic model can not reproduce. However, from further understanding of the shape of $N(t)$, an explanation for the patterns in detection times observed can be proposed. Sub-MIC detection times displayed concentration dependent variation, at its greatest at intermediate inoculum sizes ($N(0) = 10^3 - 10^5$ cell/well) where detection times were seen up to 24 hours later. Detection times from single cell inocula and those as high as $10^7 - 10^8$ cells/ml showed less variation with detection times spanning 100 and 200 min respectively.

It is postulated that stochasticity in detection times becomes noticeable when N has dropped to small numbers before regrowth. For each $N(0)$ the magnitude of the variation observed increases with how low N is when $dN/dt = 0$ occurs (*i.e.* with $P(0)$). Stochasticity leads to exponential growth (which quickly becomes deterministic) taking off at different times, and hence reaching N_{det} at different times. At intermediate values of $N(0)$, an immediately sub-MIC $P(0)$ causes the population to spend a longer period of time at low cell numbers than at low inoculum sizes, due to a lengthy drop in numbers before regrowth. This leads to a larger amount of variation between replicates. At high $N(0)$ death occurs rapidly at early times, thus the situation at low $N(0)$ is replicated, producing a similar magnitude of variation.

In summary, comparison of the experimental results to those from a deterministic model has allowed proposed explanations for the patterns in population dynamics and thus detection times witnessed. The comparison has also suggested future avenues of exploration in the study of the IE displayed by the pexiganan MIC.

8.7 Other agents: Amhelin and poly-L-lysine

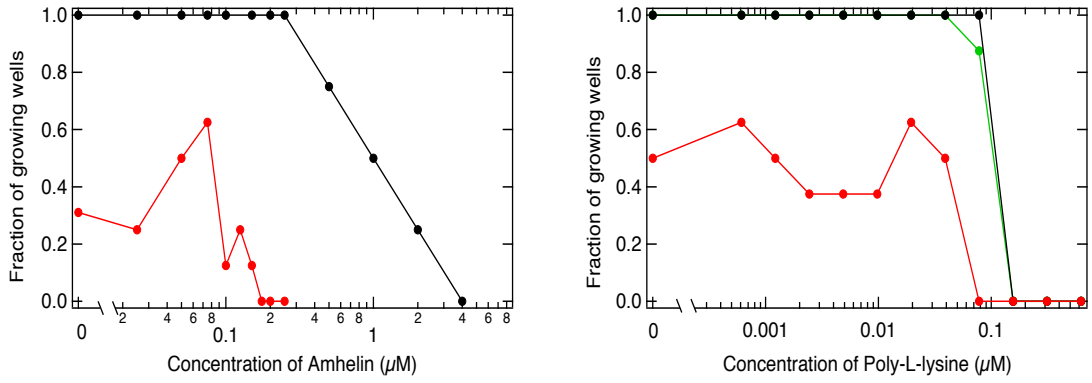

Figure 8.31 The fraction of growing wells from amhelin and poly-L-lysine MIC assays. Plotted against concentration of (a) amhelin (0μM plotted at 0.01μM) and (b) poly-L-lysine (0μM plotted at 0.0006μM), for $N(0) = 1 \times 10^5$ cell/well (black), $N(0) = 1 \times 10^3$ cell/well (green) and $N(0) \sim 1$ cell/well (red).

To determine whether the observations and conclusions presented throughout this chapter are specific to pexiganan, general to AMPs or more widely general to other classes of antibiotics would require large scale research which has not been undertaken. Nevertheless, MIC assays with *E. coli* MG1655 in the antimicrobial peptide amhelin and the antimicrobial polymer poly-L-lysine were studied. They provide a comparison with pexiganan MIC results presented at the beginning of this chapter in section 8.2, which are now at least partially understood. Amhelin was designed and synthesised by Rakowska *et al.* and has been observed to form pores in supported lipid bilayers [242]. Poly-L-lysine is a cationic polymer used by some countries in food preservation. It is commonly used by microbiologists to attach bacteria to glass surfaces. The antimicrobial action of poly-L-lysine is due to disturbance of the membrane leading to entry to the cell, reactive oxygen species response and interaction with DNA [239].

For both of these agents, growth curves measured in the plate reader as part of a MIC assay appear similar to those obtained with pexiganan. At sub-MIC concentrations the detection times are lengthened without the maximum growth rate being affected. The diauxic lag was seen to disappear on addition of sufficient amhelin, but did not at any concentration for poly-L-lysine. The fraction of growing wells and the measured detection times $T_{0.12}$ in 8 replicate MIC assays are plotted against concentration for $N(0) = 1 \times 10^5$ cell/well and $N(0) = 1$ cell/well (Figures 8.31 and 8.32(a)). $T_{0.12}$ for pexiganan, already shown, are included for comparison.

Amhelin shows similar plots to pexiganan with the fraction of growing wells reducing

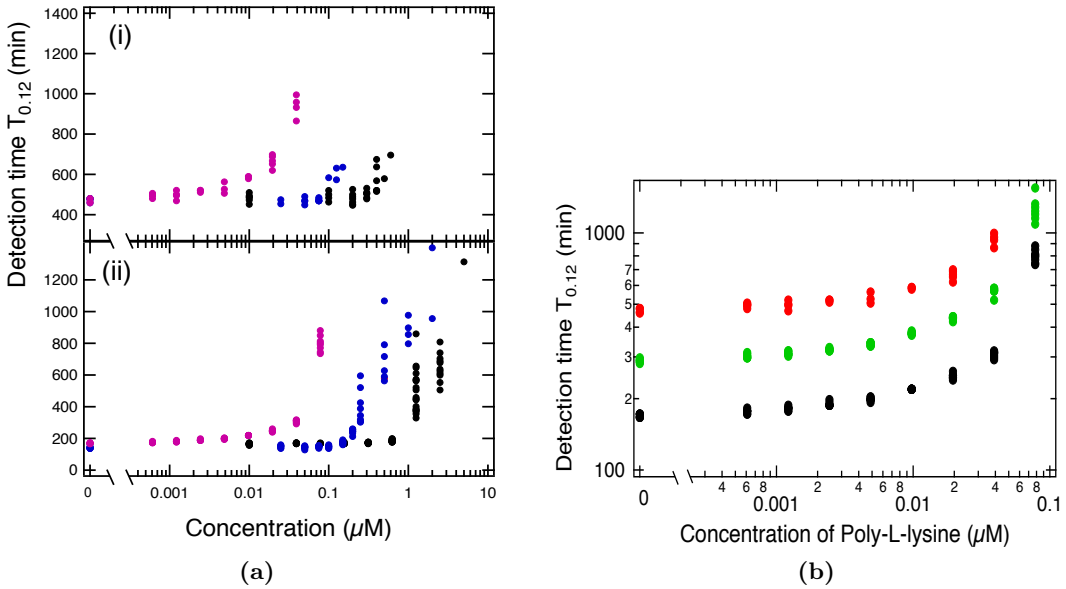

(a) (b)

Figure 8.32 Comparison of *E. coli* detection times in amhelin, poly-L-lysine and pexiganan. (a) $T_{0.12}$ against concentration of amhelin (blue), poly-L-lysine (pink) and pexiganan (black) at (i) $N(0) = 1$ cell/well and (ii) $N(0) = 1 \times 10^5$ cell/well. The detection times recorded at 0μM are plotted at 0.0001μM. (b) $T_{0.12}$ on a log scale, against concentration of poly-L-lysine at $N(0) = 1$ cell/well (green), $N(0) = 1 \times 10^3$ cell/well (black) and $N(0) = 1 \times 10^5$ cell/well (red).

over a large concentration range ($4 - 16\times$), causing an ill-defined MIC between replicates. The main difference is that the concentration at which no replicates grow is $\sim 5\times$ lower than for pexiganan. Conversely, poly-L-lysine shows a well defined MIC with the fraction of wells growing dropping to 0 over a $2 - 4\times$ concentration range. The detection times measured are influenced at much lower multiples of the MIC than for both the AMPs. They then rise gradually, over a concentration range spanning two orders of magnitude, not showing significantly more noise between replicates until the dilution immediately before the MIC. The single cell detection times are extended by up to 500 min, compared to > 150 min in pexiganan. Differences in $T_{0.12}$ patterns are seen most clearly when all three agents are plotted together (Figure 8.32(a)). Additionally, while amhelin shows a similar magnitude of IE to pexiganan, poly-L-lysine shows no change in MIC in the $N(0)$ range 10^2 to 10^7 (Figure 8.33).

Understanding of the results collected for pexiganan allows speculation of the reasons for poly-L-lysine's differences. For pexiganan, an increase in detection time coincides with an increase in variation between replicates as cell numbers drop to low levels before regrowth. For poly-L-lysine, detection times are increased substantially without any corresponding increase in variation. Only at concentrations immediately sub-MIC do stochastic effects become apparent, and even at these concentrations differences between replicates are not large enough to play a role in the determination of the MIC. Therefore

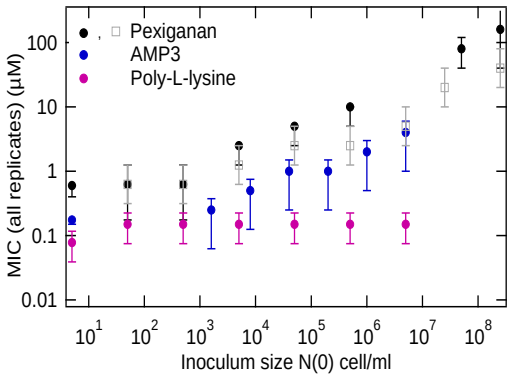

Figure 8.33 The inoculm effect of amhelin and poly-L-lysine. Data for pexiganan shown previously is plotted for comparison. The concentration at which no replicate wells grow (MIC (no replicates)) against inoculum size $N(0)$.

it is unlikely that cells drop to very low numbers during $N(t)$, despite detection times being increased over a wide range of concentrations. Potentially, either bacteriostatic effects play a larger role than for pexiganan, or the influence of the polymer on the net growth rate lasts for longer. In terms of the model constructed for pexiganan, a lower death rate b, and/or a lesser depletion of the polymer may cause net death to progress more slowly and for more time. These changes would also lead to a reduced IE in the range of inoculum sizes tested.

Despite these results leading to more questions than they answer, this section has illustrated how simple macroscopic MIC measurements can highlight differences between antimicrobial agents and focus on key areas of future population dynamics, single cell and mechanistic research.

Chapter 9

Discussion and Conclusion: Pexiganan action on growth

9.1 Discussion and comparison with the literature

Some discussion followed each of the sections presented on experimental results, but this chapter discusses to what extent the results presented have met the primary (investigation of the MIC) and secondary (live biological measurements of mechanism) aims of the study, in the context of the literature. Comments are then made on topics on which the study relied, but were not its focus, the experimental methods employed and suggestions for future studies.

9.1.1 MIC measurements with pexiganan

The importance of accurate, reproducible and understood antibiotic susceptibility tests, in particular MIC assays, was emphasised in the introduction. This study represents a first attempt to probe weaknesses of MIC measurements for antimicrobial peptides.

The bMIC (MIC at $N(0) \sim 5 \times 10^5$ cell/ml) determined in this study was comparable to those quoted in the literature for pexiganan and *E. coli* [189, 190]. This value is not the action threshold of pexiganan. In fact, there are sub-bMIC pexiganan concentrations at which the vast majority of cells from the initial inoculum become unviable. Frequently in the literature the bMIC is assumed to represent, in the words of Melo *et al.*, the 'macroscopically observable threshold for the onset of AMP

activity' [125]. An example of this assumption leading to the mis-interpretation of data can be seen in Pius *et al.* [198], where researchers see membrane disruption at pexiganan concentrations 100× below the bMIC, deemed insufficient for antimicrobial action. The work presented here demonstrates than the bMIC is roughly 10× above the macroscopically observable threshold of action. Therefore, Pius *et al.* observed membrane disruption at concentrations 10× below the threshold of action, rather than 100×. This is not a minor point: if the results of MIC assays are ever to be compared with mechanistic studies, understanding of what MIC assays mean is critical.

Not only has the value of the MIC been mis-interpreted at times, but there has been no previous mention of stochasticity playing a role in the determination of the MIC of pexiganan for *E. coli*. This study found that the MIC is not a well defined threshold, but a range of concentrations at which no growth could be observed if the test is only conducted once. For an inoculum level of a single cell this range is narrow ($\sim 0.3\mu$M), while at higher inoculum levels the range broadens ($\sim 10\mu$M at $N(0) = 10^7$ cell/ml). Ge *et al.* [189] tested 137 *E. coli* isolates and found a range of bMICs between 1 and 64μg/ml. It is unlikely that more than one replicate MIC assay was conducted for each strain, as the study tested 3109 bacterial strains in total. Stochasticity in the measurement can't account for all of the variation in bMIC measured between *E. coli* strains, but the 4× variation in bMIC measured here for a single strain accounts for part of it. If a comparison between strains is needed to more than a 4× accuracy, establishing a range of MICs by completing multiple replicates is more robust than comparing a single test.

Mirroring the findings of previous research into the weaknesses of the MIC for antibiotics [126], environmental factors are crucial to the measurement of a reproducible MIC for pexiganan. Diluting the growth medium and lowering the temperature could lengthen the division time of an *E. coli* sufficiently that regrowth does not reach the detection level in the time of incubation. Similarly, if the incubation time is shorter, regrowth which is occurring may not be noticed, leading to a greater deviation of the MIC from the MBC. Some researchers use incubation times as short as 4 hours to measure the MIC of antimicrobial peptides [191].

Our findings could influence the way in which the MIC of pexiganan is used as a marker for *e.g.* peptide stability and resistant bacteria. For example, Fluorogainin-1 an analogue of pexiganan, designed to be more stable, displays a lower bMIC against *S. aureus* [202]. In light of the findings presented we can postulate that this is because the peptide is not depleted as rapidly, reducing the gradient of its IE. *E. coli* are able to develop resistance to pexiganan [181]. The mechanism responsible may not be an

altering of surface properties, requiring more peptide to result in cellular death, but a more efficient inactivation of the peptide upon death, raising the value of the bMIC.

Inoculum effect: The IE has previously been attributed to active degradation of an antibiotic by pathogens [170]. This study has shown that it is also possible for passive degradation to lead to an IE, confirming the finding of [155]. Other non-mutually exclusive mechanisms of IE, such as decreases in *per cell* antibiotic concentration for higher inocula, SOS responses, quorum sensing and protease secretion, have not been ruled out. Indeed a comparison of single cell MICs between a multi-well plate and the MDA suggested adhesion of peptide to surfaces or cellular appendages may reduce the active concentration sufficiently for a *per cell* effect to be present. Incorporation of other causes to models may be necessary to achieve quantitative prediction of the measured magnitude.

The results collected represent the first quantification of the IE displayed by the MIC of pexiganan. The power law recorded at high inoculum sizes coincided within uncertainty to that seen for 5 out of the 6 antibiotics investigated by Udekwu *et al.* [155] (powers between 0.3 and 0.5). As the researchers found no depletion of the antibiotic for 3 of these 5 antibiotics, the reason all of the powers observed are so similar presents a fascinating opportunity for further research. To date, no explanation as to why powers below 1 are recorded has been proposed.

Knowledge of an IE and its mechanism are deemed crucial to successful treatment strategy [155, 168]. Udekwu *et al.* [155] model the IE of their antibiotics with a Hill function. In modelling pexiganan pharmacodynamics, a Hill function would not describe the IE measured, as the MIC does not plateau at the highest inocula studied.

Regardless of the mechanism responsible for the IE, the measurement of its magnitude is an important tool, not previously quoted. The plot provides an estimate of the minimum pexiganan concentration required to result in reproducible inhibition of an *E. coli* population of a known density.

An alternative measure of pexiganan efficacy: The antibiotic susceptibility measurement needed depends on the research or clinical need. Clinically, the concentration at which no net regrowth is seen in a given time period after pexiganan treatment (the MIC) remains a useful threshold. But in other cases the concentration at which normal growth is influenced is more relevant. Here I found that the detection times of sub-MIC growth curves can provide a measurement of the NIC, the 'non-inhibitory concentration' defined by Lambert *et al.* [163].

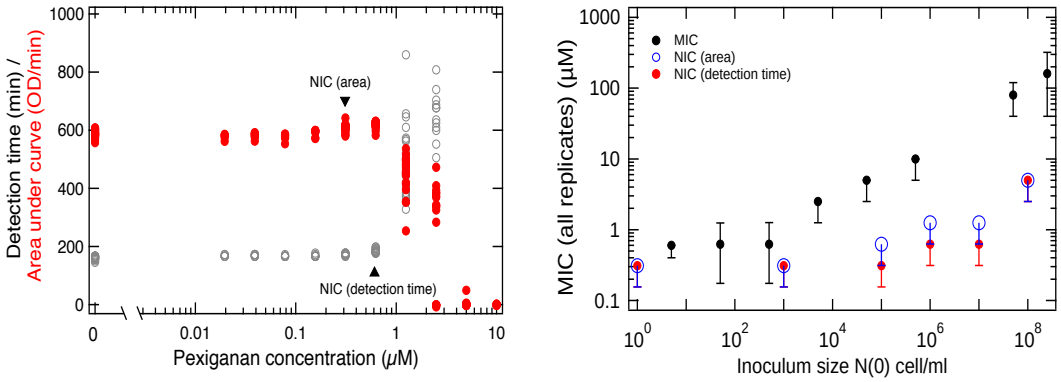

(a)

Figure 9.1 The NIC and its IE from detection times compared to those from measuring the area under the curve. (a) Detection times (black) and area under the growth curve (red) plotted for a pexiganan bMIC assay. Concentration interpreted as the NIC shown on plot. (b) A comparison of the IE seen in the measurement of the MIC, the NIC from the area under the growth curve and the NIC from detection times.

Figure 9.1(a) compares the area under the curve, used previously by Lambert *et al.* (see Figure 6.7(b)), and detection time inhibition profiles from a pexiganan bMIC assay. The advantage of judging the NIC from detection times is that they do not incorporate the noise in OD measurements at later times, when evaporation and condensation occur. Also the detection times at 0μM stay constant within uncertainty between plates and days, whereas the area under the curve fluctuates more. A loss of diauxic lag is seen as a slight increase in the area under the curve.

Figure 9.1(b) shows an IE plot of the MIC, the NIC determined with detection times, and the NIC determined with an area under the curve approach. Both NICs were determined visually as being the first concentration at which the measurement returned values different from the control. The detection times of inoculum sizes $N(0) = 1 - 10^5$ cell/well begin to deviate from those of the control at $\sim 0.3 - 0.6\mu$M pexiganan. This represents a peptide concentration at which a sufficient proportion of the inoculum dies to influence the subsequent growth curve. At inoculum levels higher than 10^5 cell/well, it requires more peptide to influence detection times. It is likely that, despite cell death occurring at $\sim 0.3 - 0.5\mu$M for every $N(0)$, too few cells die at high $N(0)$ to influence the growth curve. The plot emphasises the fact that the IE is a function of the measurement made and cannot be compared between antibiotics unless the same quantity is being measured.

Finally, the single cell MIC is not a quantity which is often determined. It could provide a useful comparative value between peptides.

9.1.2 Pexiganan mechanism of action

Pexiganan caused concentration dependent growth halt, leakage of the cytoplasm over time, bleb formation and lysis. Experimental observations on the mechanism of action of pexiganan are a valuable addition to the two previous mechanistic studies of pexiganan action on *E. coli*, both of which only made population measurements.

Strikingly, on the addition of pexiganan at a concentration sufficient for action, a clonal population of *E. coli* contained cells which underwent death, lysis or survival to continue growing normally. No theoretical study has predicted this level of difference in peptide action between live cells, it is a feature which requires explanation. Given the enormous number of peptides per bacterium in the system, the heterogeneity is not due to fluctuations in the number of peptides received by each cell. Heterogeneity must arise from phenotypic variation in a property or properties of single cells. The survivors were not a sub-population of non-dividing cells, and susceptibility to the peptide was un-related to cell length. AMPs are known to interact with the surface of *E. coli*, a complex charged environment the properties of which fluctuate with its surroundings. At a given time there is heterogeneity in the surface properties of single cells, *e.g.* in the structure of the LPS [243] or in the expression of fimbrae [244]. Surface appendages may change their conformation on the addition of charged molecules to the medium [245], potentially influencing the ease at which pexiganan reaches the lipid membrane.

This study supports the claim made by both publications on pexiganan action [192, 198], that it causes concentration dependent membrane disruption. But microscopy did not reveal why membrane disruption should be maximal at 5 min, claimed by Ramamoothy *et al.* [192]. The lysis rate observed slowed on roughy this timescale. It is possible that 5 min represented the first time point available to the researchers and membrane disruption thereafter decreased due to disintegration of the membrane.

Although there is a consensus that pexiganan's bactericidal action is through the formation of toroidal pores, the true pore forming capabilities of the majority of AMPs have been questioned [203, 204]. Some researchers believe that non-selective membrane disruption is a more likely mechanism of action in both in GUVs and in live bacteria. GUVs show stochastic bursting [246], and on occasions leakage of their contents over seconds to minutes [247]. These features are similar to those observed in *E. coli* with microscopy in this study. *E. coli* which stopped growing were never seen to recover, and eventually these cells all lost their cytoplasmic contents. Cell lysis appeared stochastic, with cells lysing from 1 min after peptide addition to much later times.

As it is unknown how the formation of pores over membrane disruption would influence microscopy on live bacteria, it is not possible to draw any firm conclusions on the mechanism of pexiganan. However, both microscopy and a comparison of CFU to OD suggested that viability is lost before observable cellular damage occurs and lysis takes place. Blebbing is frequently seen before lysis, suggesting that curvature strain leads to lysis rather than the formation of stable pores.

This study has begun the process of linking population measurements to single cell observations of pexiganan action. The next step in this process is to link single cell measurements to biophysical studies of mechanism. The single cell observations presented should provide a useful living cell reference in this process.

9.1.3 Comments on time-kill and growth curves

Density curves: Density curves (time-kill) showed partial killing of populations by pexiganan, concentration dependent and inoculum dependent features. The measurements represent a significant improvement on the only previous publication of time-kill curves for pexiganan [189], which only collected data for 120 min.

Survival was attributed to the growth rate balancing the death rate before complete eradication of the population. The literature has only recently suggested that fractional killing can be due to a dynamic state of balanced division and death rather than the historically assumed sub-population of non-dividing persister cells [233]. Wakamoto *et al.* [233] imaged a colony of *Mycobacterium smegmatis* in the drug isoniazid. Survival on addition of the drug was not correlated with single cell growth rates, but was found to be related to the stochastic pulses of an enzyme KatG. The definition of persistence and the fundamental features that are attributed to persisters are current areas under discussion [248].

Depletion of the peptide in time leads to regrowth. Regrowth in the time-kill curves of peptides [199, 207, 208] has been attributed to resistance, with little evidence, introduced as one of the perceived problems in the field of antimicrobial peptide research. This study has illustrated that depletion or inactivation of the peptide due to cell death is the cause of regrowth in suspensions containing pexiganan. Experiments conducted to verify this hypothesis were rapid and straightforward and should be performed as a check in all cases of regrowth.

Growth curves: The OD growth curves recorded from MIC assays were distinctive in the shape, with the lengthening detection time being the primary feature seen

on addition of pexiganan. Growth curves are not routinely shown in the literature, so comparative plots for other antibiotics are only available from research into the accuracy and reproducibility of the MIC measurement. Examples of antibiotics studied with *E. coli* include; cefotaxime which decreases the stationary level and growth rate systematically as its concentration increased, without affecting the detection time [164] (Figure 6.7(a)) and tetracycline, which increases the detection time and decreased the stationary level and growth rate [126] (Figure 6.8(a)). There is no common pattern to growth curves at sub-MIC concentrations of antibiotic, therefore there is no common meaning to the MIC measurement (*i.e.* it is not the same growth curve feature for each antibiotic which leads to no growth above the detection level in a given period of time), but it seems likely that other lytic peptides would return the same growth curve features as pexiganan.

There is no mention of variation between replicates in the growth curve examples quoted above. From this I infer that for many antibiotics it plays a more minor role than for the AMPs used in this study, where it was always an obvious feature. If other antibiotics do not cause a drop to low numbers of cells during the growth curve, then it is unlikely that stochastic effects play as large a role in the subsequent growth. Either this is the case, or researchers believe that variation seen is a function of experimental inconsistencies and therefore do not report it as a real and interesting feature.

In section 8.2.2 it was mentioned that the diauxic growth of *E. coli* in MHB, which shows a brief lag phase without peptide addition, did not display this lag in sub-MIC concentrations of pexiganan. Following the finding that many cells undergo lysis at these concentrations leads to the postulate that the medium has been supplemented by cell death. After peptide depletion, cells appear to thrive in the medium; they do not require time to adjust to a second metabolite and they reach a slightly higher stationary phase. These features were not seen for single cell inoculum levels, presumably because the total number of dead cells which have undergone lysis by the time the peptide is depleted is far below that for higher $N(0)$ and $P(0)$. The retention of the feature in all concentrations of poly-L-lysine implies that the overall number of cells undergoing lysis is low, despite the increase in detection time.

9.1.4 Comments on experimental methods

Following the collection of data for this study, there are observations to be made on the suitability of the methods employed.

Detection times: Detection times proved a useful tool for characterising the growth of *E. coli* in a well and studying the effects of pexiganan on single cells. In particular, they were crucial to visualising large numbers of growth curves and interpreting what they meant for the MIC measurement.

As a caution; plots of detection times published for preservatives sometimes display the same patterns as those presented in this study of a bactericidal agent, but are interpreted differently. As an example, the lengthening of *L. monocytogenes* detection times by 1.2MmM NaCl has been attributed to a density dependent population lag time and an 'unspecified medium conditioning effect' [143], rather than early-time loss of viability.

CFU: The CFU density curves collected were not a straightforward measurement to conduct. Partly this was due to the laborious nature of the procedure and partly it was due to the difficultly of precise density prediction due to the variation between replicates seen. I believe data collection would have been helped significantly by using a drop-plate method rather than a spread plating method. Drop plating is able to count every dilution in the series, by pipetting 10μl of suspension onto a section of an agar plate in triplicate. The protocol would reduce the counts at the optimum dilution, increasing the uncertainty in the density calculated, but this disadvantage is outweighed by increased likelihood of successful data collection. An alternative approach would be to use live-dead staining of cells in a flow cytometer for these viability curves.

Millifluidic droplet analyser: MIC assays in the MDA confirmed features already seen in multi-well plates, proving that they were not specific to the well environment. In some cases better statistics were obtained. However, use of the apparatus was significantly more complex than a multi-well plate, and the growth curves collected contained large amounts of apparatus noise, in some cases preventing further analysis. An explanation for change in single cell MIC with the volume of the incubating fluid remains a question for further research.

9.1.5 Clinical implications

When pexiganan is added to a population of *E. coli*, unless all of the bacteria are killed before the growth rate balances the death rate, they will eventually regrow completely un-inhibited. Total eradication of the population, before peptide depletion, is necessary to result in any improvement of population size from a clinical point of view. This being said, at some sub-MIC concentrations the peptide is able to transiently reduce

numbers. In application, this may be sufficient for either the immune system or a second antibiotic, acting synergistically, to eradicate the remaining cells. Another consideration is that pexiganan may not be an appropriate treatment for very high density bacterial infections. Its MIC at a density of 10^8 cells/ml is roughly that of the concentration required for 100% heomolysis (100μM) [184].

Pexiganan is not an orally taken agent, such were discussed in publications which simulate pharmacodynamic treatments, but would be incorporated into a topically applied cream. There is potential for the dosing procedure of an externally applied agent, where the antibiotic is delivered directly to the site of infection, to differ to oral delivery [249]. Therefore, there is room for a study into how an IE, such as is seen with pexiganan would influence a topical treatment program. During the clinical trial patients were instructed to apply cream twice daily [187, 188]. This was not adjusted according to the severity of the infection. Clearly the $>$ 100 times increase in MIC with changing inoculum level must be taken into consideration in the design of any future treatment protocol with pexiganan.

Finally, dynamic persistence was observed. Continued division in a concentration of drug high enough to kill some of the cells promotes the likelihood of genetic mutations which confer genetic resistance.

9.1.6 Future work

There are two future experimental studies which have been mentioned repeatedly throughout. Yet again, the most pressing experiment is to construct a single cell microscopy technique which probes any bacteriostatic action of pexiganan. Secondly, the cause of the peptide depletion presents another important avenue of exploration. An experimental investigation could begin by adding protease inhibitors to assays and/or monitoring whether the use of stationary phase cells, which package anionic DNA differently to those growing exponentially, influences results.

Previously, daptomycin and vancomycin, both of which target the cell membrane, have shown a similar depletion in suspensions of *S. aureus* [155]. Any links between the mechanism of action of an agent and its depletion could be explored by a large scale screening of antibiotic compounds to decipher which exhibit this effect. Depending on the mechanism of peptide depletion, it is possible that by adding another compound to the medium *e.g.* a protease inhibitor, the MIC of pexiganan could be lowered.

Although the peptide depletion assays used showed depletion/inactivation, they were

not extended to probe the timescale on which this occurred. It is possible that ultraviolet absorbance at 205nm could return the concentration of peptide in the medium with time, although this is not a straightforward experiment to conduct and may require a large amount of peptide. Changes in peptide concentration with time would allow comparison with modelled $P(t)$.

Further work on the modelling of the system is needed. Instead of simulating the deterministic model proposed numerically it could be solved analytically. Fitting of the solutions to the experimental time-kill curves could return a functional form for the concentration dependent death rate, assumed to be linear previously only for simplicity. Whether the experimental data collected is sufficient for the fitting of a model remains to be seen.

Ideally, any model to describe the system would be stochastic as this was such a prominent feature in experimental results. The most straightforward approach would be to model both the growth and death of cell as stochastic chemical reactions. However, bacterial growth is more complex than a stochastic chemical reaction with levels of noise which may be better represented by other approaches, such as the stochastic model of growth developed by Baranyi [136]. Simulations could be extended to include a peptide binding rate and subsequent death rate and a rate of lysis after death (this would allow comparison with OD time-kill data as well as CFU).

A plethora of less closely related possible investigations have been suggested by this study. For example, the appearance, dynamics and lysis of AMP induced membrane blebs and bulges could provide an interesting area of research. Also, a quantification of the OD drop due to lysis for pexiganan or AMPs in general is needed.

9.2 Conclusion

In summary, the MIC of pexiganan is not the threshold of its action, but can be > 100 times above this concentration due to a substantial inoculum effect above 10^3 cells/ml, described by a power law, power $0.3 - 0.5$. The IE displayed is a consequence of peptide depletion or inactivation during the death of cells. The cells do not display a lag on peptide depletion, but immediately resume growth at their maximum specific growth rate for those conditions. When cell numbers drop to low levels, stochasticity plays a role in the population dynamics and therefore the MIC determination. Detection times could be used for an estimation of an alternative threshold of pexiganan action.

Research into the pharmacodynamics of antimicrobial peptides is not as advanced as for some other classes of antibiotics. The study presented has contributed to the field by inspecting the growth and death of *E. coli* in pexiganan. Pharmacodynamics are often described by a single value, the MIC. This work found that, for pexiganan and *E. coli* the meaning of this threshold is: a concentration at or above that required for bactericidal action on cells which provides a sufficient *amount* of peptide to achieve population eradication before depletion, preventing regrowth.

Chapter 10

Motility in the presence of pexiganan

10.1 Background

One of the earliest antibiotic susceptibility signs recorded was loss of microorganism motility in the presence of a drug [150]. Understandably, since then, growth has been the primary marker of antibiotic action, as not all pathogens are motile. The final results chapter of this thesis applies the motility techniques studied in Part 1 to the antimicrobial peptide suspensions of Part 2. The aim was to investigate whether DDM measurements could return population information on peptide activity. In comparison with the other studies presented in this thesis, results and interpretation are preliminary.

Swimming and swarming behaviours are of relevance to the study of biofilm formation, thus there are previous reports of motility in the presence of a drug from this literature. The majority of the research quotes the diameter of swimming or swarm fronts, on agar plates containing the drug (typically LB 0.3% agar). Comparison with control plates results in a semi-quantitative test. In this manner it was shown that colisitin [250] and ciprofloxacin [251] reduced the motility of *Pseudomonas aeruginosa*, while tetracycline had no effect and tobramycin induced motility. Ampicillin and tetracycline have been seen to slow *E. coli* [252] as have linear cationic octameric and hexameric peptides [253]. Microscopy has been used to observe that magainins reduce the swimming speed of hamster *Spermatozoa* but the motility of protozoa was preserved even whilst they were swelling and bursting [185].

Quantitative temporal changes in the motility of *E. coli* on the addition of antibiotics have been little researched, but could be useful in two ways. Firstly, motility assays could represent an alternative antibiotic susceptibility test to the commonly used methods. It is probable that the information provided by the assay would vary greatly between antimicrobial compounds, but in some cases could be a useful addition to the information already routinely collected. CFU time-kill curves are labour intensive, prone to mistakes, return poor statistics and require 24 hours to incubate before results are available. OD measurements of net-death only show cells which have undergone lysis. DDM can provide a fast, high-throughput, bulk measurement of the proportion of motile cells α in a dilute suspension of bacteria. This chapter reports a preliminary study into whether measuring α after the addition of the antimicrobial peptide pexiganan can reproduce the concentration and density dependent features of the CFU time-kill curves.

Secondly, changes of swimming behaviour on the addition of a drug may also provide clues towards its mechanism of action. To this end, measurements of v are presented. Changes in the average swimming speed are likely related to the average change in proton motive force (PMF) across its the bacterial membrane (see section 2.2), assuming a constant geometry of flagella bundle [254] and no structural changes due to cyclic di-GMP [33, 34]. Antimicrobial peptides have been reported to depolarise membranes by collapsing the membrane potential [207, 208] and lowering the ΔpH across the membrane [255], both of which dissipate the PMF [255]. The precise physical mechanism by which the PMF is dissipated remains a topic of research, either it is actively dissipated or its generation is hampered. Magainin2 is thought to decrease the transmembrane proton gradient by the formation of transient pores which allow the release of protons [256, 257]. Currently, it is unknown whether changes in PMF can be observed by the slowing of swimming cells.

10.2 Methods

Ideally, cells would have been cultured and measured in MHB at 37°C to allow direct comparison with the results of Chapter 8. However, as anticipated from DDM results for growth in LB, presented in section 5.4.1, *E. coli* display limited motility in MHB at 37°C. On removal of *E. coli* in MHB from a 37°C incubator to room temperature, motility is recovered with time (Figure 10.1 (red)). If cells are grown into TB, but then transferred into MHB to conserve the medium of measurement, v drops at a rate of $\sim 4\mu$m/s per 100 min in MHB (Figure 10.1 (green)). Neither of these situations

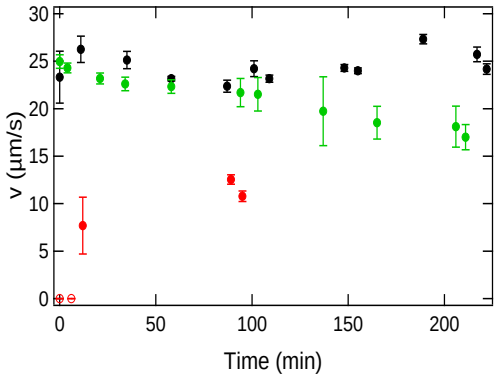

Figure 10.1 The average swimming speed of *E. coli* grown and measured in conditions relevant for the study of antimicrobial peptides. Grown in MHB at 37°C and diluted into MHB at room temperature at $t = 0$ min (red), grown in TB at 30°C and diluted into MHB at room temperature at $t = 0$ min (green), and grown in TB at 30°C and diluted into TB at room temperature at $t = 0$ min (black). Time points plotted with empty symbols at $v = 0$ represent samples for which the motility model would not fit the DDM data collected.

represent a stable control to investigate the effects of antimicrobial peptides. Therefore experiments were conducted with a culture grown under the standard protocol and measured in TB, a growth medium in which motility with time is further understood and characterised.

It is unknown how changing the medium and temperature of samples influences the action of the peptide in comparison to results shown in MHB at 37°C in Chapter 8. However, MIC assays at 20°C in TB returned the same MIC within uncertainty.

Protocol: An overnight culture of MG1655 in LB was diluted 100× into TB and incubated for 4 hours at 30°C and 200rpm. The culture was removed at OD∼0.5 and diluted to the required density with fresh TB. Densities are quoted as ODs in this chapter, calibrated to CFU by $N = 1.5 \times 10^9$ cell/ml at OD=1.

Prepared cells were divided into two tubes and the antimicrobial peptide added to one. A capillary was loaded with sample immediately after the addition of the peptide to provide the first data point at $t \sim 1$ min. All following measurements were made after gently turning the tube to ensure oxygenation and filling a new capillary. Capillaries were loaded as efficiently as practical, keeping the time before recording a constant. Adjustments to protocols in response to issues raised in Chapter 5 were adhered to.

Movies were recorded at ×10 magnification and analysed using DDM, as previously described in section 3.3.2. Dark field movies were recorded for ~ 8 seconds immediately after the phase contrast movies, following the procedure described in section 3.4.2.

Analysis: The average swimming speed v and the motile fraction α were extracted from the analysis following procedures described previously (section 3.3.2).

10.3 Motile fraction in pexiganan

To reproduce features of pexiganan time-kill curves by measuring α requires two assumptions to hold; that non-viable cells stop swimming (reasonable) and that pexiganan does not prevent cells which remain viable from swimming. Unfortunately, an experiment to compare α to CFU data for the same pexiganan sample was not conducted. However, the two measurements were compared for a sample of *E. coli* in BMB with amhelin added, and they corresponded closely (not shown). Quantitative agreement could be achieved by incorporating OD measurements, believed to correct the DDM data for changes in density due to lysis. These results indicate that both assumptions are valid for amhelin, which is believed to have a similar mechanism of action to pexiganan [242].

The concentration and density ranges available for exploration are limited both by the experimental setup and DDM analysis. $N(0)$ is required to be between 0.15×10^9 (OD=0.1) and 0.75×10^9 (OD=0.5) cells/ml to ensure enough bacteria in the field of view whilst maintaining a low enough oxygen consumption rate to allow a motility measurement before oxygen depletion. $P(0)$ is limited to concentrations which maintain α >20%, as below this, changes in α cannot be monitored.

The fraction of motile bacteria α is plotted with time after peptide addition for two concentrations of pexiganan in Figure 10.2(a). Both samples began at OD=0.3 ($N(0) = 4.5 \times 10^8$ cell/ml). At both 2.5μM and 5μM α drops immediately after peptide is added to the sample and continues to drop for the next $\sim$ 40 min. At later times α rises again, but the next day is still lower than that of the control. The rate and extent of α decrease is concentration dependent; 5μM causes more bacteria to stop swimming than 2.5μM, while no bacteria swam at short times after 10μM was added. When the density of the bacterial suspension is increased to OD=0.5 ($N(0) = 7.5 \times 10^8$ cell/ml), α drops to 0.6 rather than 0.25 at $t = 40$ min after the addition of 5μM (Figure 10.2(b)).

Although measuring α with DDM yields the same concentration and density dependence as seen in $N(t)_{CFU}$ at a similar $N(0)$ (Figure 8.10(b)), the shapes of the curves differ. Potential explanations for the short-time disagreements are that CFU data at 5μM is sparse compared to the motility data, potentially missing features, and that variation is known to be present. Discrepancies at longer times are likely to be due

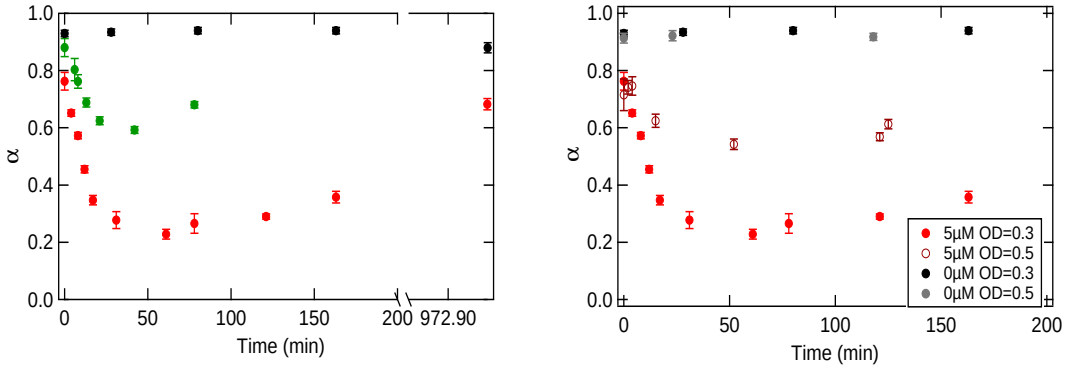

(a) **(b)**

Figure 10.2 Fraction of motile *E. coli* with time at room temperature in TB with pexiganan added at $t = 0$ min. (a) OD=0.3 containing 5μM pexiganan (red) and 2.5μM pexiganan (green). (b) ODs and pexiganan concentrations shown in the legend.

to the fact that α was measured in different conditions to CFU. The slower growth rate of *E. coli* in TB results in it taking far longer for regrowth to become noticeable. Morevover, the following day, α is no longer expected to directly correspond to the proportion of viable cells as the medium has been supplemented by cell death, affecting motility behaviour. Also, at times this long motility in the control has reduced.

The only inexplicable feature is the fact that CFU display a much larger drop at $t = 2$min compared to motility measurements. This implies the peptide acts faster in MHB at 37°C than in TB at room temperature. Alternatively, cells may lose the ability to divide in the future sooner than they stop swimming *i.e.* they may succumb to the peptide after being spread onto the plate. Following the observation of cells on agar after peptide exposure (section 8.5.2), this explanation is plausible. Whether this disagreement is a function of the method or the conditions is impossible to know without comparing CFU, OD and motility measurements simultaneously under these conditions, clearly a priority for future experiments.

In conclusion, motility measurements in pexiganan provide an efficient means of displaying the concentration dependence, density dependence and regrowth displayed by CFU and OD time-kill curves, within the same peptide concentration range. They are able to monitor differences between relatively small changes in inoculum size ($N(0) = 4.5 \times 10^8$ *vs* 7.5×10^8 cell/ml), which would be overridden by uncertainty in CFU where comparison is typically between orders of magnitude. The advantage of motility measurements over CFU is that they return results much faster given an adequately fast computer, as there is no need to wait 24 hours for colonies to form before analysing the data. However, there are limitations to the quantitative applicability of

the method, depending on the environmental conditions of interest.

10.4 Swimming speed in pexiganan

Alongside providing measurements of α, DDM analysis yielded measurements of the average speed v of a population of *E. coli* in pexiganan. These results are unrelated to the growth and death of *E. coli* in pexiganan and are a measurement of the survivors only. Figure 10.3 shows v data corresponding to the α measurements in Figure 10.2.

While the motile fraction in the sample decreases at short times after peptide addition, v also drops. The drop in v is peptide concentration dependent, but not density dependent. The average speed is at its lowest value ~ 10 min after peptide addition and then recovers over the next $50 - 60$ min to almost the level of the control. After recovery, at approximately the same time as regrowth begins, v begins to drop once again at a rate of 4μm/s per 100 min. It is postulated that this slowing is due to the increased level of nutrients in the media, supplemented by the death and lysis of non-surviving cells. Comparison with Figure 10.1 shows the same slowing rate within uncertainty as when cells are placed in MHB from TB.

Dark field microscopy, measuring the cell body rotation rate Ω, was used to provide information on the changing width of the swimming speed distribution. Results for Ω peak position showed the same drop and recovery as seen in v (not shown). The width of the distribution doubles on peptide addition and then drops over the following $50-60$ min until it reaches the level of the control (Figure 10.3(b)). Quantitative interpretation of results is reliant on the assumption that the Ω distribution measured is representative of the v distribution, which would require more work to justify. However, it is likely that trends in width are related.

The results presented suggest that PMF across the *E. coli* membrane is reduced and then recovers. The extent to which the PMF is disrupted is highly heterogeneous between surviving cells; the v distribution widens. Spindler *et al.* measured membrane depolarisation in *E. coli* 5 min after the addition of sub-lethal Bac8 concentrations, but natural defence systems were able to recover normal PMF in 90 min [208]. An increased population heterogeneity under stress is often seen in bacterial studies, for example on the addition of Poly-L-lysine to *E. coli* [258].

In this study of pexiganan, these are the only measurements of surviving cells to have indicated that they are influenced by the peptide. As discussed at length already, none

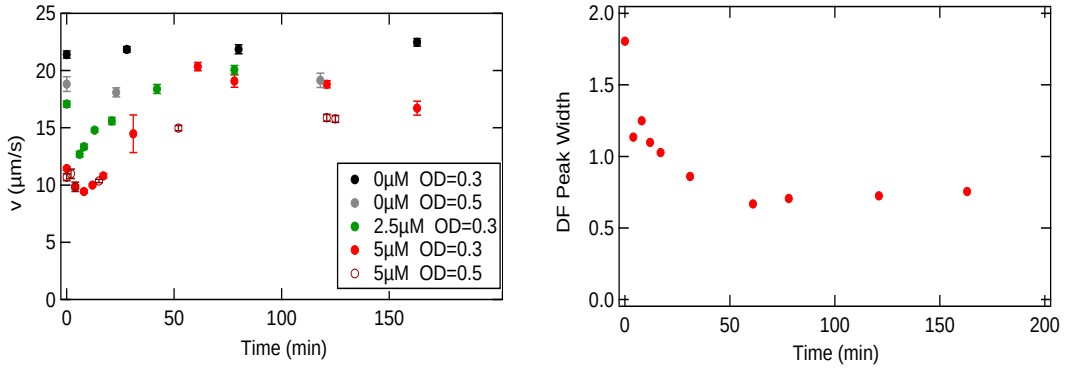

(a) (b)

Figure 10.3 The average swimming speed of *E. coli* with time in TB with pexiganan added at $t = 0$ min. (a) v measured with DDM for the $N(0)$ and $P(0)$ shown in the legend. (b) Width of the Ω distribution, measured with dark field microscopy and fitted with a Log-normal function.

of the single cell measurements showed any slowing of growth in survivors, however no experimental situation tested a constant peptide concentration. The PMF is crucial in ensuring the localisation of proteins required for cell division. Any dissipation of PMF is expected to impact on growth [259]. Therefore, the results shown in this section reinforce the need for an experiment which tackles this question directly.

Finally, it is possible that, instead of disruption to the PMF, the reduction in v indicates a changing morphology of the flagella bundle. A flagellum straining technique being developed in the department would allow this possibility to be checked.

10.5 Aggregation

The motility experiments presented in this chapter represent the only microscopy of bacteria in bulk media in the presence of peptides undertaken. A feature seen frequently and reproducibly with pexiganan was the aggregation of cells on the addition of the peptide. This feature was not the subject of any systematic investigation, but should be in the future, thus the observation is included.

Aggregates formed within the first minute of peptide addition (the time required for imaging), but then disappeared over time. It is not known whether their disappearance was due to the aggregates dispersing or their constituent cells lysing. For the conditions reported above, aggregation was not sufficient to disrupt data collection, but at 5μM in BMB, aggregates were visible and took $\sim$ 8 min to disperse (Figure 10.4(a)). If higher concentrations of peptide were added, aggregates were larger and took longer to

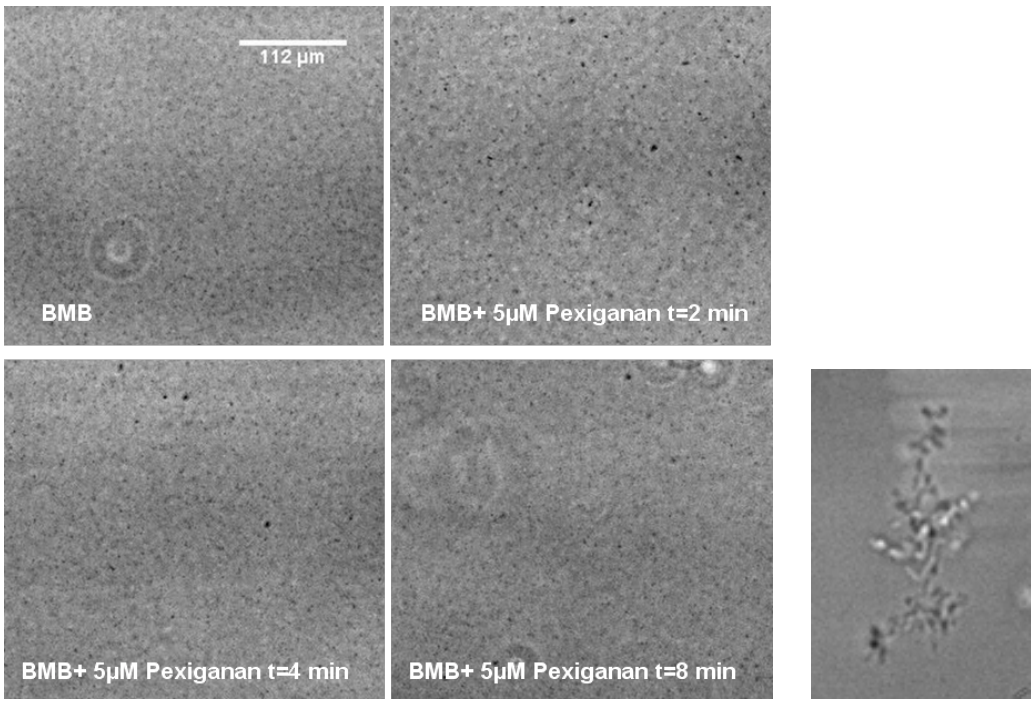

(a) **(b)**

Figure 10.4 *E. coli* aggregation on the addition of an antimicrobial peptide. (a) Phase contrast microscopy at 10× magnification, of *E. coli* at OD=0.3 in BMB. Pexiganan was added at $t = 0$ min. The time at which the image was recorded is noted on the image. Aggregation can be seen at $t = 2$ min, but has disappeared by $t = 8$ min. (b) Phase contrast microscopy at 100× magnification of an *E. coli* aggregate in MHB, formed 2 min after amhelin was added at 100μM and the capillary filled.

disperse. For example, at 100μM amhelin, cells remained in enormous aggregates for 16 hours (Figure 10.4(b)). It is unknown whether these aggregated cells remained viable, but un-aggregated single cells in the sample at this time were motile. Aggregation was observed in BMB, TB and MHB.

Physical mechanisms cause the aggregation of cells, for example the depletion mechanism on the addition of non-adsorbing polymers, and the bridging mechanism on addition of adsorbing polymers. Without further experimental work, speculation on the mechanism acting here is dangerous, although peptides are assumed to be strongly adsorbent. Reports and studies of aggregation due to AMPs are sparse, but Moiset *et al.* [241] noticed that when they added an active peptide (BPC194) to their suspension, *E. coli* aggregated. On addition of an inactive peptide with the same charge (BPC193) no aggregation was seen. The researchers ran MD simulations to show that multiple peptides inserted into bacterial membranes could lead to bridges between adjacent cells formed by multiple peptides and disrupted lipids. They believe pore formation and membrane bridging happen simultaneously.

Aggregation leads to rapid sedimentation. The presence of a surface may protect some cells by allowing biofilms to form. Once the peptide is depleted it only requires a single viable cell to repopulate the environment. Berditsch and co-workers [256] inspected wells at MIC/2 concentrations of antimicrobial peptide (magainin2, PGLa, MAP) and found small adherent colonies. They believe these colonies represent surviving cells with a different phenotype, persistent or biofilm forming, induced by membrane depolarisation.

Wimley perceived that one of the problems of the AMP field of study was the infrequent reports of vesicle aggregation on the addition of peptide [204]. This comment should be extended to living bacterial cells; from the limited microscopy conducted here, it seems likely that this effect is frequently seen, but not reported.

10.6 Conclusion

Future work should repeat these experiments with other peptides. Initial results have indicated a slowing of v at concentrations proportional to the MIC of that peptide. This suggests v slows due to peptide action rather than simply a physical or chemical (charge or pH) consequence of an abundance of peptide in the solution surrounding the cell. Indeed, no reduction in v has been seen without a corresponding decrease in α. Likewise, aggregation has been observed for other peptides at concentrations proportional to the MIC of the peptide.

To summarise, motility measurements can be used to measure concentration and density dependent features of time-kill curves for the antimicrobial peptide pexiganan. The swimming speed of *E. coli* is reduced by the addition of peptide, but recovers. Cells in bulk medium demonstrate concentration and time dependent aggregation on the addition of sufficient cationic peptide.

In conclusion, although growth in the presence of antimicrobial peptides is heavily researched, motility is not. Motility measurements prove a useful complement to traditional biological tests of antimicrobial peptide activity and provide hints towards their mechanism.

Chapter 11

Concluding remarks

11.1 Outlook

In this thesis future experiments were proposed as each study was discussed in turn. This section reiterates some of the more immediate experiments which could result from the work presented, and comments on the broad outlook for these areas of research.

Following the development of DDM for motile *E. coli* [13, 79], it was believed that the technique would provide a powerful research tool. Chapters 4, 5 and 10 confirm this belief by reporting applications of the technique in *E. coli* motility research and the quantification of active suspensions. These in turn invite further DDM experiments in a continuation of these studies.

In particular, the method of monitoring added fluorescent tracers in motile suspensions with DDM (Chapter 3) could be applied to an experimental investigation of whether a suspension of smooth swimmers reduce the enhanced diffusion seen in 3D, as predicted theoretically [40]. Also, the method could be used to investigate the motion of tracers in a suspension containing higher concentrations of active swimmers, displaying collective motion.

To maximise the utility of motile *E. coli* in the research of active suspensions, further work on its swimming behaviour under different preparative conditions is needed. Chapter 5 used DDM to begin this work and there are a plethora of closely related DDM investigations which could follow. Although swimming in a motility buffer is well characterised, motility in other conditions has been studied less. Most pressing is an experiment to follow the motility of *E. coli* throughout the growth curve in different

growth media. With further understanding of motility in different conditions, DDM can be used to provide information on little explored research areas, such as AMP action on motility. This was demonstrated in Chapter 10. Further work in the area of motility in AMPs would directly compare DDM measurements with other techniques and test other peptides.

In the longer term, to incorporate tumbling into the modelled ISF (recent theoretical work on tumbling [260] requires experimental verification) to allow reporting of a tumbling rate alongside v would be an exciting development in this field. Broadly speaking, further understanding of *E. coli* motility and its influence on their environment addresses evolutionary and ecological questions. For example, although it is believed that bacteria evolved motility to perform chemotaxis, the reason this is necessary in their native environment of the human gut is less clear.

Every part of the study reported in Chapter 8 could be developed into an interesting research project, by extending pexiganan measurements or incorporating measurements with other peptides. However, in consideration of swimming speed measurements presented, the priorities are to modify the tunnel chamber to allow continuous flow of medium and to improve tunnel chamber data collection. Of clinical relevance, the characterisation of the IE should be extended to other peptides and antibiotics to probe how general the effect is, and to aid understanding of its cause. It is possible that a project researching cell aggregation on addition of peptide would contribute to understanding of the IE, and be interesting in its own right. In the longer term, other researchers working in the area of antimicrobial peptides will want to know why the peptide is deactivated or depleted. There have been investigations with similar aims [179, 180], but which do not answer precisely this question for a simple MIC assay.

A common theme throughout the thesis was the significant variation between cells within a genotypically homogenous population. Awareness of phenotypic heterogeneity was necessary to interpret results in all of the studies presented. Additionally, suggestions for future experiments include investigations of sub-populations in both parts of the thesis *e.g.* the non-swimmers in a motile population, and the survivors in a suspension containing pexiganan. Phenotypic heterogeneity has emerged as a central theme of interdisciplinary work on bacteria, and from the evidence of these studies, an increased understanding of the effect would benefit many areas of bacterial research.

11.2 Conclusion

This thesis reports an experimental investigation into *E. coli* motility and how it influences its environment, as well as an investigation into *E. coli* growth and how it is influenced by an environment containing antimicrobial peptides.

The primary conclusion to the first part of the thesis was that in dilute 3D suspensions the enhanced diffusion of passive bacteria due to active motility scales with activity flux as was found in 2D, but is almost 2 times smaller in magnitude. DDM provides an effective technique for quantifying the suspension activity and for monitoring how the growth, preparation and measurement of *E. coli* can influence its motility. These findings contribute to the field of active suspensions and their physical properties.

The second part of the thesis concluded that the minimum inhibitory concentration of pexiganan does not represent its threshold of action against growing *E. coli*, but, due to peptide depletion, can be up to two orders of magnitude higher than this, depending on the inoculum size. DDM of *E. coli* motility in antimicrobial peptides can provide a measure of antibiotic efficacy as well as hints towards their mechanism. Antimicrobial peptides have potential as future therapeutic agents, but their pharmacodynamics, including an understanding of their MIC, requires further research, an area this study has contributed to.

E. coli suspensions are a well-studied experimental system. Nonetheless, an interdisciplinary approach to population measurements of the system continue to contribute towards both physical and microbiological research on bacteria.

Bibliography

[1] Jepson, A, Martinez, V. A, Linek, J. S, Morozov, A, & Poon, W. C. K. (2013) Enhanced diffusion of nonswimmers in a three-dimensional bath of motile bacteria. *Physical Review E* **88**, 041002+.

[2] Einstein, A. (1905) The motion of elements suspended in static liquids as claimed in the molecular kinetic theory of heat. *Annalen der Physik* **17**, 549–560.

[3] Balescu, R. (1975) *Equilibrium and Non-equilibrium Statistical Mechanics.* (Wiley).

[4] Palacci, J, Cottin-Bizonne, C, Ybert, C, & Bocquet, L. (2010) Sedimentation and Effective Temperature of Active Colloidal Suspensions. *Physical Review Letters* **105**, 088304+.

[5] Ramaswamy, S. (2010) The Mechanics and Statistics of Active Matter. *Annual Review of Condensed Matter Physics* **1**, 323–345.

[6] Valeriani, C, Li, M, Novosel, J, Arlt, J, & Marenduzzo, D. (2011) Colloids in a bacterial bath: simulations and experiments. *Soft Matter* **7**, 5228–5238.

[7] Gaspard, P. (2007) Time Asymmetry in Nonequilibrium Statistical Mechanics. *Advances in Chemical Physics* **135**, 83–133.

[8] Wu, X. L & Libchaber, A. (2000) Particle Diffusion in a Quasi-Two-Dimensional Bacterial Bath. *Physical Review Letters* **84**, 3017–3020.

[9] Underhill, P. T, Hernandez Ortiz, J. P, & Graham, M. D. (2008) Diffusion and Spatial Correlations in Suspensions of Swimming Particles. *Physical Review Letters* **100**, 248101+.

[10] Kim, M. J & Breuer, K. S. (2004) Enhanced diffusion due to motile bacteria. *Physics of Fluids* **16**, L78–L81.

[11] Leptos, K. C, Guasto, J. S, Gollub, J. P, Pesci, A. I, & Goldstein, R. E. (2009) Dynamics of Enhanced Tracer Diffusion in Suspensions of Swimming Eukaryotic Microorganisms. *Physical Review Letters* **103**, 198103+.

[12] Chen, D. T. N, Lau, A. W. C, Hough, L. A, Islam, M. F, Goulian, M, Lubensky, T. C, & Yodh, A. G. (2007) Fluctuations and Rheology in Active Bacterial Suspensions. *Physical Review Letters* **99**, 148302+.

[13] Wilson, L. G, Martinez, V. A, Linek, J. S, Tailleur, J, Bryant, G, Pusey, P. N, & Poon, W. C. K. (2011) Differential Dynamic Microscopy of Bacterial Motility. *Physical Review Letters* **106**, 018101+.

[14] Poon, W. C. K. (2013) in *Physics of Complex Colloids*, eds. Bechinger, C, Sciortino, F, & Ziherl, P. (IOS Press), pp. 317–386.

[15] Berg, H. C. (2004) *E. coli in Motion*. (Springer Science & Business Media).

[16] Ford, B. J. (1991) *The Leeuwenhoek legacy*. (Biopress).

[17] Marwan, W, Alam, M, & Oesterhelt, D. (1991) Rotation and switching of the flagellar motor assembly in Halobacterium halobium. *Journal of bacteriology* **173**, 1971–7.

[18] Fenchel, T & Thar, R. (2004) 'Candidatus Ovobacter propellens': a large conspicuous prokaryote with an unusual motility behaviour. *FEMS microbiology ecology* **48**, 231–8.

[19] Mitchell, J. G & Kogure, K. (2006) Bacterial motility: links to the environment and a driving force for microbial physics. *FEMS Microbiology Ecology* **55**, 3–16.

[20] Purcell, E. M. (1977) Life at low Reynolds number. *American Journal of Physics* **45**, 3–11.

[21] Nelson, P. (2003) *Biological Physics: Energy, Information, Life*. (W. H. Freeman), 1st edition.

[22] Purcell, E. M. (1997) The efficiency of propulsion by a rotating flagellum. *Proceedings of the National Academy of Sciences of the United States of America* **94**, 11307–11311.

[23] Polin, M, Tuval, I, Drescher, K, Gollub, J. P, & Goldstein, R. E. (2009) Chlamydomonas Swims with Two Gears in a Eukaryotic Version of Run-and-Tumble Locomotion. *Science* **325**, 487–490.

[24] Gaffney, E. A, Gadêlha, H, Smith, D. J, Blake, J. R, & Brown, J. C. K. (2011) Mammalian Sperm Motility: Observation and Theory. *Annual Review of Fluid Mechanics* **43**, 501–528.

[25] Berg, H. C & Anderson, R. A. (1973) Bacteria Swim by Rotating their Flagellar Filaments. *Nature* **245**, 380–382.

[26] Silverman, M & Simon, M. (1974) Flagellar rotation and the mechanism of bacterial motility. *Nature* **249**, 73–74.

[27] Eisenbach, M. (2001) in *Nature Encyclopedia of Life Sciences*. (London: Nature Publishing group).

[28] Sowa, Y & Berry, R. M. (2008) Bacterial flagellar motor. *Quarterly Reviews of Biophysics* **41**, 103–132.

[29] Lo, C.-J, Sowa, Y, Pilizota, T, & Berry, R. M. (2013) Mechanism and kinetics of a sodium-driven bacterial flagellar motor. *Proceedings of the National Academy of Sciences* **110**, E2544–E2551.

[30] Thomas, D. R, Morgan, D. G, & DeRosier, D. J. (1999) Rotational symmetry of the C ring and a mechanism for the flagellar rotary motor. *Proceedings of the National Academy of Sciences of the United States of America* **96**, 10134–10139.

[31] Chattopadhyay, S, Moldovan, R, Yeung, C, & Wu, X. L. (2006) Swimming efficiency of bacterium Escherichia coli. *Proceedings of the National Academy of Sciences* **103**, 13712–13717.

[32] Gabel, C. V & Berg, H. C. (2003) The speed of the flagellar rotary motor of Escherichia coli varies linearly with protonmotive force. *Proceedings of the National Academy of Sciences* **100**, 8748–8751.

[33] Paul, K, Nieto, V, Carlquist, W. C, Blair, D. F, & Harshey, R. M. (2010) The c-di-GMP binding protein YcgR controls flagellar motor direction and speed to affect chemotaxis by a 'backstop brake' mechanism. *Molecular cell* **38**, 128–39.

[34] Boehm, A, Kaiser, M, Li, H, Spangler, C, Kasper, C. A, Ackermann, M, Kaever, V, Sourjik, V, Roth, V, & Jenal, U. (2010) Second messenger-mediated adjustment of bacterial swimming velocity. *Cell* **141**, 107–16.

[35] Macnab, R. M & Aizawa, S. I. (1984) Bacterial Motility and the Bacterial Flagellar Motor. *Annual Review of Biophysics and Bioengineering* **13**, 51–83.

[36] Turner, L, Ryu, W. S, & Berg, H. C. (2000) Real-Time Imaging of Fluorescent Flagellar Filaments. *Journal of Bacteriology* **182**, 2793–2801.

[37] Darnton, N. C, Turner, L, Rojevsky, S, & Berg, H. C. (2007) On torque and tumbling in swimming Escherichia coli. *Journal of Bacteriology* **189**, 1756–1764.

[38] Berg, H. C & Brown, D. A. (1972) Chemotaxis in Escherichia coli analysed by Three-dimensional Tracking. *Nature* **239**, 500–504.

[39] Wei, Y, Wang, X, Liu, J, Nememan, I, Singh, A. H, Weiss, H, & Levin, B. R. (2011) The population dynamics of bacteria in physically structured habitats and the adaptive virtue of random motility. *Proceedings of the National Academy of Sciences of the United States of America* **108**, 4047–52.

[40] Morozov, A & Marenduzzo, D. (2014) Enhanced diffusion of tracer particles in dilute bacterial suspensions. *Soft Matter* **10**, 2748–2758.

[41] Brown, R. (1828) On the Existence of Active Molecules. *Edinburgh New Philosophy Journal* **5**, 358+.

[42] Wray, D & Fowler, D. (2004) Lucretius on Atomic Motion: A Commentary on De Rerum Natura Book Two, Lines 1-332. *The Journal of Roman Studies* **94**, 238+.

[43] Sutherland, W. (1905) A Dynamical Theory of Diffusion for Non-Electrolytes and the Molecular Mass of Albumin. *Philosophical Magazine* **9**, 781–785.

[44] Perrin, J. (1920) *Atoms*. (Constable, London).

[45] Lindner, P & Zemb, T. (2002) *Neutrons, X-rays, and light : scattering methods applied to soft condensed matter*. (Elsevier), Rev sub edition.

[46] Tavaddod, S, Charsooghi, M, Abdi, F, Khalesifard, H, & Golestanian, R. (2011) Probing passive diffusion of flagellated and deflagellated Escherichia coli. *The European Physical Journal E: Soft Matter and Biological Physics* **34**, 1–7.

[47] Angelani, L, Di Leonardo, R, & Ruocco, G. (2009) Self-Starting Micromotors in a Bacterial Bath. *Physical Review Letters* **102**, 048104+.

[48] Kolomeisky, A. B & Fisher, M. E. (2007) Molecular Motors: A Theorist's Perspective. *Annual Review of Physical Chemistry* **58**, 675–695.

[49] Mauro Mobilia, T. R. (2008) Generic principles of active transport. *Banach Center Publications* **80**, 101–120.

[50] Fielding, S. M, Marenduzzo, D, & Cates, M. E. (2011) Nonlinear dynamics and rheology of active fluids: Simulations in two dimensions. *Physical Review E* **83**, 041910+.

[51] Paxton, W. F, Kistler, K. C, Olmeda, C. C, Sen, A, St. Angelo, S. K, Cao, Y, Mallouk, T. E, Lammert, P. E, & Crespi, V. H. (2004) Catalytic Nanomotors: Autonomous Movement of Striped Nanorods. *Journal of the American Chemical Society* **126**, 13424–13431.

[52] Ke, H, Ye, S, Carroll, R. L, & Showalter, K. (2010) Motion Analysis of Self-Propelled Pt-Silica Particles in Hydrogen Peroxide Solutions. *The Journal of Physical Chemistry A* **114**, 5462–5467.

[53] Sambelashvili, N, Lau, A. W. C, & Cai, D. (2007) Dynamics of bacterial flow: Emergence of spatiotemporal coherent structures. *Physics Letters A* **360**, 507–511.

[54] Voituriez, R, Joanny, J. F, & Prost, J. (2006) Generic Phase Diagram of Active Polar Films. *Physical Review Letters* **96**, 028102+.

[55] Sokolov, A & Aranson, I. S. (2009) Reduction of Viscosity in Suspension of Swimming Bacteria. *Physical Review Letters* **103**, 148101+.

[56] Sokolov, A, Apodaca, M. M, Grzybowski, B. A, & Aranson, I. S. (2010) Swimming bacteria power microscopic gears. *Proceedings of the National Academy of Sciences* **107**, 969–974.

[57] Grossart, H.-P, Riemann, L, & Azam, F. (2001) Bacterial motility in the sea and its ecological implications. *Aquatic Microbial Ecology* **25**, 247–258.

[58] Drescher, K, Dunkel, J, Cisneros, L. H, Ganguly, S, & Goldstein, R. E. (2011) Fluid dynamics and noise in bacterial cell-cell and cell-surface scattering. *Proceedings of the National Academy of Sciences* **108**, 10940–10945.

[59] Drescher, K, Goldstein, R. E, Michel, N, Polin, M, & Tuval, I. (2010) Direct measurement of the flow field around swimming microorganisms. *Physical Review Letters* **105**, 168101+.

[60] Cheung, C, Hwang, Y. H, Wu, X. l, & Choi, H. J. (1996) Diffusion of particles in free-standing liquid films. *Physical Review Letters* **76**, 2531–2534.

[61] Grégoire, G, Chaté, H, & Tu, Y. (2001) Comment on "Particle Diffusion in a Quasi-Two-Dimensional Bacterial Bath". *Physical Review Letters* **86**, 556+.

[62] Miño, G, Mallouk, T. E, Darnige, T, Hoyos, M, Dauchet, J, Dunstan, J, Soto, R, Wang, Y, Rousselet, A, & Clement, E. (2011) Enhanced Diffusion due to Active Swimmers at a Solid Surface. *Physical Review Letters* **106**, 048102+.

[63] Miño, G. L, Dunstan, J, Rousselet, A, Clément, E, & Soto, R. (2013) Induced diffusion of tracers in a bacterial suspension: theory and experiments. *Journal of Fluid Mechanics* **729**, 423–444.

[64] Berg, H. C & Turner, L. (1990) Chemotaxis of bacteria in glass capillary arrays. Escherichia coli, motility, microchannel plate, and light scattering. *Biophysical Journal* **58**, 919–930.

[65] Lauga, E, DiLuzio, W. R, Whitesides, G. M, & Stone, H. A. (2006) Swimming in Circles: Motion of Bacteria near Solid Boundaries. *Biophysical Journal* **90**, 400–412.

[66] Martinez, V. A, Schwarz-Linek, J, Reufer, M, Wilson, L, Morozov, A. N, & Poon, W. C. K. (2014) Flagellated bacterial motility in polymer solutions: newtonian and non-newtonian effects. *Unpublished manuscript.*

[67] Miño, G. L. (2012) *Study of the diffusion, rheology and microrheology of complex mixtures of bacteria and particles under flow confined in thin channels.* Ph.D. thesis (Ecole superieure de physique et de chimie industrielles, France).

[68] Dunkel, J, Putz, V. B, Zaid, I. M, & Yeomans, J. M. (2010) Swimmer-tracer scattering at low Reynolds number. *Soft Matter* **6**, 4268.

[69] Lin, Z, Thiffeault, J. L, & Childress, S. (2011) Stirring by squirmers. *Journal of Fluid Mechanics* **669**, 167–177.

[70] Lighthill, M. J. (1952) On the squirming motion of nearly spherical deformable bodies through liquids at very small reynolds numbers. *Communications on Pure and Applied Mathematics* **5**, 109–118.

[71] Pushkin, D. O, Shum, H, & Yeomans, J. M. (2012) Fluid transport by individual microswimmers. *Journal of Fluid Mechanics* **726**, 5–25.

[72] Pushkin, D. O & Yeomans, J. M. (2013) Fluid Mixing by Curved Trajectories of Microswimmers. *Physical Review Letters* **111**, 188101.

[73] Kaplan, P. D, Trappe, V, & Weitz, D. A. (1999) Light-Scattering Microscope. *Applied Optics* **38**, 4151–4157.

[74] Amin, M. S, Park, Y, Lue, N, Dasari, R. R, Badizadegan, K, Feld, M. S, & Popescu, G. (2007) Microrheology of red blood cell membranes using dynamic scattering microscopy. *Optics Express* **15**, 17001–17009.

[75] Crocker, J. (1996) Methods of Digital Video Microscopy for Colloidal Studies. *Journal of Colloid and Interface Science* **179**, 298–310.

[76] Nossal, R, Chen, S, & Lai, C. (1971) Use of laser scattering for quantitative determinations of bacterial motility. *Optics Communications* **4**, 35–39.

[77] Berne, B. J & Pecora, R. (2000) *Dynamic light scattering : with applications to chemistry, biology, and physics*. (Dover Publications), Unabridged edition.

[78] Stock, G. B & Jenkins, T. C. (1978) The measurement of bacterial translation by photon correlation spectroscopy. *Biophysical Journal* **22**, 79–96.

[79] Martinez, V. A, Besseling, R, Croze, O. A, Tailleur, J, Reufer, M, Schwarz-Linek, J, Wilson, L. G, Bees, M. A, & Poon, W. C. K. (2012) Differential Dynamic Microscopy: A High-Throughput Method for Characterizing the Motility of Microorganisms. *Biophysical Journal* **103**, 1637–1647.

[80] Croccolo, F, Brogioli, D, Vailati, A, Giglio, M, & Cannell, D. S. (2006) Effect of Gravity on the Dynamics of Nonequilibrium Fluctuations in a Free-Diffusion Experiment. *Annals of the New York Academy of Sciences* **1077**, 365–379.

[81] Cerbino, R & Trappe, V. (2008) Differential Dynamic Microscopy: Probing Wave Vector Dependent Dynamics with a Microscope. *Physical Review Letters* **100**, 188102+.

[82] Giavazzi, F, Brogioli, D, Trappe, V, Bellini, T, & Cerbino, R. (2009) Scattering information obtained by optical microscopy: Differential dynamic microscopy and beyond. *Physical Review E* **80**, 031403+.

[83] Ferri, F, DAngelo, A, Lee, M, Lotti, A, Pigazzini, M. C, Singh, K, & Cerbino, R. (2011) Kinetics of colloidal fractal aggregation by differential dynamic microscopy. *The European Physical Journal Special Topics* **199**, 139–148.

[84] Reufer, M, Martinez, V. A, Schurtenberger, P, & Poon, W. C. K. (2012) Differential dynamic microscopy for anisotropic colloidal dynamics. *Langmuir : the ACS journal of surfaces and colloids* **28**, 4618–24.

[85] Schwarz-Linek, J, Martinez, V. A, Arlt, J, Jepson, A, Pilizota, T, & Poon, W. C. K. (2014) How to keep E.coli swimming. *Unpublished manuscript*.

[86] Vladescu, I, Marsden, E, Schwarz-Linek, J, Martinez, V. A, Arlt, J, Morozov, A. N, Marenduzzo, D, Cates, M. E, & Poon, W. C. K. (2014) Filling an emulsion drop with motile bacteria. *Unpublished manuscript*.

[87] Dean, G. E, Macnab, R. M, Stader, J, Matsumura, P, & Burks, C. (1984) Gene sequence and predicted amino acid sequence of the motA protein, a membrane-associated protein required for flagellar rotation in Escherichia coli. *Journal of Bacteriology* **159**, 991–999.

[88] Terashima, H, Kojima, S, & Homma, M. (2008) Flagellar motility in bacteria structure and function of flagellar motor. *International Review of Cell and Molecular Biology* **270**, 39–85.

[89] Cheng, H. P & Walker, G. C. (1998) Succinoglycan is required for initiation and elongation of infection threads during nodulation of alfalfa by Rhizobium meliloti. *Journal of Bacteriology* **180**, 5183–5191.

[90] Bertani, G. (1951) Studies on lysogenesis. I. The mode of phage liberation by lysogenic Escherichia coli. *Journal of Bacteriology* **62**, 293–300.

[91] Adler, J & Dahl, M. M. (1967) A method for measuring the motility of bacteria and for comparing random and non-random motility. *Journal of General Microbiology* **46**, 161–173.

[92] Adler, J & Templeton, B. (1967) The Effect of Environmental Conditions on the Motility of Escherichia coli. *Journal of General Microbiology* **46**, 175–184.

[93] Roche, A, McFadden, J, & Owen, P. (2001) Antigen 43, the major phase-variable protein of the Escherichia coli outer membrane, can exist as a family of proteins encoded by multiple alleles. *Microbiology* **147**, 161–9.

[94] Dorken, G, Ferguson, G. P, French, C. E, & Poon, W. C. K. (2012) Aggregation by depletion attraction in cultures of bacteria producing exopolysaccharide. *Journal of the Royal Society: Interface* **9**, 3490–502.

[95] Lowe, G, Meister, M, & Berg, H. C. (1987) Rapid rotation of flagellar bundles in swimming bacteria. *Nature* **325**, 637–640.

[96] Wilson, L, Zhang, R, Martinez, V. A, Li, M, Schwarz-Linek, J, Morozov, A, Arlt, J, & Poon, W. C. K. (2014) High speed, high-throughput screening of molecular motor speed in a free-swimming bacterial population. *Unpublished manuscript.*

[97] Min, T. L, Mears, P. J, Chubiz, L. M, Rao, C. V, Golding, I, & Chemla, Y. R. (2009) High-resolution, long-term characterization of bacterial motility using optical tweezers. *Nature methods* **6**, 831–835.

[98] Magariyama, Y, Sugiyama, S, & Kudo, S. (2001) Bacterial swimming speed and rotation rate of bundled flagella. *FEMS Microbiology Letters* **199**, 125–129.

[99] Taylor, B. L & Koshland, D. E. (1975) Intrinsic and extrinsic light responses of Salmonella typhimurium and Escherichia coli. *Journal of Bacteriology* **123**, 557–569.

[100] Martinez, V. A, Bryant, G, & van Megen, W. (2008) Slow dynamics and aging of a colloidal hard sphere glass. *Physical review letters* **101**, 135702+.

[101] Martinez, V. A, Thijssen, J. H, Zontone, F, van Megen, W, & Bryant, G. (2011) Dynamics of hard sphere suspensions using dynamic light scattering and X-ray photon correlation spectroscopy: dynamics and scaling of the intermediate scattering function. *The Journal of chemical physics* **134**, 054505+.

[102] Happel, J & Brenner, H. (1983) *Low Reynolds number hydrodynamics: with special applications to particulate media (Mechanics of Fluids and Transport Processes).* (Springer), Softcover reprint of the original 1st ed. 1983 edition.

[103] Clausznitzer, D, Oleksiuk, O, Løvdok, L, Sourjik, V, & Endres, R. G. (2010) Chemotactic Response and Adaptation Dynamics in Escherichia coli. *PLoS Compututational Biology* **6**, e1000784+.

[104] Pushkin, D. O & Yeomans, J. M. (2014) Stirring by swimmers in confined microenvironments. *Journal of Statistical Mechanics: Theory and Experiment* **2014**, P04030.

[105] Molina, J. J & Yamamoto, R. (2014) Diffusion of colloidal particles in swimming suspensions. *Molecular Physics* pp. 1–9.

[106] Amsler, C. D, Cho, M, & Matsumura, P. (1993) Multiple factors underlying the maximum motility of Escherichia coli as cultures enter post-exponential growth. *Journal of Bacteriology* **175**, 6238–6244.

[107] Turner, L, Stern, A. S, & Berg, H. C. (2012) Growth of Flagellar Filaments of Escherichia coli Is Independent of Filament Length. *Journal of Bacteriology* **194**, 2437–2442.

[108] Rosu, V & Hughes, K. T. (2006) sigma28-dependent transcription in Salmonella enterica is independent of flagellar shearing. *Journal of Bacteriology* **188**, 5196–5203.

[109] Berke, A. P, Turner, L, Berg, H. C, & Lauga, E. (2008) Hydrodynamic Attraction of Swimming Microorganisms by Surfaces. *Physical Review Letters* **101**, 038102+.

[110] Levin, B. R & Rozen, D. E. (2006) Non-inherited antibiotic resistance. *Nature Reviews Microbiology* **4**, 556–562.

[111] Chien, A.-C, Hill, N. S, & Levin, P. A. (2012) Cell size control in bacteria. *Current biology : CB* **22**, R340–9.

[112] Makinoshima, H, Aizawa, S.-I, Hayashi, H, Miki, T, Nishimura, A, & Ishihama, A. (2003) Growth Phase-Coupled Alterations in Cell Structure and Function of Escherichia coli. *Journal of Bacteriology* **185**, 1338–1345.

[113] Lund, R. D. (2012) Analyzing the Effect of Pipette Tip Geometries on Fluid Velocity and Shear Strain Rate: Biomek Wide Bore vs. Standard Pipette Tips, Technical report.

[114] Higdon, J. J. L. (1979) The hydrodynamics of flagellar propulsion: helical waves. *Journal of Fluid Mechanics* **94**, 331–351.

[115] Wei, X & Bauer, W. D. (1998) Starvation-Induced Changes in Motility, Chemotaxis, and Flagellation of Rhizobium meliloti. *Applied and Environmental Microbiology* **64**, 1708–1714.

[116] Riedel, T. E, Berelson, W. M, Nealson, K. H, & Finkel, S. E. (2013) Oxygen consumption rates of bacteria under nutrient-limited conditions. *Applied and Environmental Microbiology* **79**, 4921–31.

[117] Aminov, R. I. (2010) A brief history of the antibiotic era: lessons learned and challenges for the future. *Frontiers in Microbiology* **1**, 134.

[118] Emmerich, R & Löw, O. (1899) Bakteriolytische Enzyme als Ursache der erworbenen Immunität und die Heilung von Infectionskrankheiten durch dieselben. *Zeitschrift für Hygiene und Infectionskrankheiten* **31**, 1–65.

[119] Mahoney, J. F, Arnold, R. C, & Harris, A. (1943) Penicillin Treatment of Early Syphilis-A Preliminary Report. *American Journal of Public Health and the Nation's Health* **33**, 1387–91.

[120] Fleming, A. (1929) On the Antibacterial Action of Cultures of a Penicillium, with Special Reference to their Use in the Isolation of B. influenzæ. *British Journal of Experimental Pathology* **10**, 226–236.

[121] Murray, P, Pfaller, M, & Rosenthal, K. (2005) *Medical Microbiology.* (Elesvier Mosby, Philadelphia), 5th edition.

[122] Goossens, H. (2009) Antibiotic consumption and link to resistance. *Clinical Microbiology and Infection* **15 Suppl 3**, 12–5.

[123] ECDC/EMEA Joint Working Group. (2009) The bacterial challenge: time to react, Technical report.

[124] Yount, N. Y & Yeaman, M. R. (2012) Emerging themes and therapeutic prospects for anti-infective peptides. *Annual Review of Pharmacology and Toxicology* **52**, 337–60.

[125] Melo, M. N, Ferre, R, & Castanho, M. A. R. B. (2009) Antimicrobial peptides: linking partition, activity and high membrane-bound concentrations. *Nature reviews. Microbiology* **7**, 245–50.

[126] Schuurmans, J. M, Nuri Hayali, A. S, Koenders, B. B, & ter Kuile, B. H. (2009) Variations in MIC value caused by differences in experimental protocol. *Journal of Microbiological Methods* **79**, 44–7.

[127] Neidhardt, F. C. (1999) Bacterial Growth: Constant Obsession with dN/dt. *Journal of Bacteriology* **181**, 7405–7408.

[128] Monod, J. (1949) The Growth of Bacterial Cultures. *Annual Review of Microbiology* **3**, 371–394.

[129] Wang, G, Li, X, & Wang, Z. (2009) APD2: the updated antimicrobial peptide database and its application in peptide design. *Nucleic Acids Research* **37**, D933–7.

[130] Boye, E & Nordström, K. (2003) Coupling the cell cycle to cell growth. *EMBO Reports* **4**, 757–60.

[131] Hagen, S. J. (2010) Exponential growth of bacteria: Constant multiplication through division. *American Journal of Physics* **78**, 1290.

[132] Pin, C & Baranyi, J. (2008) Single-cell and population lag times as a function of cell age. *Applied and Environmental Microbiology* **74**, 2534–6.

[133] Sezonov, G, Joseleau-Petit, D, & D'Ari, R. (2007) Escherichia coli physiology in Luria-Bertani broth. *Journal of Bacteriology* **189**, 8746–9.

[134] Van Impe, J. F, Poschet, F, Geeraerd, A. H, & Vereecken, K. M. (2005) Towards a novel class of predictive microbial growth models. *International Journal of Food Microbiology* **100**, 97–105.

[135] Zwietering, M. H, Jongenburger, I, Rombouts, F. M, & van 't Riet, K. (1990) Modeling of the bacterial growth curve. *Applied and Environmental Microbiology* **56**, 1875–81.

[136] Baranyi, J. (2010) *Modelling and parameter estimation of bacterial growth with distributed lag time.* Ph.D. thesis (University of Szeged, Hungary).

[137] Baranyi, J. (1998) Comparison of Stochastic and Deterministic Concepts of Bacterial Lag. *Journal of Theoretical Biology* **192**, 403–408.

[138] Baranyi, J. (2002) Stochastic modelling of bacterial lag phase. *International Journal of Food Microbiology* **73**, 203–206.

[139] Baranyi, J & Pin, C. (1999) Estimating Bacterial Growth Parameters by Means of Detection Times. *Applied and Environmental Microbiology* **65**, 732–736.

[140] Mytilinaios, I, Salih, M, Schofield, H. K, & Lambert, R. J. W. (2012) Growth curve prediction from optical density data. *International Journal of Food Microbiology* **154**, 169–76.

[141] Cuppers, H. G. A. M & Smelt, J. P. P. M. (1993) Time to turbidity measurement as a tool for modeling spoilage by Lactobacillus. *Journal of Industrial Microbiology* **12**, 168–171.

[142] Jason, A. C. (1983) A deterministic model for monophasic growth of batch cultures of bacteria. *Antonie van Leeuwenhoek* **49**, 513–36.

[143] Robinson, T. P, Aboaba, O. O, Kaloti, A, Ocio, M. J, Baranyi, J, & Mackey, B. M. (2001) The effect of inoculum size on the lag phase of Listeria monocytogenes. *International Journal of Food Microbiology* **70**, 163–173.

[144] Métris, A, George, S. M, Peck, M. W, & Baranyi, J. (2003) Distribution of turbidity detection times produced by single cell-generated bacterial populations. *Journal of Microbiological Methods* **55**, 821–7.

[145] Métris, A, George, S. M, Mackey, B. M, & Baranyi, J. (2008) Modeling the variability of single-cell lag times for Listeria innocua populations after sublethal and lethal heat treatments. *Applied and Environmental Microbiology* **74**, 6949–55.

[146] Baranyi, J, George, S. M, & Kutalik, Z. (2009) Parameter estimation for the distribution of single cell lag times. *Journal of Theoretical Biology* **259**, 24–30.

[147] Francois, K, Devlieghere, F, Standaert, A, Geeraerd, A, Van Impe, J, & Debevere, J. (2003) Modelling the individual cell lag phase. Isolating single cells: protocol development. *Letters in Applied Microbiology* **37**, 26–30.

[148] Guillier, L, Pardon, P, & Augustin, J.-C. (2005) Influence of stress on individual lag time distributions of Listeria monocytogenes. *Applied and Environmental Microbiology* **71**, 2940–8.

[149] Li, Y, Odumeru, J. A, Griffiths, M, & McKellar, R. C. (2006) Effect of environmental stresses on the mean and distribution of individual cell lag times of Escherichia coli O157:H7. *International Journal of Food Microbiology* **110**, 278–85.

[150] Wheat, P. F. (2001) History and development of antimicrobial susceptibility testing methodology. *The Journal of Antimicrobial Chemotherapy* **48 Suppl 1**, 1–4.

[151] Poupard, J, Walsh, L, & Kleger, B, eds. (1994) *Antimicrobial Susceptibility Testing: Critical Issues for the 90's.* (Springer) Vol. 7, p. 191.

[152] Pea, F & Viale, P. (2006) The antimicrobial therapy puzzle: could pharmacokinetic-pharmacodynamic relationships be helpful in addressing the issue of appropriate pneumonia treatment in critically ill patients? *Clinical Infectious Diseases* **42**, 1764–71.

[153] Wiegand, I, Hilpert, K, & Hancock, R. E. W. (2008) Agar and broth dilution methods to determine the minimal inhibitory concentration (MIC) of antimicrobial substances. *Nature Protocols* **3**, 163–75.

[154] Annis, D. H & Craig, B. A. (2005) The effect of interlaboratory variability on antimicrobial susceptibility determination. *Diagnostic Microbiology and Infectious Disease* **53**, 61–4.

[155] Udekwu, K. I, Parrish, N, Ankomah, P, Baquero, F, & Levin, B. R. (2009) Functional relationship between bacterial cell density and the efficacy of antibiotics. *The Journal of Antimicrobial Chemotherapy* **63**, 745–57.

[156] Levin, B. R & Udekwu, K. I. (2010) Population dynamics of antibiotic treatment: a mathematical model and hypotheses for time-kill and continuous-culture experiments. *Antimicrobial Agents and Chemotherapy* **54**, 3414–26.

[157] French, G. L. (2006) Bactericidal agents in the treatment of MRSA infections–the potential role of daptomycin. *The Journal of Antimicrobial Chemotherapy* **58**, 1107–17.

[158] Levin, B. R & Rozen, D. E. (2006) Non-inherited antibiotic resistance. *Nature reviews. Microbiology* **4**, 556–62.

[159] Guerillot, F, Carret, G, & Flandrois, J. P. (1993) Mathematical model for comparison of time-killing curves. *Antimicrobial Agents and Chemotherapy* **37**, 1685–9.

[160] Yourassowsky, E, Van der Linden, M. P, Lismont, M. J, Crokaert, F, & Glupczynski, Y. (1985) Correlation between growth curve and killing curve of Escherichia coli after a brief exposure to suprainhibitory concentrations of ampicillin and piperacillin. *Antimicrobial Agents and Chemotherapy* **28**, 756–60.

[161] Cotroneo, N, Harris, R, Perlmutter, N, Beveridge, T, & Silverman, J. A. (2008) Daptomycin exerts bactericidal activity without lysis of Staphylococcus aureus. *Antimicrobial Agents and Chemotherapy* **52**, 2223–5.

[162] Marsch, J & Goode, J, eds. (2008) *Ciba Foundation Symposium 186 - Antimicrobial Peptides* (John Wiley & Sons), p. 292.

[163] Lambert, R & Pearson, J. (2000) Susceptibility testing: accurate and reproducible minimum inhibitory concentration (MIC) and non-inhibitory concentration (NIC) values. *Journal of Applied Microbiology* **88**, 784–790.

[164] Baraban, L, Bertholle, F, Salverda, M. L. M, Bremond, N, Panizza, P, Baudry, J, de Visser, J. A. G. M, & Bibette, J. (2011) Millifluidic droplet analyser for microbiology. *Lab on a Chip* **11**, 4057–62.

[165] Gompertz, B. (1825) On the Nature of the Function Expressive of the Law of Human Mortality, and on a New Mode of Determining the Value of Life Contingencies. *Philosophical Transactions of the Royal Society of London* **115**, 513–583.

[166] Mackey, B & Derrick, C. M. (1982) The effect of sublethal injury by heating, freezing, drying and gamma-radiation on the duration of the lag phase of Salmonella typhimurium. *Journal of Applied Bacteriology* **53**, 243–251.

[167] Soriano, F, García-Corbeira, P, Ponte, C, Fernández-Roblas, R, & Gadea, I. (1996) Correlation of pharmacodynamic parameters of five beta-lactam antibiotics with therapeutic efficacies in an animal model. *Antimicrobial Agents and Chemotherapy* **40**, 2686–90.

[168] Tan, C, Smith, R. P, Srimani, J. K, Riccione, K. A, Prasada, S, Kuehn, M, & You, L. (2012) The inoculum effect and band-pass bacterial response to periodic antibiotic treatment. *Molecular Systems Biology* **8**, 617.

[169] Craig, W. A, Bhavnani, S. M, & Ambrose, P. G. (2004) The inoculum effect: fact or artifact? *Diagnostic Microbiology and Infectious Disease* **50**, 229–30.

[170] Thomson, K. S & Moland, E. S. (2001) Cefepime, piperacillin-tazobactam, and the inoculum effect in tests with extended-spectrum beta-lactamase-producing Enterobacteriaceae. *Antimicrobial Agents and Chemotherapy* **45**, 3548–54.

[171] Haney, E. F & Hancock, R. B. E. W. (2013) Peptide design for antimicrobial and immunomodulatory applications. *Biopolymers* **100**, 572–583.

[172] Hancock, R. E. W & Sahl, H.-G. (2006) Antimicrobial and host-defense peptides as new anti-infective therapeutic strategies. *Nature Biotechnology* **24**, 1551–7.

[173] Zasloff, M. (2002) Antimicrobial peptides of multicellular organisms. *Nature* **415**, 389–95.

[174] Phoenix, D. A, Dennison, S. R, & Harris, F. (2013) *Antimicrobial Peptides.* (Wiley-VCH Verlag GmbH & Co. KGaA, Weinheim, Germany).

[175] Brogden, K. A. (2005) Antimicrobial peptides: pore formers or metabolic inhibitors in bacteria? *Nature reviews. Microbiology* **3**, 238–50.

[176] Fjell, C. D, Hiss, J. A, Hancock, R. E. W, & Schneider, G. (2012) Designing antimicrobial peptides: form follows function. *Nature reviews. Drug discovery* **11**, 37–51.

[177] Salick, D. A, Pochan, D. J, & Schneider, J. P. (2009) Design of an Injectable β-Hairpin Peptide Hydrogel That Kills Methicillin-Resistant Staphylococcus aureus. *Advanced Materials* **21**, 4120–4123.

[178] Sieprawska-Lupa, M, Mydel, P, Krawczyk, K, Wójcik, K, Puklo, M, Lupa, B, Suder, P, Silberring, J, Reed, M, Pohl, J, Shafer, W, McAleese, F, Foster, T, Travis, J, & Potempa, J. (2004) Degradation of human antimicrobial peptide LL-37 by Staphylococcus aureus-derived proteinases. *Antimicrobial Agents and Chemotherapy* **48**, 4673–9.

[179] Ulvatne, H, Haukland, H. H, Samuelsen, O. r, Krämer, M, & Vorland, L. H. (2002) Proteases in Escherichia coli and Staphylococcus aureus confer reduced susceptibility to lactoferricin B. *The Journal of Antimicrobial Chemotherapy* **50**, 461–7.

[180] Schmidtchen, A, Frick, I.-M, Andersson, E, Tapper, H, & Björck, L. (2002) Proteinases of common pathogenic bacteria degrade and inactivate the antibacterial peptide LL-37. *Molecular Microbiology* **46**, 157–68.

[181] Perron, G. G, Zasloff, M, & Bell, G. (2006) Experimental evolution of resistance to an antimicrobial peptide. *Proceedings of the Royal Society: Biological sciences* **273**, 251–6.

[182] Fedtke, I, Götz, F, & Peschel, A. (2004) Bacterial evasion of innate host defenses; the Staphylococcus aureus lesson. *International Journal of Medical Microbiology* **294**, 189–194.

[183] Buckling, A & Brockhurst, M. (2005) Microbiology: RAMP resistance. *Nature* **438**, 170–171.

[184] Gottler, L. M & Ramamoorthy, A. (2009) Structure, membrane orientation, mechanism, and function of pexiganan–a highly potent antimicrobial peptide designed from magainin. *Biochimica et Biophysica acta* **1788**, 1680–6.

[185] Zasloff, M. (1987) Magainins, a class of antimicrobial peptides from Xenopus skin: isolation, characterization of two active forms, and partial cDNA sequence of a precursor. *Proceedings of the National Academy of Sciences of the United States of America* **84**, 5449–53.

[186] Giovannini, M. G, Poulter, L, Gibson, B. W, & Williams, D. H. (1987) Biosynthesis and degradation of peptides derived from Xenopus laevis prohormones. *The Biochemical Journal* **243**, 113–20.

[187] Lamb, H. M & Wiseman, L. R. (1998) Pexiganan acetate. *Drugs* **56**, 1047–52; discussion 1053–4.

[188] Lipsky, B. A, Holroyd, K. J, & Zasloff, M. (2008) Topical versus systemic antimicrobial therapy for treating mildly infected diabetic foot ulcers: a randomized, controlled, double-blinded, multicenter trial of pexiganan cream. *Clinical infectious diseases : an official publication of the Infectious Diseases Society of America* **47**, 1537–45.

[189] Ge, Y, MacDonald, D. L, Holroyd, K. J, Thornsberry, C, Wexler, H, & Zasloff, M. (1999) In Vitro Antibacterial Properties of Pexiganan, an Analog of Magainin. *Antimicrobial Agents and Chemotherapy* **43**, 782–788.

[190] Fuchs, P. C, Barry, A. L, & Brown, S. D. (1998) In Vitro Antimicrobial Activity of MSI-78, a Magainin Analog. *Antimicrobial Agents and Chemotherapy* **42**, 1213–1216.

[191] Navon-Venezia, S, Feder, R, Gaidukov, L, Carmeli, Y, & Mor, A. (2002) Antibacterial Properties of Dermaseptin S4 Derivatives with In Vivo Activity. *Antimicrobial Agents and Chemotherapy* **46**, 689–694.

[192] Ramamoorthy, A, Thennarasu, S, Lee, D.-K, Tan, A, & Maloy, L. (2006) Solid-state NMR investigation of the membrane-disrupting mechanism of antimicrobial peptides MSI-78 and MSI-594 derived from magainin 2 and melittin. *Biophysical Journal* **91**, 206–16.

[193] Gottler, L. M. (2008) *Peptides as Model Systems, Antimicrobial Agents, and a Means for Protein Superassembly.* Ph.D. thesis (The University of Michigan, USA).

[194] Porcelli, F, Buck-Koehntop, B. A, Thennarasu, S, Ramamoorthy, A, & Veglia, G. (2006) Structures of the dimeric and monomeric variants of magainin antimicrobial peptides (MSI-78 and MSI-594) in micelles and bilayers, determined by NMR spectroscopy. *Biochemistry* **45**, 5793–9.

[195] Hallock, K. J, Lee, D.-K, & Ramamoorthy, A. (2003) MSI-78, an analogue of the magainin antimicrobial peptides, disrupts lipid bilayer structure via positive curvature strain. *Biophysical Journal* **84**, 3052–60.

[196] Yang, P, Ramamoorthy, A, & Chen, Z. (2011) Membrane orientation of MSI-78 measured by sum frequency generation vibrational spectroscopy. *Langmuir : the ACS Journal of Surfaces and Colloids* **27**, 7760–7.

[197] Mecke, A, Lee, D.-K, Ramamoorthy, A, Orr, B. G, & Banaszak Holl, M. M. (2005) Membrane thinning due to antimicrobial peptide binding: an atomic force microscopy study of MSI-78 in lipid bilayers. *Biophysical Journal* **89**, 4043–50.

[198] Pius, J, Morrow, M. R, & Booth, V. (2012) H solid-state nuclear magnetic resonance investigation of whole Escherichia coli interacting with antimicrobial peptide MSI-78. *Biochemistry* **51**, 118–25.

[199] Matsuzaki, K, Sugishita, K.-i, Harada, M, Fujii, N, & Miyajima, K. (1997) Interactions of an antimicrobial peptide, magainin 2, with outer and inner membranes of Gram-negative bacteria. *Biochimica et Biophysica Acta (BBA) - Biomembranes* **1327**, 119–130.

[200] Meincken, M, Holroyd, D. L, & Rautenbach, M. (2005) Atomic force microscopy study of the effect of antimicrobial peptides on the cell envelope of Escherichia coli. *Antimicrobial Agents and Chemotherapy* **49**, 4085–92.

[201] Juretić, D, Chen, H.-C, Brown, J. H, Morell, J. L, Hendler, R. W, & Westerhoff, H. V. (1989) Magainin 2 amide and analogues Antimicrobial activity, membrane depolarization and susceptibility to proteolysis. *FEBS Letters* **249**, 219–223.

[202] Gottler, L. M, Lee, H.-Y, Shelburne, C. E, Ramamoorthy, A, & Marsh, E. N. G. (2008) Using fluorous amino acids to modulate the biological activity of an antimicrobial peptide. *ChemBioChem* **9**, 370–3.

[203] Wimley, W. C. (2010) Describing the mechanism of antimicrobial peptide action with the interfacial activity model. *ACS Chemical Biology* **5**, 905–17.

[204] Wimley, W. C & Hristova, K. (2011) Antimicrobial peptides: successes, challenges and unanswered questions. *The Journal of Membrane Biology* **239**, 27–34.

[205] Gee, M. L, Burton, M, Grevis-James, A, Hossain, M. A, McArthur, S, Palombo, E. A, Wade, J. D, & Clayton, A. H. A. (2013) Imaging the action of antimicrobial peptides on living bacterial cells. *Scientific Reports* **3**, 1557.

[206] Sochacki, K. A, Barns, K. J, Bucki, R, & Weisshaar, J. C. (2011) Real-time attack on single Escherichia coli cells by the human antimicrobial peptide LL-37. *Proceedings of the National Academy of Sciences of the United States of America* **108**, E77–81.

[207] McGrath, D. M, Barbu, E. M, Driessen, W. H. P, Lasco, T. M, Tarrand, J. J, Okhuysen, P. C, Kontoyiannis, D. P, Sidman, R. L, Pasqualini, R, & Arap, W. (2013) Mechanism of action and initial evaluation of a membrane active all-D-enantiomer antimicrobial peptidomimetic. *Proceedings of the National Academy of Sciences of the United States of America* **110**, 3477–82.

[208] Spindler, E. C, Hale, J. D. F, Giddings, T. H, Hancock, R. E. W, & Gill, R. T. (2011) Deciphering the mode of action of the synthetic antimicrobial peptide Bac8c. *Antimicrobial Agents and Chemotherapy* **55**, 1706–16.

[209] Levison, M. E, Pitsakis, P. G, May, P. L, & Johnson, C. C. (1993) The bactericidal activity of magainins against Pseudomonas aeruginosa and Enterococcus faecium. *The Journal of Antimicrobial Chemotherapy* **32**, 577–85.

[210] Pag, U, Oedenkoven, M, Papo, N, Oren, Z, Shai, Y, & Sahl, H.-G. (2004) In vitro activity and mode of action of diastereomeric antimicrobial peptides against bacterial clinical isolates. *The Journal of Antimicrobial Chemotherapy* **53**, 230–9.

[211] Casteels, P & Tempst, P. (1994) Apidaecin-type peptide antibiotics function through a non-poreforming mechanism involving stereospecificity. *Biochemical and Biophysical Research Communications* **199**, 339–45.

[212] Jones, E, Smart, A, Bloomberg, G, Burgess, L, & Millar, M. (1994) Lactoferricin, a new antimicrobial peptide. *Journal of Applied Bacteriology* **77**, 208–214.

[213] Bachmann, B. J. (1972) Pedigrees of some mutant strains of Escherichia coli K-12. *Bacteriological Reviews* **36**, 525–57.

[214] Elowitz, M. B, Levine, A. J, Siggia, E. D, & Swain, P. S. (2002) Stochastic gene expression in a single cell. *Science (New York, N.Y.)* **297**, 1183–6.

[215] Pilizota, T & Shaevitz, J. W. (2012) Fast, multiphase volume adaptation to hyperosmotic shock by Escherichia coli. *PloS one* **7**, e35205.

[216] Andreu, D & Rivas, L. (1998) Animal antimicrobial peptides: an overview. *Biopolymers* **47**, 415–33.

[217] Giacometti, A, Cirioni, O, Barchiesi, F, Del Prete, M. S, Fortuna, M, Caselli, F, & Scalise, G. (2000) In vitro susceptibility tests for cationic peptides: comparison of broth microdilution methods for bacteria that grow aerobically. *Antimicrobial Agents and Chemotherapy* **44**, 1694–6.

[218] Pin, C & Baranyi, J. (2006) Kinetics of single cells: observation and modeling of a stochastic process. *Applied and Environmental Microbiology* **72**, 2163–9.

[219] Métris, A, George, S. M, & Baranyi, J. (2006) Use of optical density detection times to assess the effect of acetic acid on single-cell kinetics. *Applied and Environmental Microbiology* **72**, 6674–9.

[220] Rasch, M, Métris, A, Baranyi, J, & Bjørn Budde, B. (2007) The effect of reuterin on the lag time of single cells of Listeria innocua grown on a solid agar surface at different pH and NaCl concentrations. *International Journal of Food Microbiology* **113**, 35–40.

[221] Sutton, S. (2003) Accuracy of Plate Counts. *Journal of Validation Technology* **17**, 42–46.

[222] Forster, L. I. (2003) Measurement uncertainty in microbiology. *Journal of AOAC International* **86**, 1089–94.

[223] Young, J. W, Locke, J. C. W, Altinok, A, Rosenfeld, N, Bacarian, T, Swain, P. S, Mjolsness, E, & Elowitz, M. B. (2012) Measuring single-cell gene expression dynamics in bacteria using fluorescence time-lapse microscopy. *Nature Protocols* **7**, 80–8.

[224] Niven, G. W, Fuks, T, Morton, J. S, Rua, S. A, & Mackey, B. M. (2006) A novel method for measuring lag times in division of individual bacterial cells using image analysis. *Journal of Microbiological Methods* **65**, 311–317.

[225] Irwin, P. L, Nguyen, L.-H. T, Paoli, G. C, & Chen, C.-Y. (2010) Evidence for a bimodal distribution of Escherichia coli doubling times below a threshold initial cell concentration. *BMC Microbiology* **10**, 207.

[226] Zhao, X, Pan, F, & Lu, J. R. (2009) Interfacial assembly of proteins and peptides: recent examples studied by neutron reflection. *Journal of the Royal Society, Interface* **6 Suppl 5**, S659–70.

[227] Kogot, J. M, Sarkes, D. A, Val-Addo, I, Pellegrino, P. M, & Stratis-Cullum, D. N. (2012) Increased affinity and solubility of peptides used for direct peptide ELISA on polystyrene surfaces through fusion with a polystyrene-binding peptide tag. *BioTechniques* **52**, 95–102.

[228] Small, D. M, Wang, L, & Mitsche, M. A. (2009) The adsorption of biological peptides and proteins at the oil/water interface. A potentially important but largely unexplored field. *Journal of Lipid Research* **50 Suppl**, S329–34.

[229] Goebel-Stengel, M, Stengel, A, Taché, Y, & Reeve, J. R. (2011) The importance of using the optimal plasticware and glassware in studies involving peptides. *Analytical Biochemistry* **414**, 38–46.

[230] Firsov, A, Vostrov, S, Shevchenko, A, & Cornaglia, G. (1997) Parameters of bacterial killing and regrowth kinetics and antimicrobial effect examined in terms of area under the concentration-time curve relationships: action of ciprofloxacin against Escherichia coli in an in vitro dynamic model. *Antimicrobial Agents and Chemotherapy* **41**, 1281–1287.

[231] Jacoby, G. H & Young, K. D. (1991) Cell cycle-independent lysis of Escherichia coli by cefsulodin, an inhibitor of penicillin-binding proteins 1a and 1b. *Journal of Bacteriology* **173**, 1–5.

[232] Sear, R. P. (2003) The effects of added salt on the second virial coefficients of the complete proteome of E. coli. *The Journal of Chemical Physics* **118**, 5157.

[233] Wakamoto, Y, Dhar, N, Chait, R, Schneider, K, Signorino-Gelo, F, Leibler, S, & McKinney, J. D. (2013) Dynamic persistence of antibiotic-stressed mycobacteria. *Science* **339**, 91–5.

[234] Niven, G. W, Morton, J. S, Fuks, T, & Mackey, B. M. (2008) Influence of environmental stress on distributions of times to first division in Escherichia coli populations, as determined by digital-image analysis of individual cells. *Applied and Environmental Microbiology* **74**, 3757–63.

[235] Métris, A, Le Marc, Y, Elfwing, A, Ballagi, A, & Baranyi, J. (2005) Modelling the variability of lag times and the first generation times of single cells of E. coli. *International Journal of Food Microbiology* **100**, 13–19.

[236] Yao, Z, Kahne, D, & Kishony, R. (2012) Distinct single-cell morphological dynamics under beta-lactam antibiotics. *Molecular Cell* **48**, 705–12.

[237] Gottenbos, B, Grijpma, D. W, van der Mei, H. C, Feijen, J, & Busscher, H. J. (2001) Antimicrobial effects of positively charged surfaces on adhering Gram-positive and Gram-negative bacteria. *The Journal of Antimicrobial Chemotherapy* **48**, 7–13.

[238] Kim, S. H, Yamamoto, T, Fourmy, D, & Fujii, T. (2011) An electroactive microwell array for trapping and lysing single-bacterial cells. *Biomicrofluidics* **5**, 24114.

[239] Ye, R, Xu, H, Wan, C, Peng, S, Wang, L, Xu, H, Aguilar, Z. P, Xiong, Y, Zeng, Z, & Wei, H. (2013) Antibacterial activity and mechanism of action of ϵ-poly-L-lysine. *Biochemical and Biophysical Research Communications* **439**, 148–53.

[240] Regoes, R. R, Wiuff, C, Zappala, R. M, Garner, K. N, Baquero, F, & Levin, B. R. (2004) Pharmacodynamic functions: a multiparameter approach to the design of antibiotic treatment regimens. *Antimicrobial Agents and Chemotherapy* **48**, 3670–6.

[241] Moiset, G, Cirac, A. D, Stuart, M. C. A, Marrink, S.-J, Sengupta, D, & Poolman, B. (2013) Dual action of BPC194: a membrane active peptide killing bacterial cells. *PloS one* **8**, e61541.

[242] Rakowska, P. D, Jiang, H, Ray, S, Pyne, A, Lamarre, B, Carr, M, Judge, P. J, Ravi, J, Gerling, U. I. M, Koksch, B, Martyna, G. J, Hoogenboom, B. W, Watts, A, Crain, J, Grovenor, C. R. M, & Ryadnov, M. G. (2013) Nanoscale imaging reveals laterally expanding antimicrobial pores in lipid bilayers. *Proceedings of the National Academy of Sciences of the United States of America* **110**, 8918–23.

[243] Lerouge, I & Vanderleyden, J. (2002) O-antigen structural variation: mechanisms and possible roles in animal/plantâmicrobe interactions. *FEMS Microbiology Reviews* **26**, 17–47.

[244] Abraham, J. M, Freitag, C. S, Clements, J. R, & Eisenstein, B. I. (1985) An invertible element of DNA controls phase variation of type 1 fimbriae of Escherichia coli. *Proceedings of the National Academy of Sciences of the United States of America* **82**, 5724–7.

[245] Gall, I, Herzberg, M, & Oren, Y. (2013) The effect of electric fields on bacterial attachment to conductive surfaces. *Soft Matter* **9**, 2443.

[246] Domingues, T. M, Riske, K. A, & Miranda, A. (2010) Revealing the lytic mechanism of the antimicrobial peptide gomesin by observing giant unilamellar vesicles. *Langmuir : the ACS journal of surfaces and colloids* **26**, 11077–84.

[247] Tamba, Y & Yamazaki, M. (2009) Magainin 2-induced pore formation in the lipid membranes depends on its concentration in the membrane interface. *The journal of physical chemistry. B* **113**, 4846–52.

[248] Balaban, N. Q, Gerdes, K, Lewis, K, & McKinney, J. D. (2013) A problem of persistence: still more questions than answers? *Nature Reviews Microbiology* **11**, 587–591.

[249] Adams, J. L & Kashuba, A. D. M. (2012) Formulation, pharmacokinetics and pharmacodynamics of topical microbicides. *Best Practice & Research. Clinical Obstetrics & Gynaecology* **26**, 451–62.

[250] Cummins, J, Reen, F. J, Baysse, C, Mooij, M. J, & O'Gara, F. (2009) Subinhibitory concentrations of the cationic antimicrobial peptide colistin induce the pseudomonas quinolone signal in Pseudomonas aeruginosa. *Microbiology* **155**, 2826–37.

[251] Linares, J. F, Gustafsson, I, Baquero, F, & Martinez, J. L. (2006) Antibiotics as intermicrobial signaling agents instead of weapons. *Proceedings of the National Academy of Sciences of the United States of America* **103**, 19484–9.

[252] Xu, C, Lin, X, Ren, H, Zhang, Y, Wang, S, & Peng, X. (2006) Analysis of outer membrane proteome of Escherichia coli related to resistance to ampicillin and tetracycline. *Proteomics* **6**, 462–73.

[253] Hou, S, Liu, Z, Young, A. W, Mark, S. L, Kallenbach, N. R, & Ren, D. (2010) Effects of Trp- and Arg-containing antimicrobial-peptide structure on inhibition of Escherichia coli planktonic growth and biofilm formation. *Applied and environmental microbiology* **76**, 1967–74.

[254] Gabel, C. V & Berg, H. C. (2003) The speed of the flagellar rotary motor of Escherichia coli varies linearly with protonmotive force. *Proceedings of the National Academy of Sciences of the United States of America* **100**, 8748–51.

[255] Montville, T. J & Bruno, M. E. (1994) Evidence that dissipation of proton motive force is a common mechanism of action for bacteriocins and other antimicrobial proteins. *International Journal of Food Microbiology* **24**, 53–74.

[256] Berditsch, M, Afonin, S, Vladimirova, T, Wadhwani, P, & Ulrich, A. S. (2012) Antimicrobial Peptides can Enhance the Risk of Persistent Infections. *Frontiers in Immunology* **3**, 222.

[257] Matsuzaki, K, Mitani, Y, Akada, K. Y, Murase, O, Yoneyama, S, Zasloff, M, & Miyajima, K. (1998) Mechanism of synergism between antimicrobial peptides magainin 2 and PGLa. *Biochemistry* **37**, 15144–53.

[258] Colville, K, Tompkins, N, Rutenberg, A. D, & Jericho, M. H. (2010) Effects of poly(L-lysine) substrates on attached Escherichia coli bacteria. *Langmuir : the ACS Journal of Surfaces and Colloids* **26**, 2639–44.

[259] Strahl, H & Hamoen, L. W. (2010) Membrane potential is important for bacterial cell division. *Proceedings of the National Academy of Sciences of the United States of America* **107**, 12281–6.

[260] Angelani, L, Di Leonardo, R, & Paoluzzi, M. (2014) First-passage time of run-and-tumble particles. *The European physical journal. E, Soft matter* **37**, 15.

Appendix

Publication:

Enhanced diffusion of nonswimmers in a three-dimensional bath of motile bacteria

---

PHYSICAL REVIEW E **88**, 041002(R) (2013)

Enhanced diffusion of nonswimmers in a three-dimensional bath of motile bacteria

Alys Jepson, Vincent A. Martinez, Jana Schwarz-Linek, Alexander Morozov, and Wilson C. K. Poon
SUPA, School of Physics & Astronomy, The University of Edinburgh, Mayfield Road, Edinburgh EH9 3JZ, United Kingdom
(Received 3 July 2013; published 28 October 2013)

We show, using differential dynamic microscopy, that the diffusivity of nonmotile cells in a three-dimensional (3D) population of motile *E. coli* is enhanced by an amount proportional to the active cell flux. While nonmotile mutants without flagella and mutants with paralyzed flagella have quite different thermal diffusivities and therefore hydrodynamic radii, their diffusivities are enhanced to the same extent by swimmers in the regime of cell densities explored here. Integrating the advective motion of nonswimmers caused by swimmers with finite persistence-length trajectories predicts our observations to within 2%, indicating that fluid entrainment is not relevant for diffusion enhancement in 3D.

DOI: 10.1103/PhysRevE.88.041002 PACS number(s): 47.63.Gd, 47.63.mf, 05.40.Jc

A collection of swimmers in a liquid (fish, motile algae, Janus colloids in "fuel", etc.) is an example of intrinsically nonequilibrium "active matter" [1], which show multiple intriguing activity-driven phenomena, e.g., novel pattern formation and counterintuitive rheology [2]. In particular, swimmers perturb the motion of passive species in their vicinity, from turning microgear wheels [3,4] to enhancing the motion of tracer colloids [5–10]. Understanding such phenomena is a challenge to statistical physics; it is also relevant biologically. Motile microorganisms live in the presence of and interact with nonswimmers of the same or different species, and nonliving debris such as food, substrates for colonization, etc. Such active-passive interactions are important ecologically [11], e.g., in cross-species predator-prey relationships.

The most well-studied active-passive mixture to date is colloids in a bacterial bath [5–9]. Experiments show that swimming bacteria enhance the long-time (nonthermal) diffusivity D of colloidal tracers linearly with the swimmer concentration [5] or, more generally, the active particle flux [6,7], $J_A = \bar{v} n_A$, where $\bar{v}$ and n_A are the average speed and number density of the swimmers, i.e.,

$$\Delta D = D - D_0 = \beta J_A, \tag{1}$$

with D_0 the (thermal) diffusivity in the absence of swimmers.

Significantly, all experiments supporting Eq. (1) [5–8] have been in two dimensions (2D), with the swimmers in a thin film [5] or close to one [6,7] or two [7,8] walls; in [5], the swimmers were at interacting concentrations. It remains unknown whether Eq. (1) holds under much simpler, bulk (3D) conditions far from any boundaries at low swimmer concentrations. Moreover, existing calculations [7] considering only far-field advection of tracer motion [12,13] significantly underestimate 2D observations [6,7]. One factor may be the presence of a range of swimmer-wall distances in the experiments. It has also been proposed recently [14] that advection and fluid entrainment [15] both contribute in 3D, but entrainment dominates in 2D. This theory predicts a value of β in 3D that is more than an order of magnitude larger than that given in [7].

Thus, the current situation, given in Table I, is far from satisfactory. To progress, confrontation of theory with 3D data is essential. We report a 3D study of enhanced diffusion in a bacterial bath using differential dynamic microscopy (DDM), which is uniquely able to deliver high-throughput 3D averaging [16]. We predict the measured β to within 2% by considering advection alone, showing that entrainment is negligible in 3D.

DDM measures the intermediate scattering function (ISF), $f(q,t)$, of a population of swimming *E. coli* [17], where q is the scattering vector and t is the time. Fitting the ISF gives the swimming speed distribution, and hence the average speed $\bar{v}$, the fraction of nonmotile organisms α, and the diffusivity of the nonmotile species D. The method has been validated in detail for wild-type (WT), i.e., run-and-tumble, and smooth swimming *E. coli* [18].

We use nonswimming cells as tracers. Since the fraction of motile organisms in as-prepared ("native") populations does not vary significantly from day to day, we add nonswimmers to native populations to study ΔD as a function of J_A. Thus, in general, there are three subpopulations in each of our samples: *native* motile (M) and nonmotile (N1) cells, and *added* nonmotile (N2) cells, with the latter being fluorescent and therefore distinguishable from native nonmotile cells. We performed DDM in phase contrast and fluorescence [19] modes, probing the motion of all the cells and only the diffusion of the added, fluorescent nonmotile mutants (N2), respectively.

K12-derived wild-type (WT) *E. coli* AB1157 and fluorescent nonmotile fliF (no flagella) or motA (paralyzed flagella) mutants [20] were grown and harvested as described before [18]. Suspensions at optical density OD = 0.5 (at 600 nm), corresponding to $7.8 \pm 0.2 \times 10^8$ cells/ml (=cell body volume fraction $\phi \approx 0.1\%$ based on cell volume of $V = 1.4 \pm 0.1\ \mu\text{m}^3$ [24]), were obtained by dilution.

DDM showed that as-prepared WT populations (M + N1) contained 20–40% native nonmotile (N1) cells (i.e., $\alpha =$ 0.6–0.8), and motile cells swam with $\bar{v} =$ 13–16 μm/s [17,18]. We studied the effect of $J_A = \bar{v} n_A = \bar{v}\alpha\phi/V$ on enhanced diffusion using three protocols. In most cases, we varied α directly by mixing WT and mutant cell suspensions at different ratios to obtain samples with fixed $\phi = 0.1\%$ and $\bar{v}$ in the narrow range $\bar{v} =$ 13–16 μm/s. To check that it is the combination $\bar{v}\alpha\phi$ that controls ΔD, we repeated these experiments but added glucose (0.006 wt%) into cell mixtures immediately before loading into capillaries, which increased $\bar{v}$ to $\lesssim$25 μm/s [25]. Finally, we studied a limited number of mixtures in which we varied ϕ at fixed α, or varied ϕ

TABLE I. Experiments (E) and theory (T) on tracer diffusion.

	Dimensionality	Effect(s) included	β (μm^4)[a]
E [7]	Next to wall		13 ± 0.7[b]
T [7]	Next to wall	Advection	2.0
T [7]	3D	Advection	0.48[c]
T [14]	3D	Advection + Entrainment	9.0
E [this work]	3D		7.1 ± 0.4
T [this work]	3D	Advection	7.24

[a]See Eq. (1) for the definition of β; cf. Fig. 2.
[b]Fitted value reported in [7] based on their Fig.8.
[c]Approximating swimmers as point dipoles, as in this work.

and α together. Taken together, these experiments accessed $0 \leqslant J_A \leqslant 14 \times 10^{-3}$ μm^{-2} s^{-1} by varying the component parameters of J_A in the range $0 \leqslant \alpha \lesssim 0.7$ and $0.04\% \lesssim \phi \lesssim 0.1\%$, and $\bar{v} \approx 15$ μm/s and $\approx$25 μm/s.

Observations began immediately after a glass capillary (depth 400 μm) was filled with $\approx$200 μl of solution and sealed with Vaseline to prevent drift. Forty-second-long phase-contrast movies (Nikon Plan Fluor 10× objective, NA = 0.3, 100 frame per second, 500^2 pixels) capturing all cells ($\sim 10^4$ M + N1 + N2), and fluorescence movies (Nikon Plan Fluor 20× objective with NA = 0.5, 20 fps, 1024^2 pixels excited at 450–490 nm) capturing only the added nonmotile mutants ($\sim 10^2$–10^3 N2), were consecutively recorded on an inverted microscope (Nikon TE300 Eclipse) with a Mikrotron high-speed camera (MC 1362) and frame grabber (Inspecta 5, 1 Gb memory). We image at 100 μm from the bottom of the capillary. This is significantly larger than the persistence length of WT *E. coli* (1 s run time $\equiv \lesssim$ 15–20 μm run length), so that they execute 3D motion. We have previously shown that the depth at 10× or 20× is large enough for DDM to return the 3D ISF of swimming *E. coli* [18].

Figure 1(a) shows ISFs from fluorescence DDM performed on a typical sample containing 70% WT cells (M + N1) and 30% motA mutants (N2) at a range of q values. Since only N2 cells fluoresce, the decay of these ISFs is exclusively due to the motion of the nonmotile motA mutants. The data collapse against $q^2\tau$, shown in Fig. 1(b), which means that their motion is well described as diffusive, and there is little evidence for non-Gaussianity [5,8,10] over our experimental window. As

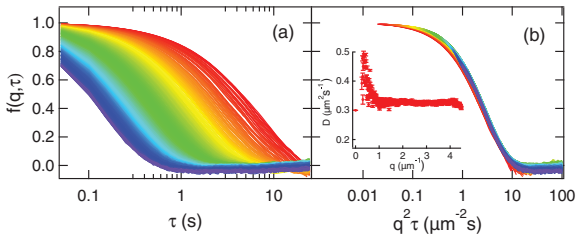

FIG. 1. (Color online) The ISF from fluorescence DDM of a sample at $\phi = 0.1\%$ with WT cells and motA mutants at a number ratio of 7:3 plotted against (a) τ and (b) $q^2\tau$. In each case, q increases from red to purple in a rainbow scale in the range $0.62 < q < 4.46$ μm^{-1}. The inset to (b) plots the fitted diffusivity of the nonmotile motA (N2) cells as a function of q.

a check, we plotted $\ln[w(q,\tau)]$ versus $\ln(\tau)$, where $w(q,\tau) = -\ln[f(q,\tau)]/q^2$ [26,27]. Only a hint of superdiffusion appears at very short times. The fitted values of D_{N_2} are shown as a function of q in the inset of Fig. 1(b). Averaging over the flat part of $D(q)$ ($1 \lesssim q \lesssim 3$ μm^{-1}) gives $\bar{D}_{N_2}^{(motA)} = 0.326 \pm 0.003$ μm^2/s. Repeating this procedure by mixing populations of native cells and nonmotile fliF or motA mutants, but always at a total $\phi = 0.1\%$, yields the dependence of D_{N_2} on n_A for each of the two different kinds of added motile cells, fliF and motA [Fig. 2(a), red], showing that ΔD increases linearly with n_A. In the same plot, we show data for swimmers in glucose with higher $\bar{v}$ (black). A linear dependence remains, but with a higher slope.

Before discussing diffusion enhancement, we first comment on the thermal diffusivity of various nonmotile cells. Measurements of fliF and motA mutants on their own [$J_A = 0$ in Fig. 2(a)] gave $D_{0,N2}^{(motA)} = 0.29 \pm 0.01$ μm^2/s and $D_{0,N2}^{(fliF)} = 0.39 \pm 0.01$ μm^2/s $\approx 1.4 \times D_{0,N2}^{(motA)}$. This is consistent with tracking measurements [28], which found that deflagellated cells diffused $\approx$50% faster than cells with paralyzed flagella. The unenhanced diffusivity of native nonmotile cells (N1) cannot be accessed directly, but can be obtained by performing DDM on more and more dilute suspensions of AB1157 (i.e., using a native mixture of M + N1 cells and taking the limit $J_A \to 0$), from which we found $D_{0,N1} = 0.37 \pm 0.02$ μm^2/s. This value is, within uncertainties, the same as that of the fliF mutants, suggesting that nonmotile WT cells probably have had their flagella sheared off during preparation. Indeed, DDM measurements showed that gentler preparative protocols (e.g., using blunted pipette tips to reduce shear) generally increased the motile fraction α.

Returning to diffusivity enhancement, we find that all four data sets in Fig. 2(a) collapse onto a universal line if we plot the change in diffusivity, $\Delta D_{N2} = D_{N2} - D_{0,N2}$, versus the swimmer flux, J_A; see Fig. 2(b). All the data in Fig. 2(a) were obtained at fixed overall cell concentration $\phi = 0.1\%$. Figure 2(b) includes data points in which J_A is varied by changing ϕ (green points) or by changing ϕ and α together (blue points). These also fit into the universal linear dependence within experimental errors. Thus, $J_A = \bar{v}\alpha\phi/V$ is indeed the operative variable in controlling diffusion enhancement: $\Delta D_{N2} = \beta J_A$, with the best-fit value of $\beta = 7.1 \pm 0.4$ μm^4.

An implicit assumption so far has been that the diffusivity of each nonswimmer is enhanced *independently*. Figure 2(b) includes experiments performed over $0.04\% \lesssim \phi \lesssim 0.1\%$,

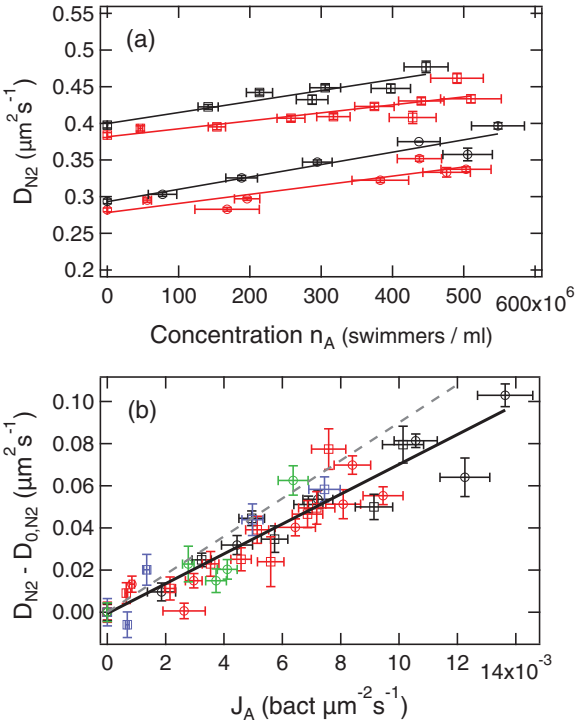

FIG. 2. (Color online) (a) Effective diffusivity D_{N2} of motA (circles) and fliF (squares) in suspensions of *E. coli* AB1157 containing no glucose (red, $\bar{v} = 13$–16 μm/s) or containing glucose (black, $\bar{v} \lesssim 25$ μm/s), while α is varied at a fixed total cell density $\phi = 0.1\%$, with best-fit lines. (b) The same data plotted as diffusivity enhancement $\Delta D = D_{N2} - D_{0,N2}$ for both motA and fliF data sets with and without glucose vs the active particle flux, $J_A = \bar{v} n_A = \bar{v}\alpha\phi/V$. Green and blue points: data taken by varying ϕ or by varying both ϕ and α. Equation (1) fitted through all points gives $\beta = 7.1 \pm 0.4$ μm^4. Dashed line: prediction of [14]. All error bars give $\pm$ standard deviation.

$0 < \alpha \lesssim 0.7$, giving in each case a volume fraction of $(1-\alpha)\phi$ of nonmotile cells (N1 or N1 + N2). The observed data collapse is consistent with little or no interaction between the nonswimmers. We checked this directly by measuring the diffusivity of fliF or motA cells on their own at $\phi = 0.01\%$ and $\phi = 0.1\%$, and found no change within experimental errors.

Equation (1) has been demonstrated before in 2D [6,7]. In a bath of *E. coli* and 2 μm beads between two glass walls separated by $h = 20$ μm, tracking gave $\beta \approx 45$ μm^4, dropping to ≈ 10 μm^4 for $h = 110$ μm, where bacteria and tracers remain close to one wall, so that surface effects still dominate. Our bulk value of $\beta \approx 7$ μm^4 is smaller than any of these values [29].

Significantly, although motA and fliF have different thermal diffusivities (and therefore hydrodynamic radii), their motion is enhanced to the same extent (same β); see Fig. 2(b). Previously, enhancement in 2D close to a wall was found to be the same for 1 and 2 μm tracers [6]. These findings recall particle imaging velocimetry (PIV), where small tracers sufficiently close to being neutrally buoyant follow the streamlines in a flow field. Corrections due to finite tracer size (radius R) scale as $(R/\ell)^2$ according to Faxén's law [30], for an average swimmer-tracer distance ℓ. The "PIV regime" is obtained if $(R/\ell)^2 \ll 1$.

To estimate ℓ, we approximate swimming *E. coli* cells by equivalent-volume spheres of diameter $d \approx 1.4$ μm, so that $\ell \sim d\phi^{-1/3} \approx 14$ μm at our highest total cell concentration ($\phi \approx 10^{-3}$). For native nonswimmers and fliF mutants without flagella, we take $2R = d \approx 1.4$ μm, so that $(R/\ell)^2 \approx 0.003$. Thus, we are in the PIV regime as in previous work using 1–2 μm colloidal tracers [6]. However, for motA mutants with $\lesssim 10$ μm paralyzed flagella, $(R/\ell)^2 \lesssim 0.5$. Thus, at ϕ somewhat higher than our highest value, motA mutants will be out of the PIV regime; the physics in this case remains to be explored.

A tracer near a passing swimmer executes a not-quite-closed loop [7,12,13,15] due to far-field fluid advection, resulting in a net displacement. We adapt a theory developed for "squirmers" [13] to *E. coli* [31], and show that integrating these motions over bacterial trajectories with finite persistence length accurately explains our data.

Each flagellated *E. coli* cell is a pusher; the far-field fluid velocity at a distance $\mathbf{r}$ from a cell is dipolar [32]:

$$\mathbf{v}(\mathbf{r}) = \frac{p\,\mathbf{r}}{r^3}[3\cos^2\theta - 1], \tag{2}$$

with strength $p = kv$, v the swimming speed, and k a geometric constant with dimensions (length)^2. We model WT cells using particles that swim straight over a persistence length λ before randomly changing direction.

The total displacement of a tracer is the sum of many "elementary scattering events", each of which is characterized by two "impact parameters": the distance a from the tracer and the distance b from the start of the straight trajectory, to the point of the closest approach; see Fig. 3. If $\lambda \to \infty$, such scattering events result in closed or almost-closed loop trajectories of the tracer [7,12,13,15] and a slightly enhanced tracer diffusivity. Real swimmers have finite λ, so that tracers only execute parts of these looplike trajectories, giving larger net displacements during each scattering event and higher ΔD [13].

The mean-squared displacement of a tracer $\langle|\mathbf{x}(t)|^2\rangle$ comes from summing individual displacements $\delta(a,b)$ over all

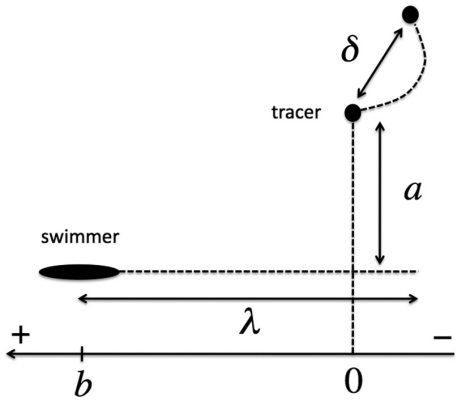

FIG. 3. Schematic of an "elementary scattering event" between a swimmer and a tracer. See text for definition of symbols.

possible scattering configurations a and b. Assuming identical, noninteracting, isotropic swimmers and statistically independent events [13]:

$$\langle|\mathbf{x}(t)|^2\rangle \equiv 6\Delta D t = \left(\frac{2\pi n_A v t}{\lambda}\right)\int_0^\infty\int_{-\infty}^\infty a\delta^2(a,b)dbda. \quad (3)$$

To understand the prefactor (...), note that in time t, each swimmer "tumbles" $v\,t/\lambda$ times to give $n_A\,v\,t/\lambda$ scattering events of the type shown in Fig. 3. To evaluate Eq. (3), we numerically integrate the tracer equations of motion, $\dot{\mathbf{r}}_t(t) = \mathbf{v}[\mathbf{r}_t(t) - \mathbf{r}_s(t)]$, where $\mathbf{r}_t(t)$ and $\mathbf{r}_s(t) = \mathbf{r}_s(0) + v\,t\,\hat{\mathbf{e}}$ are the positions of the tracer and swimmer, respectively. The initial position and swimming direction $\hat{\mathbf{e}}$ are set by the scattering parameters a and b. Repeating for sets of (a,b) and summing up the resulting displacements, we find an enhanced diffusivity for the dipolar pusher velocity field [Eq. (2)]:

$$\Delta D = 3.44\,n_A\,v\left(\frac{p}{v}\right)^2 = 3.44k^2J_A. \quad (4)$$

Detailed calculations [31] show that, as for squirmers [13], the numerical prefactor in Eq. (4) is not very sensitive to the range of (λ,p,v) relevant for swimming *E. coli* [32], for which $k = 1.45\ \mu\text{m}^2$, and Eq. (4) predicts $\Delta D = \beta J_A$ with $\beta = 7.24\ \mu\text{m}^4$, in remarkably good agreement with our value (Fig. 2) of $\beta = 7.1 \pm 0.4\ \mu\text{m}^4$.

Previous calculations at $\lambda \to \infty$ give $\beta = 0.48\ \mu\text{m}^4$ [7] because, here, tracers execute almost-closed loops [12]. For finite λ, the largest contribution to the integral in Eq. (3) comes from $b = 0$ and $b = \lambda$ [13]. At these scattering events (Fig. 3), a swimmer starting or finishing at the point of closest approach causes a tracer to perform approximately half of the infinite-λ almost-closed loop, giving significantly larger total displacements. Indeed, preliminary DDM measurements using a smooth swimming mutant, which has a significantly higher λ than a run-and-tumble swimmer, showed lower enhanced diffusion of the nonswimmers.

To summarize, we have observed that the enhanced diffusion of nonmotile cells in a 3D bath of motile *E. coli* scales linearly with the motile cell flux (Fig. 2). The scaling is accurately accounted for by summing tracer displacements due to far-field advection induced by individual swimmers with long but finite persistence-length trajectories. Interestingly, it has been recently suggested [14] that fluid entrainment is also important, which, together with advection, give $\beta = 9\ \mu\text{m}^4$ in 3D, which is a value incompatible with our observations [Fig. 2(b)] [33].

We have worked at $\phi \lesssim 0.1\%$, where the diffusivities of nonmotile fliF and motA mutants are enhanced equally. At higher ϕ, this situation should change because motA cells with paralyzed flagella are then too large to be considered tracers. Separately, it should be interesting to probe concentrated systems in which the density of tracers is increased until they interact with each other.

A.J., V.A.M., A.N.M., and W.C.K.P. were funded by an EPSRC studentship, Grants No. EU FP7-PEOPLE (PIIF-GA-2010-276190), No. EPSRC EP/I004262/1, and No. EPSRC EP/J007404/1, respectively. We thank G. Dorken for assisting with plasmid transformations and M. E. Cates, E. Clément, G. Miño, and D. Pushkin for discussions.

[1] S. Ramaswamy, Annu. Rev. Condens. Matter Phys. **1**, 323 (2010).
[2] M. E. Cates, Rep. Prog. Phys. **75**, 042601 (2012).
[3] A. Sokolov, M. M. Apodaca, B. A. Grzybowski, and I. S. Aranson, Proc. Natl. Acad. Sci. USA **107**, 969 (2010).
[4] L. Angelani, R. Di Leonardo, and G. Ruocco, Phys. Rev. Lett. **102**, 048104 (2009).
[5] X. L. Wu and A. Libchaber, Phys. Rev. Lett. **84**, 3017 (2000).
[6] G. L. Miño, T. E. Mallouk, T. Darnige, M. Hoyos, J. Dauchet, J. Dunstan, R. Soto, Y. Wang, A. Rousselet, and E. Clément, Phys. Rev. Lett. **106**, 048102 (2011).
[7] G. L. Miño, J. Dunstan, A. Rousselet, E. Clément, and R. Soto, J. Fluid Mech. **729**, 423 (2013).
[8] C. Valeriani, M. Li, J. Novosel, J. Arlt, and D. Marenduzzo, Soft Matter **7**, 5228 (2011).
[9] D. T. N. Chen, A. W. C. Lau, L. A. Hough, M. F. Islam, M. Goulian, T. C. Lubensky, and A. G. Yodh, Phys. Rev. Lett. **99**, 148302 (2007).
[10] K. C. Leptos, J. S. Guasto, J. P. Gollub, A. I. Pesci, and R. E. Goldstein, Phys. Rev. Lett. **103**, 198103 (2009).
[11] H. Grossart, L. Riemann, and F. Azam, Aquat. Microb. Ecol. **25**, 247 (2001).
[12] J. Dunkel, V. B. Putz, I. M. Zaid, and J. M. Yeomans, Soft Matter **6**, 4268 (2010).
[13] Z. Lin, J. L. Thiffeaul, and S. Childress, J. Fluid Mech. **669**, 167 (2011).
[14] D. O. Pushkin and J. M. Yeomans, arXiv:1307.6025v1.
[15] D. O. Pushkin, H. Shum, and J. M. Yeomans, J. Fluid Mech. **726**, 5 (2013).
[16] R. Cerbino and V. Trappe, Phys. Rev. Lett. **100**, 188102 (2008).
[17] L. G. Wilson, V. A. Martinez, J. Schwarz-Linek, J. Tailleur, G. Bryant, P. N. Pussey, and W. C. K. Poon, Phys. Rev. Lett. **106**, 018101 (2011).
[18] V. A. Martinez, R. Besseling, O. A. Croze, J. Tailleur, M. Reufer, J. Schwarz-Linek, L. G. Wilson, M. A. Bees, and W. C. K. Poon, Biophys. J. **103**, 1637 (2012).
[19] P. J. Lu, F. Giavazzi, T. E. Angelini, E. Zaccarelli, F. Jargstorff, A. B. Schofield, J. N. Wilking, M. B. Romanowsky, D. A. Weitz, and R. Cerbino, Phys. Rev. Lett. **108**, 218103 (2012).
[20] Step 1 in flagellar synthesis in fliF [21] and synthesis of the stator complex in the motor in motA [22] are disrupted. Fluorescence comes from inclusion of the Green Fluorescent Protein-encoding plasmid pHC60 [23].
[21] H. Terashima, S. Kojima, and M. Homma, Int. Rev. Cell. Mol. Biol. **270**, 39 (2008).
[22] G. E. Dean, R. M. Macnab, J. Stader, P. Matsumura, and C. Burks, J. Bacteriol. **159**, 991 (1984).
[23] H. P. Cheng and G. C. Walker, J. Bacteriol. **180**, 5183 (1998).

[24] From measuring 60 cells using $\times 100$ phase-contrast microscopy.
[25] J. Adler and B. Templeton, J. Gen. Microbiol. **46**, 175 (1967).
[26] V. A. Martinez, G. Bryant, and W. van Megen, Phys. Rev. Lett. **101**, 135702 (2008).
[27] V. A. Martinez, J. H. J. Thijssen, F. Zontone, W. van Megen, and G. Bryant, J. Chem. Phys. **134**, 054505 (2011).
[28] S. Tavaddod, M. Charsooghi, F. Abdi, H. Khalesifard, and R. Golestanian, Eur. Phys. J. E **34**, 1 (2011).
[29] Cell densities in [5] were $\sim 10^2\times$ those used here or in [6,7]; the data cannot be compared directly.
[30] J. Happel and H. Brenner, *Low Reynolds Number Hydrodynamics* (Prentice-Hall, Englewood Cliffs, NJ, 1965).
[31] A. Morozov and D. Marenduzzo, arXiv:1308.3387.
[32] K. Drescher, J. Dunkel, L. H. Cisneros, S. Ganguly, and R. E. Goldstein, Proc. Natl. Acad. Sci. USA **108**, 10940 (2011).
[33] Note, however, that [14] predicts $\beta = 7.6\ \mu\text{m}^4$ for 3D advection alone, consistent with our work.